UNBURNED HYDROCARBON EMISSION MECHANISMS IN SMALL ENGINES

By

Victor M. Salazar

A disertation submitted in partial fulfillment of the requirements for the degree of

Doctor of Philosophy

(Mechanical Engineering)

at the

UNIVERSITY OF WISCONSIN-MADISON

2008

ABSTRACT

The effect of the liquid fuel in the intake manifold, the ring pack crevices and the oil film on the unburned hydrocarbon (HC) emissions of a spark-ignited, carbureted, air-cooled V-twin engine was studied. Tests were performed for a range of engine load, two engine speeds, various air-fuel ratio and with a fixed ignition timing. To isolate liquid fuel effects due to the poor atomization and vaporization of the fuel when using a carburetor, a specially conditioned homogeneous, pre-vaporized mixture system (HMS) was developed. The results from carburetor and HMS are compared. To verify the existence of liquid fuel in the manifold, and to obtain an estimate of its mass, a carburetor-mounted liquid fuel injection (CMLFI) system was also implemented. Stop-injection tests performed with the CMFLI system show that 60-80 cycles worth of liquid fuel is held in the intake manifold depending on operating condition. The results of the comparison show that the liquid fuel in the intake manifold does not have a statistically significant influence on the averaged HC emissions. In addition, the cycle-resolved HC emissions for both systems follow the same trends and are comparable in magnitude. Heat release analysis showed little difference between fuel mixture delivery system. These results suggest that under steady state operation the HC emissions for this engine are not sensitive to the presence of liquid fuel in the intake manifold.

The ring pack contribution to the engine-out HC emissions was estimated using a simplified ring pack gas flow model; the model was tested against the experimentally

measured blowby. The tests were performed using the homogeneous fuel mixture system. The integrated mass of HC leaving the crevices from the end of combustion (the crank angle that the cumulative burn fraction reached 90%) to exhaust valve closing was taken to represent the potential contribution of the ring pack to the overall HC emissions; post-oxidation in the cylinder will consume some of this mass. Time-resolved exhaust HC concentration measurements were also performed, and the instantaneous HC mass flow rate was determined using the measured exhaust and cylinder pressure. At high load the model predicts that the ring pack returns approximately three times as much HC mass to the cylinder as is measured in the exhaust, indicating that the HC emissions are dominated by the ring pack contribution. At the lightest load condition tested, the ring pack model predicts less mass returning to the cylinder from the ring pack than is observed in the exhaust, clearly indicating that another HC mechanism is significantly contributing to the exhaust HC emissions. The integrated exhaust HC mass from the time-resolved HC measurement was found to correlate inversely with the IMEP on a cycle-by-cycle basis, which strongly suggest that incomplete combustion is materially contributing to the exhaust HC emissions. A statistical analysis showed that the correlation was significant. The intermediate load condition represents a combination of these two extremes. The ensemble-average ring pack model results indicate that the mass returned to the cylinder from the ring pack is slightly higher than the amount measured in the exhaust. But, a conditional sampling analysis indicates that there are sub-groups, *i.e.* late-burning cycles, for which this is not true. There is expected to be some in-cylinder post-oxidation of the ring pack HC mass at this condition, and the late burning cycles

were not found to excessively contribute to the HC emissions, which both strongly suggests that there are other mechanisms besides the ring pack that are significantly contributing to the HC emissions at this condition. The most likely mechanism is incomplete combustion.

The contribution of fuel adsorption in engine oil and its subsequent desorption following combustion to the engine-out hydrocarbon (HC) emissions was studied by comparing steady state and cycle-resolved HC emission measurements from operation with a standard full-blend gasoline, and with propane, which has a low solubility in oil. Experiments were performed at two speeds and three loads, and for different mean crankcase pressures. The crankcase pressure was found to impact the HC emissions, presumably through the ringpack mechanism, which was largely unaltered by the different fuels. The average and cycle-resolved HC emissions were found to be in good agreement, both qualitatively and quantitatively, for the two fuels. Further, the two fuels showed the same response to changes in the crankcase pressure. The experiments were supported by a numerical analysis. The simulation of the liquid-gas phase equilibrium of the fuel-oil system showed the solubility of propane in the oil was approximately an order of magnitude lower than for gasoline. Further the numerical analysis of the adsorption-desorption of the fuel in the oil along the cycle showed that the oil layer contribution is very small compared with the ring pack contribution. This suggests that the effect of fuel adsorption in the oil is not significant for small air-cooled utility-type engines.

Dedicated to the memory of my father

Alfredo Salazar

ACKNOWLEDGEMENTS

I would like to acknowledge to all who directly or indirectly help me out while I was at the Engine Research Center (ERC). In special, I want to acknowledge my advisor Professor Jaal B. Ghandhi, for his guidance and valuable support along my studies. Jaal is a real advisor.

I also would like to acknowledge the Wisconsin Small Engine Consortium (WSEC) for providing the project funding. The feedback and technical support from its members was extremely helpful. Thus, I would like to express thanks to Eric Hudak from Kohler, Chuck Eichinger from Mercury Marine, and Blake Suhre from MotoTron for providing component for the test cell.

At the ERC, thanks to Ralph Braun for helping me in the machine shop and for sorting out several mechanical problems during the implementation of the test cell.

I would like to express my appreciation as well to my officemates Ben Petersen, Nate Huagle, John Brossman and Doug Heim for being such nice guys.

Finally, I want to acknowledge the support of all my family and specially of my wife Janette for her comprehension and love along my PhD endeavor.

CONTENTS

TABLES

FIGURES

NOMENCLATURE

A	Area
AF	mixture air-fuel ratio
a_p	piston acceleration
$aTDC$	after top dead center
B	bore
$bTDC$	before top dead center
C	constant, concentration
c	speed of the sound in the gas
CA	crank angle
$CA50$	crank angle at the mass fraction burned of 50%
$CA90$	crank angle at the mass fraction burned of 90%
$CA90\text{-}EVO$	time interval from CA90 to EVO
C_D	discharge coefficient
CO	carbon monoxide
CO_2	carbon dioxide
COV	coefficient of variance
$CMFIS$	carburetor mounted fuel injection system
c_v	specific heat at constant volume
D	diffusivity
d	diameter
$d1L$	diameter of the bottom edge of the first piston groove
$d1U$	diameter of the upper edge of the first piston groove
$d3L$	diameter of the bottom edge of the second piston groove
$d3U$	diameter of the upper edge of the second piston groove
$di2$	internal diameter of the first piston groove
$di4$	internal diameter of the second piston groove
Dv	exhaust valve diameter
E_a	activation energy

ECU	electronic control unit
EG-RI	first ring end gap
EG-RII	second ring end gap
EIi	emission index of species *i*
EVO	exhaust valve opening
EVC	exhaust valve closing
$EIHC_{M,EXH}$	HC emission index measured at the exhaust
$EIHC_{C,RP}$	HC emission index calculated using the ring pack model
$EIHC_{C,MB}$	HC emission index calculated from the mass balance at the exhaust
F	force
FID	flame ionization detector
FFID	fast-flame ionization detector
h	relative position of the ring in the grove
H_2	hydrogen
H_2O	water
h1	first piston groove height
h2	second piston groove height
h3	top inter-grove height
h4	bottom inter-grove height
h_c	heat transfer coefficient
HC	hydrocarbon
hR	ring height
hRI	height of the first ring
hRII	height of the second ring
HMS	homogeneous mixture system
IMEP	indicated mean pressure
IVC	intake valve closing
IVO	intake valve opening
K	static sensitivity, constant equilibrium
k	specific heat ratio
Lv	lift exhaust valve

LHV	lower heating value
m	mass
$\dot{m}$	mass flow rate
MAP	manifold absolute pressure
MW	molecular weight
N	mole
$\dot{N}$	molar flow rate
N_2	nitrogen
NOx	oxides of nitrogen
O_2	oxygen
P	pressure
P_c	unprobability correlation
ppm	parts per million
R	gas constant
Q	heat
RPM	revolutions per minute
RSS	root-sum-squares
S	stroke
S_p	mean piston speed
t	time
T	temperature
TDC	top dead center
u_p	piston velocity
U	internal energy
V	volume, volts
V_A	molar volume of solute A at its normal boiling temperature
V_c	critical volume
wRI	width of the first ring
$wRII$	width of the second ring
x	ring pack parameter, distance
X	molar fraction

y	hydrogen to carbon ratio
y_{res}	in cylinder residual mass fraction
Y	mass fraction
#	number
[i]	concentration of species i
$\propto$	infinity

GREEK SYMBOLS

δ	oil layer thickness
Δ	increment
η	compressibility factor, efficiency
γ	specific heat ratio of the gas
$\mu_{\mathbf{B}}$	viscosity of the solvent B
ρ	density of the gas
ϕ	angle
θ	angle
Φ	equivalence ratio
τ	time constant

SUB- AND SUPER-SCRIPTS

act	actual
air	air
C	carbon
c	combustion
C_1	1 carbon basis
C_3	3 carbon basis
carb	carburetor
corr	corrected
cr	crankcase
crev	crevice
crk_offset	crankcase offset
cyl	cylinder
d	downstream
disp	displaced
evo	exhaust valve opening
exh	exhaust
fuel	fuel
f	friction

fuel/cycle	fuel per cycle
fuel-engine/cycle	fuel injected per cycle
fuel-cum.-norm	normalized cumulative mass of fuel
hr	heat release
H	hydrogen
HV	heating value
i	index, species
in-cum	in cumulative
m	motoring
max	maximum
mix	mixture
n	potytropic exponent
out-cum	out cumulative
p	products
ref	reference
s	stick, system
u	upstream
uncer	uncertainty
w	wall

CHAPTER I

INTRODUCTION

1.1 OVERVIEW

Small engines are identified as a major source of air pollution by the California Air Resources Board (CARB) and the Environmental Protection Agency (EPA). Every year approximately 100 million of small engines are produced worldwide [1]. From this total about 35 million are sold in the US. This is very significant compared with the approximately 17 million of cars sold in the US [2]. Small engines usually run for shorter periods of time than the automotive engines however their emissions levels are significantly higher accounting as much as 13% of the total hydrocarbon emissions in some regions of the US [3]. Therefore there is a considerable pressure on the manufacturers to reduce the emissions levels by way of new, lower emission standards.

1.2 LEGISLATION

The CARB is the leading regulatory agency regarding emissions from small engines followed by the EPA. Table 1.1 shows the general status of the CARB and EPA legislations for the handheld and non-handheld small engines. The CARB 3 emission regulations have been already implemented and the CARB Blue Skies have been

implemented voluntarily as well. The EPA 3, regulations which are very similar to the CARB 3, regulations will be implemented starting in 2008. Since the introduction of the emissions regulations in 1995, small engines have been subject to a decade-long reduction in emission levels. However, it is important to note that the carbon monoxide (CO) levels have remained the same with no further reduction. One of the main reasons for this trend is that small air-cooled engines, for structural reasons, need to operate under rich conditions, which makes the reduction of the CO levels difficult without major changes. This operating regime keeps the engine temperature at safe levels.

Table 1. 1 Legislations and limits on emissions for small engines (Source CARB/EPA)

Status →		2001-2007 and later		2000-2005 and later		2005-2008 and later		Implemented voluntary	
	Legislation→	EPA-2		CARB-2		CARB-3		CARB BLUE SKY	
Products	Engine Capacity	HC + NOx (g/kWhr)	CO (g/kWhr)	HC + NOx (g/kWhr)	CO (g/kWhr)	HC + NOx (g/kWhr)	CO (g/kWhr)	HC + NOx (g/kWhr)	CO (g/kWhr)
Handheld	<50cc	50	805	72	536	50	536	25	536
	>50cc	72	603	72	536				
	50cc to 80cc					72	536	36	536
Non handheld	<66cc/65cc	50	610	72	536				
	66cc-100cc	40	610						
	100cc-225cc	16.1	610						
	>225cc			16.1	549				
	80cc-225cc	12.1	610	12.1	549	10	549	5	549
	>225 cc					8	549	5	549

1.3 MOTIVATION

Small engine manufacturers are being pushed to find cost-effective methods to meet ever-tightening future emission regulations, but they cannot directly benefit from the technologies developed by automotive engine producers, such as electronic fuel injection, exhaust gas recirculation (EGR), and after-treatment devices, that represent a

significant increase in production costs. Therefore, small engines will still use simple, reliable and low-cost devices like the carburetor, and the study of engines using such accessories is still important.

Hydrocarbons emissions are the product of the incomplete combustion of the fuel, which arises from storage of the fuel in regions of the chamber that the flame can not reach. There are several mechanisms of fuel storage to avoid the complete oxidation of the fuel during flame propagation. The mechanisms of unburned hydrocarbon emissions (HC) from automotive engines have been widely studied, and at the moment there is a good understanding of the relative contribution of each source to the total HC emissions [4, 5]. The main sources of HC described in the literature are: crevice regions, adsorption and desorption of fuel by the oil layers and deposits, liquid fuel films, flame quenching, and exhaust valve leakage. The ring pack contribution is believed to be the major source of engine-out HC emissions, however other mechanisms such as the liquid films are also important and their contribution can be significant, especially under cold-start and transient conditions. It is important to note that not all the combustible mixture that escapes the main combustion contributes to the total HC emissions. Depending on the engine operating condition a significant quantity of this mixture can be partially oxidized during post-flame processes, reducing its contribution to HC emissions. The extent of post-flame oxidation depends on the time available for the unburned mixture to diffuse into the hot burned gases; provided that there is sufficient oxygen and that the temperature is high enough, the unburned mixture can oxidize.

Small engines, however, operate under different conditions than the automotive engines. Small engines: use carburetors as a fuel delivery system; are air cooled, and therefore have high operating temperature, which can give significant, uneven bore distortion; and run with rich air-fuel ratios.

The atomization and subsequent vaporization of the fuel by the carburetor is poor. Consequently, liquid fuel films in the intake manifold are formed and can adversely impact the HC emissions. Another important aspect in small engines is that the residence time in the intake manifold can be very short because in many cases the carburetor is directly mounted to the head. Under such conditions, the fuel may not have enough time to vaporize, producing a poorly vaporized and inhomogeneous air-fuel mixture.

Air cooling of small engines using external fins and an integral fan does not provide a uniform cooling pattern, causing the engine to run hot in locations away from the fan. This generates significant and uneven bore distortion. The bore distortion could directly affect the mass flow through the ring pack crevices and the blowby, consequently creating an impact on the HC emissions. In addition the adsorption-desorption mechanism of the fuel in the oil could also be affected by the high operating temperature.

The rich operation in small engines has the advantage of higher output power levels at cooler operating temperatures, which reduces thermal problems, and increases the lifetime of the engine. Running under such conditions also gives good transient response without the use special compensation systems in the carburetor. However part

of the fuel is not oxidized completely mainly due to the lack of oxygen, which generates higher HC and CO emissions.

Hydrocarbon emissions have a negative impact on the environment and human health, and represent a fraction of fuel that does not produce useful work, and therefore, a reduction in the engine efficiency. In small engines for partial load conditions, mainly because of the rich operation, the HC emissions dominate over the NOx in the legislated HC+NOx emissions. Therefore, the HC mechanisms under the particular conditions of small engine operation need to be studied

1.4 OBJECTIVES

The purpose of the present work is to study the relative contribution of each of the unburned hydrocarbons mechanisms of a spark-ignited, carbureted, air-cooled V-twin engine.

The HC mechanisms that were studied in depth were: the liquid fuel in the cylinder, the ring pack crevices, and oil adsorption-desorption. The individual contribution of each source on the total HC emissions will be studied for a wide range of load, speed and spark timing conditions. Other HC sources that are known contributors will be discussed and shown to be of lesser importance.

The remainder of the thesis will be presented as follows. In Chapter 2 a literature review of the hydrocarbon emission mechanisms is provided. The majority of the literature review comes from previous studies carried out in automotive engines. In

Chapter 3 the test cell and experimental apparatus are described. Chapter 4 details the study of the liquid fuel mechanism and its impact on the hydrocarbon emissions. Chapter 5 discusses the estimation of the ring pack contribution on the HC emissions. The findings of the effect of the fuel-oil adsorption-desorption on the HC are provided in Chapter 6. Finally Chapter 7 covers the conclusions regarding to the main findings and the recommendations for future work.

CHAPTER II

LITERATURE REVIEW

Hydrocarbon emission mechanisms for automotive engines have been studied extensively. Detailed information about each possible mechanism and their relative contribution to engine-out emissions has been obtained by using both experimental and computational techniques. However, little small-engine-specific work been done; therefore, the major source of information available in the literature is pertinent to automotive engines.

Cheng *et al.* [4], estimated the relative contribution of the different mechanisms to the HC emissions for fully warmed up conditions, see Table 2.1.

Table 2.1 Relative contribution of the different HC mechanisms to engine-out HC emissions [4]

Source	**%HC**
Combustion chamber crevices	38
Single-wall flame quenching	5
Oil Film Layers	16
Combustion Chamber Deposits	16
Exhaust Valve Leakage	5
Liquid Fuel	20

The main contributors of the total output HC emissions are: the crevices, liquid fuel, oil films and the combustion chamber deposits [5].

In §2.1 a literature review of the previous studies related to small engine emissions is given, and is followed by a literature review of the different HC mechanism for automotive engines in §2.2-2.9

2.1 PREVIOUS STUDIES OF EMISSIONS FROM SMALL ENGINES

There are no specific studies focused solely on HC emission mechanisms from small engines. However, there are some studies reporting the general CO, HC and NOx emission trends of small engines [6]. Thus, it is well known that the output power requirement of small engines has a direct effect on the amount of HC, CO and NOx emitted [6-11]. Hydrocarbon and CO emissions decrease as the load increase. In addition, small engines, due to their particular design, run with rich air-fuel mixtures, producing low levels of NOx and high levels of CO. It has been reported, that the air-fuel ratio has a direct effect on the HC, CO and NOx emissions [8]. Swanson [10] implemented an electronic port fuel injection system (EFI) on a small engine and showed that the air-fuel mixture preparation had a significant impact on the emissions levels. Using the EFI system, the brake specific CO (BSCO) and brake specific hydrocarbon plus oxides of nitrogen (BSHC + NOx) were reduced 14.2% and 16.6% respectively.

Currently small engines still use carburetors as a fuel system, and the resulting fuel atomization and subsequent vaporization of the fuel is poor and inefficient. Thus, a significant amount of the fuel can enter the cylinder in the liquid phase. In addition, some

of the fuel impinges on the intake manifold and intake port walls, generating liquid fuel films. The liquid fuel films can adversely affect the HC emissions [4]. Another important aspect in small engines is that the residence time of the fuel in the intake manifold is very short because in many engines the carburetor is directly mounted to the cylinder head. Therefore, under steady-state operation the fuel may not have enough time to vaporize, producing a poorly vaporized and inhomogeneous air-fuel mixture.

Itano *et al.* [12], studied the exit flow of several common carburetors. The idea was to characterize the quality of the air-fuel mixture preparation by the carburetor. To that end the air-fuel ratio was measured, and the exit flow was visualized with high speed movies. The main findings of these tests were that there was a significant amount of liquid fuel film formation on the wall of the manifold. In addition, the air-fuel ratio measurements at the exit plane, revealed that the mixture was not uniform, having higher air-fuel ratio close to the liquid fuel film. The problem of poor mixture preparation is exacerbated under transient conditions [13].

It is known that the transient operation of the engine generates excursions in the air-fuel ratio which are responsible for an increase in the HC, CO, and NOx emissions. In the same way, transient conditions increase the formation of liquid fuel films in the intake manifold, which act as a sink or source of fuel, causing a fluctuation in the air fuel ratio. The transient behavior of the liquid films in the intake manifold of a four-stroke small engine has been characterized by Jehlik *et al*. [13], who modified the stock engine carburetor by incorporating a fuel injector. This setup allowed total control of the

injection process on a single-cycle basis. Transient tests like: step-fueling changes with constant air flow, step-throttle changes with constant fuel flow, skip-injection and stop-injection were performed. The idea was to characterize the liquid fuel films dynamics under transient conditions. The engine was fueled with indolene, iso-octane, and propane to isolate the vaporization effect. The main findings of this work were: the film dynamics are dominated by the airflow in the intake manifold, and that the vaporization from the fuel film in the intake walls contributed approximately 30% of the fuel inducted per cycle regardless of load.

Bonneau [14] compared the operation of a small engine using two different fuel systems at 10% and 50% load. In this study, the engine was first operated with the carburetor, and then with a homogeneous pre-vaporized fuel mixture system. The results showed that for a range of air-fuel ratios from 11.5 to 16 the carburetor did not have a significant impact on the HC emissions; the behavior of both systems was remarkably similar. However, for leaner air-fuel ratios the carburetor fuel system showed increased levels of HC emissions.

2.2 LIQUID FUEL FILMS

In port-injected (PFI) engines the fuel spray usually impinges on the back side of the intake valve and the surrounding intake port surfaces. Depending of the operating condition of the engine, part of the fuel evaporates and part of the fuel forms a liquid film on the back side of the valve, intake manifold and intake port. As a consequence, part of the fuel enters to the cylinder as liquid films, droplets and ligaments. In the automotive

industry most of the engine-out HC emissions are oxidized using a catalyst. However, due to the stringent emission regulations, the HC emissions are still being investigated especially during the cold start transient, which accounts for 80-90% of the total tailpipe HC emissions. Another area of recent interest is the formation of fuel films on the piston surface in a direct-injection engine. It is believed that under such conditions there is also a fuel film contribution to the particulate matter formation.

The reduction of HC emissions in a port-injected (PFI) engine using a pre-vaporized fuel system during the cold star and warm up periods was studied by Boyle and Boam [15]. They compared the HC emissions when different engines were fueled with liquid gasoline, and with pre-vaporized gasoline, which eliminated the liquid fuel film effect. The results showed a reduction of 15 to 40% in the HC emissions when operating the engine in the pre-vaporized fuel mode. This finding highlights the importance of the liquid fuel in the HC emissions.

The phenomena that determine the inflow process of the liquid fuel past the intake valve in a PFI engine was addressed experimentally by Meyer *et al.* [16]. The study simulated a cold-start process in a transparent engine. Detailed characterization of the fuel droplets entering the cylinder was made using a Phase Doppler Particle Analyzer (PDPA). In addition, Planar Laser-Induced Fluorescence (PLIF) visualization of the fuel spray was carried out. Based on the droplet measurements and the qualitative geometrical information of the PLIF measurements, a method to determine the amount of fuel mass going into the cylinder was estimated for both closed-valve and open-valve injection

cases. The tests identified four transports mechanisms of liquid fuel into the cylinder: forward flow atomization, spray contribution, high-speed intake flow transport, and fuel film squeezing. The evolution in time of the liquid fuel going to the cylinder showed a different behavior for both the closed-valve and open-valve injection cases. The estimated fraction of liquid fuel entering the cylinder was 40 % and 25% of the injected fuel 15 seconds after the start for closed-valve and open-valve cases respectively. Meyer and Heywood [17], continuing the work of Meyer *et al.* [16], qualitatively studied the influence of several engine and injector design parameters, and fuel parameters, on the characteristics of the liquid fuel droplets entering the cylinder. Using a PDPA, measurements of fuel droplet size distributions in the vicinity of the intake valve were performed. The effect of the fuel volatility, injection timing, intake valve warming, injector type, spray geometry, and spray targeting in the intake port were studied for both closed-valve and open-valve injection cases. The results showed that there is a significant dependence of the above-mentioned parameters on the liquid fuel in the cylinder, both during the cold starting and the fully warmed up conditions. It was found that the influence of the studied parameters on the amount of liquid fuel in the cylinder is enough to be reflected on the HC output emissions. However no HC emissions measurements were reported.

Takahashi and Nakase [18], using a non-intrusive optical technique, measured the liquid fuel thickness in the intake port, the combustion chamber, and cylinder liner of a port fuel injected engine. The measurements showed the evolution in time of the liquid fuel film in the walls of the intake port, combustion chamber, and cylinder liner, during a

cold start. They found that the fuel film thickness in the intake port reaches its peak value after 6 cycles of the start, and that the liquid fuel stored in the intake port started to enter the cylinder three cycles after starting. Increasing the engine speed, load, coolant temperature, and valve overlap resulted in thinner liquid fuel films.

As can be seen from the different sources above, liquid fuel films are considered an important source of HC emissions, but their relative contribution is not clear.

2.3 RING PACK CREVICES

Combustion chamber crevices are an important source of HC emissions from engines. As seen from Table 2.1, the crevices are the greatest contributors under fully warmed up steady-state operation. However, for other particular conditions of engine operation such as cold start, other sources are considered to be equally important. Several studies regarding the HC crevices have been performed mainly focused on the impact of reducing crevices volumes and on understanding the post flame oxidation. At the present, it appears that there is a very good understanding of the crevice mechanism.

The crevices in the combustion chamber are (see Fig. 2.1): the ring pack crevice, the cylinder head gasket crevice, the spark plug crevices (which includes the thread and the central electrode crevices), and the valve-seat crevice.

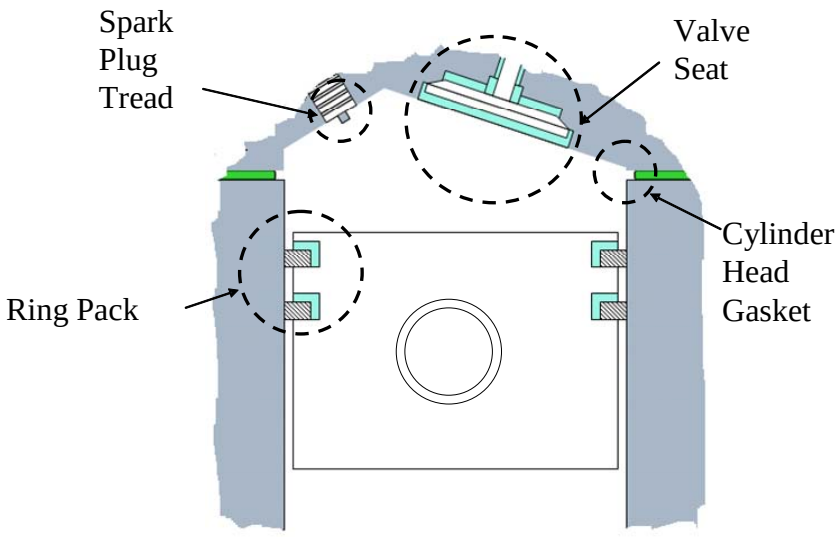

Figure 2.1 Combustion chamber crevices

A crevice in the SI engine field is defined as a small space surrounded by walls that is directly connected to the combustion chamber. The characteristic of a crevice is that the small size of the passageway that connects the crevice with the main chamber prevents the flame propagation, and thus, prevents oxidation of the combustible mixture stored in the crevice. An easy way to characterize the ability of a flame to propagate into a narrow passageway is the two wall quenching distance [19]. This distance is the critical distance between two parallel plates below which the flame will not propagate. The concept has been very useful to explain why the mixture stored in the crevices escapes the main combustion. Several expressions that correlate the quench distance with other parameters have been developed for internal combustion engines [20, 21]. The quench distance depends on the equivalence ratio and the amount of charge dilution. Off-stoichiometric air-fuel ratios and high dilution increases the quench distance [22].

A detailed view of the ring pack is presented in Fig. 2.2. The ring pack crevices consist of the piston upper crevices and the piston lower crevices. The piston upper crevice (V_1) is the space that is formed by the walls of the top piston land, the first ring, and the cylinder wall. The lower piston crevice is the space formed between the two rings (V_2).

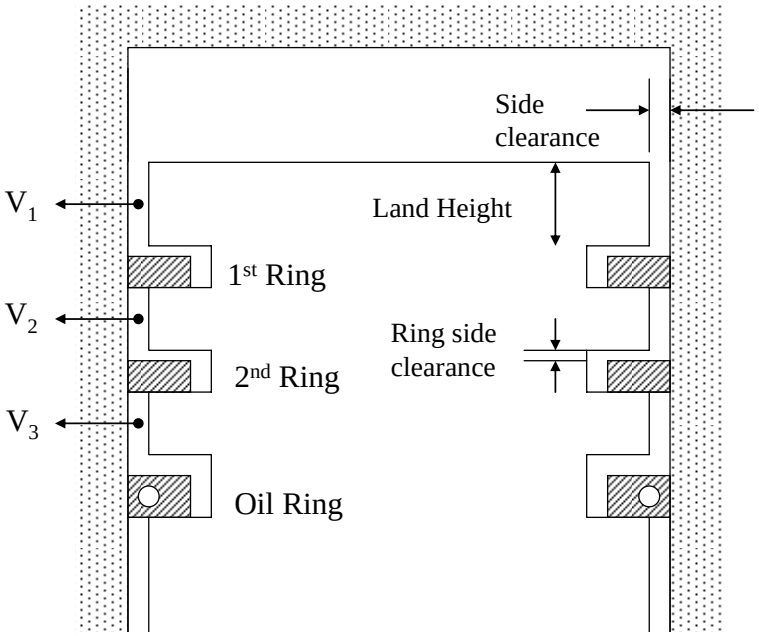

Figure 2.2 Ring pack crevice detail

Wentworth [23] used a specially designed top ring in order to almost completely eliminate the piston crevices (see Fig. 2.3). Using that arrangement the HC emissions were reduced 25%-52% from the normal ring pack configuration. This identified the crevices as critical to the HC emissions. Alkidas [24] showed that there is a dependence of the HC emissions on the volume of the ring pack crevices. However the dependence of the HC on the geometric parameters such as the top land distance and piston-cylinder

radial clearance shows a complicated relationship that involves not only the quench distance but also other factors such as flame propagation.

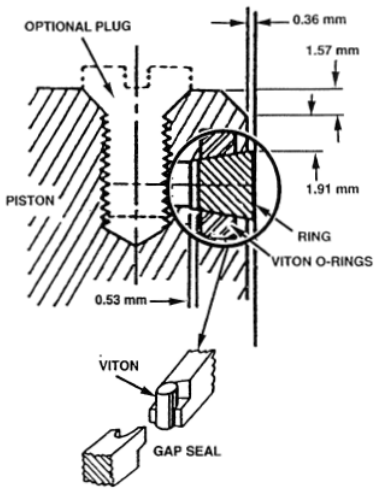

Figure 2.3 Sealed-ring orifice design [23]

The change in HC emissions in response to changes in the top land height has been studied by Alkidas [24]. Using a production engine, the HC emissions were reduced 22% when the top land height was reduced from 6 to 3 mm, which represented a 47% reduction in the top land crevice volume.

Later, taking a different approach Bigninon and Spicher [25], tested six pistons with different top land crevice geometry. Each piston had a different chamfer configuration, ranging from 2 to 4 mm at 45°, and being either only half or continuous around the top land. The observation of the flame intrusion into the top land crevice was performed with the implementation of an optical fiber technique. The relation between the top land crevices, output HC emissions and the flame penetration frequency in the crevice were studied. An HC emissions reduction of 30% was obtained for the case

where the piston had the largest top land crevice. For this case the optical tests showed an increase in the frequency of intrusion of the flame in the crevice.

The top land radial clearance, combined with the quench distance is an important design parameter. Alkidas [24], observed that there is a critical radial clearance beyond which the HC emissions are not affected by further increases in the radial clearance. Below the critical value, the reduction in radial clearance results in a reduction on the HC emissions, which was explained using the wall quench distance phenomena. When the distance between the piston and the cylinder wall is large enough, the flame can propagate into the crevice and oxidizes the stored mixture. However, when the distance is too small the flame cannot propagate into the crevice, resulting in an increase in HC emissions. Reitz and Kuo [26], develop a multidimensional model to assess the effects of the flow through the ring pack on the HC emissions, and combustion. Several operating conditions were simulated for different top land crevice designs. No significant effect on the combustion was found. However HC emissions were increased when the top radial clearance was increased. The authors also found that HC emissions were more sensitive to top land radial clearance than to the top land height.

When analyzing engine-out HC emissions, it is important to also consider the characteristics of the stored gas mixture. The main factor is the amount of unburned gases, or the mass fraction of fresh combustible mixture. The composition of the crevice mixture is highly dependent on the location of the spark plug in the combustion chamber [22]. With a spark plug located at the center of the combustion chamber, the greatest HC

emissions are obtained. This is because the flame propagation takes more time to get the cylinder walls, and therefore, more fresh combustible mixture can be stored in the ring pack crevices. On the other hand as the spark plug is moved from the center towards the cylinder wall, the amount of HC emissions are reduced, because part of the mixture stored in the crevices are burned gases.

Another parameter that appears to affect the amount of HC emissions is the relative location of the ring end gap with respect to the spark plug location in the combustion chamber. Wentworth [23] fixed the ring gap position by pinning the top ring. Several angular positions of the end gap relative to the spark plug were tested. The minimum HC emissions were found to occur with a ring gap orientation of 60 degrees, which was near to the exhaust valve. The total variation with respect to the average was of about 27% of the average. Thus, this study shows the complexity of the HC emission coming from the ring pack.

Blowby, which is the gas that flows from the combustion chamber to the crankcase through the ring pack, affects the HC emissions. The magnitude of the blowby is affected by the ring end gap of the two compression rings. Wentworth [23], and later Namazian and Heywood [27], found that the blowby flow rate is controlled by the smallest of the two compression ring gaps. However, Alkidas [22] showed that the reduction of the top ring end gap by a factor of two only produces a small reduction of the HC emissions. Namazian and Heywood [27] showed that reducing the crevice

volume between the first and second ring by 75% reduced HC emissions by approximately 20%.

As it can be observed from this brief review the ring pack crevices have been extensively studied, and represent the major source of the HC emissions.

2.4 CYLINDER HEAD GASKET CREVICE

The cylinder head gasket crevice [4, 22] is an important contributor to the HC emissions. However, its relative contribution depends on the thickness of the gasket. If the gasket thickness is relatively large (1-1.5 mm) [22], which make it greater than the two-wall quench distance, the flame can propagate within the crevice and there is no contribution of this crevice to the HC emissions. Experiments carried out at GM [22], showed that when the gasket thickness was reduced from 2 to 1.3 mm the HC emissions for low EGR levels were not affected. However, for high EGR levels there was a small difference between the two gasket thicknesses. The difference observed at higher dilution level can be explained by the fact that the two wall quench distance increases as the dilution level increases. The effects of using multilayer steel and composite gaskets were evaluated by Alkidas [28]. Thicknesses of 0.43 to 1.5 mm were tested. The lowest HC emissions were obtained with a thickness of around 1mm. By reducing the thickness to 0.4 mm the HC emissions were significantly increased. The maximum amount of HC reduction for the range of gasket thicknesses studied was of about 15%.

2.5 SPARK PLUG CREVICES

The crevices related with the spark plug are the thread and the space between the electrode and the body of the spark plug. The relative contribution to the output HC emissions has been reported by Alkidas [22], who found that the reduction of the thread crevice does not have a significant impact on the HC emissions. However a four-fold reduction in the central electrode crevice can result in a 5-11% reduction in engine-out HC emissions.

2.6 TRANSPORT MECHANISMS OF HC CREVICE GASES AND POST OXIDATION

As explained above, the crevices prevent the oxidation of the stored combustible mixture from taking place during the main combustion. However, some of the mixture that escapes the main combustion can totally or partially oxidize in the combustion chamber during the expansion and exhaust strokes.

The measured cylinder pressure and the calculated inter-ring pressure using a simplified ring pack model are shown in Fig. 2.4, and the history of the mass flow rate of crevice gases as a function of the crank angle is shown in Fig. 2.5. It can be observed from Fig. 2.5 that the outflow from the crevices into the combustion chamber starts as soon as the cylinder pressure starts to drop. The speed at which the gases leave the crevices is small when compared with the piston during the expansion stroke [22]. Therefore, a thin layer of crevice gas is developed near the cylinder wall during the

expansion stroke. The understanding of the crevice outflow is extremely important to quantify extent of the post oxidation process.

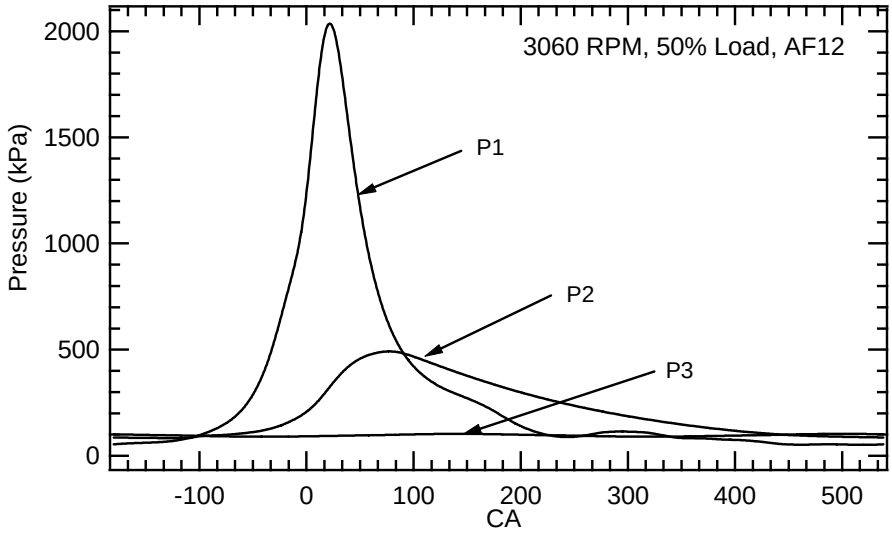

Figure 2.4 Measured cylinder pressure and calculated inter-ring pressure. Numbering convention based on Fig.2.2.

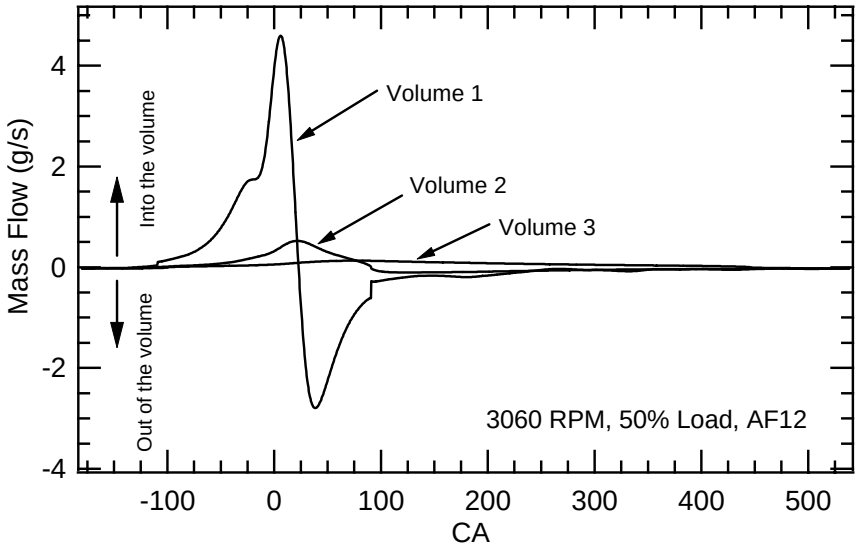

Figure 2.5 Mass flow through the ring pack crevices. Numbering convention based on Fig.2.2.

Namazian and Heywood [27] developed a simplified model to study the gas flow into and out of the crevices. The simulated results were accompanied with Schlieren imaging of the outflow mechanism in a square-piston optical engine. Two kinds of flows were observed. The first starts just after the peak in-cylinder pressure is reached and consists of a low velocity flow coming from the crevices around the circumference of the piston. The other flow appears later in the expansion stroke and consists of a wall-jet-type flow that has its origin at the ring end gap. Green and Cloutman [29], using PLIF in a fired optical engine, qualitatively studied the outflow gas of the ring pack crevice. Two planes around the piston land crevice were observed. One plane opposite to the ring end gap (180°), and the other at the plane of the ring end gap. The plane opposite the ring gap did not show any outflow during the expansion stroke, and a wall-jet-type flow was observed during the start of the exhaust stroke. The authors believe that this type of jet flow has its origin in the mass stored between the two compression rings. The results are in conflict with those obtained by Namazian and Heywood [27]. In the plane of the ring end gap, a different flow structure was observed. For this case, outflow gases were observed at the end of the expansion stroke, and they formed a thin layer of fuel-air mixture near the cylinder wall. Then during the exhaust stage the HC layer was scraped in a roll-up type vortex by the piston. The transport of HC in the wall layer into the bulk cylinder gases occurs by two mechanisms. The gases are engulfed by diffusion and by the roll-up vortex generated at the top of the piston head [5], then diffused at a molecular level.

Not all the combustible mixture that escapes the main combustion stored in the ring pack crevices contributes to the engine-out HC emissions. Under fully warmed up conditions, there can be significant post-flame oxidation in the cylinder during the expansion and exhaust stroke. The amount of HC post oxidation depends of the operating condition of the engine, however some experimental [30] and computational [31] results show that about 50-90% of the trapped HC are oxidized within the cylinder before the exhaust valve opening. It has been found that the critical cut-off temperature for the HC oxidation is approximately 1500 K [32]. Therefore, the rate of HC consumption is limited by the diffusion of the relatively cold HC from the boundary layer to the bulk of the high temperature burned gas. This fact has been verified by Eng *et al.* [30], who experimentally found that the HC emissions for neat paraffinic fuels scales inversely with the diffusion coefficient.

Eng *et al.* [30] developed a global hydrocarbon consumption correlation based on the hydrocarbons stored in the ring pack crevices. The *HC consumption* was defined as the complete conversion of the fuel to CO, CO_2 and H_2O. On the other hand *HC conversion* was defined as decomposition of the parent fuel to intermediate HC species. The correlation developed was able to accurately predict the amount of engine-out HC emissions based on the amount of HC stored in the ring pack crevices calculated using a simplified ring pack flow model [27]. The correlation was able to capture the particularities of different loads, speeds, air-fuel ratio, amount of dilution, and spark timing. Also, the sensitivity of the correlation to different fuels was tested. Initially experiments with n-butane were carried out because its diffusivity in the oil layer is very

small and the HC output emission should not be affected by the oil adsorption and desorption mechanism. Later iso-octane was used as a fuel. Iso-octane has a higher solubility in oil than the iso-butene, therefore some oil film adsorption effect was expected. However when the results of both fuels were compared, no significant difference was observed. Thus it was concluded that the oil adsorption and desorption mechanism under fully warmed up conditions does not play a significant role in the HC emissions.

Since the hydrocarbon global consumption correlation was heuristic in nature, it was subject to several refinements to account for different factors affecting the HC consumption. The integration of scaling factors like engine speed (to account for the increased turbulence and diffusion rates), and fuel-air binary diffusivity were necessary. The final correlation obtained was:

$$\text{Global Consumption Rate} = \frac{\ln\left[(1-y_{res})\dfrac{EIHC_{crev}P_{\max}}{EIHC_{exh}P_{evo}}\right]}{D^{c}S_{p}^{a}(P_{\max}/RT_{\max})^{b}X_{O_2}^{b}\tau} \qquad (2.1)$$

$$\text{Global Consumption Rate} = C\exp(-E_a/RT_{\max}) \qquad (2.2)$$

In equation (2.1) and (2.2), C is a pre-exponential constant, E_a the activation energy, R the gas constant, T_{max} the in cylinder maximum temperature, y_{res} is the in-cylinder residual mass fraction, $EIHC_{crev}$ the emission index of the maximum HC mass stored in the ring pack and calculated with the simplified ring pack model. $EIHC_{exh}$ is the measured output HC engine emissions, D is the diffusivity of the fuel, S, the mean piston

speed, P_{max} the maximum in-cylinder pressure, P_{evo} the in-cylinder pressure at the time that exhaust valve opens (EVO), X_{O_2} is the oxygen molar fraction in the exhaust gases, and τ is the time period from when the cylinder reaches the peak pressure to EVO. It is important to note that the difference between $EIHC_{crev}$ and $EIHC_{exh}$, represents the amount of fuel that has been oxidized after the main combustion process. The fact that the experimental results were fit very well by this correlation suggests that the correlation is catching all the factors that affect the HC consumption. At the same time, it is important to appreciate the significance of the ring pack crevices on the engine-out HC emissions under warmed up conditions. The experimental results also allowed the calculation of the global consumption rate against the maximum temperature in the cylinder. Using this available information, an extrapolation of the maximum in-cylinder temperature for a global consumption rate of zero was performed, and the extrapolated temperature was found to be around 1500 K. This means that the minimum in-cylinder temperature must be 1500 K in order to have post-flame oxidation. This critical value of 1500 K is in agreement with values found by other authors [32, 33].

More recently Eng [34] studied the effect of spark retard on the HC emissions using heat release analysis and a simple model of the HC flow through the ring pack crevices. A conceptual HC mechanism model was outlined to explain the storage and post-flame oxidation. The ring pack crevice model was the same as the one used in [30], and the influence of the spark retard for both lean and rich mixtures was studied. The end of the main combustion was defined as the crank angle (CA) where the cumulative heat release reached 90% (CA90). It was found that with significant retard of the spark timing,

a greater amount of HC was released from the crevices before the flame reached the cylinder walls (as defined by CA90). As a consequence, the amount of HC initially stored in crevices that is consumed by the flame increased, resulting in lower HC emission. For all the conditions tested there was sufficient HC mixture in the crevices after CA90 (end of the main combustion) to account for the engine-out HC emissions, and therefore, post oxidation took place if the following conditions were present: 1) The temperature of the bulk burned gases was greater than 1500 °K, 2) there was enough oxygen present to oxidize the unburned HC, and 3) the residence time of the HC in the hot burned gases was sufficient for the gases to diffuse and mix with the hot gases. For the conditions tested, the majority of the HC consumption takes place inside the cylinder before exhaust valve opening.

2.7 FUEL ADSORPTION-DESORPTION IN THE OIL FILM

Early experimental studies carried out in a closed vessel [35], in an engine [36] and through simulation [37] showed that the fuel-oil adsorption-desorption problem could be a significant contributor to the HC emissions despite the short exposure time of the oil to the fuel during the engine cycle. The lubricanting oil on the cylinder liner adsorbs unburned fuel mixture during the compression stroke [4, 5]. Therefore, part of the fuel is hidden from the flame during the main combustion and escapes oxidation. Later during the expansion and exhaust strokes the stored fuel desorbs, releasing unburned fuel into the cylinder and contributing to the HC emissions. Figure 2.6 schematically shows the adsorption-desorption process. The magnitude of this phenomenon depends on the solubility of the fuel in the oil layer. Currently, together with the crevices, the oil films

are considered to be the greatest contributor to the total HC emissions. Cheng *et al.* [4] report that the oil films are responsible for up to 16% of the total HC emissions.

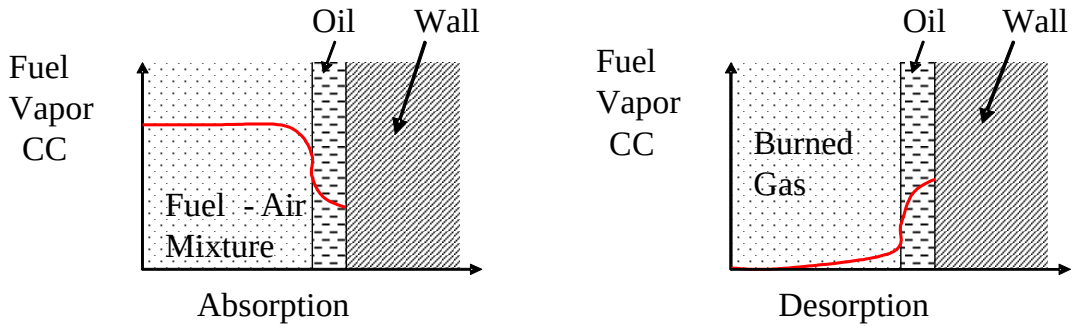

Figure 2.6 Adsorption–desorption process in an oil layer

Gatellier *et al.* [38] studied the contribution of the oil film to the HC emissions by testing different fuel-oil combinations. Initial studies of the fuel solubility showed that different fuels have different solubility in oil and that the solubility was reduced as the temperature increased. In engine tests they found that by reducing the fuel solubility by a factor of 40 (from iso-pentane to iso-octane), the engine HC emissions were reduced by a 30%. However, when a commercial fuel was used a reduction of only 10% was observed compared with when the engine was run with no oil between the cylinder liner and the piston rings using a specially designed extended piston. The difference was attributed to the different solubility of the commercial gasoline in the lubricant oil.

Several estimates of the oil film's contribution to the total HC emissions have been reported in the literature. Linna *et al.* [39] reported that the upper limit contribution of the oil film is below 10%. The small impact was explained by the fact that the fuel is stored in the upper part of the liner, and when the desorption flux comes out it is burned

by the hot bulk gases of the main combustion. Testing different oil film thicknesses with a synthetic multi-component fuel they found that the oil thickness did not contribute significantly to the HC emissions, and that if there was some contribution of the oil films this it was being masked by other factors.

Kaiser *et al.* [40] studied the effect of the fuel stored in the crankcase oil using a single cylinder spark ignited engine. The oil sump was saturated with fuel through exposure to the blowby gases, while the engine was fired using a certification gasoline. After approximately 200 hours of operation motored tests were performed. During the motored tests a relatively high concentration of HC was measured in the exhaust. Gas chromatography analysis showed that most of HC species were from the low volatility components of the diffused fuel. When the engine was fired using iso-octane as a fuel, the observed species in the motored case reduced drastically. The authors explained the reduction by the fact that under fully warmed up condition up to 80% of the desorbed fuel can be oxidized in the cylinder as it mixes with the hot cylinder gases. Thus the total contribution of the crankcase-derived emissions was of approximately 1.5+-0.5%.

The post-flame oxidation of desorbed fuel in the cylinder was studied by Norris and Hochgreb [41]. The oil of an SI engine was doped with a known fuel, and the engine was fired using hydrogen as fuel. This kind of arrangement isolated the HC emissions from the fuel, so the only HC source could be the desorbed fuel from the oil film. The studies showed that a large amount of the desorbed fuel was burned during the post-flame

period. The amount of post-flame oxidation was strongly affected by the engine load, air-fuel ratio, and fuel chemical reactivity.

Kaiser *et al.* [42] studied the effect of fuel composition on the oil-film-related HC emissions. The base gasoline was doped with n-alkanes of wide range of solubility levels. The effect of the different fuels on the engine-out HC emission was studied for two coolant temperatures (339 and 380 K). The HC emissions were not changed significantly over the range of fuels tested, suggesting that the oil adsorption-desorption mechanism does not contribute significantly to the HC emissions above the temperatures tested.

Recently, the effect of the adsorption of fuel in the oil film under cold conditions was studied by Parks *et al.* [43], who experimentally measured the amount of fuel adsorbed into the oil during cold start engine operation. The amount of fuel stored was comparatively higher than in a normal steady state warmed up condition, because the solubility of the fuel is increased as the lower temperature. The results showed that the fuel concentration in the oil film reached a maximum of 50% in volume. This large increase of fuel concentration in oil could contribute significantly to the HC emissions during the cold start period.

The magnitude of the fuel-oil contribution to the HC has been also addressed numerically [44-46]. The results show that the Henry's constant, which is related to the fuel solubility in oil, is the most dominant parameter in the adsorption-desorption mechanism. The Henry's constant of the components of a typical gasoline in several commercial oils has been experimentally measured [47] and it has been very useful for

experimentalists and for modelers as well [43]. In addition due to the complexity of the composition of commercial oils and the lack of experimental data, surrogates such as Squalane (C_{30} H_{62}) [48, 49], which has similar characteristics than some engine oil are used to assess the severity of the fuel-oil diffusion problem [46].

As can be seen from the literature review, the impact of oil film adsorption on HC emissions is less well understood. The diversity of results can be due to the fact that the researchers use different fuel and oil formulations, which makes it difficult to compare the different results. However, in spite of those differences it is believed that the contribution of oil film adsorption to the total HC emissions is small and it should decrease at elevated temperature.

2.8 FLAME QUENCHING AT THE CYLINDER WALL

The flame quenching at the cylinder wall has been identified as a HC emissions contributor [4, 20, 21], and initially it was considered to be a major contributor. However, experimental measurements and detailed modeling of the flame quench phenomenon showed that the majority of the fuel layer that was not oxidized during the main combustion diffuses into the hot gases and burns up during the expansion [50, 51]. On the other hand, for diluted mixtures the flame quench phenomenon can be the greatest contributor to the HC emissions [4, 30]. The estimate of wall quenching contribution to the HC emissions at steady state conditions for a stoichiometric air-fuel ratio is less than 3%.

2.9 DEPOSITS

Deposits in the combustion chamber are formed in proportion to the engine operation time. The effects of the deposits on the HC emissions are well known [4], and the mechanism of contribution to the HC emissions is similar to the adsorption and desorption process of the fuel in oil. Deposits are porous organic compounds that adsorb and desorb the fuel in the same way as the oil film. In the case of port-fueled engines, the deposits on the intake valve contribute to the HC emissions during transient conditions. The deposits make the engine operation leaner during the acceleration and richer during the deceleration. However, it is known that under steady state conditions the intake valve deposits do not contribute significantly to the HC emissions [4].

On the other hand, the combustion chamber deposits are known to increase the HC emissions for both steady and transient conditions. Currently there is not detailed information about the effect of the deposits on the HC emissions. However, some estimates show that the deposits are responsible for up to 16% of the total engine-out HC emissions. It is important clarify that the deposit size is highly dependent on the age of the engine and those reported values must be used very cautiously.

CHAPTER III

EXPERIMENTAL SET-UP, DATA ANALYSIS, MATERIALS AND TEST METHODOLOGY

3.1 INTRODUCTION

Chapter III describes the main components of the test cell, the data acquisition system, the materials, the experimental methodology for taking the data, and the data analysis used along this investigation. Some specific schematics and programs used to analyze the data are provided in Appendices of the thesis.

3.2 ENGINE TEST CELL

The test cell consisted of the engine, the air and fuel supply systems, the engine control system, the dynamometer, the emissions sampling systems, and the data acquisition systems. A detailed description of each of these systems is given below.

3.2.1 ENGINE

The engine chosen for this study was the four stroke V-twin Kohler model CH23 engine. This is a spark-ignited air-cooled engine with overhead valves (OHV) and a horizontal shaft. It comes equipped with a carburetor and has fixed spark timing. The engine is representative of the small engine group. In part, this two-cylinder engine was

chosen because measuring the emissions of each cylinder could provide new insights about the individual cylinder contribution to the HC emissions and the large manifold was expected to exaggerate liquid film effects. The specifications of the engine are given in Table 3.1. Typical applications of this utility engine are: ridding lawnmowers, electric power generators, boats, recreational vehicles, industrial applications, and construction applications.

Table 3.1 Engine specifications

Type	Two cylinder 90° V
Bore	80 mm
Stroke	67 mm
Displacement	674 cc (for the two cylinders)
Compression ratio	8.15
Spark timing	22 bTDC
Intake valve timing	IVO: 22 bTDC/IVC:134 bTDC
Exhaust valve timing	EVO:130 aTDC/EVC:26 aTDC

The engine was modified in order to carry out the experiments in a controlled way. Changes were made to the intake system, the exhaust system, the ignition system and the fueling system. Regarding the intake system, the engine air filter was removed and clean air from the building compressed air supply was used. The intake port temperatures were monitored using thermocouples. The intake pressure was also measured with a MAP sensor model SENS-PRES-001H-00 from MotoTron. The exhaust system was custom made, and it was designed to allow sampling the exhaust gases for average and cycle-resolved emission measurements, and to measure the temperature and cycle-resolved pressures at the exhaust ports. The fuel system was modified so that the engine could be fired either using a homogeneous pre-vaporized mixture system or with

the carburetor. The fixed-timing magneto ignition system was removed and an electronic MotoTron mode IGN-COIL-003-00 ignition system was installed. Additional changes included the installation of the cylinder pressure transducer in each cylinder. A thermocouple in the oil sump was installed to monitor the time when the engine reached steady state operation. The details of these modifications are provided in the following sections of this chapter.

3.2.2 FUEL SYSTEMS

The stock fuel system of the engine was modified with several goals in mind. First, in order to identify the effects of liquid fuel films on the HC emissions, a homogeneous, pre-vaporized air-fuel mixture system was built. This fuel system avoided the presence of liquid fuel in the intake manifold, so the effect of the poor fuel atomization by the carburetor on the HC emissions could be inferred. The stock carburetor was replaced with an adjustable carburetor. With this carburetor a fixed air-fuel ratio could be achieved at any speed and load. Finally, to estimate the mass of fuel stored in the intake manifold a carburetor-mounted fuel injection system was built. This device emulated the behavior of the carburetor but provided the flexibility of precise control of fuel supply. In addition the engine ignition could be deactivated with the fuel injection simultaneously. The following subsections provide a detailed description of each fuel system.

3.2.2.1 CARBURETOR FUEL SYSTEM

The stock carburetor is calibrated by the manufacturer to provide a fixed amount of fuel according to the engine speed and load. This air-fuel ratio may vary between operating conditions. However, in this study the air-fuel ratio needed to be changed at a variety of loads and speeds. Therefore, the stock Keihin model 24-053-031 carburetor converted into an adjustable carburetor was used. Two special adjustable needle type valves were installed in the carburetor body to control the fuel flow through the main and idle jets. Adjusting the main jet fuel flow provided a gross tuning of the air-fuel ratio. The fine adjustment was carried out adjusting the needle valve of the idle jet. Figure 3.1 shows the adjustable carburetor used for the tests.

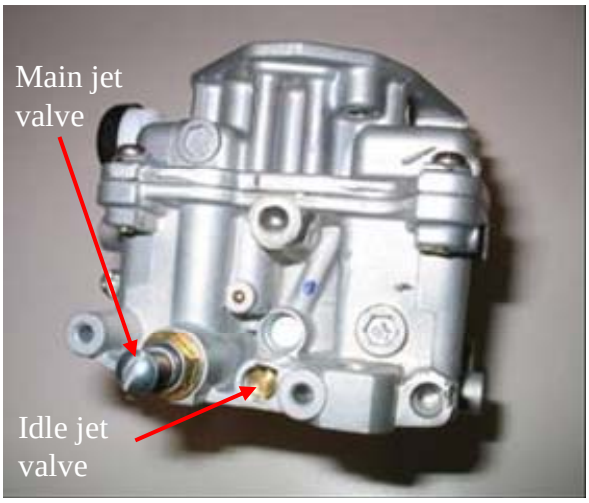

Figure 3.1 Adjustable air-fuel ratio carburetor

Figure 3.2 shows the schematic of the test cell. A complete layout of the carburetor and homogenous fuel systems are shown. It is important to mention that the fuel systems were designed to allow easy switching between them. When the engine was

operating with the carburetor fuel system, the fuel was taken from the high pressure side of the high pressure fuel pump. Then, the pressure was reduced to around 34.5 kPag using a pressure regulator. This is a typical pressure operation of a carburetor.

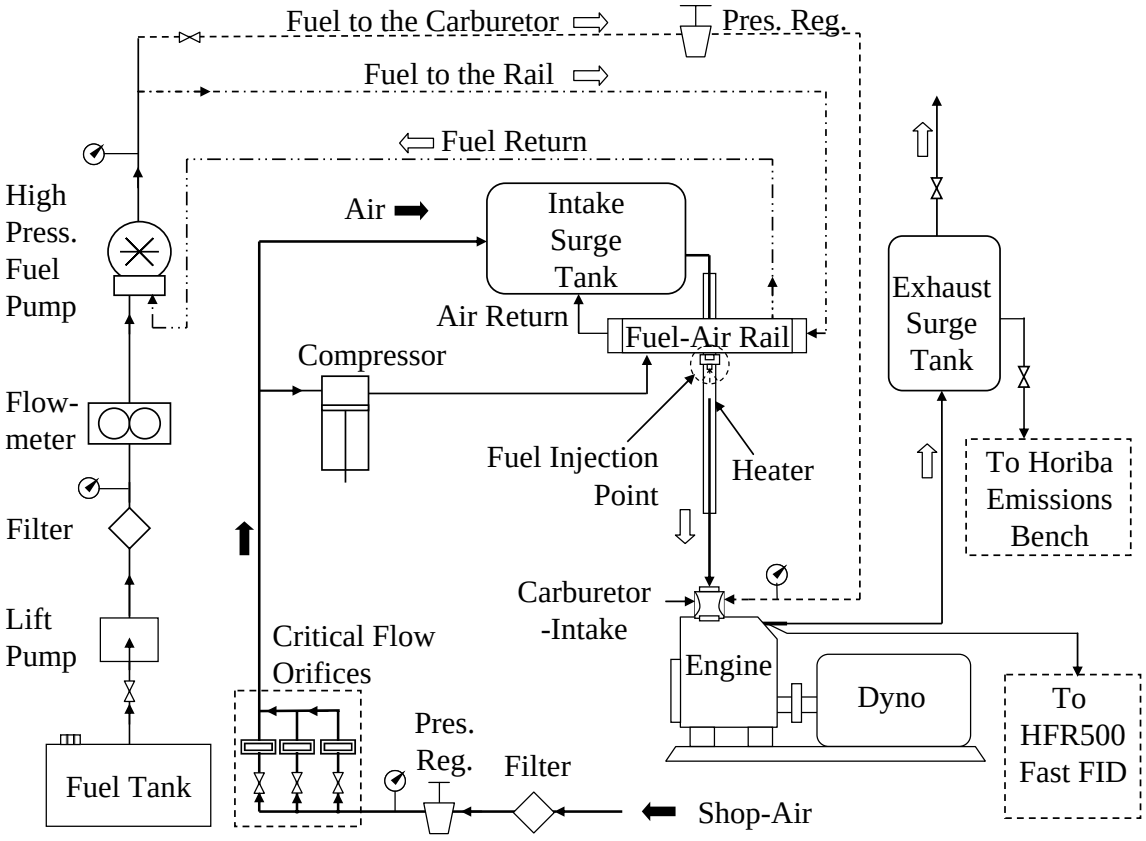

Figure 3.2 Schematic of the test cell

3.2.2.2 HOMOGENEOUS MIXTURE SYSTEM (HMS)

The homogeneous mixture system was designed and built to provide a completely vaporized and homogeneous mixture to the engine. In the HMS system the atomization of the fuel was performed using an Orbital air-assisted fuel injection system similar to the fuel injection system used by the 3.0 liter Optimax Mercury Marine direct-injection

engine [52]. The components of the Orbital air-assisted fuel injection are: a lift pump (low pressure fuel pump), a low pressure fuel filter, a high pressure electric fuel pump, an Orbital air-fuel rail (includes the rail and the fuel and air injectors), and an air compressor (see Fig. 3.2).

The fuel path is described following (Fig. 3.2). First, the fuel is taken from the fuel tank using the low pressure lift pump. Then, the fuel passes through the low pressure filter and through a model 940620 mass flow meter MicroMotion Inc. The fuel that leaves the mass flowmeter enters to the low pressure side of the high pressure electric fuel pump. The high pressure electric fuel pump increases the fuel pressure up to approximately 620.5 kPa. This maximum high pressure is controlled by a fuel pressure regulator located in the air-fuel rail body. In the rail the fuel is metered by the fuel injector, and then atomized by the air injector (Fig. 3.3). The air supply for the air injector was provided by an oil-less air compressor model LGH-310-260463 from Thomas Industries. The compressor took the air from the intake air surge tank. In this way it was not necessary measure the mass flow of air going through the air injector. The pressure of the air in the rail was regulated by the fuel pressure regulator as well and it was kept at approximately 69 kPa below the fuel pressure. The amount of fuel injected per cycle, and the injection timing was controlled by the electronic control unit (ECU).

The fuel was injected at approximately 1 meter upstream of the intake port and the injector was oriented at an angle of 45° against the air stream. This configuration reduced the possibility of fuel impingement on the pipe walls.

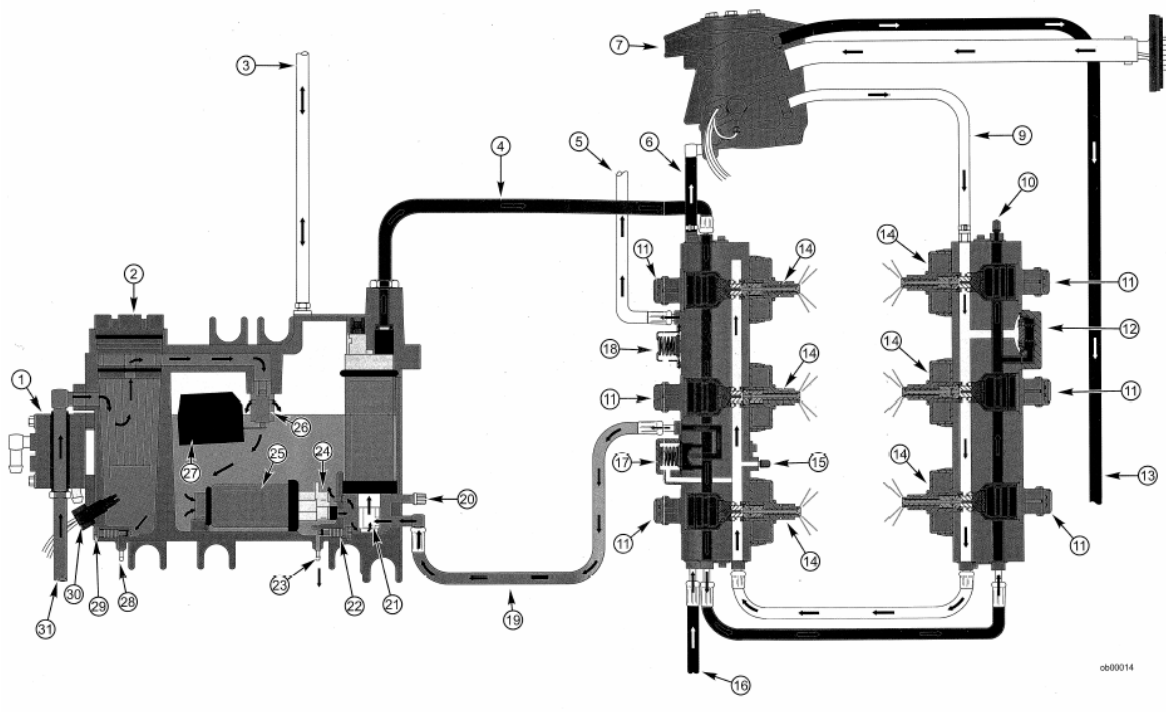

Figure 3.3 Schematic of the air assisted fuel injection system [52]

To vaporize the fuel injected heat was added to the stream through the external surface of the intake pipe near the fuel injector. Two 1 kW Omega heater bands were used to maintain the intake temperature of 50° C. The heaters provided the power to completely vaporize the injected fuel. The intake air temperature was maintained at 50 °C using a closed-loop controller implemented via MotoHawk.

The fuel flow was measured with a model 940620 mass flow meter MicroMotion Inc. (Now part of Rosemount). The output signal of the mass flowmeter sensor was converted to a 4-20 mA signal by a model RTF9712 1PNU transmitter also from MicroMotion Inc. This signal then was read by the LabView data acquisition system. The flowmeter was calibrated for the range of mass flows expected during the engine

operation (see Appendix I). It is important to mention that there was significant variability in the data, and for some conditions the reading of the flowmeter was not accurate. Despite the inaccuracies, the mass flow meter was used to double check the air-fuel ratio obtained from the emissions analysis. In general they were in good agreement.

3.2.2.3 CARBURETOR-MOUNTED FUEL INJECTOR SYSTEM (CMFIS)

As mentioned above, due to poor fuel atomization by the carburetor, part of the fuel is stored in the intake manifold as liquid films. To understand the extent of their contribution to the engine-out HC emissions, a quantification of the mass of fuel stored was necessary. This was accomplished by carrying out stop-fuel-injection tests. To that end, a carburetor mounted fuel injection system was built. This device consisted of a carburetor body and an Orbital fuel injector that delivered the fuel directly to the carburetor main jet (Fig. 3.4). The CMFIS emulated the carburetor behavior (poor atomization) while providing accurate control of the delivered mass of fuel and the ability to precisely stop fuel injection. The fuel injector was controlled with the ECU and the fuel supplied to this system came from the same low pressure line that provided fuel to the carburetor. However, the fuel pressure for this system was regulated to 58.5 kPa. During the stop injection tests the fuel injector was simultaneously deactivated with the ignition to avoid combustion of fuel vaporized in the intake and ingested by the engine.

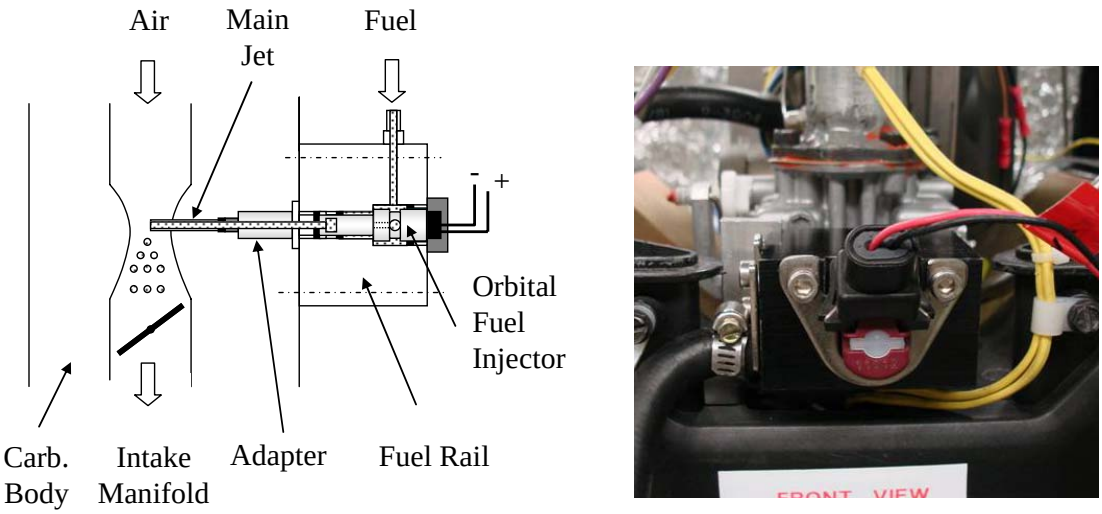

Figure 3.4 Carburetor-mounted fuel injector. Schematic (left), picture (right)

3.2.2.4 PROPANE FUEL SYSTEM

The study of the oil film effect on the engine-out HC emissions required the use of a fuel with very low solubility in oil. Propane was chosen for the study because it is known from the literature to have low solubility in oil [13]. To fire the engine with propane in a controlled manner, the HMS fuel system was slightly modified. A new fuel rail, as shown in Fig. 3.5 was built. The difference of this new fuel rail is that it only holds the Orbital air injector and there is no built-in pressure regulator. The air injector delivered the propane to the intake air stream in the same way as the HMS system. Propane was supplied from a commercial tank where it was a two-phase liquid-vapor mixture. The propane pressure at the rail was controlled with the pressure regulator on the propane tank. The pressure was kept at approximately 655 kPag. For the high load and high speed engine operating conditions the tank was not able to provide the propane

mass flow required by the engine due to the insufficient heat transfer from the room to the tank to vaporize the liquid propane at the rate required by the engine. Therefore, a heater was attached to the external surface of the tank. The power delivered by the heater was controlled to 40 °C with an Omega temperature controller. This resulted in a propane pressure of 1275 kPag.

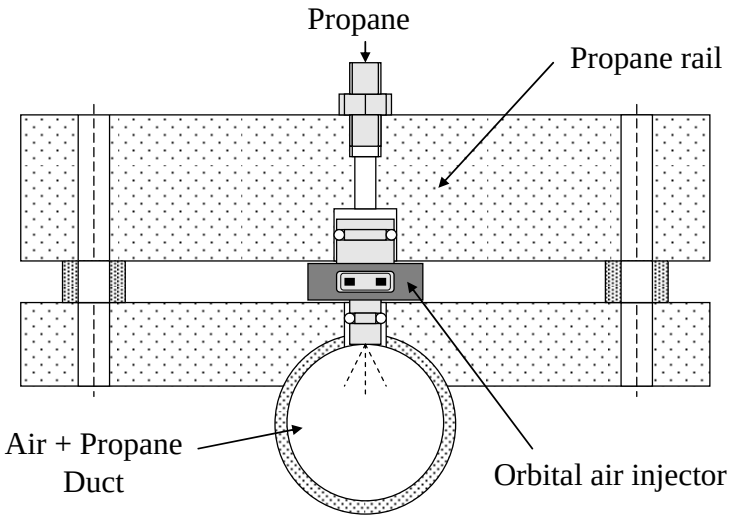

Figure 3.5 Schematic of the propane rail

3.2.3 AIR SUPPLY SYSTEM

The schematic of the air supply system is shown in Fig. 3.2. The air was supplied from the compressed air line of the building and filtered with a coalescing filter model M30-08-000 from Wilkerson Corporation. The air mass flow rate was controlled using critical flow orifices. A calibration between the upstream pressure and air mass flow for each orifice plate was required [53, 54]. The details of the calibration are presented in Appendix II. During the tests the upstream pressure of the orifice plate was continuously

adjusted to match required engine air mass flow rate. The air supplied to the rail of the air-assisted fuel injection was taken from the intake surge tank and there was no need to individually measure the mass flow through the air injector (see Fig. 3.2). The air-fuel mixture was heated and delivered to the engine at a constant temperature of 50 °C, measured at approximately 10 cm above the carburetor body.

3.2.4 CONTROL SYSTEM

The engine was controlled using the MotoTron suite of products [55]. This consists of three main software components MotoHawk, MotoTune and MotoServer, and the hardware engine control unit (ECU).

MotoHawk is software that is used to develop, test, and validate control applications using Simulink from MathWorks [56]. The program that controls the engine operation was created in MotoHawk. The MotoHawk-Simulink integration helps to reduce the time and complexity of working with a wide variety of engine control applications. The model created in MotoHawk can be simulated and verified for errors before it is transferred to the ECU hardware. However, an intermediate step to transfer the model into the ECU is required. The Simulink-based model has to be translated into the ECU language. The Multi2000 compiler from Green Hills Software Inc. was used for that purpose [57]. The files generated with the Multi2000 compiler (.srz and .dll type files) are the ones used to program the ECU.

MotoTune is a calibration development tool that establishes communication between the ECU and the command computer during the engine operation. This software

has an interactive spreadsheet-type interface, in which the calibration parameters stored in the ECU can be modified and adjusted at any time during the engine operation. MotoTune is also for flash programming of the ECU. Other important features of MotoTune include: activation and deactivation of specific engine systems (fuel injector, spark coils, throttle, etc), management of the calibration files, parameter display, override and logging capabilities.

MotoServer is the licensing software and it allows the configuration of the communication ports. Figure 3.6 shows a schematic of the interaction of the several components of the MotoTron suite of products. MotoHawk, MotoTune and MotoServer were continuously being updated, however, during this work the following versions were used: MotoHawk version 0.8.3 beta 14, MotoTune version 8.10, and MotoServer version 8.10. The Matlab version plays an important role during the installation of MotoHawk, and it must be compatible with the MotoHawk version being installed. The ECU program was written using Matlab version 2006b.

The engine was equipped with a Motorola model ECM-0565-128 [58]. This ECU uses the Motorola MPC565 microprocessor at 56 MHz. The main features of the ECU include the availability of 34 analog inputs, 8 digital inputs, 2 inputs for 2 wide band oxygen sensors (Bosch LSU4.2), outputs for injector drivers, TTL signals for ignition systems, PWM outputs, and 2 CAN 2.0B channels, within other resources.

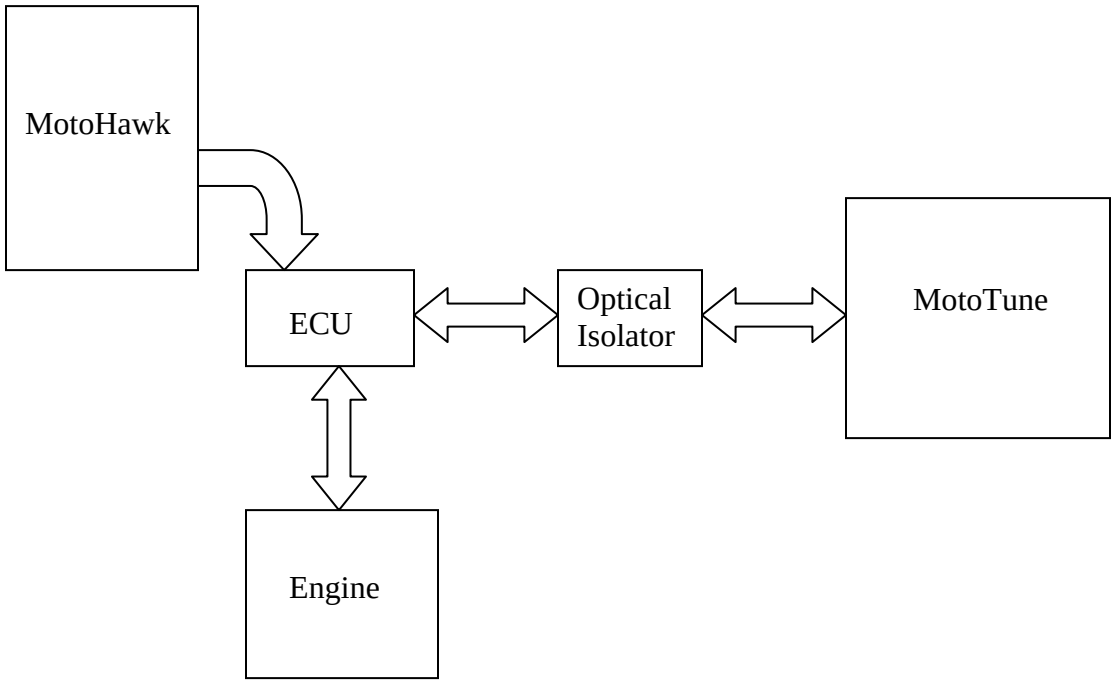

Figure 3.6 Schematic of the interaction between the components of the MotoTron suite of products and the engine

The ECU received the signals (inputs) from: the intake MAP sensor, the intake temperature sensor, the oil pressure sensor, throttle position sensor (embedded in the throttle controller), crank sensor, cam sensor, and 2 wide band oxygen sensors. Based on the input signals the ECU controlled the following components: the fuel injector, the air injector, the throttle position controller, the electronic spark coil, and the intake heaters. One of the main features of the ECU is that it allowed close-loop control of the throttle position controller, the air-fuel ratio, and the intake temperature.

The activation of the spark coils generated high levels of electrical noise (ground loops and surges) in the engine electrical system. This caused communication problems

between the ECU and the command computer (MotoTune). The problem was eliminated using an USB optical isolator model UISOHUB4 from B&B Electronics Manufacturing Company [59], which was installed between the ECU and the command computer (Fig. 3.6).

3.2.5 DYNAMOMETER

The dynamometer consisted of a direct current motor and a controller. The motor was a General Electric model 5CY977E1 direct current motor, with a rated power of 25 HP and maximum speed of 3600 RPM. The dynamometer was controlled with the Dyn-Loc digital dynamometer controller [60]. This controller allowed control of either the speed or the torque. However, during the tests only the speed was controlled. The torque was controlled adjusting the engine throttle position via MotoTune.

The engine was coupled to the dynamometer with a TB Wood's SureFlex coupling of Size 7 with a neoprene insert [61]. A considerable amount of time was spent in finding the right size and type of coupling that matched the engine-dynamometer dynamic behavior. Several types of couplings were tested. Some couplings were very stiff (Falk Wrapflex coupling from Rexnord) [62] producing intolerable levels of vibration. Other couplings were very soft and failed after a very short time of operation (TB Wood's DuraFlex) [61].

3.2.6 EMISSIONS BENCH

The average engine-out emissions were measured with a standard 5 gas analyzer Horiba emissions bench. This bench had the following analyzers: Horiba AIA-23 non-dispersive infrared analyzer for the CO and CO2, Horiba MPA-21A paramagnetic oxygen analyzer, Horiba CLA-22A chemiluminescence analyzer for the NOx, and the flame ionization detector (FID) FIA-23A for the total HC.

The emissions were sampled from individual-cylinder exhaust surge tanks of a specially designed separated exhaust system (Fig. 3.7). With this arrangement the individual cylinder contribution to the total emissions was estimated. The surge tanks were designed to damp the pressure fluctuations and to promote mixing of the exhaust gases. The tanks were made from steel with capacity of 7570.8 cm^3 (2 gal) and they satisfied the ASME pressure vessel code. The gas diffuser and the sampling probe were built following the SAE norms [63]. The sampling probe was located at approximately 80 cm from the exhaust port.

The hot exhaust gases leaving the sampling probe were passed through a chiller to remove the water before they entered the emissions bench. The cold FID can cause some oxygenated species present in the exhaust gases to not be measured [30]. In the emission bench the gases were passed through a chiller to further condense water. The readings of the gas analyzers were recorded using a LabView-based data acquisition system.

A typical test using the emissions bench included at least 1 hour of warming up followed by a spanning of all the analyzers with the span gases that are specified in section §3.4.1

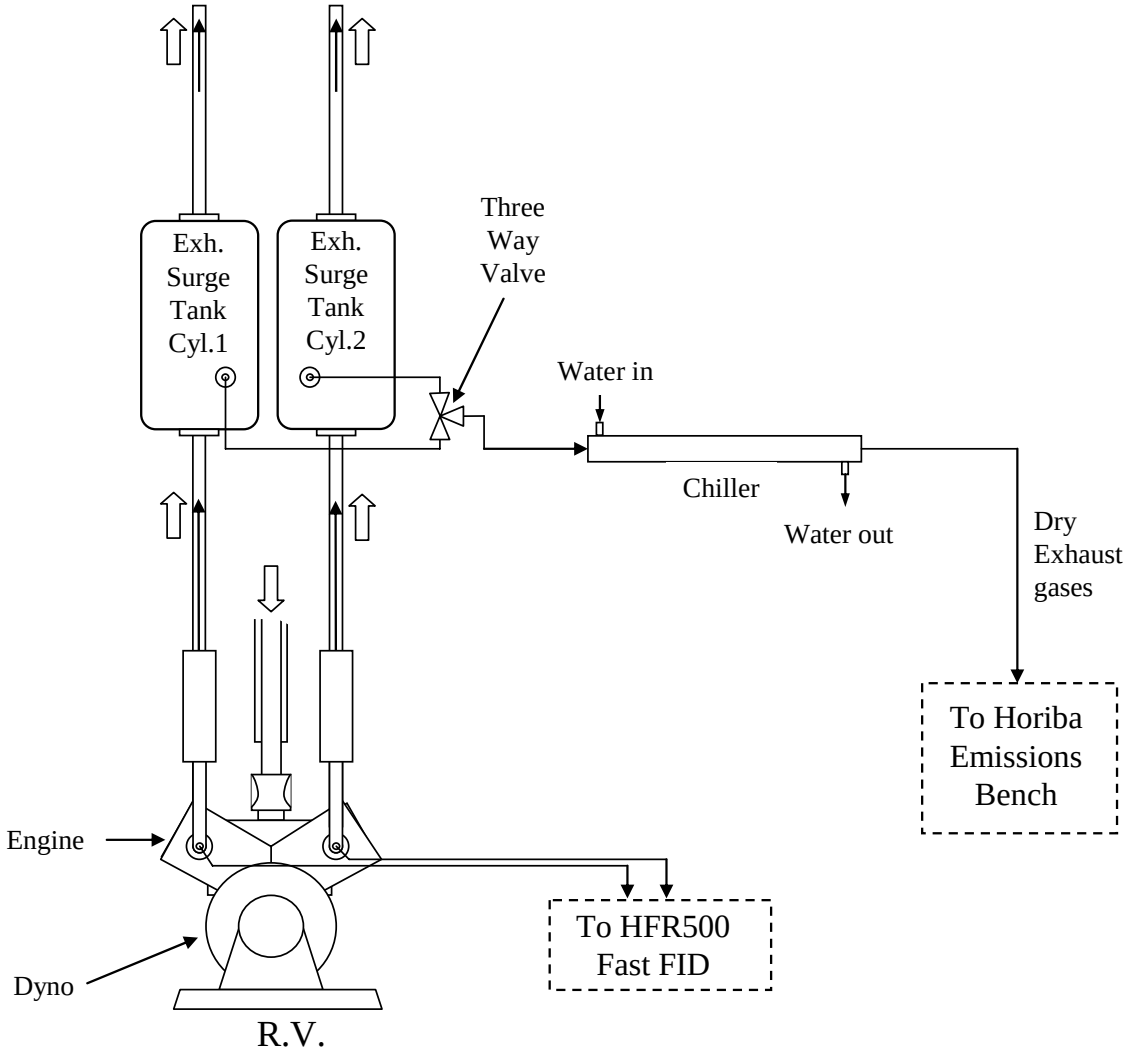

Figure 3.7 Schematic of the split exhaust emission gas sampling system

3.2.7 FAST FLAME IONIZATION DETECTOR

The cycle-resolved total HC emissions were measured using a Combustion model HFR-500 fast flame ionization detector (FFID). This system consists of the remote sampling heads (containing the FID), the service control unit, and the PC user interface. Detailed description of the system is provided in the HFR-5000 user manual [64]. The location of the sample probe plays an important role in the observed history of the HC emissions [65, 66]. Therefore, in order to resolve the history of the HC leaving the engine, the sample probe was located at the exhaust port at 12 mm downstream from the exhaust valve stem (Fig. 3.8) of each cylinder. The HFR-500 was calibrated with propane at a concentration of 2500 ppm.

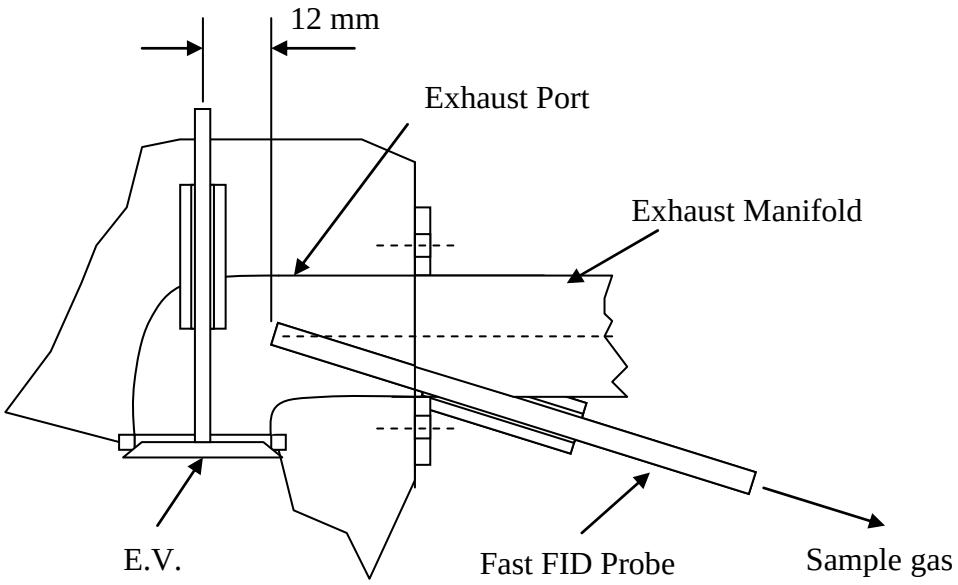

Figure 3.8 Fast FID Probe location in the Exhaust Port

3.2.8 BLOWBY MEASUREMENT AND CRANKCASE AND EXHAUST PRESSURE CONTROL SETUP

For all the tests, the crankcase pressure was kept at a constant value because it was found to significantly affect the HC measurements. The pressure was adjusted by restricting the mass flow of the crankcase breather. A gate valve (as indicated in Fig. 3.9) was used to restrict the breather mass flow. The pressure was measured using a Magnehelic differential pressure gage from Dryer Instruments Inc [67]. This gage used as reference the intake surge tank pressure, which was maintained at 101.35 kPa for all the testing conditions. Crankcase differential pressures of 0.5 kPa above the intake pressure were used for the majority of the tests, however during the study of the crankcase effect on the HC emissions, pressures below and above this value were tested. The average intake surge tank pressure was measured using a model SEN-PRES-00200 1 bar MAP sensor from MotoTron.

The blowby was measured with a bellows meter (from American Meter Company) [68] installed in series with the crankcase pressure control valve (Fig.3.9). To determine the mass flow, temperature measurements at the inlet side were carried out. The outlet of the bellows meter was connected to the exhaust vacuum line of the building.

The pressure of each exhaust surge tank was held at a constant pressure that was 0.5 kPa greater than the intake surge tank pressure (101.35 kPa). Gate valves located at the exit of the exhaust surge tanks were adjusted to achieve the target pressure (Fig. 3.9).

Magnehelic differential pressure gages were used to measure the differential pressures [67].

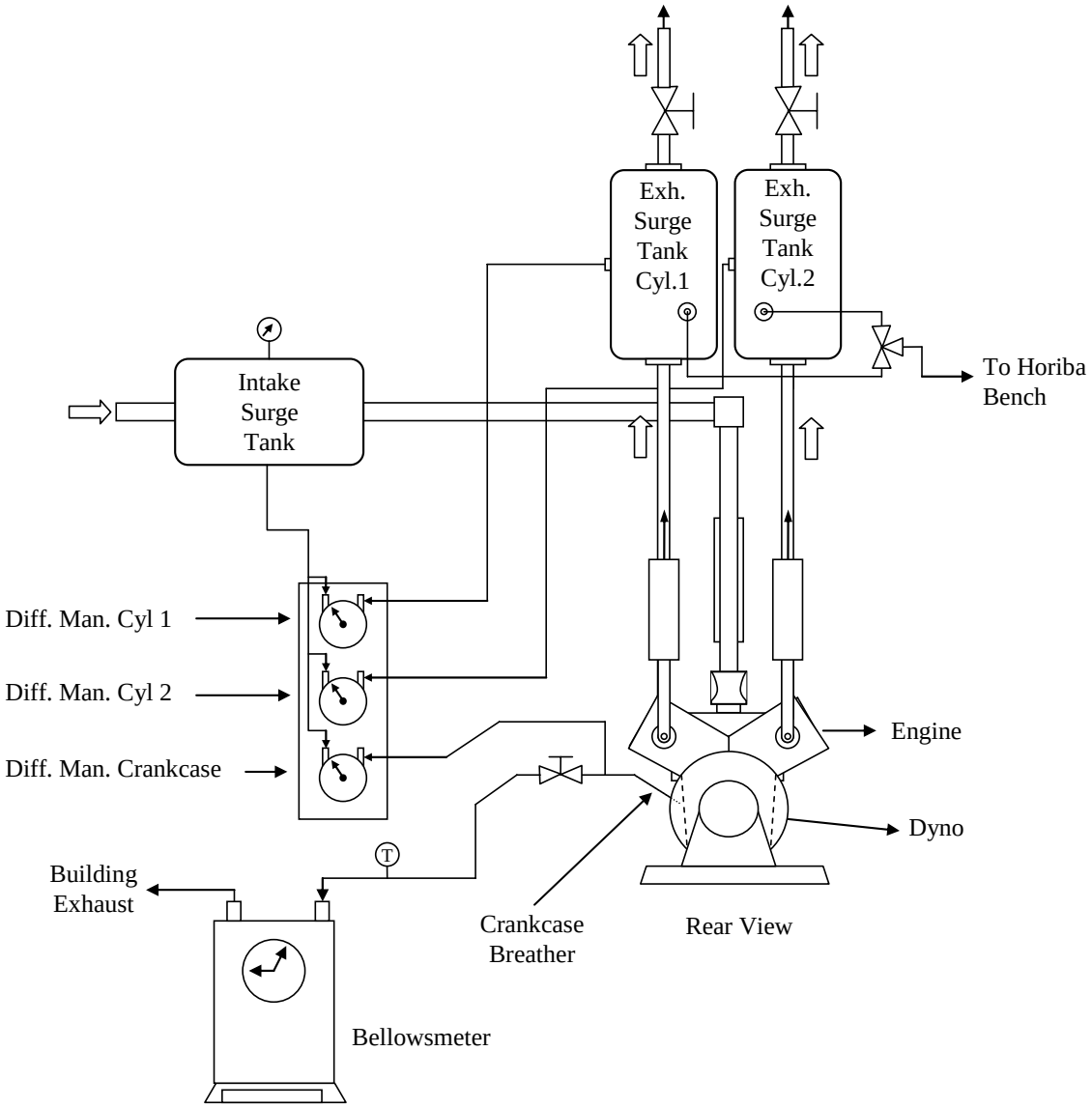

Figure 3.9 Schematic of the arrangement for the crankcase pressure control and blowby measurement

3.2.9 CYCLE-RESOLVED PRESSURE MEASUREMENT

Cycle-resolved measurements of the in-cylinder, exhaust manifold, and intake manifold pressures were performed.

The in-cylinder pressure was measured with water-cooled Kistler 7061 and 7063A pressure transducers [69] for cylinder 1 and cylinder 2, respectively. A special threaded hole was made in the cylinder head to accept the pressure transducer. The pressure transducers were calibrated using a weight dead tester, and the calibration curves are shown in Appendix III.

The exhaust and intake manifold pressures were measured with a 2 bar MAP pressure sensor, model SEN-PRES-0001H from MotoTron. The sensors located in the exhaust required a special cooling system to avoid the high temperatures of the exhaust gases. The cooling system is shown in Fig. 3.10. Typical operating temperatures of these sensors were around 30-40 °C. The intake side sensor did not require cooling, and temperatures at the intake location ranged from 50-70 °C. The intake and exhaust pressure transducers described above have relatively slow time response (approximately 1 kHz) and do not accurately follow the dynamics of the intake and exhaust manifold pressure waves. Therefore, a first-order correction was performed on the pressure traces. A detailed explanation of the correction process is presented in Appendix IV. The corrected pressure traces showed satisfactory agreement with a piezoelectric sensor, showing that a low cost sensor could be used to measure accurately the cycle-resolved exhaust and intake pressure traces.

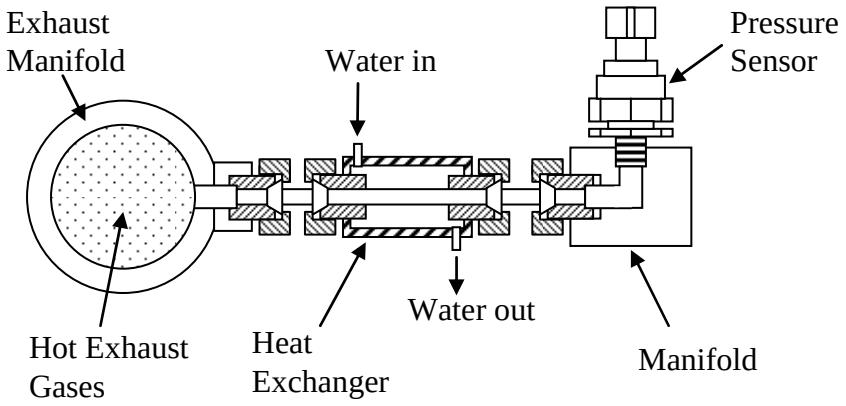

Figure 3.10 Exhaust pressure sensor cooling configuration.

3.3 DATA ACQUISITION

Two data acquisitions systems were used to record the data. One system collected the average emissions data and the other recorded the cycle-resolved data (in-cylinder pressure, HC, intake and exhaust manifold pressures, and crankcase pressure). A description of each system is provided below.

3.3.1 AVERAGE DATA ACQUISITION

The average CO, CO2, NOx, O2, and HC emissions data were recorded using a National Instruments data acquisition 6024E card [70]. A program to acquire and process the data was implemented in LabView version 7.1. This program calculated the air-fuel ratio, emissions index, combustion efficiency, power and air mass flow rate. The part of the program that calculates the emission index, air-fuel ratio, and efficiency calculations is shown in Appendix V. The program outputs text type files that were used for subsequent post processing.

The air-fuel ratio was calculated using several methods available in the literature and were implemented in the program: carbon-based, oxygen-based, Bartesville, Spindt and one locally developed. The details of the calculations are given in section §3.6 and in Appendix VI

3.3.2 CYCLE-RESOLVED DATA ACQUISITION

The cycle-resolved data were acquired using a HiTechniques [71] data acquisition system. This system has capabilities to record up to 8 cycle-resolved input signals (channels) at a sampling rate up to 1 MHz. The Win600 software, also from HiTechniques, was used to configure the acquisition of the in cylinder pressure and all the cycle resolved-traces. The data acquisition required the signal A, and Z of an incremental rotary encoder to phase the data with the corresponding stages of the engine combustion cycle. The A and Z signals were provided by a model H25D-SS-720-ABZC-5406R-SM18-S optical encoder from BEI Electronics Inc. [72]. This encoder has 0.5 crank angle (CA) resolution providing 1440 data points per cycle per trace. The system memory allowed recording 8 channels of data for 200 cycles. The data traces were recorded in phase with either the first or second cylinder of the engine. However, the first channel was reserved for the in-cylinder pressure of cylinder 1, and the other channels could be configured in any order. The channel configuration for the present research is show in Table 3.2. However, it is important to mention that the configuration does not affect the acquisition process. The data acquisition recorded the data in binary format.

The binary file then was post processed using a Matlab program. Details of the program are provided in section §3.6

Table 3.2 HiTechniques Channel Configuration

Channel #	Resource
1	Cylinder 1 Pressure
2	Cylinder 2 Pressure
3	Intake Manifold Pressure (pegging)
4	Exhaust Manifold Pressure Cylinder 1
5	Exhaust Manifold Pressure Cylinder 2
6	Fast FID Cylinder 1
7	Fast FID Cylinder 2
8	Crankcase Pressure

3.4 MATERIALS

3.4.1 EMISSIONS BENCH AND FAST FID GASES

The emissions bench required gases to operate and span the analyzers. The spanning of the analyzers was carried out using the following gases at the specified concentration:

Oxygen: 1%, nitrogen balance

Propane: 2500 ppm, nitrogen balance

NOx: 750 ppm, nitrogen balance

Carbon monoxide: 10%, nitrogen balance

Carbon dioxide: 10%, nitrogen balance

Nitrogen zero, <0.5 ppm HC

In addition to the calibration gases, the FID of the emissions bench and the fast-FID required the following two gases:

Hydrogen 40%, nitrogen balance, <0.5 ppm total HC

Zero air (Oxygen 21.5%, <1.0 ppm total HC)

3.4.2 FUELS

The engine was fueled with two fuels: gasoline and propane. The majority of the tests were carried out using a fully blended US EPA TIER II EEE certification fuel provided by Halterman Products [73]. However, to study the impact of the oil layer on the HC emissions the engine was fueled with propane. The propane was industrial grade 99% purity, and it was purchased from Airgas Inc. The specifications of the EEE are presented in Appendix VII.

3.4.3 ENGINE OIL

The engine lubricant oil used along all the tests was the Delo general-use SAE 30 oil from Chevron. The engine oil and filter were changed as specified by the engine manufacturer. It is important to mention that before firing the engine with propane, the oil was changed and the engine was fired for about 5 hours before taken emissions data. This avoided any possible biasing on the measured HC emissions due to the vaporization of some light HC fractions from the new oil.

3.5 EXPERIMENTAL METHODOLOGY

The contribution of the different HC mechanisms to the engine-out HC emissions was estimated by carrying out various types of tests. In general the experimental methodology for all the tests was similar. However, some studies required very specific procedures. The details of the experimental procedure for the different sets of experiments is provided below.

3.5.1 GASOLINE TESTS

The majority of the tests were carried out fueling the engine with gasoline. There were three types of tests were the engine was fired with gasoline. These used the adjustable carburetor, the homogeneous mixture system and the carburetor mounted fuel injector.

3.5.1.1 CARBURETOR TESTS

These tests were performed to study the effect of the liquid fuel on the HC emissions. The following is an explanation of the carburetor tests. Before the engine was run, the emissions bench, fast FID and dynamometer were turn on for at least 30 minutes. This provided enough time to warm up the instruments and to make sure they were fully stabilized. In the case of the emissions bench of the gas analyzers were spanned previous to runing the engine. However, a recalibration to verify any possible drift respect to the initial calibration was performed. This could be done usually with the engine firing. The fast FID required a more diligent calibration process before spinning the engine because this instrument can not be calibrated when the engine is motoring or firing. The

instrument is very sensitive to pressure fluctuations. A common practice was to calibrate the dynamometer prior to every run, thus, the zero and span values were adjusted as required. Then, the engine was spun at the required speed with the throttle opened to a position near to the target load. Next, the intake heaters were activated and the engine was motored until the intake air reached the temperature of 50°C. After this the engine was fired and the air-fuel ratio was adjusted to the required value. The engine was warmed up in that condition until steady state operation was achieved. The engine reached the steady state when no change in the oil temperature was observed. The time to reach the steady state operation depended of the load, speed and air-fuel ratio; for the majority of the conditions it was around 45 minutes. Typical steady-state oil temperatures between 85-135 °C were observed. When the engine was approximately half of the way to reach steady state, the engine was supplied with air coming from the orifice plates. The pressure upstream of the orifice plate was adjusted to obtain an intake surge tank pressure of 101.35±0.1 kPa. Taking as reference this pressure the exhaust manifold pressure was adjusted to 101.85 kPa (a differential pressure of 0.5 kPa). At the same time the torque and air-fuel ratio were adjusted to the required values. This was carried out by changing the throttle position, and the needle valves of the adjustable carburetor. It is important to mention that in order to reach a run condition an iterative adjustment of the intake air pressure, throttle position and air-fuel ratio was required. A change in one of these parameters compromised the other two. A good advantage of the test cell was that the dynamometer maintained an accurate control of the speed. Once the desired air-fuel ratio, torque and speed were reached the engine was fired for

approximately 15 minutes. Subsequently, all the pressures, temperatures, and emissions were recorded.

3.5.1.2 HOMOGENEOUS MIXTURE SYSTEM TESTS

The homogeneous mixture system was used for the study of the liquid fuel, ring pack and oil film HC mechanisms. The majority of the tests were carried out using this fuel system. The methodology followed during the tests using the HMS system is very similar to the procedure followed for the carburetor tests. However, in this case the fuel was delivered with the Orbital air-assisted fuel injection system. An advantage of this system was that the air-fuel ratio was close-loop controlled via MotoHawk. The air fuel ratio was read with a wide band oxygen sensor installed at 40 cm from the exhaust port of cylinder 1 (right cylinder). It is important to mention that the low and high pressure fuel pumps were turned on before or at the same time that the intake heaters to avoid formation of vapor bubbles in the high pressure fuel line.

3.5.1.3 STOP FUEL INJECTION TESTS

The methodology for the stop fuel injection tests was a little bit different from the other tests, although the warming up process was the same. The main difference was that data from only three channels were recorded, i.e. the cylinder pressure, the signal indicating that the spark and the fuel injector were disabled, and the fast FID data. For these tests, the program that controlled the engine was modified so the spark and fuel injector were disabled simultaneously. Once the engine was fully warmed up and the desired operating steady operating condition was reached, data from 2000 consecutive

cycles were recorded. The recording was started 4 to 5 seconds before the spark and fuel injection were halted. The timing of the fast FID with the stop fuel injection was carried out by recording fuel injector electrical pulse using a current probe. A Matlab program was written to perform the post processing (Appendix VIII). Average emissions of the steady state operation were also recorded with the National Instruments data acquisition system.

3.5.2 PROPANE TESTS

The experimental procedure for the propane tests was similar to the one followed for the HMS tests. The main difference was that the vapor phase propane was injected only using the air injector. To control the mass of fuel delivered per cycle the program for the HMS tests was used. The closed-loop air-fuel ratio control was not used in these types of tests. The air-fuel ratio was adjusted by changing the start of injection so the air injector was open for a shorter or longer time.

3.6 DATA ANALYSIS

Several codes were implemented to process and analyze the emissions and pressure data. These codes calculated the air-fuel ratio, emissions indexes, heat release, ring pack contribution to the HC emissions, and mass of HC leaving the engine. A brief description of each of these calculations is given below.

3.6.1 PRESSURE CODE

This code was implemented in Matlab to extract and process the HiTechniques data which was recorded in binary format. The program carried out the pegging process of the in-cylinder pressure and calculated the average and single-cycle IMEP and CA of peak pressure. The in-cylinder pressure was pegged at 180 CA bTDC with the dynamic intake manifold pressure. The program also performed the first order correction of the intake and exhaust pressure transducers. Correction of the fast FID traces for transit time and time response was also carried out by the program. It is important to mention that all the traces were filtered using the built-in `csaps` smoothing function in Matlab before any processing. Additional options of the code included plotting capabilities and output files with the average data of all the traces. Single-cycle pressure and fast-FID output data files were also available for further post-processing. The main section of the program is shown in the Appendix IX

3.6.2 AIR FUEL RATIO

In engines the mixture air-fuel ratio is an important parameter to characterize the engine operation and it is defined as:

$$AF = \frac{\dot{m}_{air}}{\dot{m}_{fuel}} \qquad (3.1)$$

where AF is the mixture air-fuel ratio and $\dot{m}_{air}$ and $\dot{m}_{fuel}$ are the mass flow rate of air and fuel respectively. During the tests the air-fuel ratio was calculated from the exhaust

measured emissions using several methods. The methods used were: carbon balance, oxygen balance [5, 74], Bartlesville [75], Spindt [76], and one ERC method [77]. No significant differences were observed between methods, however, the oxygen-balance method was used as a reference. The equations used to calculate the *AF* using these methods are shown in the Appendix VI. These equations, as mentioned before, were implemented in a LabView program that allowed the air-fuel ratio to be continuously monitored and recorded.

The air-fuel ratio was also monitored using the wide band oxygen sensor (Bosch LSU4.2) which was installed in exhaust manifold of cylinder 1. This sensor provided direct information of the air-fuel ratio, and it was used by MotoTron to automatically adjust the air-fuel ratio to the desired value. The sensor was calibrated for a wide range of air-fuel ratios taking the oxygen-balance method as reference.

3.6.3 EMISSIONS INDICES

The emissions index for species *i*, is defined as the ratio of the mass flow of the specie *i* at the exhaust gases to the mass flow of fuel delivered to the engine *i.e.* [19, 74]:

$$EI_i = \frac{\dot{m}_{i,exhaust}}{\dot{m}_{fuel}} \qquad (3.2)$$

where the EI_i is the emission index of species *i*, and $m_{i,exhaust}$ and m_{fuel} are the mass flow of measured species *i* at he exhaust and the fuel mass flow respectively. The emission indices have some advantages over the other emissions units used in engines. The

emission index provides an indication of the amount of pollutant formed per mass of fuel independently of the efficiency of the combustion process. The former is particularly useful when comparing emissions from different applications. Therefore, all the emission analysis was carried out using emission indices. The equations used for its calculation are described in Appendix X

3.6.4 COMBUSTION EFFICIENCY

The combustion efficiency indicates the fraction of fuel supplied that is released as energy in the combustion process. It is a useful parameter to monitor the engine performance, and it can be estimated from the exhaust gas composition [5, 74]. In this work the combustion efficiency was calculated using the combustion inefficiency concept [5], and the details of the calculation are presented in Appendix XI.

The estimation of the combustion efficiency is extremely useful because it give an indication of the extent of completeness of the combustion process. Additionally it is useful parameter in the estimation of other performance parameters such as the rate of heat release.

3.6.5 HEAT RELEASE ANALYSIS

A single-zone heat release analysis was performed to characterize the combustion event. In the analysis the heat transfer between the cylinder wall and the gases was modeled using the Woschni [78] correlation. An overall energy balance was employed to correctly scale the heat transfer based on the fuel energy released correcting for the

combustion efficiency. The residual mass fraction was calculated from the Yun and Mirsky [79] correlation, which assumes that the gases remaining at EVO undergo a polytropic expansion during the exhaust stroke. The combustion phasing was characterized by calculating the cumulative heat release where the mixture mass fraction burned reached the 10% (CA10), 50% (CA50), and 90% (CA90). The heat release analysis was carried out for the average pressure traces and for single-cycle pressure traces. The details of the equations and the Matlab program are shown in Appendix XII

The heat release analysis requires the knowledge of the mass trapped in each cylinder. This was estimated by considering that the charging of each cylinder was proportional to the IMEP in each cylinder. To avoid the influence of incomplete combustion and other factors, spark sweep tests at constant throttle position were carried out. The mass trapped in each cylinder was considered to be proportional to the maximum IMEP in each cylinder as follows:

$$\frac{m_{cyl-1}}{m_{cyl-2}} = \frac{IMEP_{\max,cyl-1}}{IMEP_{mac,cyl-2}} \qquad (3.3)$$

$$m_{cyl-1} + m_{cyl-2} = m_{total} \qquad (3.4)$$

where m_{cyl-1}, m_{cyl-2} are the mass per cycle trapped in cylinder 1 and cylinder 2, respectively; m_{total} is the mass of fuel and air that is delivered to the engine per cycle (both cylinders), and is measured experimentally; and $IMEP_{\max,cyl-1}$ and $IMEP_{\max,cyl-2}$ are

the maximum IMEP obtained from the spark sweep tests. Figure 3.11 shows the sweep spark timing tests at constant throttle positon for the 1750 RPM, 25% load, AF12.

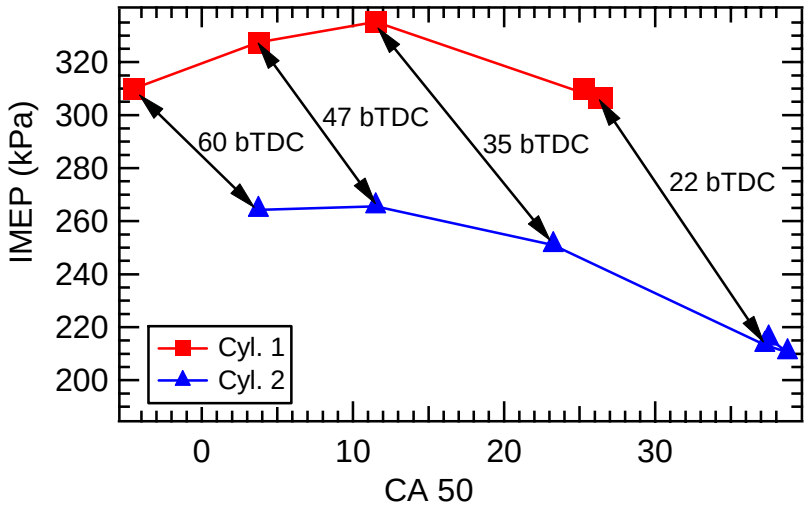

Figure 3.11 Sweep spark timing tests to determine the individual-cylinder mass for 1750 PRM, 25% load, AF12

CHAPTER IV

STUDY OF THE LIQUID FUEL EFFECTS ON THE HC EMISSIONS

4.1 INTRODUCTION

The liquid fuel film effects were easily isolated, and the results obtained from this study were necessary to setup the required experimental conditions for the following studies of the other HC mechanisms.

Two main goals were pursued in the liquid fuel study: the estimation of the stored mass of fuel in the intake manifold and the characterization of its effects on the HC emissions. The estimation of the mass of fuel in the intake manifold was performed by carrying out stop-fuel-injection tests. The effect of the liquid fuel on the hydrocarbon emissions was inferred from the comparison of two sets of engine-out HC emissions. The first set was obtained fueling the engine with the carburetor, while the second set was acquired fueling the engine with the homogeneous mixture systems (Both fueling system were described in detail in §3.2.2). For both fueling strategies, the engine was run over a wide range of loads, speeds and air-fuel ratios. Cycle-resolved HC measurements and heat release analysis were carried out to elucidate the implications of the liquid fuel on the engine performance.

4.2 STOP-FUEL-INJECTION TESTS

As mentioned above, the stop-fuel-injections tests provided an estimation of the mass of fuel stored in the intake manifold. Knowing the quantity of the liquid fuel present was necessary to fully characterize its contribution on the HC engine-out emissions.

In order to perform the stop-fuel-injection tests the carburetor-mounted fuel injector system was used. As described in section §3.2.2.3, this system consists of a stock carburetor modified so that the fuel was supplied directly through the carburetor main jet with a fuel injector (Fig. 3.4). This device emulates the carburetor fuel atomization, but allows very accurate control of the fuel injection timing, the mass of fuel delivered per cycle, and the simultaneous deactivation of the fuel injector and the ignition of the engine.

During a typical stop-fuel-injection test, the engine was fired until the steady state condition was reached (desired load, speed and air-fuel ratio). This condition was attained when the engine oil temperature reached a constant value. Depending of the engine operating condition this usually took around 30-45 minutes. Then, the injection and the ignition were suddenly halted. After this sudden cut, the engine was kept motoring at the same engine speed and air mass flow rate. Thus, only air was supplied to the engine, which continued the vaporization of the liquid fuel stored in the intake manifold. At the exhaust port, the post-stop-injection fuel concentration history was recorded with the fast FID for about 2000 cycles.

4.2.1 INTAKE PORT LIQUID FUEL MASS ESTIMATION

The HC concentration in the exhaust following cessation of fuel injection is the result of vaporization of liquid fuel in the intake system. The fast FID measures the HC concentration, or mole fraction, X_{HC}. In order to convert this concentration to a mass of fuel exhausted per cycle, the fuel mole fraction was recast as the mass fraction and the mixture in the exhaust was considered to consist of just fuel and air. The air mass flow rate is measured independently, and the compilation of these effects gives the mass of fuel per cycle as:

$$m_{fuel/cycle} = m_{air/cycle} \cdot \frac{X_{fuel} MW_{fuel}}{(1 - X_{fuel}) MW_{air}} \tag{4.1}$$

where, $m_{fuel/cycle}$ is the mass of fuel per cycle, $m_{air/cycle}$ is the measured amount of air per cycle, X_{fuel} is the mean HC mole fraction for the cycle on a C_1 basis ($3X_{HC}$), MW_{fuel} the molecular weight of the fuel per C_1, and MW_{air} the molecular weight of the air.

The fuel mass per cycle can be integrated, and then normalized by the mass of fuel delivered per cycle as follows:

$$m_{fuel-cum.-norm.} = \frac{\sum_{\#cycles} m_{fuel/cycle}}{m_{fuel-engine/cycle}} \tag{4.2}$$

where $m_{fuel\text{-}cum.\text{-}norm.}$ represents the normalized cumulative mass of fuel, and $m_{fuel\text{-}engine/cycle}$ is the mass of fuel delivered to the cylinder under steady state firing conditions for that

operating condition. Since this measurement was made in just one exhaust runner, $m_{fuel\text{-}cum.\text{-}norm}$ corresponds to only one half of the total in the intake port.

4.2.2 FUEL CONCENTRATION HISTORY OF THE TRANSITION FIRING-MOTORING DURING THE STOP-INJECTION TEST

During a stop injection test the HiTechniques data acquisition started to record data approximately five seconds before the fuel injection and ignition were stopped. This allowed the observation of the transition from the firing mode to the motoring mode, and the evolution in time of the fuel concentration at the exhaust.

As mentioned before the program that controls the ECU was modified to deactivate the fuel injection and the spark ignition simultaneously. To identify the cycle in which the stop fuel injection happened the fuel injector coil signal current was recorded in phase with the fast-FID data. The electrical current was converted to voltage using a Tektronic model A622 current probe. Figure 4.1 shows the sequence of the HC concentration and the fuel injector coil current for three consecutive cycles, including the cycle where the fuel injection is halted. In Fig. 4.1a, the injector is still energized, however in the next two consecutive cycles Figs. 4.1b-c, the fuel injector has been deactivated. The cycle where the fuel injector current signal disappeared indicated the starting point where the mass of fuel leaving the engine was integrated and was accounted as coming from the vaporization from the intake manifold.

a)

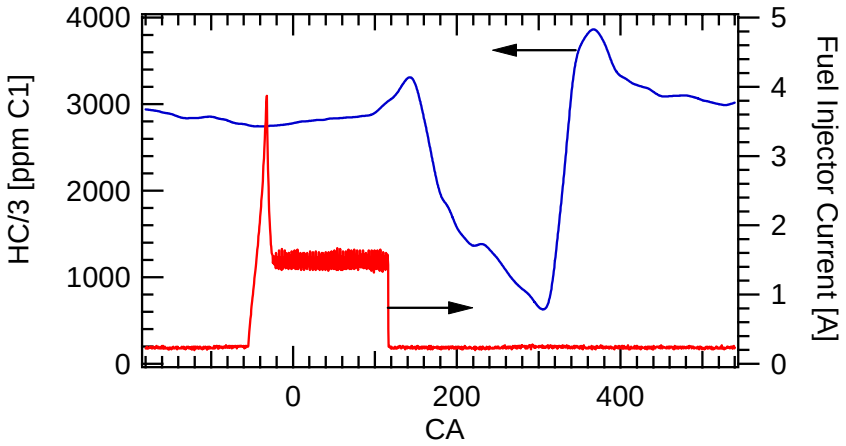

b)

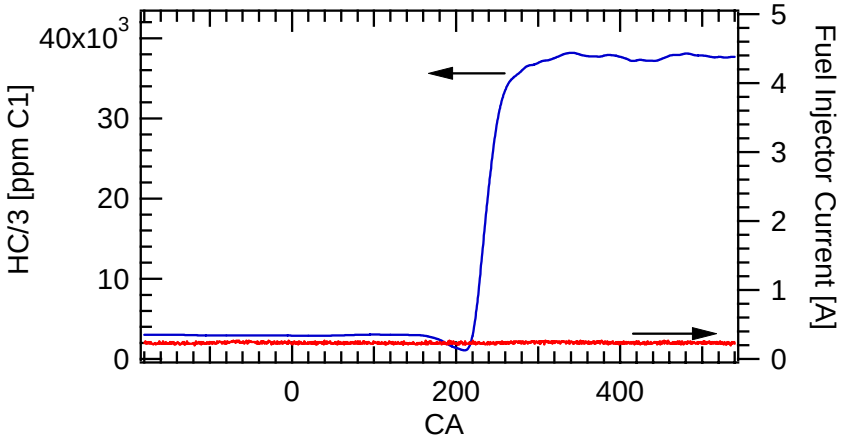

c)

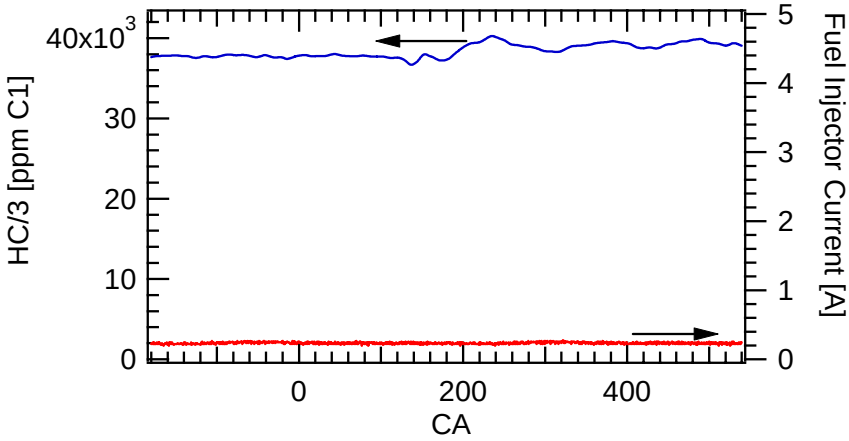

Figure 4.1 Consecutive cycles showing the time when the fuel and the spark ignition are halted: (a) Cycle -1, (b) Cycle 0 and (c) Cycle 1 (3060 RPM, 25% Load, AF11)

The detail of the HC concentration change from the cycle before and after the fuel injection was stopped is shown in Fig. 4.2. In this plot cycle 0 (left axis) represents the concentration of the firing cycle and has a typical concentration profile observed in the literature [66]. However, in cycle 1 (right axis) immediately after the fuel injection and the spark ignition were halted, a sudden increase in the concentration is observed during the main blown down period of the cycle. It can be seen that when the engine is firing the concentration is around 2,500 ppmC_3, however, as soon as the injection is stopped the concentration increases abruptly up to about 40,000 ppmC_3. This sudden increase indicates the presence of liquid fuel films on the walls of the intake manifold, which are being vaporized by the air stream. The vaporized fuel then passes to the cylinder, where the mixture does not ignite. Due to the absence of in cylinder combustion the air-fuel mixture is released through the exhaust port.

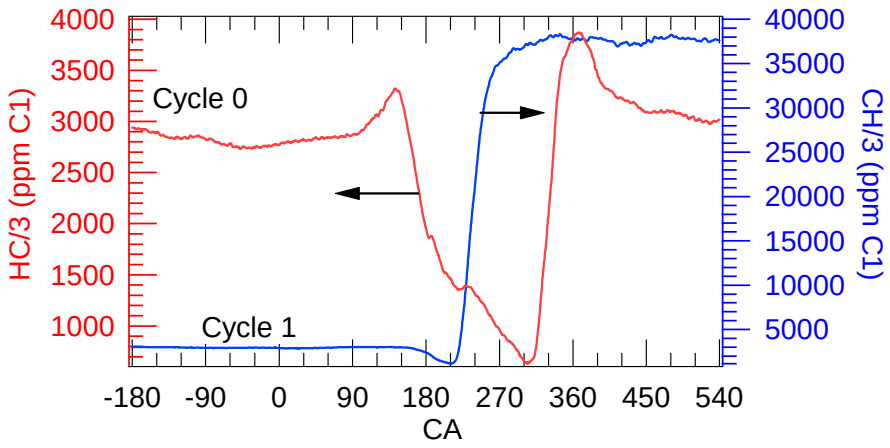

Figure 4.2 HC concentration for the cycle 0 (firing) and the cycle 1(immediately after the fuel injector and spark timing were halted), for the condition of 3060 RPM, 25% Load, AF 11

4.2.3 FUEL CONCENTRATION HISTORY

The HC concentration histories were logged for approximately 2000 cycles to ensure complete vaporization of the liquid fuel. No significant change of the HC concentration indicated that the liquid fuel films of the intake system were completely vaporized by the air stream. Figure 4.3 shows the evolution in time of the HC concentration for a typical stop-injection test. Each data point represents the average concentration for a cycle. This was considered to be representative of the cycle, because the concentration does not change significantly during the cycle, e.g. Fig. 4.1-c. Looking at the HC concentration trend (Fig. 4.3), it can be seen that when the engine is firing the concentration is low and around a typical level reported in the literature; however, as soon as the injection is stopped the concentration increases abruptly (up to about 40,000 ppmC_3). Then, the concentration decays due to the reduction of fuel available for vaporization. After a certain number of cycles, the fuel concentration does not show significant decrease or change, indicating that there is negligible amount of fuel to be evaporated in the intake manifold. At the end of the 2000 cycles the concentration was approximately 300 ppmC_3, which was similar to the concentrations measured when the engine was motored.

4.2.4 INJECTION PRESSURE SENSITIVITY

The carburetor main jet introduces the fuel into the air stream at differential pressures that are governed by the venturi flow characteristics. This differential pressure

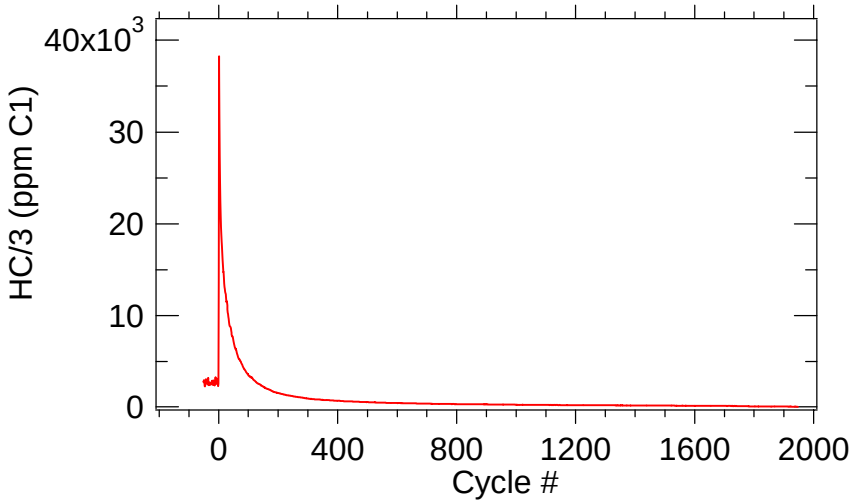

Figure 4.3 HC concentration history measured at the exhaust in at typical stop injection test (3060 RPM, 25% Load, AF11)

depends of the engine operating condition, and can be no more than ~ 50kPa (corresponding to choked flow at the throat).

In the case of the carburetor-mounted fuel injector the fuel was pressurized using a high pressure electrical fuel pump. Then, the pressure was reduced to typical carburetor fuel supply pressures (around 58.5 kPag). It is very important to note that the injection of fuel in the carburetor-mounted fuel injector is pulsating. Therefore, the fuel injection pressure could impact the atomization, and consequently the HC emissions. In addition, high injection pressures could promote high levels of fuel impingement on the carburetor walls affecting the stored mass of fuel. Hence, the effect of the injection pressure on the wall wetting was assessed. Several tests at different injection pressures were carried out under static conditions i.e. with no air stream through the carburetor. The pseudo encoder option of MotoTron was used to simulate the engine speed and the mass of fuel injected per cycle. During the tests, the fuel pressure was increased until the point that the fuel

impinged the carburetor wall. This pressure was approximately 58.5 kPag. Above this pressure excessive wetting of the carburetor venturi was observed. Below that pressure the droplets fell within the cross section of the venturi without hitting the walls. Wall wetting can also happen if the fuel is injected at very low pressure. Hence, test at very low injection pressures were performed, as well. The lowest pressure without seeing wetting effects was 21 kPag. As mentioned before, the goal was to emulate the atomization of the stock carburetor as close as possible, so a representative injection pressure should be used.

It is important to mention that if the fuel is injected within 21-58.5 kPag, the air flow through the carburetor will deflect the fuel jet. This will help to prevent the fuel impingement on the carburetor venturi walls, and the system will closely emulate the carburetor behavior. The effect of the fuel injection pressure on the stored mass of liquid fuel was investigated carrying out stop-injection tests at the two extreme injection pressures: 21 and 58.5 kPag. Figure 4.4 shows the cumulative mass of fuel for the two injection pressures. As it can be seen from the tests, the injection pressure does not affect the stored mass of fuel. Hence, all the stop injection tests were carried out with injection pressures of 58.5 kPag.

4.2.5 STOP FUEL INJECTION TESTS REPEATABILITY

The repeatability of the stop injection tests was verified by performing tests for the 1750 RPM, 25% load, AF 12 case several times over several days. Figure 4.5 shows the results of the different runs. The variability between runs was on the order of 10 mg

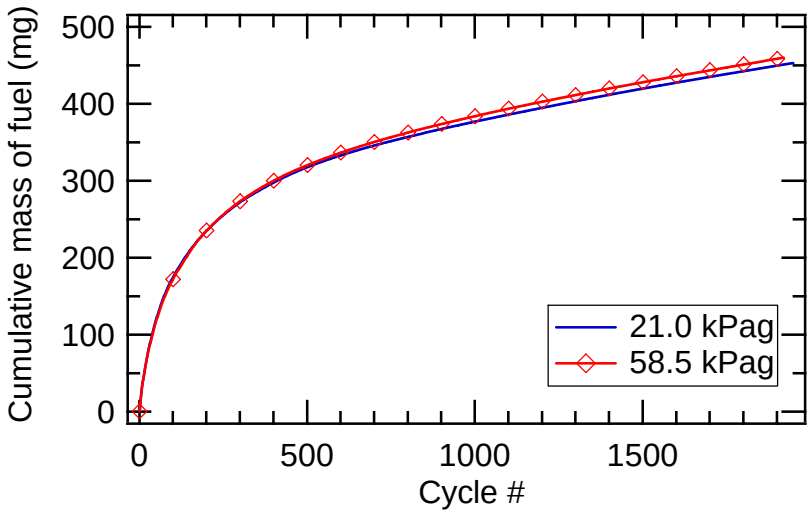

Figure 4.4 Dependence of the Fuel injector pressure on the mass of fuel stored in the intake manifold for the condition of 1750 RPM, 25% load, AF12

of fuel which represents approximately one cycle worth of fuel or approximately a 2.2 % of the total mass stored. This variability was low indicating that the tests are very repeatable, and that the technique was very robust.

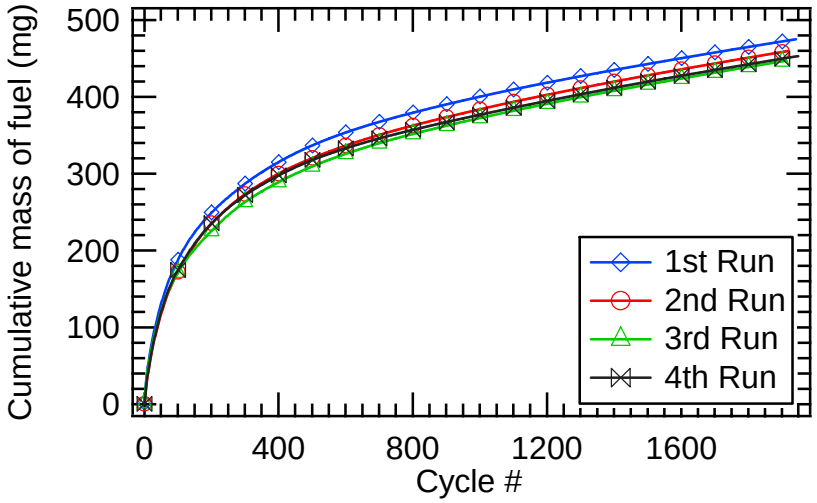

Figure 4.5 Stop injection repeatability tests at 1750 RPM, 25% load, AF 12

4.2.6 CUMULATIVE MASS OF FUEL RESULTS

The liquid fuel mass was measured for several speeds, loads and air-fuel ratios. Figure 4.6 shows the results of the tests in terms of cumulative mass of fuel. It can be seen that the stored mass depends of the engine operating condition. Specifically, the stored mass scales with the engine load. This is true for both speed conditions, i.e. 1750 rpm and 3060 rpm. However, no clear dependence is observed with respect to the engine speed. To better visualize the results as a function of the speed and load, the cumulative mass was normalized with the mass of fuel injected per cycle. The normalized results are shown in Fig. 4.7. This figure shows details that were not evident, before. Thus, a clear dependence of the fuel mass with the speed is observed.

Independent of how the cumulative mass of fuel is presented, the results show that there is a considerable amount of fuel in the intake manifold. For the 1750 RPM for 10% and 25% load conditions, Fig. 4.7 shows that approximately of 40 cycles worth of fuel is stored in the intake manifold as liquid fuel films. For the 3060 RPM, 25% and 50% load conditions the results show a presence of about 30 cycles worth of fuel. It is important to mention that the results of Fig. 4.7 represent the contribution of cylinder 1. Therefore, for the two cylinders of the engine a total mass of up to 80 cycles worth of fuel, is expected. The presence of liquid fuel in the intake manifold is unquestionable. The stored mass of fuel is relatively high compared with those reported for automotive engines, where reports show that no more than ten cycles worth of fuel is stored in the intake system [80]. Finally, it is important to mention that although the intake manifold temperature was 50 °C, this could not impact the liquid fuel film vaporization [81].

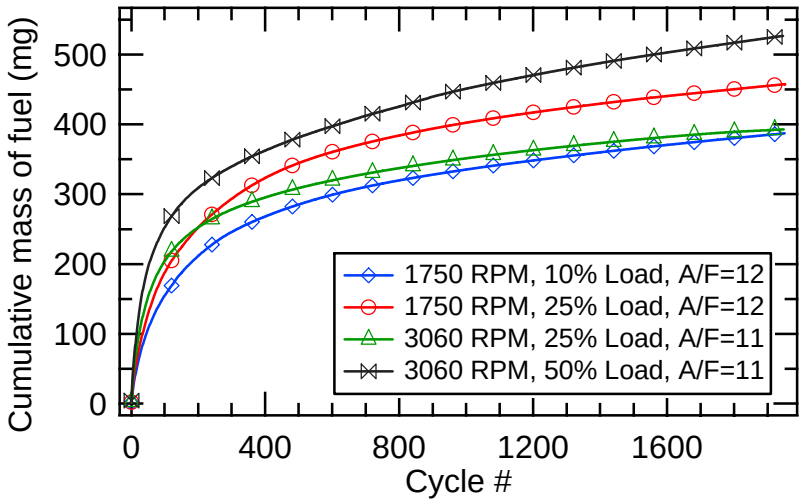

Figure 4.6 Cumulative mass of fuel results for low and high speed conditions

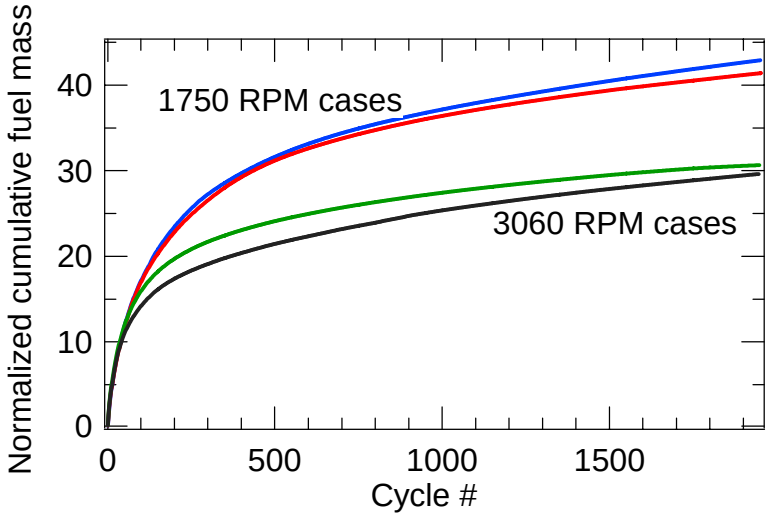

Figure 4.7 Cumulative mass of fuel results for low and high speed conditions

4.3 LIQUID FUEL EFFECT ON THE AVERAGE EMISSIONS

The stop-fuel-injection tests showed that a significant amount of fuel was present in the intake manifold. Hence, the liquid fuel effect on the average engine-out emissions was studied. The effect of the liquid fuel was inferred comparing the emissions when the

engine was fueled with the carburetor and the homogeneous mixture system. This was performed for the wide range of speed, load and air fuel ratios, showed in the Table 4.1.

Table 4.1 Test matrix

	LOAD										
SPEED (RPM)	10%			25%				50%		100%	
	AF			AF				AF		AF	
	12	13	14	11	12	13	14	11	12	11	12
1750	x	x	x		x	x	x				
3060				x	x			x	x	x	x

4.3.1 AVERAGE HC EMISSIONS

The homogeneous mixture system eliminates the possibility of liquid fuel film formation. Thus, the comparison of the HC emissions from the carburetor and homogeneous mixture system will show the extent of impact the liquid fuel films have on the HC emissions. This comparison is shown in Fig. 4.8, where symbols of the same shape correspond to the same operating condition and the filled symbols are for the HMS and the open symbols are for the carburetor.

Various observations can be made from Fig. 4.8. First, the HC emissions show a strong dependence on the air-fuel ratio. It can be seen that for all the loads and speeds the engine-out HC emissions are reduced as the air-fuel ratio is increased. This is in agreement with the trends reported in the literature for automotive engines [5, 82] and for small engines [11, 14]. One of the reasons for the reduction of the HC emissions as the air-fuel ratio increases is the increment of oxygen in the combustible mixture. This allows

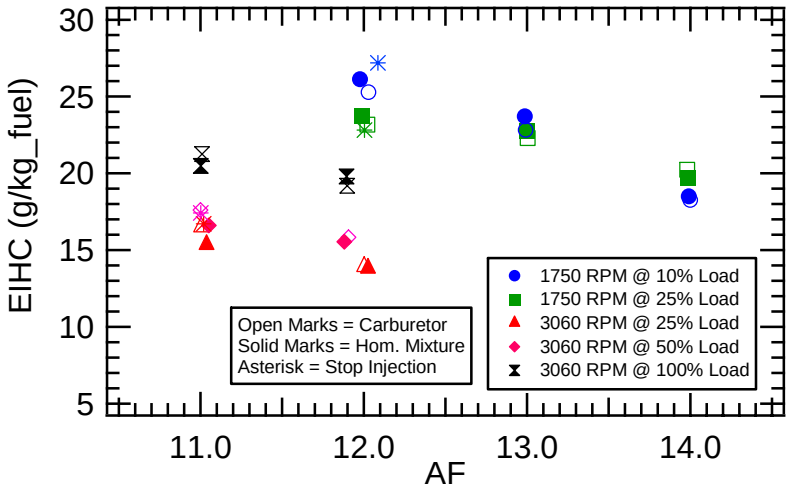

Figure 4.8 Engine-out HC emissions for the carburetor and homogeneous mixture system.

the oxidation of more fuel during the main combustion event, which increases the combustion efficiency and reduces the HC emissions [5]. However, the air fuel ratio also affects the relative contribution of other HC sources such as the crevice storage, the in-cylinder post-flame oxidation, and the residual mass fraction [82]. The effect of the air fuel ratio on the relative contribution of the HC mechanisms is complex; however, overall in Fig. 4.8 an increase in air fuel ratio reduces the HC emissions. Other important observation is that the slope $\frac{dEICH}{dAF}$ depends of the speed for a given load. Thus, the engine-out HC emissions are more sensitive to the air fuel ratio at 1750 RPM, than at 3060 RPM.

At 1750 RPM, the engine-out emissions for the 10 and 25% load are almost identical for the air-fuel ratio of 13 and 14. The slope of both loads also is similar in this range. However, for the air fuel ratio of 12 the 1750 RPM, 10% load shows a higher level

of engine-out HC emissions. This trend is shown for the carburetor, homogeneous mixture system and carburetor-mounted fuel injector.

For the 3060 RPM cases, the HC emissions levels are smaller compared with the 1750 RPM cases. Specifically, for the 25% load a reduction of approximately 50% is observed when the engine speed is increased from 1750 RPM to 3060 RPM. The reduction in emissions as the engine speed is increased has been observed by [82, 83-85], where a reduction of 20 to 50 % was observed when the speed was increased from 1000 to 2000 RPM. The main reason for the reduction is attributed to the reduction of the heat transfer from the cylinder gases. This increases the in-cylinder temperature, the exhaust temperature and the post-flame oxidation of the unburned hydrocarbons [82]. Another important factor is that as the speed is increased the in cylinder turbulence intensity increases, promoting a post-oxidation.

The dependence of the HC emissions with the load is a little bit more complex (see Fig. 4.8). For the 1750 RPM cases no appreciable difference is observed when the load is increased from 10 to 25%. However, for the 3060 RPM case it is clear that the HC emissions are increased as the load increases from 25 to 100%. The fact that for the 3060 RPM cases the emissions are increased with the load suggests that for this operating condition the HC emissions may be dominated by the ring pack storage, i.e. as the load increases the mass of HC stored in the ring pack increases. As a result a greater mass of air-fuel mixture escapes the main combustion producing higher engine-out HC emissions levels.

It is important to mention that at the 3060 RPM condition the engine could not be run at air-fuel ratios higher than 12.2, especially at the 25 and 100% load. The operation of the engine at these conditions was limited by extremely high temperatures at the exhaust. At air fuel ratios of 12.2 the exhaust temperature was approximately 770 °C. Hence, the engine was not tested at higher air-fuel ratio values for safety reasons.

The most important outcome of Fig. 4.8 is regarding the comparison of the HC emission coming from both fueling strategies. For better visualization of the comparison, the data of Fig. 4.8 were rearranged and presented in a different way in Fig. 4.9.

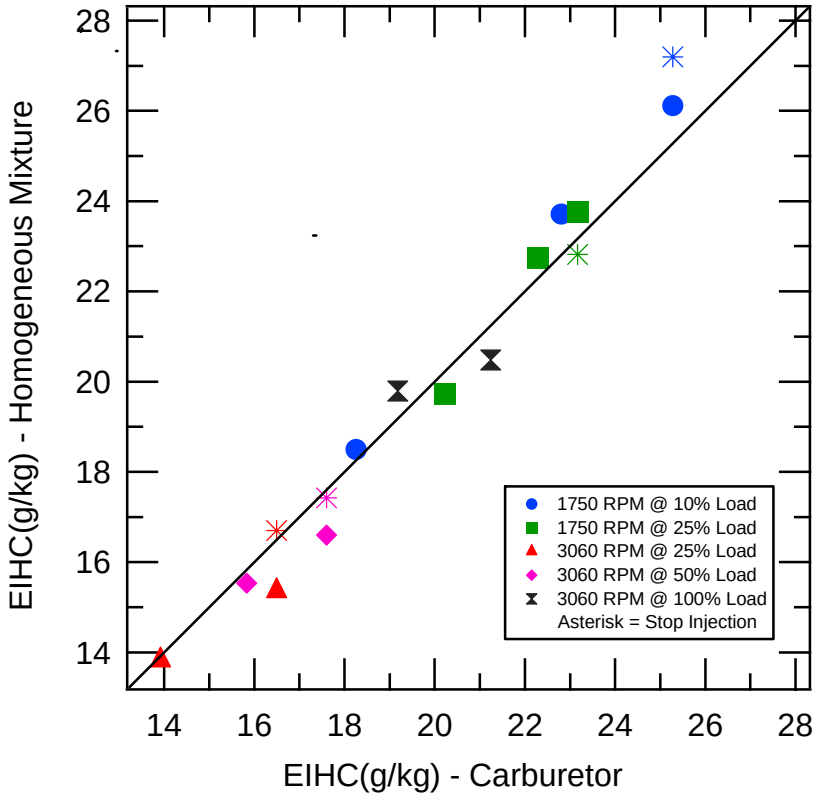

Figure 4.9 HC emissions comparison for the carburetor and the homogeneous mixture system

From Fig. 4.9 it can be seen that the HC emissions do not differ significantly between the systems. The greatest difference can be observed at the 1750 RPM case for the 10% load, AF12. For the 3060 RPM case, the differences are even smaller.

In order to determine if the differences seen in Fig. 4.9 are meaningful, a statistical analysis was carried out. The statistical analysis considered the following sources of uncertainty: instrument error, the variability within a given run, and the day-to-day variability. The emissions bench HC analyzer has an accuracy of 0.5% of the full scale. The variability within a given run represents RMS variation obtained when the HC emissions data were collected for approximately 10 minutes at a sample rate of 20Hz. The day-to-day variability was determined by running the engine on several days at the same operating condition. It is important to mention that the HC emissions were recorded at fully warmed-up steady state conditions. The total error (combination of all the error sources) was calculated using the root-sum-squares (RSS) method [54]. The individual contributions and the total uncertainty obtained from the error analysis for the 1750 RPM, 25% load, AF13 are shown in Table 4.2.

The results show in Table 4.2 indicate that the biggest source of error is the day-to-day variability. The smallest source is the instrument uncertainty. The fact that the day-to-day variability is the biggest source of error indicates that the experiments should be carried out under very controlled conditions in order to obtain good repeatability. The total error was approximately 1.20 g/kg_fuel and it represents approximately 5% of the measured value.

Table 4.2 Repeatability Analysis for the 1750 RPM, 25% load, AF 13

Measured average HC emissions	22.0 g/kg-fuel
Source of error	**Contribution**
Instrument accuracy	0.25 g/kg-fuel
Variability in a given run	0.50 g/kg-fuel
Day-to-day variability	1.00 g/kg-fuel
Total uncertainty	**1.20 g/kg-fuel**
% of the measured value	5 %

To determine the significance of the difference in HC emissions between the carburetor and the HMS system ($EIHC_{carb} - EIHC_{HMS}$), the differences (see Table 4.3) were compared with the total error obtained above (Table 4.2).

Table 4.3 Differences in the HC emissions between the carburetor and the HMS in (g/kg) for all the testing conditions

	LOAD										
SPEED (RPM)	10%			25%				50%		100%	
	AF			AF				AF		AF	
	12	13	14	11	12	13	14	11	12	11	12
1750	-0.83	-0.91	-0.27		-0.59	-0.46	0.50				
3060				1.13	0.10			1.00	0.30	0.79	-0.65

From Table 4.3 it can be seen that the differences are smaller than the measurement uncertainty. This suggests that from a statistical point of view there is no difference in HC emissions between both fuel systems. Therefore, this suggests that the liquid fuel does not significantly affect the HC emissions.

It is important to note, that these findings are in contradiction with the work developed for automotive engines where the mixture preparation affects the overall engine performance and HC emissions [86]. Specifically, the presence of liquid fuel in the intake port increases the HC emissions.

4.3.2 AVERAGE CO AND NOx EMISSIONS

To further investigate the effect of the liquid fuel, the average CO and NOx emissions were compared. Figure 4.10 shows the comparison of the CO emissions. It can be seen that the levels of CO are strongly affected by the mixture air-fuel ratio, and that the speed and load do not affect the CO emission levels. The results are in agreement with the findings reported in the literature [11, 14, 87].

It is important to note that reducing the air-fuel ratio from 14 to 11 the CO emission levels were increased by 700%. This shows why small engines produce very high levels of CO emissions. Looking at the differences in CO emissions between both fuel systems, it can be seen that the emissions are not affected by the type of fuel system i.e. not appreciable differences can be observed for the entire range of speeds and loads. This observation suggests that engine performance was not affected by the liquid fuel films.

The average NOx emissions comparison is shown in Fig. 4.11. It can be seen from this figure that for a given load the NOx emissions are increased as the air-fuel ratio increases. This trend is in agreement with the results reported in the literature [5, 11, 14, 82], as well. It is very well known the NOx emissions are governed by the temperature

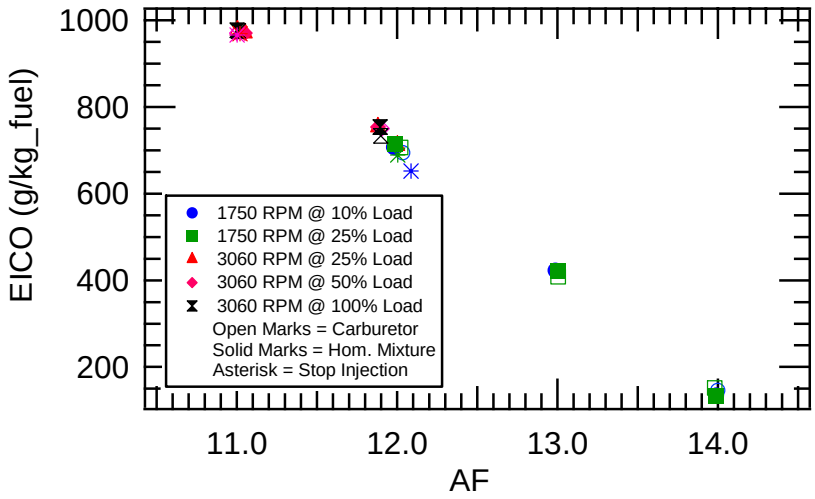

Figure 4.10 CO emissions for the carburetor and homogeneous mixture system (HMS).

history of the burned gases and the peak temperature [5, 82]. The in-cylinder peak temperatures increase with the air-fuel ratio, resulting in higher levels of NOx.

A load effect on the NOx emissions can also be observed in Fig. 4.11. For a specific speed the increase in load results in an increase of the NOx emissions. Again, this can be explained by the higher in-cylinder temperatures achieved as the load is increased. One of the main reasons for the increase of the in-cylinder temperature is the decrease of the residual mass fraction as the load is increased. On the other hand, the effect of speed is not too obvious in Fig. 4.11; this is due to the fact that the increase in speed compromises various engine parameters such as the volumetric efficiency and the net heat transfer. The increase in speed reduces the volumetric efficiency, which increases the residual mass fraction. On the other hand, an increase in the engine speed reduces the heat transfer leading to higher in-cylinder temperatures. Thus, the resulting effect of the load on the NOx emissions mainly depends of the compromise between these two factors. However, it is believed that the speed increase only has a modest effect

on the NOx emissions [82]. This is observed in Fig. 4.11 for the 25% load and AF12 where not significant effect is observed when the speed is changed from 1750 to 3060 RPM.

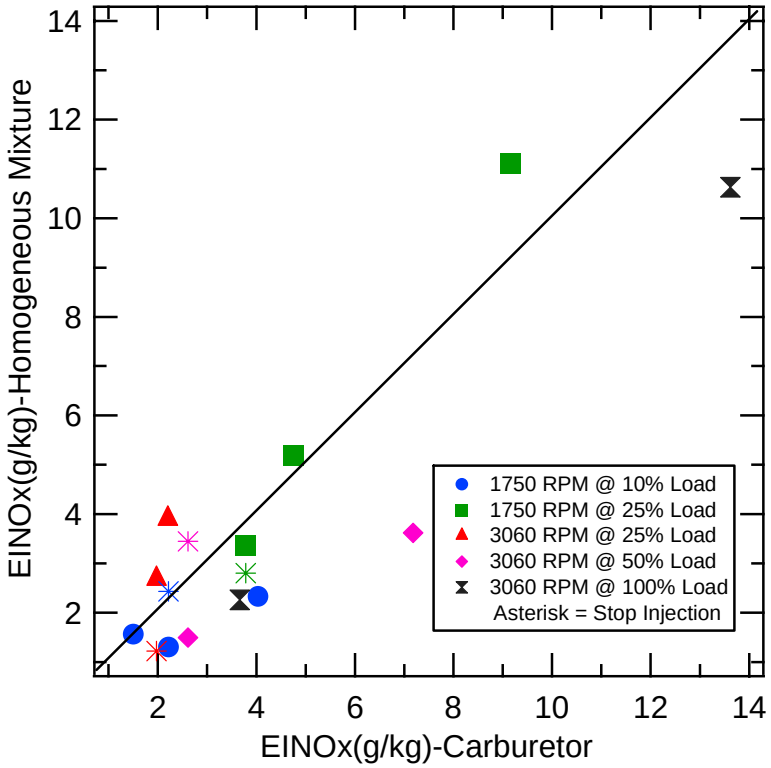

Figure 4.11 Comparison of the NOx emission for Carburetor and the homogeneous mixture system

It is important to note that in general the NOx emissions (Fig. 4.11) are very small compared with the NOx emissions obtained from automotive engines [5]. This mainly due to rich air-fuel ratios, which reduces the peak temperatures significantly.

Comparing the NOx emissions of the carburetor and the homogeneous mixture system, it can be observed that, in general, the two fuel systems show the same trends

with no significant differences except the cases of 3060 RPM, AF12, 50 and 100% load. However, the differences are small and can be attributed to the variability rather than to a physical difference between the NOx emissions. The results are in agreement with the work of Bonneau [14], who found negligible differences between fuel systems for rich air-fuel ratios. The differences for the 3060 RPM case could be attributed to the error of the NOx analyzer. The NOx analyzer exhibited a decay in the reading with time for a constant gas composition. Although, the sensor was calibrated before every run the level of signal decay was unknown in the intermediate stages of the measurement process. Finally, in spite of the small differences observed for some cases in Fig. 4.11, it can be concluded that the liquid fuel effect does not have a significant effect on the NOx emissions.

4.4 CYCLE-RESOLVED HC EMISSIONS

Cycle-resolved HC emissions measurements were performed to help elucidate the particularities of the effect of the liquid fuel on the HC emissions. Studies carried out by Stache and Alkidas [88] in a port-fuel injected automotive engine showed that the presence of the liquid fuel in the cylinder affected the cycle-resolved HC history. Specifically, the effect of the liquid fuel was observed during the exhaust stroke when the piston was near TDC. Thus, similar effects should be expected in the case of a small engine when fueled with the carburetor. Therefore, to further investigate the differences in HC emissions for the mixture preparation systems, time-resolved HC concentration measurements were performed using the fast FID.

The fast-FID results for all of the conditions tested are shown in Fig. 4.12. All of the cases investigated follow the same general shape, which agrees with literature reports [65, 66, 88]. During the time that both the intake and exhaust valves are closed, there is a relatively high, steady HC concentration in the exhaust port, however since the mass flow rate is zero it is not a significant effect. The effect of exhaust valve leakage, which would cause an increase in the concentration during the high pressure part of the cycle, i.e. starting at IVC, does not appear to be significant. When the exhaust valve starts to open at 130 °ATDC, the HC stored in the crevices of the spark plug and exhaust valve are released increasing the relative amount of HC at the exhaust port. During the blow-down period, the HC concentration is reduced because it contains the bulk gases that were burned during the main combustion event. The majority of the exhaust stroke corresponds to a relatively low HC concentration. At the end of the exhaust stroke, as the piston approaches the TDC, the HC stored in the ring pack that escaped after the combustion process are released. These HC-rich gases are located near the piston crown due to the low mixing rates, and are expelled by the piston motion at the end of the exhaust stroke.

The magnitude of the cycle-resolved HC concentrations measured at the exhaust port were comparable to the corresponding values for the averaged results, but a direct comparison is complicated by the instantaneous mass flow rate, which varies considerably during the exhaust-valve-open period. The cycle-resolved HC concentrations do, however, clearly show the expected trend with AF; for a fixed condition the cycle-resolved HC concentration decreases with increasing AF.

A comparison of the cycle-resolved HC emissions for the two different mixture systems shows that there is very little difference between the carburetor and the homogeneous system. The magnitudes of the HC emissions are not exactly the same for both systems, but the values are within 5% of the average value. Some of the differences in the magnitude of the HC concentration can be attributed to the fact that the air-fuel ratio was found to fluctuate in time with the carburetor. The nuances of the HC concentration history are, however, replicated very well between the two mixture systems. For example, the low load conditions all exhibit a decrease in HC concentration at 250 ATDC, and the phasing and magnitude of this decrease are well matched for the two mixture preparation systems. The increased HC concentration due to the fuel films observed by Stache and Alkidas [88] near TDC is not observed in Fig. 4.12 for all the cases. Overall, in accord with the average emission measurements, the cycle-resolved HC measurements show that the emissions appear to be insensitive to the air-fuel mixture preparation system, and the carburetor is not contributing to the HC emissions under these conditions.

4.5 HEAT RELEASE ANALYSIS

The characterization of the combustion event was carried out by performing a single-zone heat release analysis (see Appendix XII) in order to further identify differences in the mixture preparation system, and the results are shown in Fig. 4.13.

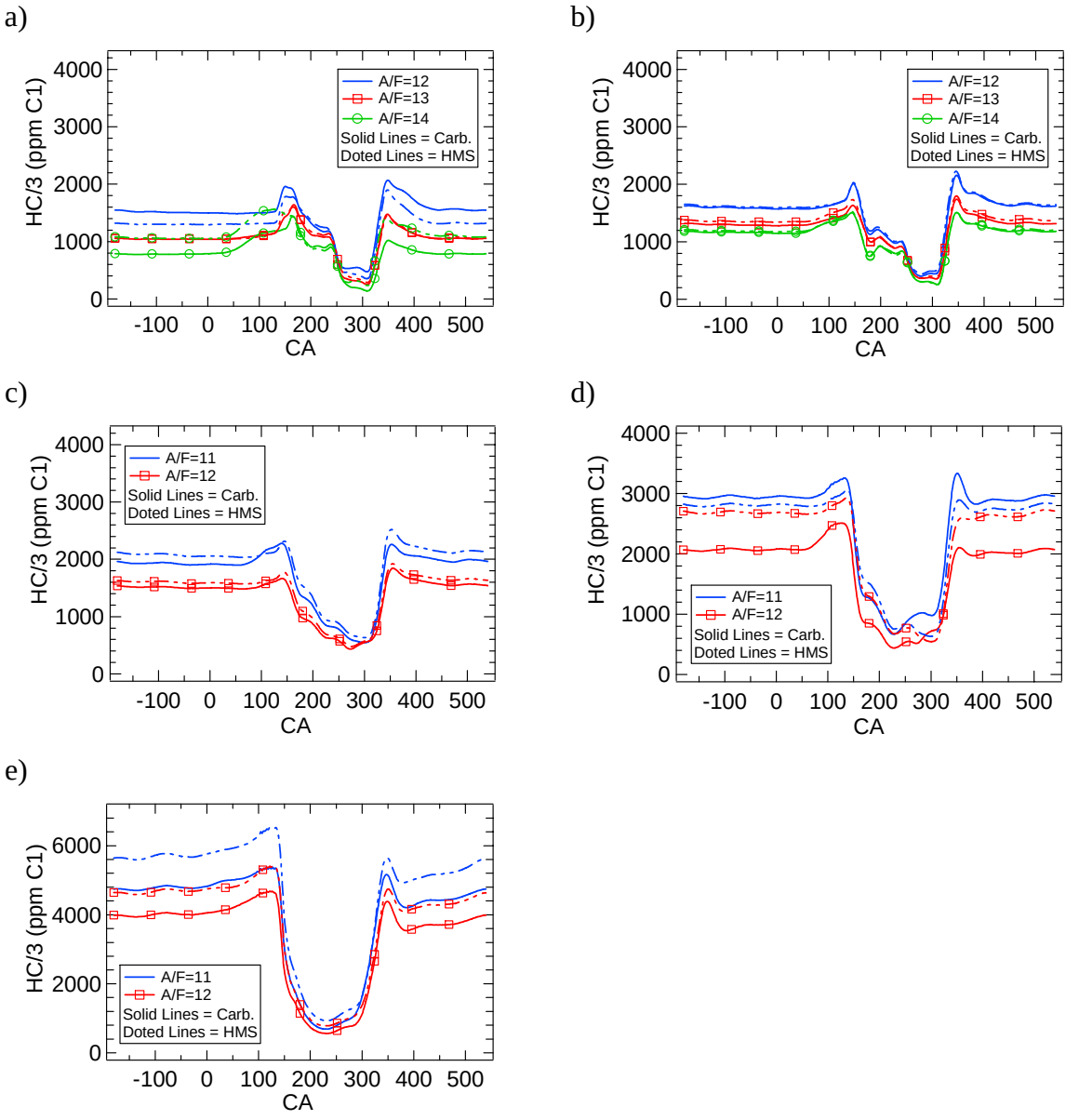

Figure 4.12 Cycle-resolved HC measurements for (a) 1750 RPM and 10% load, (b) 1750 RPM and 25% load, (c) 3060 RPM and 25% load, (d) 3060 RPM and 50% load, (e) 3060 RPM and 100% load.

In the heat release analysis the effects of heat transfer were accounted for, and an overall energy balance was enforced such that the cumulative heat release matched the measured combustion efficiency times the delivered fuel energy.

The heat release rate comparison shows that, for a given load and speed the fuel system does not have a significant effect on the energy release rate. This result further supports the negligible difference observed in the emissions measurements. The heat release data for the different operating conditions show a significant variation, which is largely because the tests were performed at fixed spark timing. The full load data show a well-phased heat release profile that has duration typical of spark-ignition engines. The lower load cases, however, have a prolonged combustion event, with the heat release continuing late into the expansion stroke. At the low load there is an indication that the heat release is extending beyond the exhaust valve opening. This, suggests that incomplete combustion could be a source of HC emissions. This will be discussed in detail in the following chapter.

4.6 SUMMARY

In the present chapter the effect of the liquid fuel on the HC emissions was studied. The study was divided in two parts. The first part was focused on the quantification of the mass of liquid fuel stored in the intake system. This was carried out performing stop-fuel-injection tests using a carburetor-mounted fuel injector. The results showed that a significant amount of liquid fuel was stored in the intake manifold and that it was highly dominated by the engine speed. For the 1750 RPM conditions the results showed that up to 80 cycles worth of fuel was stored in the intake manifold. For the 3060 RPM about 60 cycles worth of fuel was stored in the intake system. This stored mass of fuel is high, relative to port-fuel injected automotive engines [80].

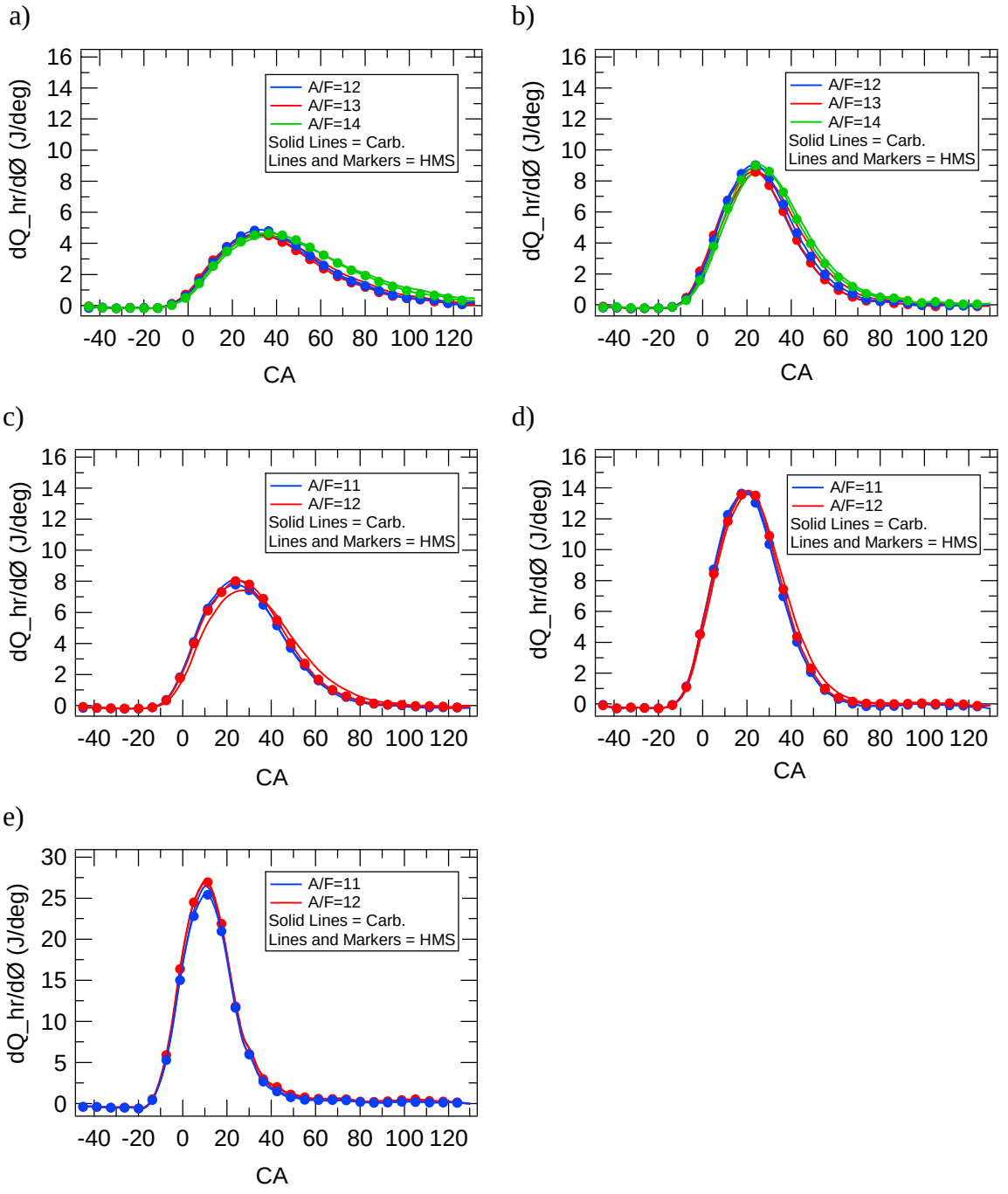

Figure 4.13 Heat release analysis for (a) 1750 RPM and 10% load, (b) 1750 RPM and 25% load, (c) 3060 RPM and 25% load, (d) 3060 RPM and 50% load, (e) 3060 RPM and 100% load.

In the second part of the study, the effect of the liquid fuel on the HC emissions was investigated. This was accomplished by comparing the engine-out HC emissions from the carburetor and the homogeneous mixture system. The HC emissions comparison showed only small differences. A statistical analysis was carried out to verify if the observed small differences were significant. The total error calculated from the statistical analysis was of 1.25 g/kg-fuel, and this was higher than the observed differences between both fuel systems. This suggested that the liquid fuel does not affect the engine out HC emissions. It is important to mention that these tests were at steady state, fully warmed up conditions with rich air-fuel ratios. The findings of the HC emissions comparison were supported by the insignificant differences in CO and NOx emissions and the heat release. Additional evidence that the liquid fuel does not affect the HC emission was provided by cycle-resolved HC measurements. The HC concentration traces for both fuel systems showed the same trend along the cycle with not significant differences, especially during the last part of the exhaust process when the piston is near TDC where the liquid fuel effect is expected to show its signature [88].

In conclusion, the results show that there is significant amount of fuel in the intake manifold, however this does not affect either the average or cycle-resolved HC emissions. In addition the average CO and NOx emissions and the heat release were not affected by the presence of liquid fuel.

CHAPTER V

ESTIMATION OF THE RING PACK CONTRIBUTION TO THE HC EMISSIONS

5.1 INTRODUCTION

As explained is section §2.3, during the main combustion event, part of the combustible mixture is stored in the ring pack crevices. The flame cannot penetrate inside these crevices due to quenching. Therefore, the mass of fuel stored in the ring pack escapes the main combustion. Part of this mass returns to the cylinder where it can be further oxidized by the hot burned gases. The part of the fuel that survives the post oxidation is exhausted and it contributes to the engine-out HC emissions. In this chapter a detailed characterization of the ring pack contribution to the HC emissions is provided. The contribution of the ring pack was estimated using a simplified ring pack model. This model was validated against the measured blowby, and a sensitivity analysis was carried out to identify the role of the different parameters that affect the ring pack HC contribution. The ring pack model was linked to the heat release code, in order to estimate the mass of HC leaving the ring pack starting at some specific combustion phasing. The ring pack results were complemented with heat release analysis, fast FID measurements, and conditional sampling. The estimated mass of HC leaving the ring pack was correlated with the combustion phasing (CA90), the mass of HC that leaves the

engine per cycle, and other parameters. Part of the analyses was carried out on a single-cycle basis. The details of the ring pack model and the results of the analysis are describe below in the detail.

5.2 RING PACK CONTRIBUTION TO THE HC EMISSIONS

The contribution of the ring-pack crevices to the HC emissions was estimated by implementing a simplified ring pack model. The ring pack model was based on the model used by Eng *et al* [30]. The model predicted the ring-pack crevice gas flow, and most importantly the mass that returns to the combustion chamber after the flame reached the cylinder wall (CA90). Several conventions were used to estimate the mass of HC that leaves the crevices. The details of the model, inputs, outputs, geometry are described in this section. The engine-out HC emission were measured, and correlated with the amount of the HC stored in the ring pack.

5.2.1 RING PACK GAS FLOW MODEL EQUATIONS

The model of the ring pack crevice flow was based on the model developed by Furuhama and Tada [89], which was later improved by Namazian and Heywood (adding ring dynamics) [27] and then simplified by Eng *et al.* [30, 34]. The main difference of the present model [30], and the Namazian and Heywood [27] model is the manner that the ring moves inside the groove. A detailed discussion of the ring motion inside the groove and its simplification for the present model are given in the subsequent part of this section.

The piston and the ring pack configuration of the engine are shown in Fig. 5.1. The ring-pack has two compression rings and an oil control ring. These rings can move freely in the axial and radial direction inside the groove.

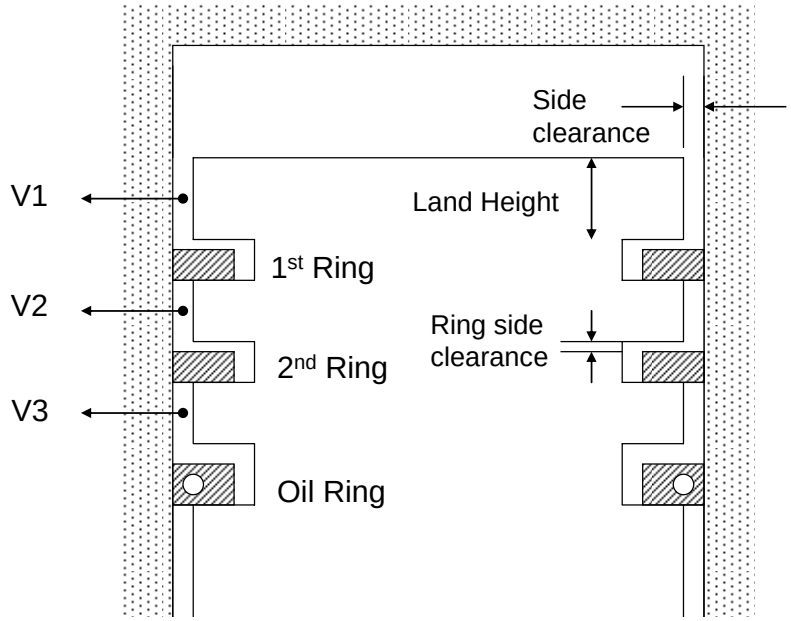

Figure 5.1 Ring pack geometry

The piston rings, piston crown and the liner form three volumes: V_1, V_2, *and* V_3 (Fig. 5.1). The axial position of the ring inside the groove changes along the cycle. Thus, the ring can be at the top, in between or at the bottom surface of the groove. The relative position of the ring changes the size of V_1, V_2, and V_3 and the manner they are interconnected, i.e. these volumes can be connected either through the ring end gap (Fig. 5.2) or through the ring side clearance (Fig. 5.1). The ring position dictates the gas flow path. When the ring is either sitting on the top or bottom edge of the groove the gas flows through the ring end gap, however when the ring is in an intermediate position the gas

flows through the ring side clearance. It is important to mention the side clearance area is significantly larger than the end gap area. Therefore, the ring movement inside the groove may affect the mass of HC that returns to the combustion chamber.

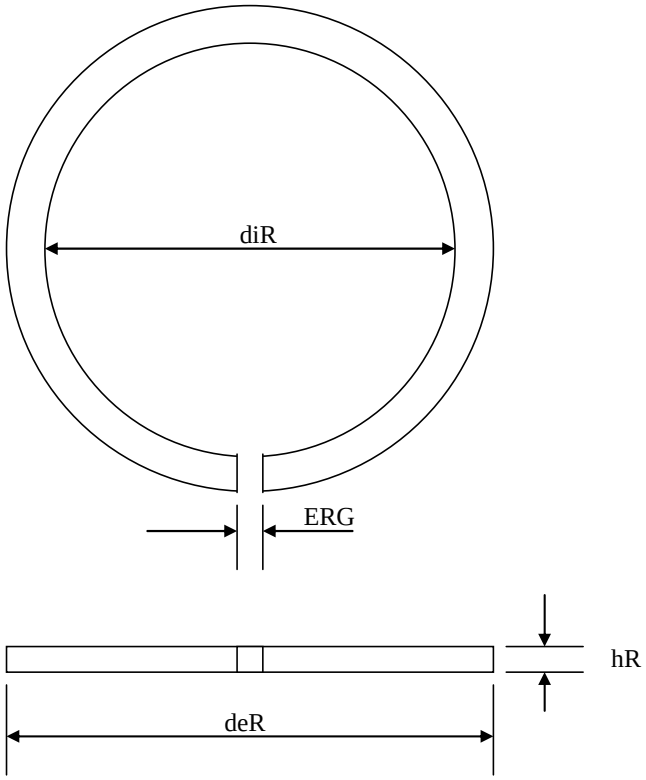

Figure 5.2 Piston Ring Geometry

5.2.2 FORCES ACTING ON THE RING

For an accurate calculation of the ring pack gas flow, the exact location of the ring inside the groove along the cycle is required. This is achieved by performing an analysis of the forces acting on the ring. Figure 5.3 shows these forces [27], where F_s is the force due to the squeezed oil, F_p is the force due to the pressure, and F_f is the friction force.

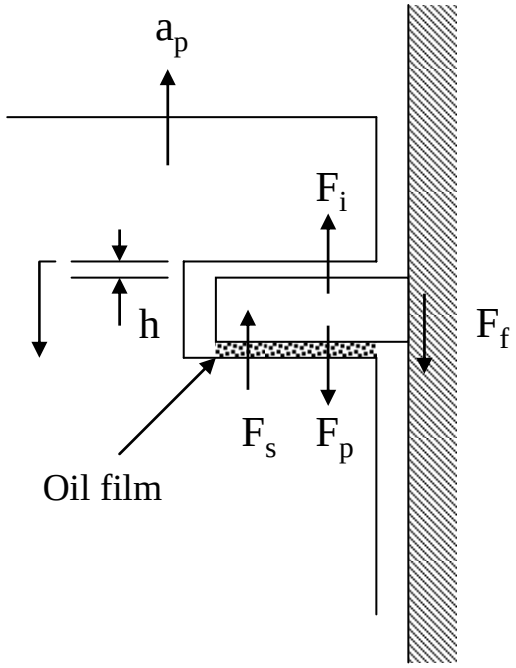

Figure 5.3 Forces acting on the ring [27]

The dynamic equilibrium of the forces acting on the ring is given by the following equation:

$$M.\frac{d^2h}{dt^2} + M.a_p = F_p + F_f - F_s \qquad (5.1)$$

where *M* is the ring mass, *h* is the relative position of the ring inside the groove (Fig. 5.3), a_p is the acceleration of the piston. In the left hand side, the first term represents the force due to the relative acceleration of the ring with respect to the piston; the second term is the force due to the acceleration of the piston. The forces of the right hand side are as described above.

In Eq. 5.1, all the terms can either be calculated directly or predicted from correlations available in the literature with very good accuracy except *Fs*. The force due

to the resistance of the squeezed oil (F_s) is difficult to predict accurately. The oil film thickness, the pressure distribution inside the oil film and the boundary conditions of the equations that govern its behavior are very difficult to estimate. An under-or-over estimation of F_s could result in significant error during the calculation of the mass flow that returns to the cylinder. Therefore, in the present work a different approach for the ring motion was taken. The ring position was governed by the net pressure force acting on the ring. When the net pressure force on the ring changes direction the ring changes position instantaneously, going from one side of the groove to the other. This approach has been successfully used in previous works [30, 34]. The success of the model may be due to the low influence of the friction and the oil resistance forces in the overall force balance, i.e. the pressure and inertial (in less degree) forces are the dominant forces, while the friction and oil resistance forces are relatively small [27]. The latter forces are significant only during a small part of the intake and exhaust process where the gas pressures on either side of the ring are small, thus no significant mass of mixture leaves the ring pack due to this problem [90].

Considering the simplification of the ring pack motion described above, the gas flow in the ring pack was modeled as the flow through connected volumes. These volumes are connected each to other by the ring end gap, which restricts the flow from one volume to another (see Fig. 5.4).

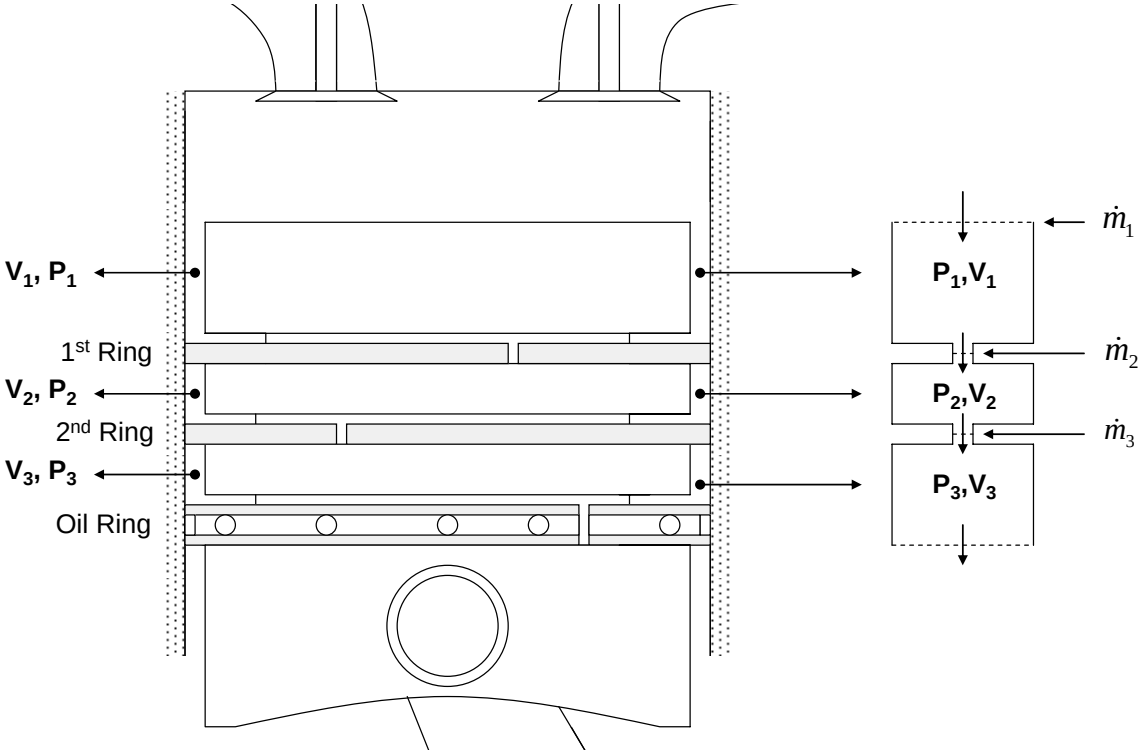

Figure 5.4 Ring pack crevices (left) and its representation as a system of interconnected volumes (right)

In Fig. 5.4, the pressure in each volume is considered uniform due to the small pressure drop across the volume (it has been shown that the pressure drop in the top land crevice is only 0.1-0.2% [27]). Thus, the first volume pressure (P_1) is considered to be the same as the cylinder pressure. In the same way, the pressure in the volume 3 (P_3) is considered equal to the crankcase pressure; this is due to the negligible resistance to the gas flow of the oil ring. Both the measured crankcase and the cylinder pressure were used to calculate the mass flow rates through the ring pack.

A very important consideration is the nature of the heat transfer process of gas that flows in the ring pack. Measurements carried out by Furuhama and Tada [91] show

that the gas temperature inside the top land crevice reaches very quickly the top land piston temperature. The explanation of their results was that the heat transfer coefficient is very large, and that it is comparatively higher than the coefficient that characterized the heat transfer between the combustion gases and the cylinder wall. A more recent investigation of the ring pack crevice flow [27], studied the nature of the flow in a stationary crevice of adjustable volume inserted in the cylinder head of an engine. The crevice volume was similar to the ring pack crevice and it was connected to the combustion chamber through a small orifice with dimensions of the order of the ring end gap. The flow through this crevice was simulated considering the flow as adiabatic and then isothermal. The results of this simulation were compared with the measured pressure. It was observed that the isothermal flow predicted very accurately the measured crevice pressure along the cycle. The authors estimated that the gas mixture takes approximately 2 CA degrees to reach the wall temperature [27]. Therefore, based on these results in the present model an isothermal flow was considered.

As indicated above, the gas temperature inside the crevices are similar to the piston wall temperature. However, the piston temperature is difficult to measure; therefore it has been approximated to the cylinder wall temperature as in previous works [26, 27, 92, 93]. This assumption provides accurate results because the piston and cylinder wall temperature do not differ significantly [91]. For all the simulations a temperature of 385 K was considered.

In the model a mass conservation equation is applied to each crevice volume. And the gas flow through the ring end gap was approximated as the flow through an orifice, which follows the equation:

$$\dot{m} = C_D A \rho c \eta \tag{5.2}$$

where:

$\dot{m}$ = mass flow through the orifice,

C_D = discharge coefficient

A = effective end gap area

ρ = density of the gas

c = speed of the sound in the gas

η = compressibility factor

It is important to mention that the effective end gap area is the area of the free passage between the cylinder wall, the ring end gap, and the edge of the groove. The compressibility factor depends of the flow regime; if the flow is subsonic the compressibility factor is given by:

$$\eta = \left(\frac{2}{\gamma - 1} \left[\left(\frac{P_d}{P_u} \right)^{2/\gamma} - \left(\frac{P_d}{P_u} \right)^{(\gamma+1)/\gamma} \right] \right)^{1/2} \tag{5.3}$$

where:

γ = specific heat ratio of the gas

P_u = upstream pressure

P_d = downstream pressure

In equation (5.3) $P_u > P_d$. When the ratio $P_d / P_u < 0.52$, the flow is choked, and the compressibility factor is calculated by the following expression:

$$\eta = \left(\frac{2}{\gamma + 1} \right)^{\frac{\gamma+1}{2(\gamma-1)}} \tag{5.4}$$

Mass conservation on each volume is enforced by the following equation that allows the calculation of the mass flow and the pressure at each time step:

$$\frac{dP_i}{dt} = \left(\dot{m}_i - \dot{m}_{i+1} \right) \frac{RT}{V_i} \tag{5.5}$$

In equation (8)

V_i = crevice volume

P_i = pressure in the volume

T = temperature of the gas

t = time

R = gas constant

$\dot{m}_i$ = mass flow into the volume i

In Eq. 5.2, a representative value for the discharge coefficient is necessary. Early experiments [91] performed under static conditions for several effective ring gap areas, temperatures and upstream pressures determined that the discharge coefficient does not change significantly with pressure, temperature and ring gap. The fluctuation of the discharge coefficient was between 0.8-0.9. They recommended that the average value of 0.86 should be used. In the present work a value of 0.85 was used to be consistent with the value used in previous works [30, 34]. The Equations (5.2) and (5.5) were integrated using the first order Euler method. An initial guess for the pressure P_2 was given and the equations were iterated until the difference $P_2(CA=-180)- P_2(CA=540)$ was below 10^{-5}. The model was implemented in Matlab and the script is given in Appendix XIII.

5.2.3 RING PACK GEOMETRICAL DIMENSIONS

The dimensions of the cylinder, piston and rings were obtained from the manufacturer and are proprietary information, therefore they cannot be disclosed. However, typical dimensions of the ring pack geometry of small engines described in the schematics in Fig. 5.1, 5.2 and 5.3 are given in the Table 5.1. The geometrical dimensions allowed the calculation of the different volumes and the ring gap effective areas. The effect of the temperature on the deformation of these parameters was not considered in the analysis.

Table 5.1 Ring pack dimensions

Volume	Land height (mm)	Groove height (mm)	Volume (cm^3)	Ring end gap (mm)
1	4.00	1.50	0.495	0.43
2	3.00	1.50	0.416	0.46

5.2.4 SAMPLE OF PREDICTED RESULTS FROM THE RING PACK MODEL

The ring pack model provided information about the pressure, relative ring position, mass flow rate going into and leaving each volume, and the net mass that goes to the crankcase (blowby). In Fig. 5.5 the history of the pressures in the top land crevice volume V_1, the inter-ring volume V_2, and the crankcase pressure are shown. The pressure P_1 is the same as the cylinder pressure and was used as an input for the model. Similarly the pressure P_3 is the measured crankcase pressure and it was used as input for the model, as well. The pressure P_2 is the pressure predicted by the model. Several important observations can be made from Fig. 5.5. First, the maximum in cylinder pressure ($P_{1,max}$ = 2036 kPa) is greater than the maximum inter-ring pressure ($P_{2,max}$ = 491 kPa); however the inter-ring maximum pressure is delayed with respect to $P_{1,\,max}$. At some point during the expansion stroke of the cycle (for this case at CA = 90.5 aTDC) the inter-ring pressure becomes greater than the cylinder pressure. This condition indicates that the first ring moves from the lower to the upper surface of the groove and that the mass from V_2 is returning to V_1 through the top ring end gap. The crankcase pressure is greater than the inter-ring pressure and the in-cylinder pressure during the intake process. This indicates that the crankcase pressure may influence the mass of fuel that returns to volume V_2 and to the combustion chamber.

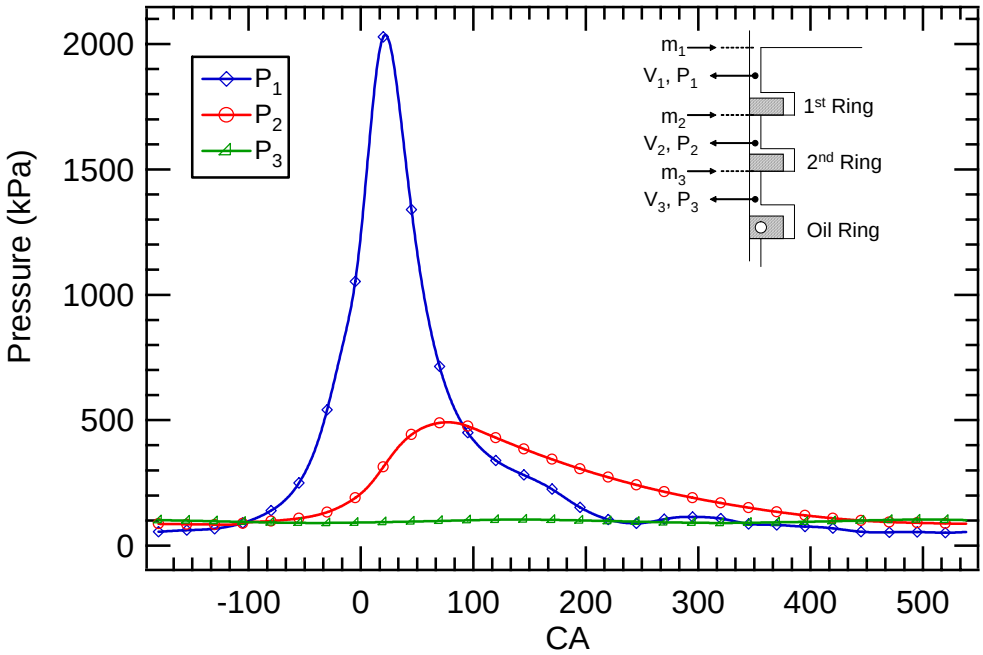

Figure 5.5 Pressure in the combustion chamber (top land crevice) P_1, in the inter-ring volume P_2 and in the crankcase P_3, for the 3060RPM, 50% Load, AF 12

The relative position of the ring inside the piston groove is shown in Fig. 5.6 for the same operating condition as Fig. 5.5. The ring is seen to move inside the groove, from one side to the other, when the net force on the ring changes its direction. The results in Fig. 5.6 show this behavior and give a better indication of the pressures acting on each side of the ring. For the first ring, it can be seen that the inter-ring pressure is higher than the cylinder pressure along the major part of the cycle. The cylinder pressure overcomes the inter-ring pressure only during part of the compression and exhaust strokes. On the other hand, for the second ring, Fig. 5.6 indicates that the inter-ring pressure is greater than the crankcase pressure for the major part of the cycle. The crankcase pressure is higher than the inter-ring pressure only during part of the intake and compression process. Indicating that certain mass of mixture can return from the crankcase to the inter-ing volume and then to the cylinder.

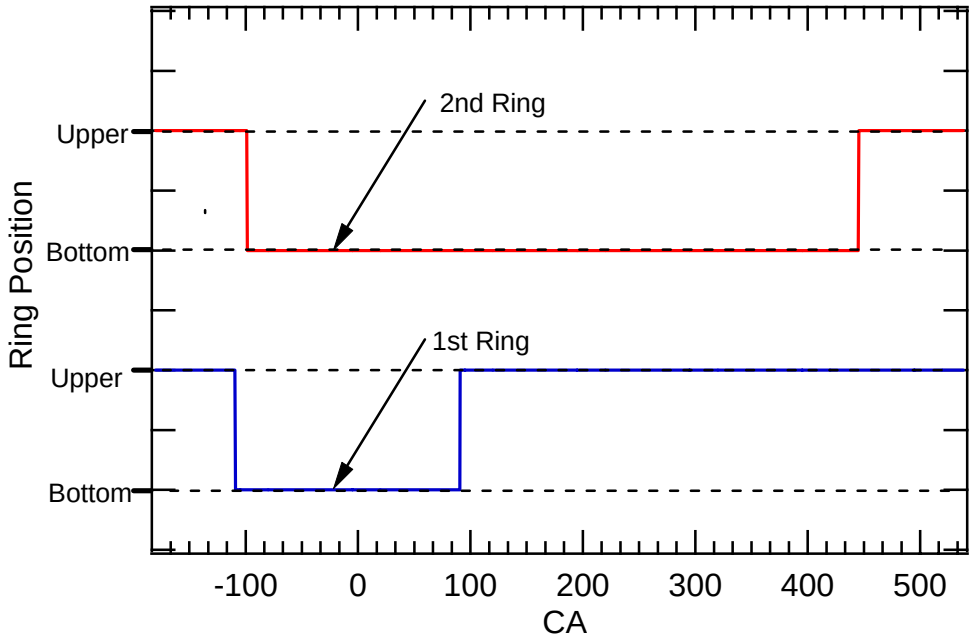

Figure 5.6 Relative position of the ring within the piston groove for the 3060RPM, 50% Load, AF 12

In the study of the HC emissions, the most important information obtained from the model is the mass of mixture that returns to the cylinder. Therefore the instantaneous mass flow rates across: the entrance of the top land crevice (m_1), the first ring end gap (m_2), and the second ring end gap (m_3) were calculated. The ring pack schematic in the right side of Fig. 5.7 shows these sections. In Fig. 5.7 a positive mass flow indicates that the mass is flowing with a direction towards the crankcase, and a negative value indicates that the mass is crossing the section with the direction towards the cylinder. The mass flow rate curve of the top land crevice (m_1) indicates that during the compression stroke the mass is flowing from the cylinder to this volume. Initially the flow rate is small, however as the in-cylinder pressure is increased the mass flow rate increases until it reaches its peak value. This peak is approximately 4.59 g/s and it occurs at

approximately 6 CA degrees aTDC. This is a little bit earlier than the peak pressure which occurs at 21.5 CA degrees aTDC. After the cylinder reaches the peak pressure the flow crossing the section of the top land crevice (m_1) reverses and the mass stored starts to return to the cylinder. The discontinuities observed at 109 CA bTDC and 90.5 CA aTDC are because of the change in position of the ring inside the groove (see Fig. 5.6). Similar trends are observed for the mass crossing the end gap of the first ring (m_2). The maximum mass flow rate is approximately of 0.53 g/s and it happens at the same CA of the maximum m_1. Then, at approximately 90.5 CA aTDC the flow across the first ring is inverted.

The maximum mass flow rate through the second ring end gap (m_3) is of 0.130 g/s and it happens at approximately 77 CA aTDC, and the flow inversion happens at 445 CA aTDC. Figure 5.7 provides excellent information of the nature of the flow through the different sections of the ring pack. However, a better visualization of the ring pack contribution is given by the normalized cumulative mass results. Figure 5.8 shows the cumulative mass of mixture (Fig. 5.8 (a)) and the cumulative mass of fuel (Fig. 5.8 (b)) normalized by the mass of mixture and mass of fuel trapped in the cylinder, respectively. Fig. 5.8 (a) shows that for the 3060 RPM, 50% load, AF 12 condition approximately 4.33% of the trapped mass is stored in the ring pack crevices escaping the main combustion. The mass that goes through the first and second ring is around 0.95 % and 0.82% respectively. The results in terms of percent of mass of fuel are shown in Fig. 5.8 (b), showing similar cumulative mass values than the show in terms of mass of mixture. This manner of presenting the results is more intuitive for the study of the HC emissions.

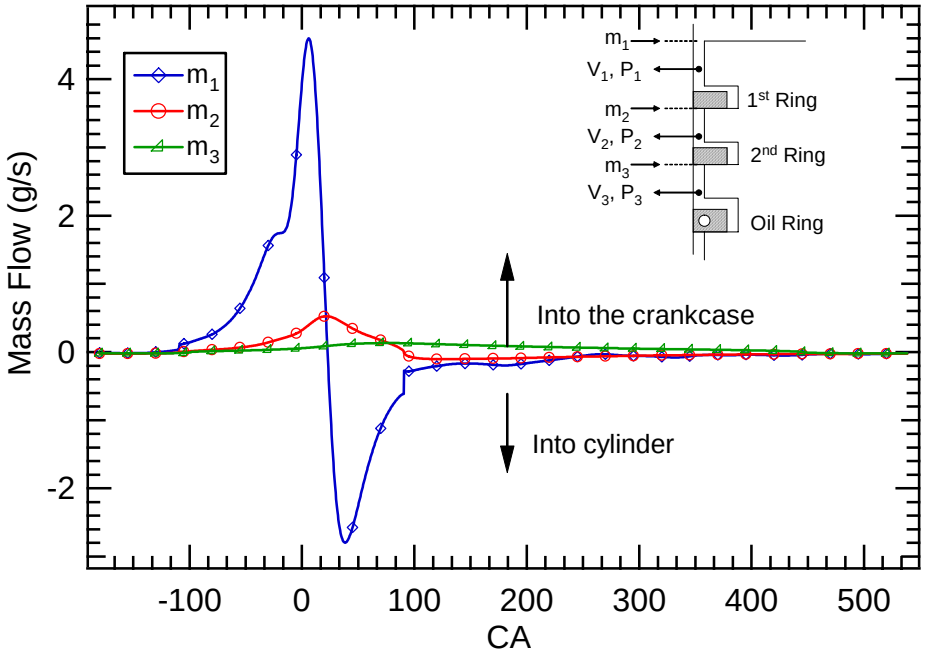

Figure 5.7 Mass flow rates crossing the entrance of the top land crevice (m_1), the first ring end gap (m_2), and the second ring end gap (m_3), for the 3060RPM, 50% Load, AF 12.

a)

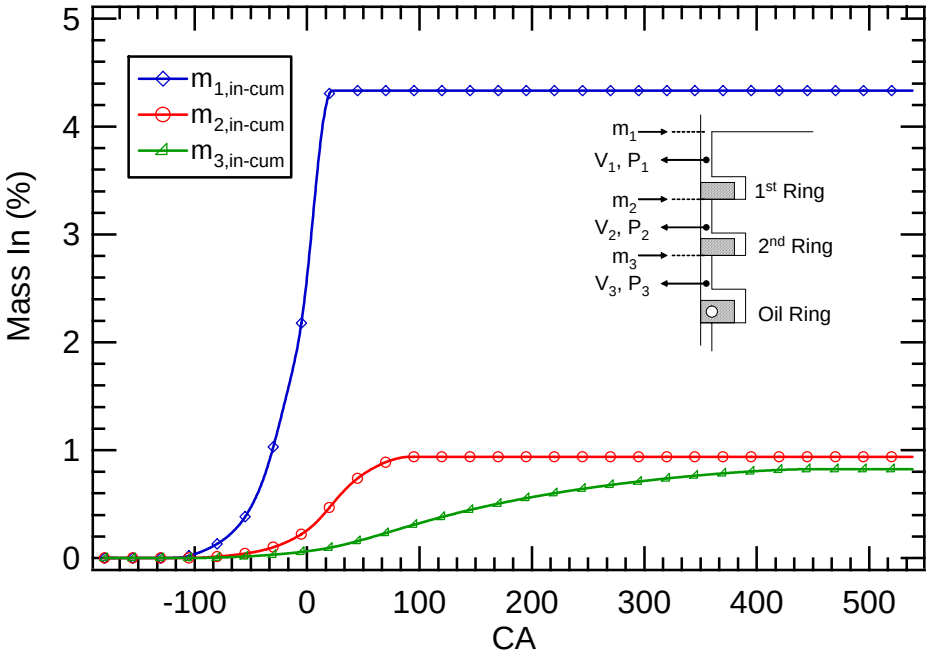

b)

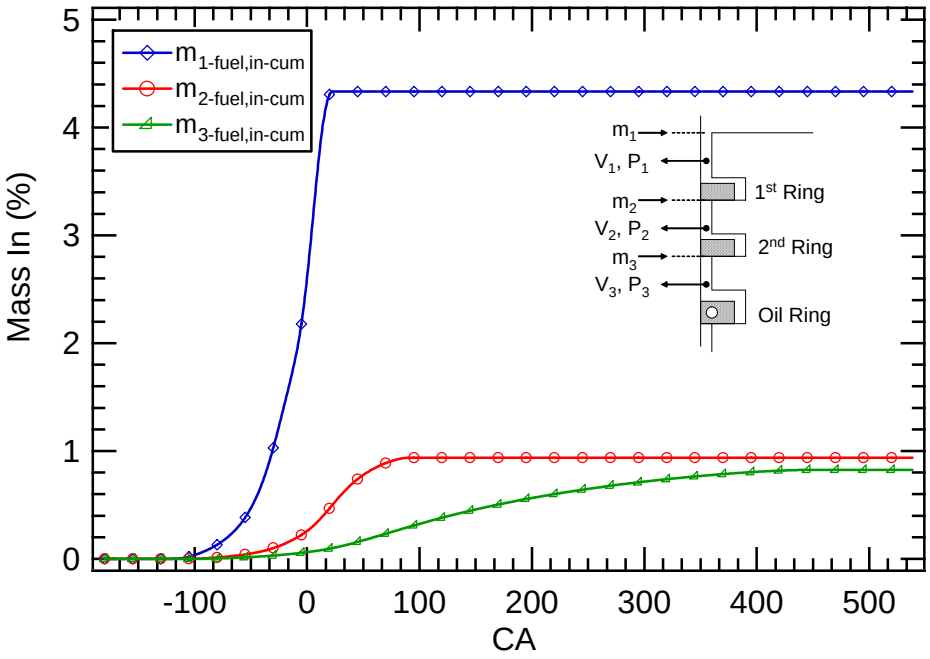

Figure 5.8 Percent of the total mass of mixture (a) and fuel (b) trapped in the cylinder that crosses the entrance of the top land crevice (m_1), the first ring end gap (m_2), and the second ring end gap (m_3) that goes into the volumes V_1, V_2, and V_3 respectively for 3060RPM, 50% Load, AF12.

Part of the mixture that is stored in the ring pack crevices returns to the cylinder. The remaining contributes to the blowby. As shown in Fig. 5.7, after the peak pressure in the top land crevice is achieved a significant amount of mixture returns to the combustion chamber. This returning mass has a significant effect on the HC emissions. Fig. 5.9 (a) shows the percent of mass trapped in the cylinder that returns to the combustion chamber ($m_{1,out\text{-}cum}$). The mass that returns to the top land crevice through the first ring end gap ($m_{2,out\text{-}cum}$), and the mass that returns to the inter-ring volume through the second ring end gap ($m_{3,out\text{-}cum}$) are also shown in Fig. 5.9 (a). The results show that approximately 3.57% of the mass trapped return to the cylinder. This indicates that an 86.6% of mass that escapes the main combustion in the ring pack crevices returns to the cylinder. The difference between the mass that goes into the top land crevice and the mass that goes out to the cylinder (0.76% of the total mass) goes to the crankcase as blowby. It is important to indicate that for the operating condition shown in Fig. 5.9, approximately 76% of the stored mass returns to the cylinder before EVO. The remaining mass returns to the cylinder during the exhaust and intake processes. The results normalized as a function of the mass of fuel trapped in the cylinder are shown in Fig. 5.9 (b), as well. As expected the trends and percent of fuel that return to the cylinder follow the same trend of Fig. 5.9 (a).

Finally, the model provided the cumulative fraction of trapped mass that went to the crankcase as blowby. These results are shown in Fig. 5.10, where it can be seen that approximately 0.76% of the total trapped mass goes to the crankcase as blowby. The calculated blowby was compared with the measured blowby to verify the accuracy in the predictions. The results of this verification are described below in next section.

a)

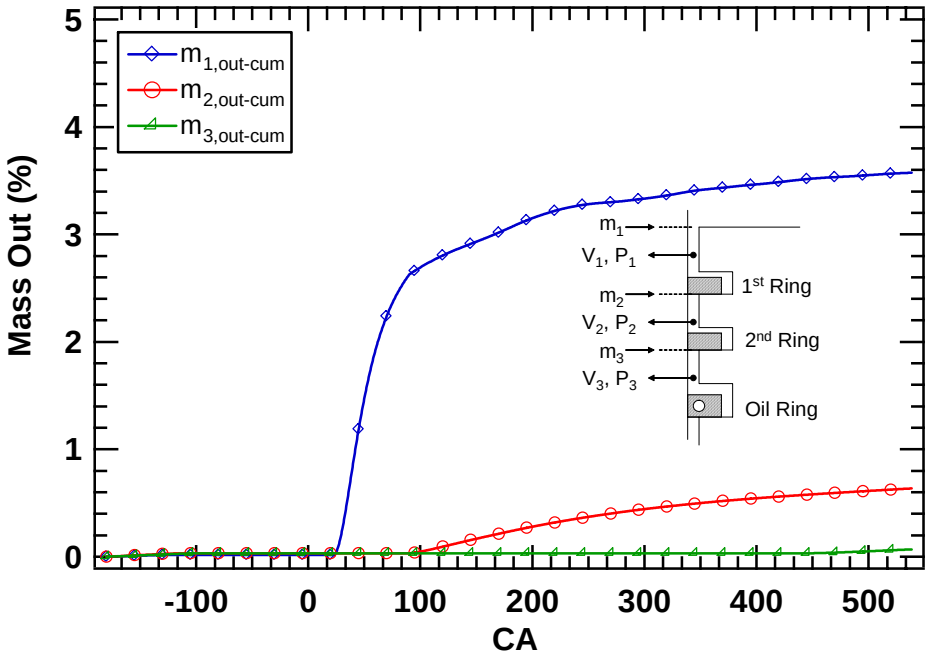

b)

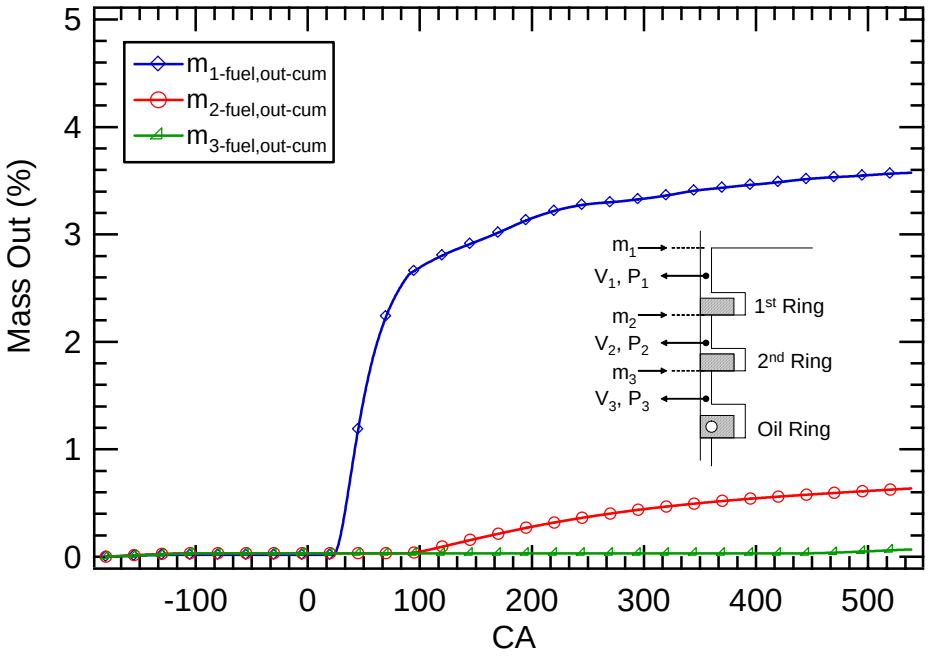

Figure 5.9 Percent of the total mass of mixture (a) and fuel (b) trapped in the cylinder that crosses the entrance of the top land crevice (m_1), the first ring end gap (m_2), and the second ring end gap (m_3) that leaves the volumes V_1, V_2, and V_3 respectively for 3060RPM, 50% Load, AF12.

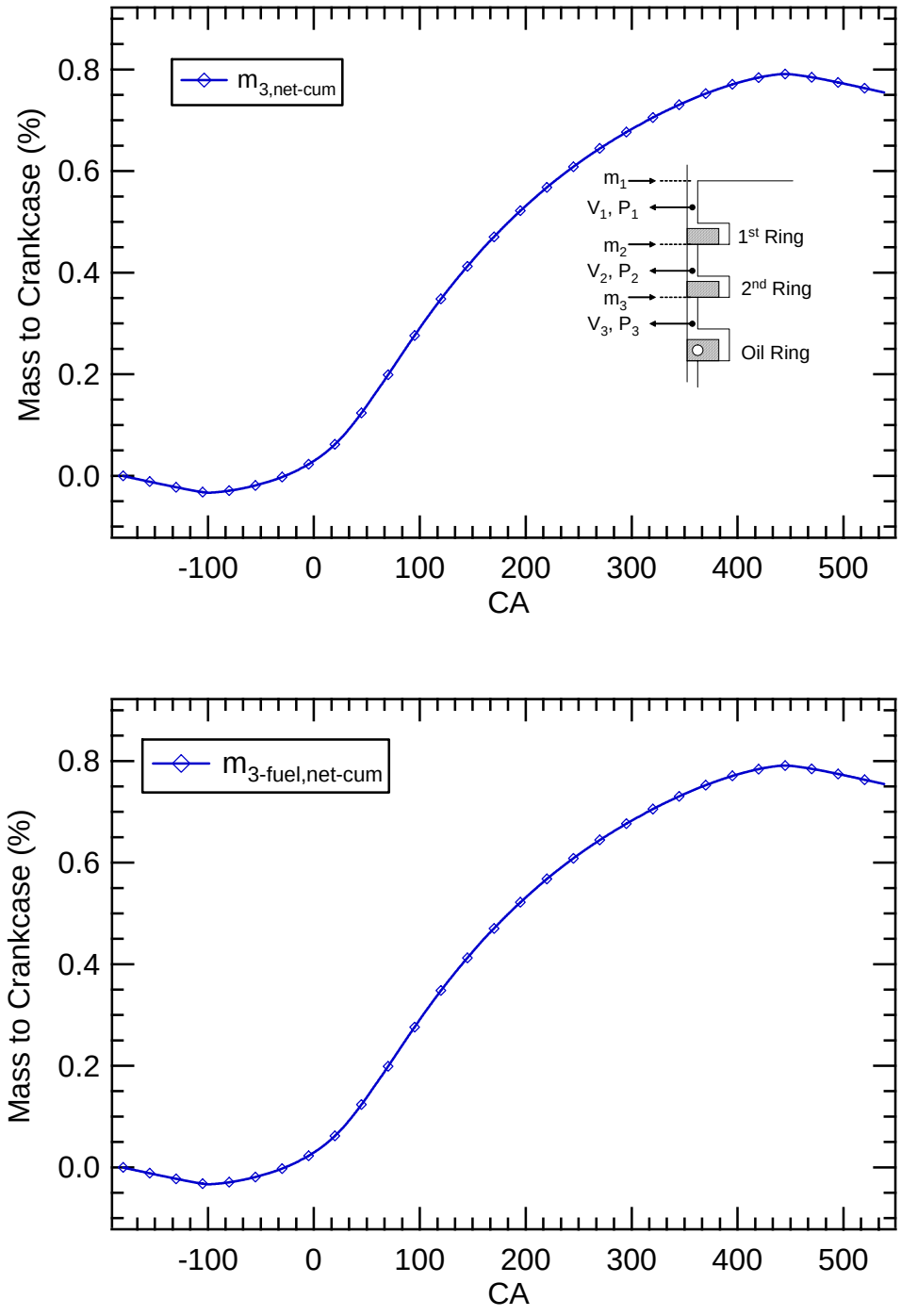

Figure 5.10 Percent of the total mass of mixture (a) and fuel (b) trapped in the cylinder that crosses the second ring end gap (m_3) that goes to the crankcase as blowby for 3060RPM, 50% Load, AF12.

5.2.5 VALIDATION OF THE RING PACK MODEL

To validate the model, blowby measurements were carried out. A flowmeter was installed on the breather element of the crankcase (see section § 3.2.7, Fig. 3.9), and the blowby was measured for all of the tested conditions. The simplified ring pack model has been successfully used in the past for automotive engines [30, 34] at low speeds, but the present study includes higher speeds where ring dynamics may be important. The significant bore distortion typical of a small engine operation could also influence the ring pack model predictions. Figure 5.11 shows the blowby comparison for all of the tested conditions. It can be seen from this figure that there is a very good agreement between the model and the experimental results; both follow the same trend, and are close in magnitude. The results show that, in general, the blowby is under-predicted by the model, being more notorious at low load were the model predicts values of up to 50% lower than the measured. At high load the model predicts better results were a difference of about 27% is observed. Similar errors in the blowby prediction were obtained by Kuo *et al* [90] using the ring pack model including the ring dynamics suggested by Namazian and Heywood [27] and with an in-house ring-friction model. It is important to mention that the results of Fig. 5.11 were obtained using the geometrical dimensions under cold conditions provided by the manufacturer, and the only parameter that was tuned to match the blowby was the first ring end gap. This was opened up to the upper allowable value as specified by the manufacturer to obtain the results shown in Fig. 5.11. It is expected that during the engine operation this dimensions may change due to thermal expansion.

However, despite the differences, the results give confidence in the use of the simple model for estimation of the amount of mass stored in the ring pack crevices.

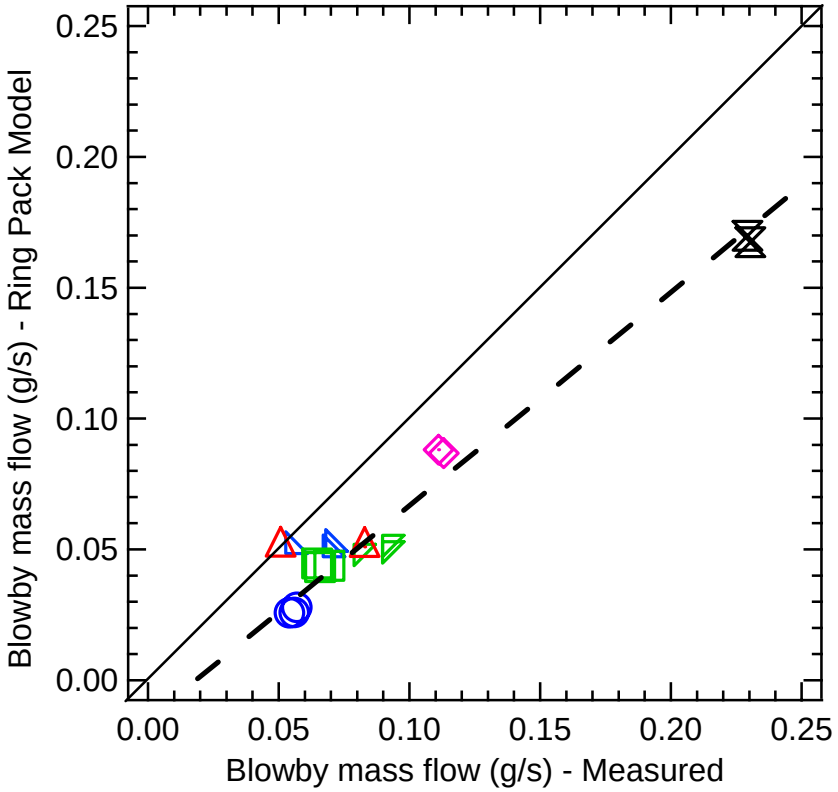

Figure 5.11 Blowby mass flow comparison between experimental and ring pack model results. The different symbol shape represents a given speed-load condition from Table 5.2.

5.2.6 SENSITIVITY ANALYSIS

The response of the model to several geometrical parameters of the ring pack was assessed through a sensitivity analysis. The objective was to evaluate whic input parameters had the largest impact on the results. This was necessary due to the uncertainty of some input parameters. As mentioned above, the dimensions given in

Table 5.1 correspond to the cold conditions. It is expected that these dimensions will change during the engine operation due to thermal expansion. In addition there was not accurate information about the piston wall temperature or discharge coefficient.

The model was tested against the measured blowby. All the changes in the considered variables were with respect to the baseline values given in Table 5.1. The changes were taken as the uncertainty in the variable's value and they are shown in Table 5.2. These values are typical for the type of engine under study. The relative sensitivity was calculated as follows:

$$\textit{Relative Sensitivity (\%)} = \left(\frac{d\dot{m}}{dx}\right)\frac{\Delta x_{uncer}}{\dot{m}_{ref}}.100 \qquad (5.6)$$

where $\frac{d\dot{m}}{dx}$ is the rate of change of the blowby with respect to the parameter x. Δx_{uncer} and $\dot{m}_{ref}$ are the uncertainty in the parameter x and the reference blowby respectively. This is a different definition of the conventional definition of relative sensitivity [94], which is defined as follows:

$$\textit{Conventional Relative Sensitivity} = \left(\frac{d\dot{m}}{dx}\right)\frac{x_{ref}}{\dot{m}_{ref}}. \qquad (5.7)$$

where x_{ref} is the value of the reference parameter. Eq. (5.7) provides an insight about how parameters that affect the blowby; however, in the present application some parameters, such as the cylinder diameter, do not change significantly i.e. the value is known with

good accuracy. Therefore, a more fair comparison of the effect of the parameters on the blowby is provided by Eq. 5.6.

Table 5.2 Parameters changed in the sensitivity analysis

Parameter x	**Units**	**Uncertainty** Δx_{uncer}
EG-RI	mm	0.25
EG-RII	mm	0.21
dcyl	mm	0.025
h1	mm	0.2
d1L	mm	0.014
d1U	mm	0.03
h2	mm	0.02
di2	mm	0.2
wRI	mm	0.52
hRI	mm	0.026
h3	mm	0.1
d3L	mm	0.014
d3U	mm	0.014
h4	mm	0.02
di4	mm	0.2
wRII	mm	0.52
hRII	mm	0.033
C_D	-	0.1
Twall	K	165
Pcrk_offset	kPa	60

Figure 5.12 shows the relative sensitivity of the model to all of the variables of interest. As it can be seen in Fig. 5.12 the most sensitive parameters controlling the blowby are the ring end gaps (EG-RI and EG-RII), the diameter of the cylinder (dcyl), the width of the first and second ring (wRI and wRII), the discharge coefficient (C_D), the wall temperature (Twall); and the crankcase offset (Pcrk_offset).

a)

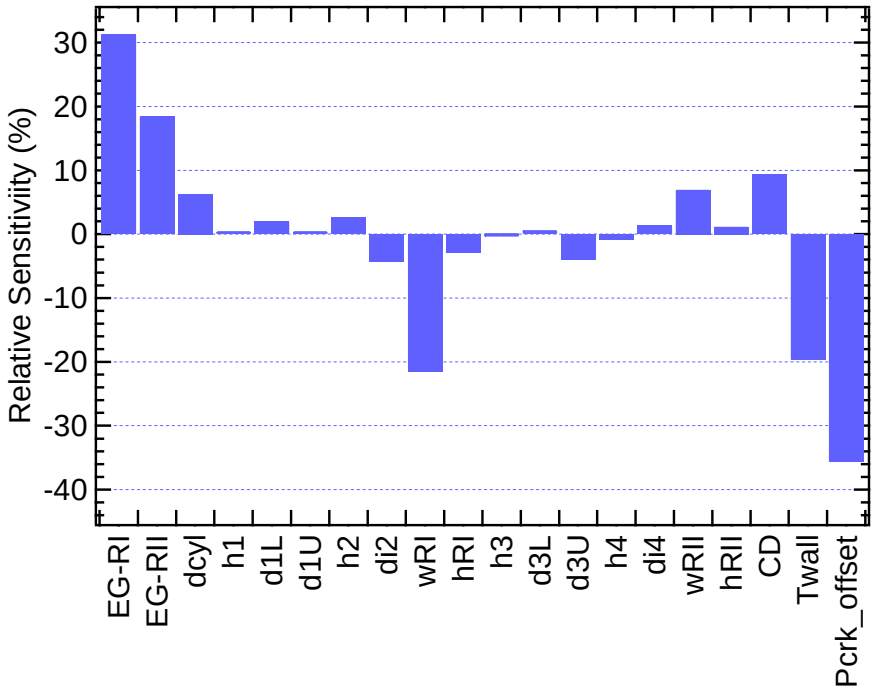

b)

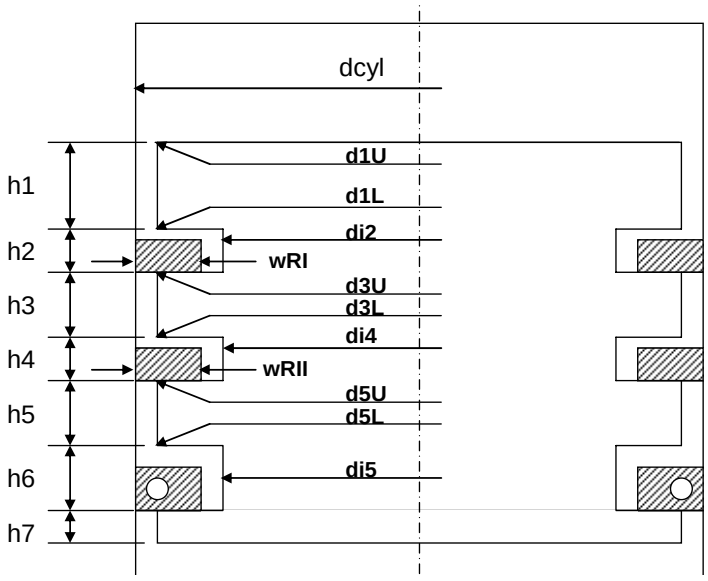

Figure 5.12 (a) Sensitivity of the blowby to several parameters, and (b) definition of the geometric parameters. EG-RI, and EG-RII stand for end gap of first and second ring respectively. C_D is the discharge coefficient, Twall the temperature of the wall in the model, and Pcrk_offset the offset in crankcase pressure.

The relative change in the ring gap does significantly change the blowby (up to 30% increase for the first ring). In a fully warmed-up engine, the ring gap could change, impacting significantly the blowby. The parameter that makes the greatest impact in the model is the crankcase pressure (up to 35% change). This is because the mass flow towards the crankcase is restricted by the crankcase pressure, especially during the period when the inter-ring pressure (P_2) is small. It is important to mention that no geometrical changes in the hardware were made to verify the dependence of the geometrical parameters on the measured blowby. The results of Figs. 5.11 and 5.12 were very useful to see how accurately the model predicts the blowby, and to have an idea of the degree of sensitivity of the model predictions. However, the estimation of the mass that returns to the cylinder is more important in the present analysis, because it directly affects the engine-out HC emissions. Therefore, a sensitivity analysis for the mass that returns to the cylinder was performed considering the changes shown in Table 5.2 and using Eq. 5.6. The results are shown in Fig. 5.13. It is important to clarify that these changes represent increments in the independent variable and the results are the mass returning to the combustion chamber. The results show that the mass returning to the cylinder is affected in a different way than the blowby. This is expected because the parameters that dominate their behaviors are different. The main parameters that affect the mass flow out of the top land crevice are: the ring end gaps (EG-RI and EG-RII), the diameter of the cylinder (dcyl), the top land height (h1), the first groove internal diameter (di2), the width of the first ring (wRI), the height of the first ring (hRI), the wall temperature (Twall), and the crankcase offset (Pcrk_offset). As it can be seen the geometrical parameters that have

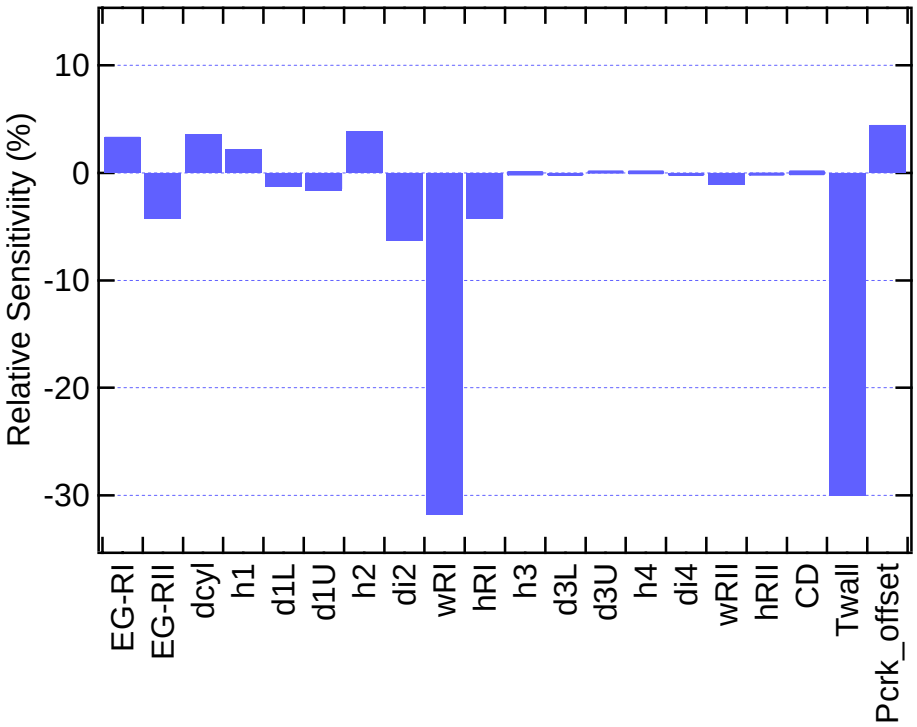

Figure 5.13 Sensitivity of the mass that returns to the cylinder to several parameters. EG-RI, and EG-RII stand for end gap of first and second ring respectively. C_D is the discharge coefficient, Twall the wall temperature in the model, and Pcrk_offset the offset of the crankcase pressure.

significant effect are the ones that increase the volume of the top land crevice. The wall temperature plays a significant effect, because it has a direct effect on the mass stored in the crevices. The effect of the discharge coefficient appears to be negligible. This results show that the predicted results should be expected to be within 30-40% of error.

5.3 TRANSPORT OF MASS RETURNING TO THE CYLINDER AND ITS CONTRIBUTION TO THE HC EMISSIONS

The transport process of the mixture stored in the ring pack crevices back into the cylinder is very complex and plays an important role in the extent to which the mixture will contribute to the engine-out HC emissions. Experimental observations [27, 29] show that as the piston moves downward during the expansion stroke a thin layer of hydrocarbons is formed along the wall due to the outflow of the HC stored in the ring pack. This begins immediately following the time that the cylinder has reached peak pressure and the out-gassing process continues until the exhaust valve is closed (see Fig. 5.7). Depending of the combustion phasing, a fraction of the mixture returns to the cylinder before the flame arrival to the cylinder wall. This mass is oxidized during the main combustion when the flame reaches and quenches on the cylinder wall. After the flame arrival, the crevice mass continues returning to the cylinder forming a layer on the cylinder wall. The transport of this HC mass to the bulk mass of the cylinder is an important process because it influences the post-flame oxidation process.

Two main transport mechanisms of the crevice outflow were described schematically by Lavoie *et al.* [83]. The first one consists in an entrainment into the bulk gases as they leave the crevices during the blowdown process mainly due to the diffusion process. The second mechanism is the roll-up vortex produced by the piston when it scrapes the HC layer off the cylinder wall. Not all of the combustible mixture that escapes the main combustion contributes to the engine-out HC emissions. Depending on the engine operating condition a significant quantity of this mixture can be partially

oxidized during post-flame processes, reducing its contribution to HC emissions. The extent of post-flame oxidation depends on the time available, the mixing rate of the unburned mixture into the hot burned gases, the availability of oxygen, and the temperature (>1500 K [30, 32]). It is believed that most of the HC that leave the ring pack are oxidized [30, 34].

From the discussion above, the ring pack crevice contribution to engine-out HC emissions was evaluated using two metrics. In the first metric the mass stored in the top piston land at the peak cylinder pressure was considered to escape the main combustion. This value, $m_{crev,max}$, is given as:

$$m_{crev,\max} = \frac{P_{cyl,\max} V_{crev}}{R T_{wall}} \tag{5.8}$$

where V_{crev} is the volume above the top ring, $P_{cyl,\max}$ is the maximum cylinder pressure, and T_{wall} is the piston wall temperature. The second metric considered that only mass that leaves the ring pack crevices after the flame propagation period contributes to engine-out HC emissions, *i.e.* the integration of the HC mass flow rate from the time that the cumulative mass fraction burn reached 90% (CA90) to the time when the exhaust valve closes (EVC) [34],

$$m_{CA90-EVC} = \int_{t_{CA90}}^{t_{EVC}} \dot{m}_{out-crev} dt \tag{5.9}$$

where t_{CA90} and t_{EVC} are the times of CA90 and exhaust valve closing.

a)

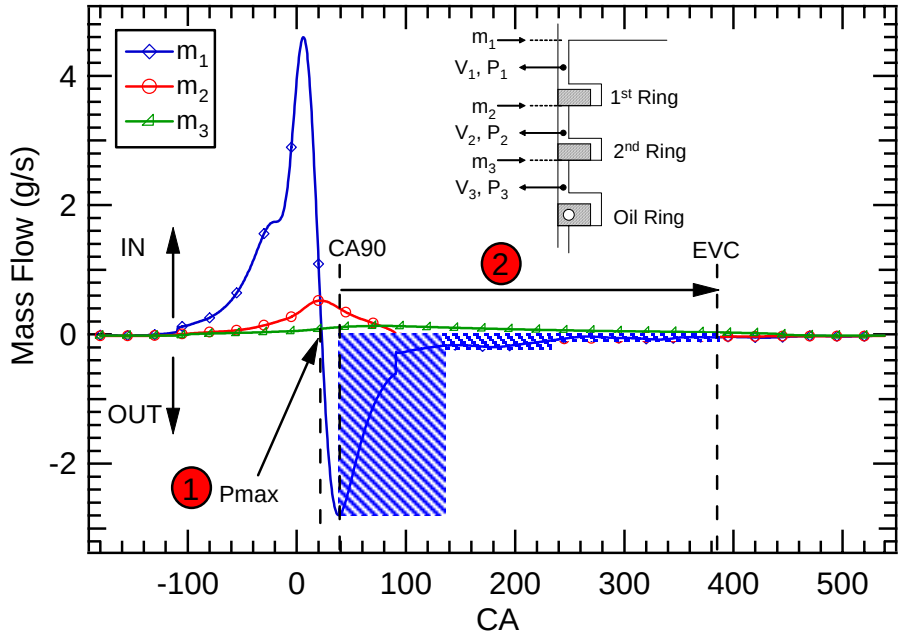

b)

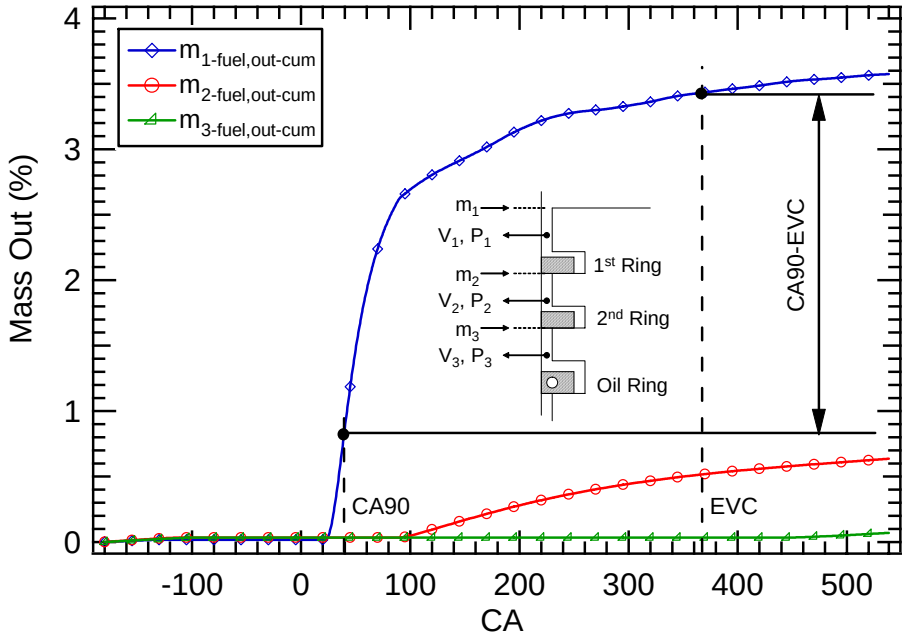

Figure 5.14 Illustration of the two metrics used to estimate the ring pack contribution to the HC emissions. (a) Mass flow rate, and (b) cumulative mass for 3060 RPM, 50% load, AF12.

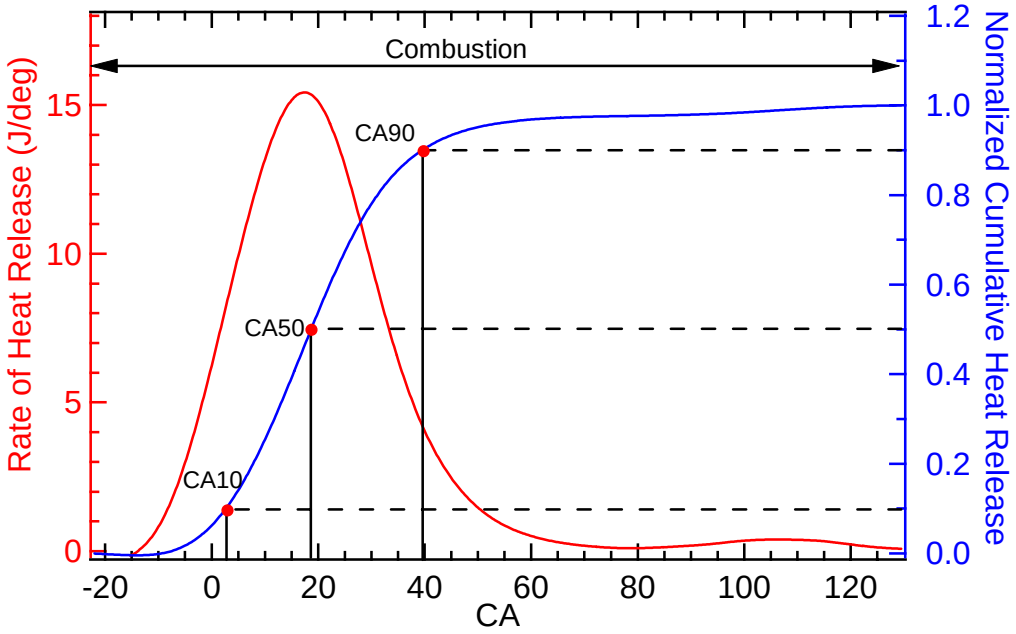

Figure 5.15 Rate of heat release and cumulative heat release diagram showing the convention to characterize the combustion phasing for 3060 RPM, 50% load, AF12.

The second method was considered to be more realistic since it assumes that the outflow of HC mass from the ring pack crevices before the flame reaches the cylinder walls is consumed by the flame. The two metrics are illustrated in Fig. 5.14, and the convention for the combustion phasing is shown in Fig. 5.15. The ring pack model was integrated with the heat release to obtain the CA90 in order to carry the mass integration from CA90 to EVO (see Appendix XIV). The mass stored in the crevices was considered to be fresh mixture, with temperature equal to the piston wall. No penetration of burned mixture in the sections of the crevices behind the flame front was considered because the nature of the flame propagation inside the combustion chamber is random and generally unknown. Thus, the assumption of any geometric shape could lead to results that are not

realistic. This results in over-prediction of the total ring-pack crevice HC contribution by the model.

5.4 RESULTS

In the following discussion, the results will be reported as the fuel-specific emission index of HC (EIHC). The HC measured in the exhaust using the steady state emission bench will be denoted as $EIHC_{M,EXH}$. The calculated mass of HC returned to the combustion chamber using the ring pack model will be denoted as $EIHC_{C,RP}$. Later, another calculated HC emission index will be developed (§5.4.2.3.3.1) from the cycle-resolved HC measurements and an estimate of the instantaneous exhaust mass flow rate, and this will be denoted $EIHC_{C,MB}$. All of these measures have been performed separately for each cylinder of the engine, referred to hereafter as cylinder 1 and cylinder 2. It is important to mention that all these tests were carried out using the homogeneous mixture system. The use of the HMS system eliminated the possible influence of any liquid fuel in the ring pack, and did not affect the HC emissions, see chapter 4.

5.4.1 ENSEMBLE-AVERAGE RESULTS

An analysis using the emsemble-average pressure data is presented in this section. The results of this section provided information about the general trends of the ring pack contribution to the engine-out HC emissions. However, the discussion will start with a brief description of the average HC emissions and IMEP for all the engine operating conditions. The HC emissions and their respective single-cylinder air-fuel ratio are provided in Table 5.3. From this table, it can be seen that each cylinder has a different

contribution to the engine-out HC emissions at a given operating condition. This behavior was observed in spite of the small air-fuel ratio difference between cylinders. The single-cylinder IMEP showed a similar behavior (see Table 5.4). From Table 5.4, it can be seen that at low load the IMEP of cylinder 1 is smaller than the IMEP of cylinder 2. However, at high load the behavior is reversed, *i.e.* cylinder 2 has higher IMEP than cylinder 1. The difference in HC emissions and IMEP is believed to be due to the difference of in-cylinder charging. Further discussion of these differences is given in §5.4.1.2.

Table 5.3 EIHC [g/kg-fuel] and air-fuel ratio for the test conditions. Upper number is cylinder 1, and lower number is cylinder 2.

	Speed (RPM)			1750	3060
Load	10%	AF	12.14 11.97	21.09 23.50	
			13.19 13.00	17.45 18.76	
			14.26 14.00	6.80 12.75	
	25%	AF	11.17 11.00		12.77 13.94
			12.20 12.00	18.82 17.11	10.06 11.12
			13.21 13.00	16.14 14.91	
			14.27 14.02	12.32 10.00	
	50%	AF	11.27 11.03		12.55 13.17
			12.29 12.00		8.72 8.87
	100%	AF	11.28 11.03		17.89 17.87
			12.19 12.00		14.93 13.88

Table 5.4 IMEP [kPa] for the test conditions. Upper number is cylinder 1, and lower number is cylinder 2.

	Speed (RPM)			1750	3060
Load	10%	AF	12.14 11.97	163.30 128.57	
			13.19 13.00	175.03 116.96	
			14.26 14.00	172.33 122.42	
	25%	AF	11.17 11.00		300.06 243.17
			12.20 12.00	315.10 220.13	294.86 245.70
			13.21 13.00	314.91 211.31	
			14.27 14.02	309.05 205.42	
	50%	AF	11.27 11.03		530.50 488.61
			12.29 12.00		527.02 487.24
	100%	AF	11.28 11.03		921.84 978.23
			12.19 12.00		867.46 916.68

5.4.1.1 RING PACK CONTRIBUTION TO THE HC EMISSIONS

The average pressure and emission data were used to estimate the ring pack contribution to the engine-out HC emissions. Figure 5.16, shows the estimation of the ring pack contribution to the HC emissions using the average pressure traces for all the conditions given in the test matrix (Table 4.1). These conditions span the operating range of the engine.

The data in Fig. 5.16 are presented with the steady-state measured emissions ($EIHC_{M,EXH}$) on the horizontal axis, and the estimated ring-pack contribution using the model on the vertical axis, $EIHC_{C,RP}$. Both the maximum stored ring pack mass and the integrated CA90-EVC mass values are shown. The direction in which the air-fuel ratio is reduced is indicated in Fig. 5.16 with a horizontal arrow. The air-fuel ratios were as indicated in the test matrix and can be identified in Fig. 5.16 considering that higher air-fuel ratios produced less measured HC.

The 1750 RPM and 10% load case, Fig. 5.16 (a), shows that for all of the cases investigated the ring pack estimation from CA90-EVC is less than the HC mass that is measured at the exhaust. Looking at the maximum possible contribution of the ring pack, the mass stored in the ring pack at peak pressure, it can be seen that for all the cases this value is greater than the value measured at the exhaust. The fact that the mass outflow from CA90 to EVC does not exceed the HC concentration measured at the exhaust suggests that for this condition the ring pack is not the main contributor to HC emissions and that other sources may be responsible for this inbalance. The increase in the measured HC emission with the AF is not reflected by the ring pack model. The ring pack model response to an air-fuel ratio change is smaller than the measured HC. Again, this could be due to the presence of other sources that are magnifying the measured HC response to the air-fuel ratio. The tests performed at near-stoichiometric air-fuel ratios (14:1) eliminated any possible strong influence of the rich combustion regime on the HC predictions. The absolute error associated with the ringpack model on these results is difficult to quantify.

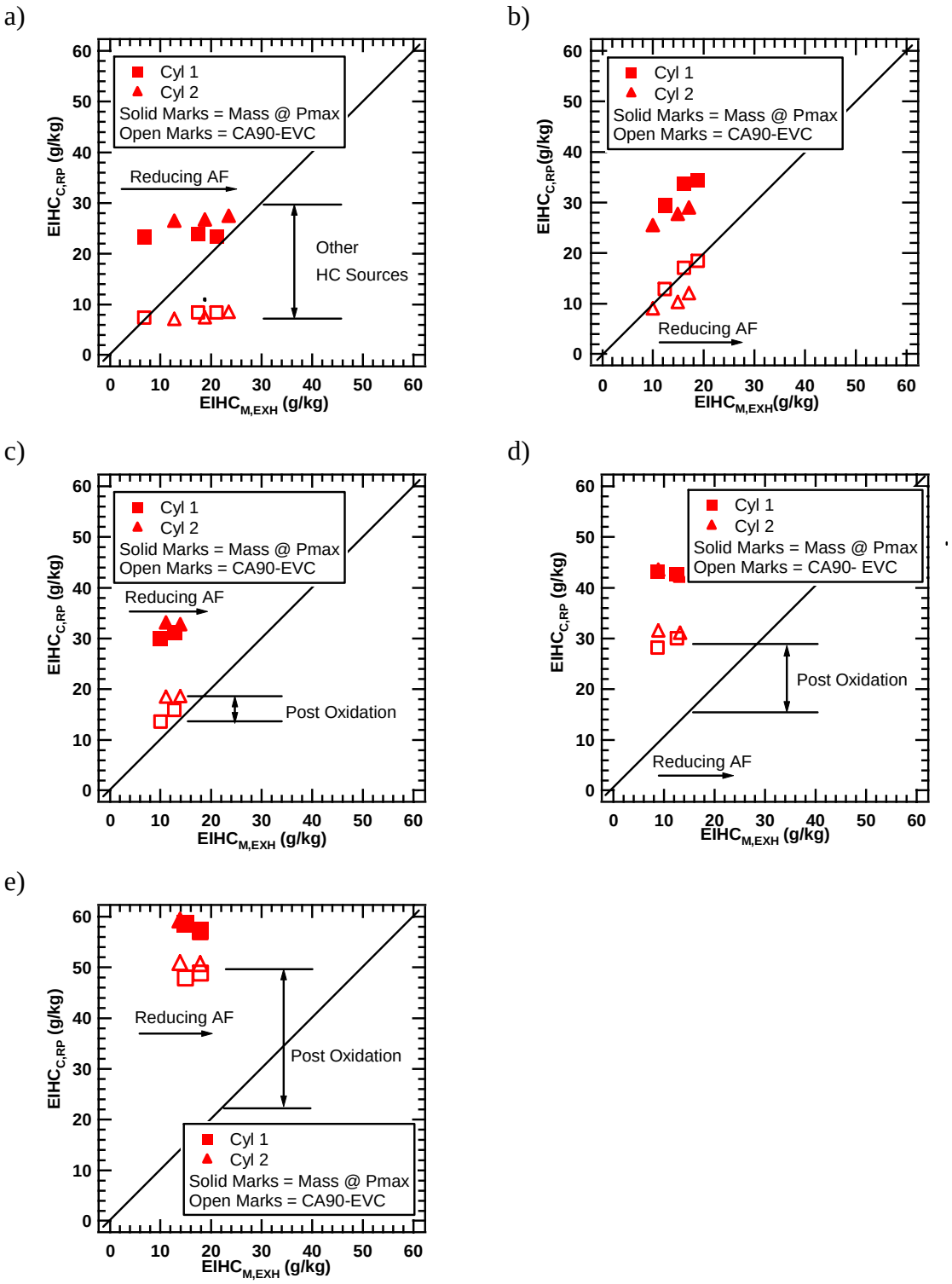

Figure 5.16 Ring pack model results for all the tested conditions, (a) 1750 RPM, 10% load, (b) 1750 RPM, 25% load, (c) 3060 RPM, 25% load, (d), 3060RPM, 50% load, (e) 3060 RPM, 100% load.

Increasing the load from 10 to 25% while keeping the engine speed at 1750 RPM, as indicated in Fig. 5.16 (b), produces an increase of the mass that leaves the ring pack from CA90 to EVC. At this condition the ring pack contribution roughly matches the measured HC at the exhaust. The mass of HC stored at maximum pressure has also been increased. This is expected because the increase of the load produces higher cylinder pressures, which increases the loading of the ring pack, increasing the stored mass of HC. The fact that at this operating condition the mass returning to the cylinder from CA90 to EVO matches the measured HC suggests that this is a limiting condition where the ring pack starts to become a significant contributor to the HC emissions. This also indicates that for this condition little or negligible post-oxidation may be taking place. Regarding the effect of the air-fuel ratio, it can be seen that for this operating condition the model shows a steeper slope than for the 1750 RPM, 10% load case. The slope appears to be of the same magnitude than of the measured HC.

As the speed is increased the ring pack contribution is increased. Thus, for the 3060 RPM, 25% load case, Fig. 5.16 (c), the mass leaving the ring pack from CA90 to EVC exceeds the value measured at the exhaust. The mass stored at peak pressure has also increased and is significantly greater than the HC measured at the exhaust. This suggests that the unburned HC mass leaving the ring pack crevice is a significant and possibly major contributor to the HC emissions. The small difference between the predicted and the measured HC can be accounted by post-oxidation. The results show that the predicted HC by the ring pack model responds in the same manner than the measured HC to the change in air-fuel ratio.

Increasing the load to 50% at the 3060 RPM engine speed (Fig. 5.16 (d)) a significant increase of the ring pack contribution is observed, for both metrics *i.e*. the ring pack mass stored at maximum pressure and the mass leaving the ring pack from CA90 to EVC. It can clearly be seen that the mass returning to the cylinder from CA90 to EVC is significantly higher than that measured at the exhaust. These results clearly indicate that at this condition the ring pack is the major contributor to the engine-out HC emissions. The air-fuel ratio effect on the model prediction is smaller than for the 3060RPM, 25% load case. However, the predicted HC is increased as the air-fuel ratio is decreased. It is important to note that the emissions index of the mass stored at maximum pressure is slightly reduced as the air-fuel ratio is reduced. This trend is different than the previous cases (Fig. 5.16 (a-c). The justification of this trend is due to the normalization of the mass stored with the mass of fuel per cycle. At this load there is a significant difference in mass injected per cycle when the air-fuel ratio is increased from 12:1 (left side cases in Fig. 5.16 (d)) to 11:1 (right side cases in Fig. 5.16(d)) , while the maximum pressure is almost identical for both cases.

If the load is further increased, as in the 3060 RPM, 100% load case, Fig. 5.16 (e), the two metrics used to evaluate the ring pack contribution to the HC show further increases. At this condition it is irrefutable that the ring pack storage prevents the oxidation of a considerable amount of fuel and there is little doubt that it is the major HC contributor. The dependence of both ring pack prediction metrics with the air-fuel ratio shows the same trend as for the 3060 RPM, 50% case. The reduction in the HC emission index at maximum pressure with the reduction of the air-fuel ratio is also observed here,

and it can be also justified due to the normalization of the maximum mass stored with the mass of fuel injected per cycle.

The increase in the ring pack contribution to HC emissions as the load is increased is the result of two phenomena. First, the loading of the ring pack crevices is increased, and second the flame reaches the cylinder walls earlier, therefore, the majority of the mass stored will contribute to the engine-out HC emissions (mass that leaves from CA90-EVC). This observation is in very good agreement with the combustion phasing obtained from the heat release analysis (Table 5.5). The difference observed between the mass that leaves from CA90 to EVC will also be affected by the post-oxidation. Table 5.5 also shows that the air-fuel ratio affects the combustion phasing, slowing the combustion as it increases. This affects the mass returning to the combustion chamber from CA90 to EVC, and together with the reduced mass of fuel in the leaner mixture case produces a decrease of the CA90 to EVC contribution.

Table 5.5 CA90 for the test conditions. Upper number is cylinder 1, and lower number is cylinder 2.

	Speed (RPM)			1750	3060
Load	10%	AF	12	92.5 96.3	
			13	94.8 104.5	
			14	103.0 106.8	
	25%	AF	11		57.3 53.0
			12	54.0 74.3	64.8 54.3
			13	58.5 83.8	
			14	72.0 92.3	
	50%	AF	11		36.3 35.5
			12		39.5 37.8
	100%	AF	11		20.5 18.5
			12		22.3 19.8

5.4.1.2 HEAT RELEASE ANALYSIS

Heat release analysis was performed in order to investigate the inability of the ring pack to explain the HC emissions at low load. The analysis of the combustion performance provided further insights. Figures 5.17-5.21 shows the rate of heat release for all the conditions of interest. It is important to mention that the analysis included the estimation of the air-fuel ratio and the mass trapped in each cylinder, which helped to improve the accuracy of the rate of heat release (see § 3.6.5 for details of the calculation).

At the low load, low speed condition, Fig. 5.17, it can be seen that neither of the cylinders complete combustion prior to EVO. For the 1750 RPM, 25% load, Fig. 5.18, the same behavior is observed; however, the degree of incomplete combustion has been decreased in comparison with the 1750 RPM, 10% load case. As expected, the air-fuel ratio affects the tail of the heat release rate. As the air-fuel ratio increases the tail of the heat release goes up, resulting in a higher level of incomplete combustion. For both loads (10 and 25%) at 1750 PRM, cylinder 2 shows more incomplete combustion prior to EVO than cylinder 1.

From Fig. 5.19, for the 3060 RPM, 25% case, the heat release analysis shows that the combustion event is finished prior EVO. This operating condition appears to be the limit where incomplete combustion is not observed. In addition, the differences in heat release between cylinders have been reduced. Still the first cylinder shows higher heat release than the second cylinder, although the difference is very small. If the load is further increased as for the 50% and 100% load cases, Figs. 5.20 and 5.21, the combustion event is clearly finished prior to EVO. For these two conditions there is no doubt that all the combustion takes place prior EVO. For the 50% load case, the heat release profile is not affected significantly by the air-fuel ratio, and both cylinders show the same heat release profile. However, for the 100% load case, cylinder 1 and cylinder 2 show different heat release profiles. At this load the air-fuel ratio does not affect the heat release profile, as well.

The above observations, suggests that at low speed, low load conditions part of the air-fuel mixture is still being oxidized during the exhaust valve opening process. As soon as the exhaust valve opens there is a sudden drop in pressure and temperature that prevent further oxidation of the remaining fuel, leading to high levels of HC in the exhaust. The observations of this section are in some way related with the ring pack contribution findings of section §5.4.1.1, supporting the idea that the incomplete combustion may be the source of high levels of HC at the low load condition. Other important observation from the discussion above is that it can be said that the 3060 RPM, 25% load is the limiting case where the incomplete combustion ceases.

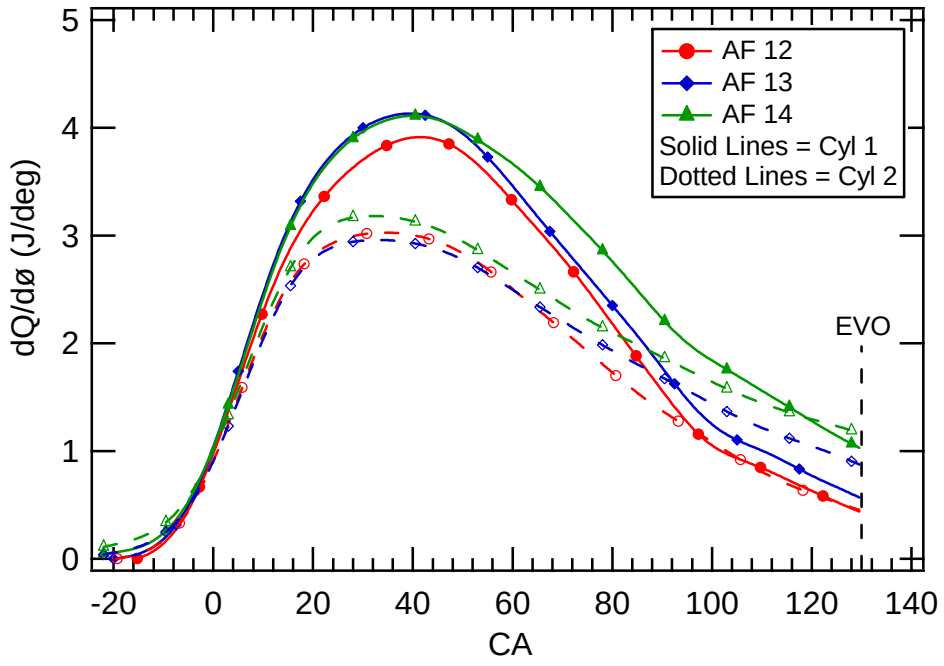

Figure 5.17 Rate of heat release for 1750 RPM and 10% load as a function of the air fuel ratio.

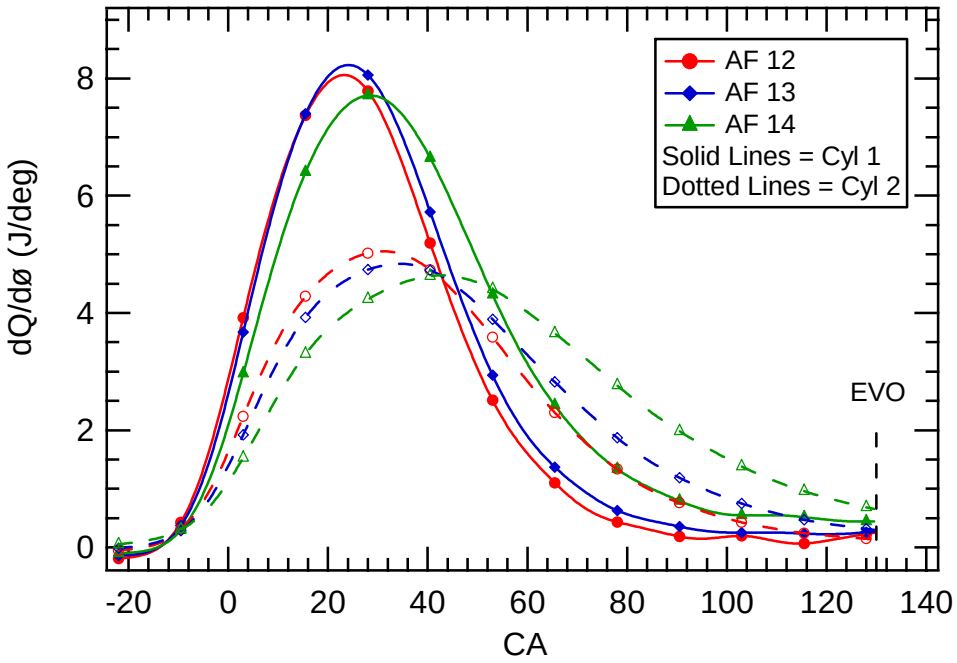

Figure 5.18 Rate of heat release for 1750 RPM and 25% load as a function of the air-fuel ratio.

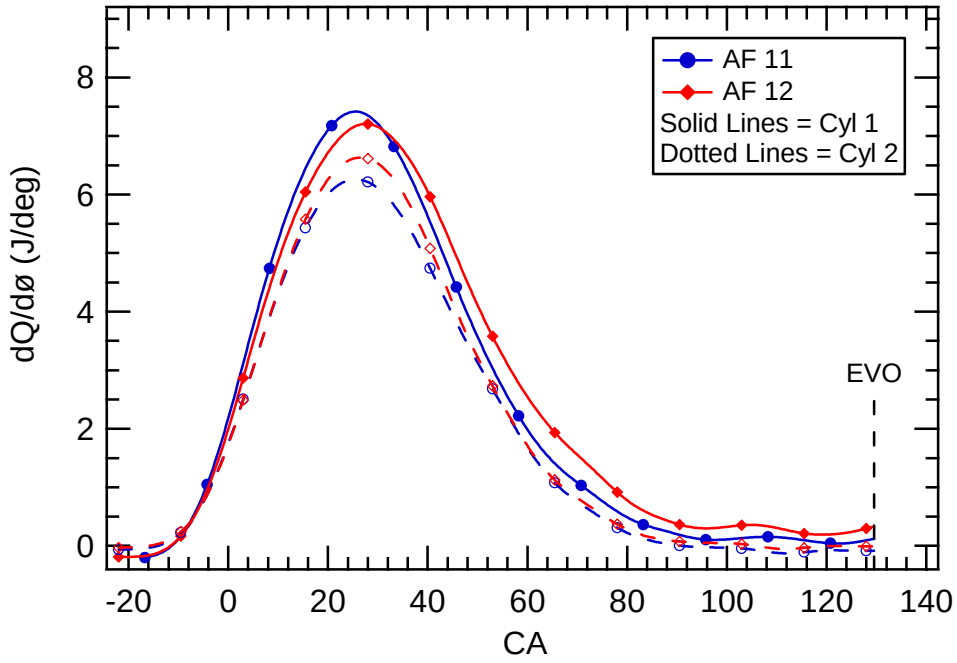

Figure 5.19 Rate of heat release for 3060 RPM and 25% load as a function of the air-fuel ratio.

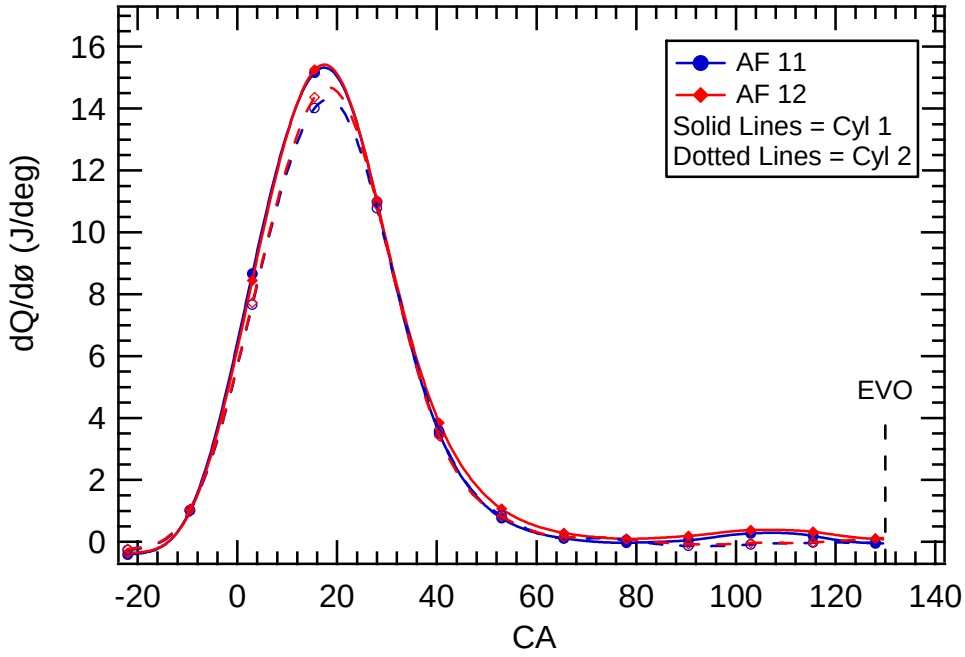

Figure 5.20 Rate of heat release for 3060 RPM and 50% load as a function of the air fuel ratio.

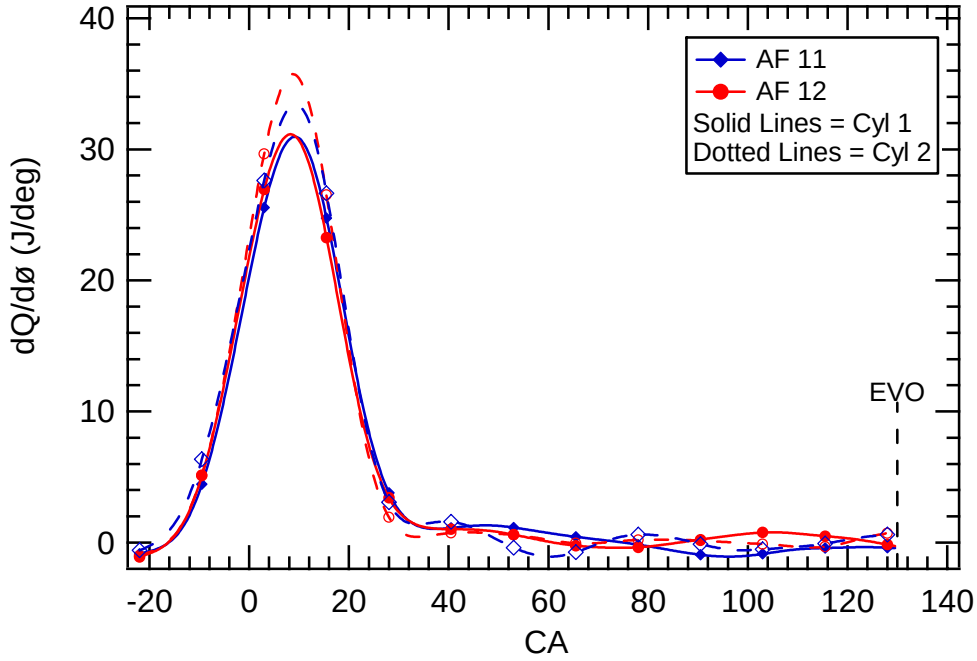

Figure 5.21 Rate of heat release for 3060 RPM and 100% load as a function of the air fuel ratio.

One important conclusion of sections §5.4.1.1 and §5.4.1.2 is that cylinder 1 and cylinder 2 behave differently and produce different amount of work for all the operating conditions except for the 3060 RPM, 50% load where both cylinders show similar rate of heat release profiles (and similar ring pack contribution). Note that cylinder 1 produces more work than cylinder 2 up to the 3060 RPM, 25% load, however for the 3060 RPM, 100% load cylinder 2 produces more work than cylinder 1, *i.e.* the behavior is inverted. This behavior was verified several times, and it is believed that the main cause of this behavior is the difference in charging between the cylinders. This was verified comparing the pressure traces, the IMEP (see §5.4.1), and by carrying out sweep spark timing tests at constant throttle position (see §3.6.5). The main reason for the difference in charging is the design of the engine, and especially of the intake system. Despite of the differences observed, the study of the engine under these conditions provided insights of the behavior that are particular of the small engines that are currently in production. Therefore, the analysis was carried out for both cylinders of the engine.

5.4.1.3 CYCLIC VARIABILITY

The indication that the ring pack was not the major contributor to the HC emissions at low load suggested the presence of other sources that could overwhelm the effect of the ring pack crevices. Incomplete combustion due to a slow burn rate is the likely cause [5]; cyclic variability is high and misfire can occur at the low load cases. At low load conditions there are other factors associated with the combustion process that may affect HC emissions. Very slow burn rate is typical because of the fixed (somewhat retarded) ignition timing. This can lead to the tail of the heat release curve extending to

the exhaust valve opening time, which can contribute to HC emissions [95]. Another issue at light load, related to the slow burning rate, is high cyclic variability. Table 5.6 shows the coefficient of variation of the IMEP (COV_{IMEP}) for the test matrix investigated. At the 1750 RPM, 10%, AF12 load condition, the COV_{IMEP} for the two cylinders were 11 and 21% respectively. Cylinder 2 had the higher COV_{IMEP}. Erratic combustion can lead to excessive emissions, and thus, a single-cycle analysis of the ring pack contribution to HC emissions was undertaken.

Table 5.6 COV of IMEP [%] for the test conditions. Upper number is cylinder 1, and lower number is cylinder 2.

	Speed (RPM)			1750	3060
Load	10%	AF	12	13.0 23.5	
			13	13.0 27.1	
			14	17.5 33.3	
	25%	AF	11		6.3 6.7
			12	5.1 11.0	6.4 7.3
			13	5.2 12.1	
			14	6.6 17.4	
	50%	AF	11		2.2 3.0
			12		2.4 2.7
	100%	AF	11		1.0 1.3
			12		0.5 0.9

5.4.2 SINGLE-CYCLE RESULTS

The single-cycle HC analysis followed the same process as described above. The codes were modified to perform the heat release and calculate the ring pack contribution on a single-cycle basis. For the heat release analysis the average heat transfer multiplier was used (see Appendix XII). It was considered to be more representative than that obtained from the single-cycle analysis, because the heat transfer was expected to be approximately constant along the 200 cycles of the data set. The heat release and ring pack filling and discharging were calculated for each cycle assuming that there was a constant cylinder charging mass, *i.e.* the value calculated from the spark timing sweep at constant throttle position. The mass of HC leaving the ring pack was integrated from CA90 to EVC on a cycle-by-cycle basis.

5.4.2.1 SINGLE-CYCLE RING PACK CONTRIBUTION TO THE HC EMISSIONS

The results of the single-cycle analysis are shown in Figs. 5.22-5.26 for the different loads and speeds. For clarity, only the air-fuel ratio of 12:1 data is shown. The results at other air-fuel ratios are shown in the Appendix XV. It can be clearly seen that while there is considerable cyclic variation in the ring pack contribution to HC, there are not isolated events that are well outside the normal range. Further, comparing the mean ring-pack EIHC of the individual cycles to the ring-pack EIHC determined from the mean cylinder pressure (horizontal lines in Figs. 5.22-5.26), there is good agreement. Over the range of operating conditions in Table 4.1, the maximum deviation between the

two means was 2.4%, indicating that a linear averaging is appropriate. One major result of Fig.5.22-5.26 is that the cyclic variation in the combustion, even at this extreme level, does not adversely impact the emissions through the ring pack mechanism.

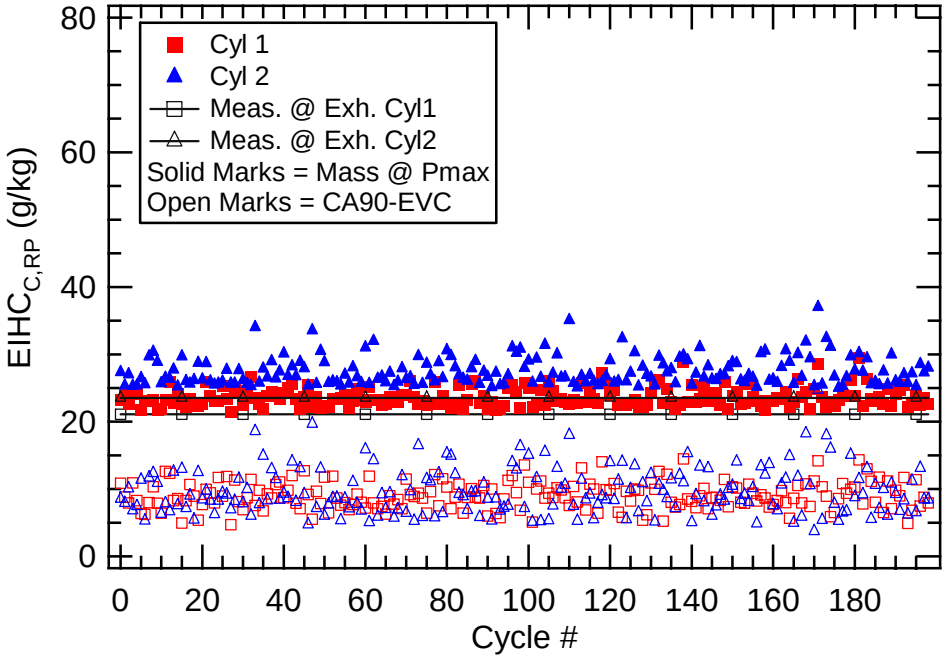

Figure 5.22 EIHC predicted by the ring pack model from single cycle analysis for 1750 RPM, 10% load, AF12.

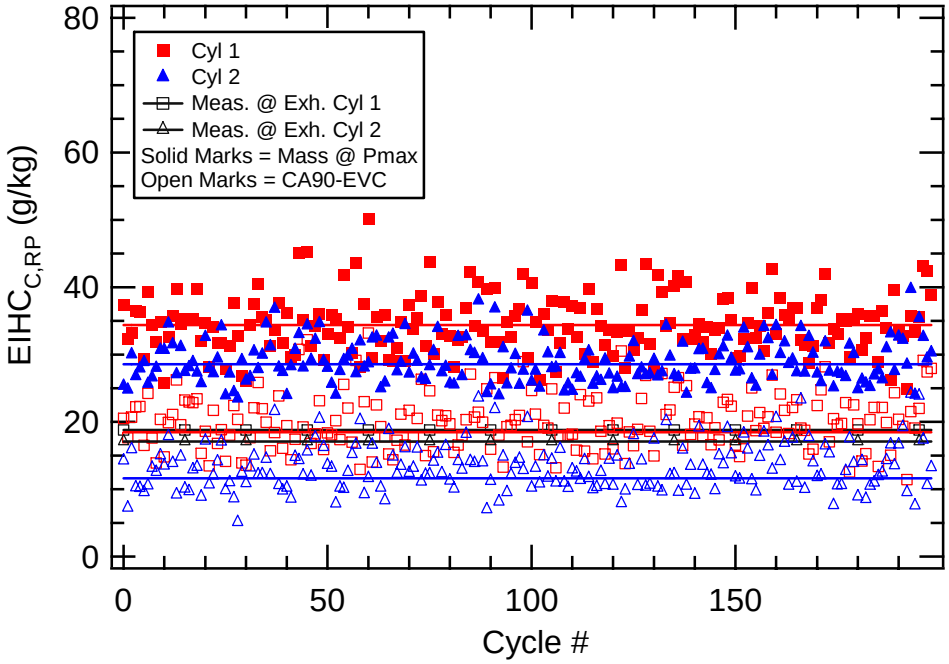

Figure 5.23 EIHC predicted by the ring pack model from single cycle analysis for 1750 RPM, 25% load, AF12.

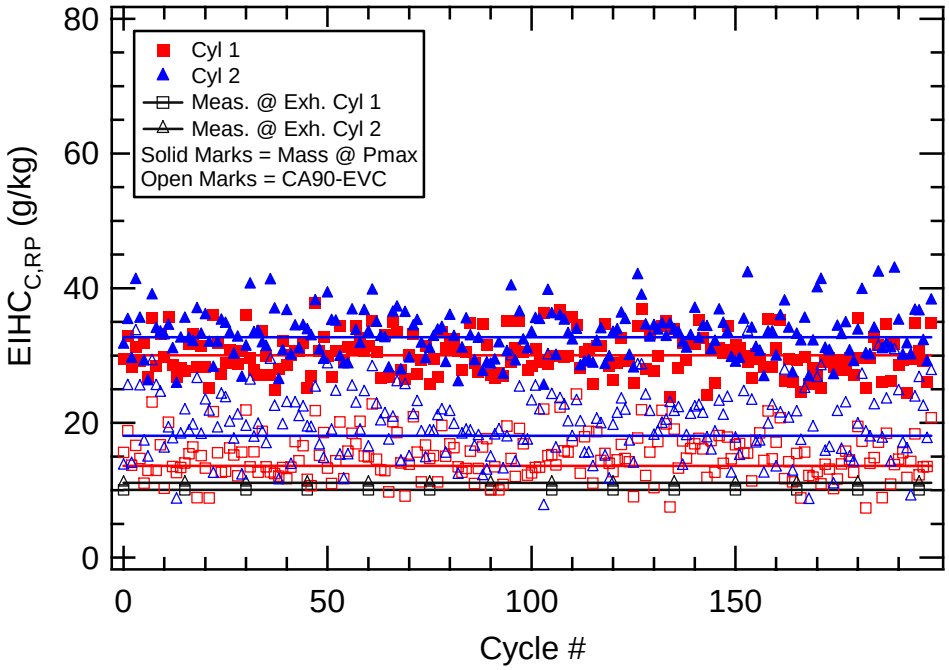

Figure 5.24 EIHC predicted by the ring pack model from single cycle analysis for 3060 RPM, 25% load, AF12.

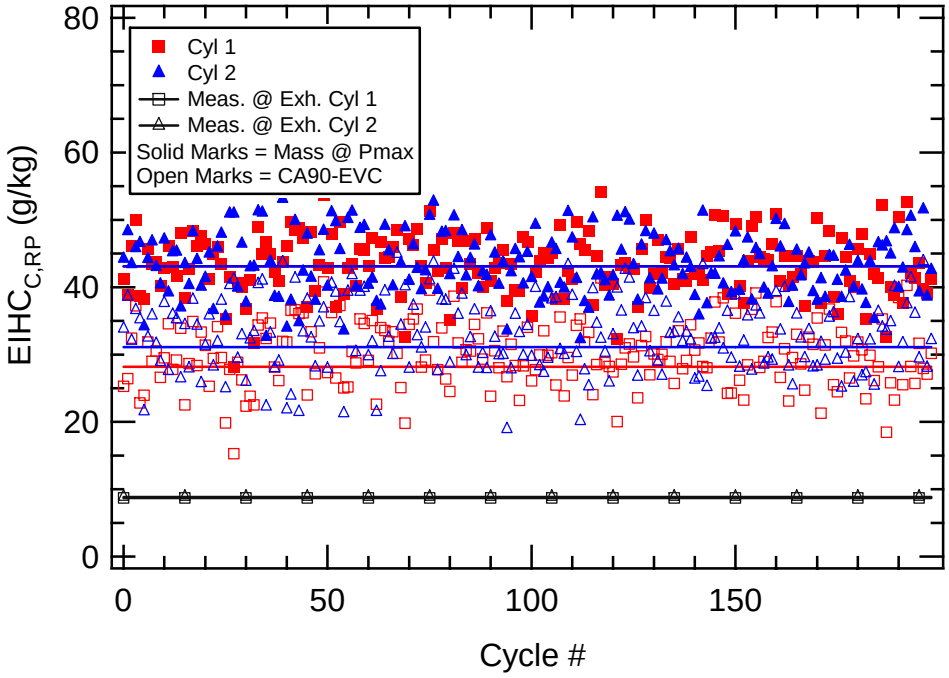

Figure 5.25 EIHC predicted by the ring pack model from single cycle analysis for 3060 RPM, 50% load, AF12.

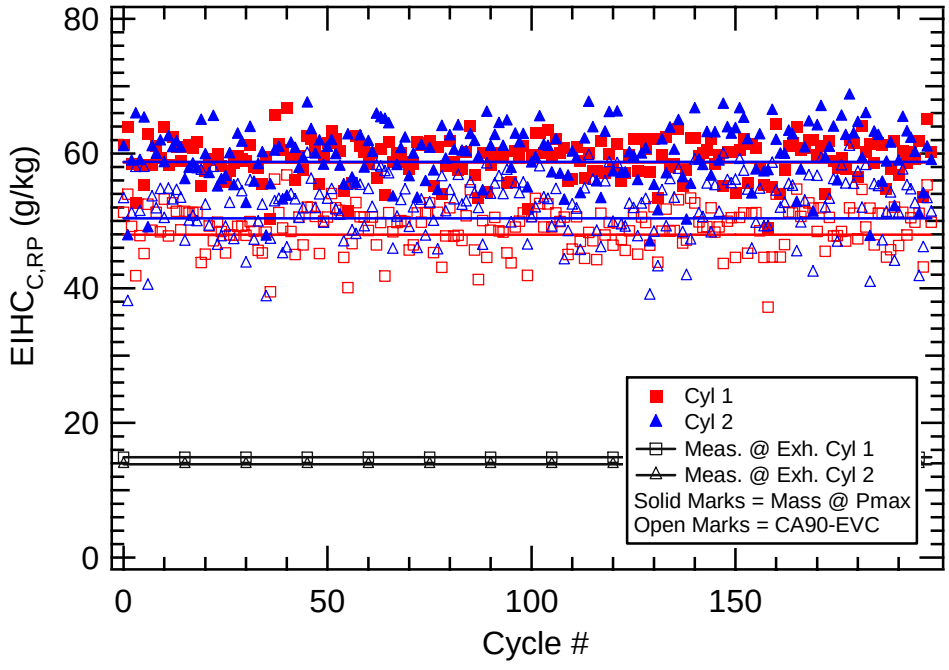

Figure 5.26 EIHC predicted by the ring pack model from single cycle analysis for 3060 RPM, 100% load, AF12.

5.4.2.2 SINGLE-CYCLE HEAT RELEASE

The ensemble average results provide insight into the global performance of the engine, but they do not fully explain the sources contributing to the HC emissions, especially at the 1750 RPM, 10% load case. In general the engine under study shows significant cycle-to-cycle variability at low load and low speed (see Table 5.6). A single-cycle-based analysis can provide more insight into the processes taking place in the engine. Therefore, the single-cycle heat release analysis was used to further investigate the inability of the ring pack filling mechanism to explain HC emissions at the light load conditions. Figures 5.27-5.31 show the single-cycle heat release analysis of each cylinder for all the operating conditions of interest.

The low load condition (10% load), Fig. 5.27, shows that for the majority of the cycles the combustion is still taking place at the time when the exhaust valve opens. For cylinder 1 in many of the cycles the combustion extends to the EVO timing. The majority of cycles in cylinder 2 have heat release extending to the point of EVO. It should be mentioned that the condition of heat release extending to the point of EVO introduces an inherent inaccuracy in the heat release calculations. It is assumed that heat release is completed by EVO in order to use the global energy balance to find the heat transfer multiplier. Because CA90 is based on the integration of the heat release rate curve, which is normalized to the total released fuel energy released at EVO, it also will be biased. The bias in CA90 would be to advance the CA90 time relative to the real CA90, therefore, it would be a conservative bias with regard to the integration of the ring pack flows. Thus, the conclusions above are not expected to be affected. As observed

before, the air-fuel ratio affects the extent of the incomplete combustion, and it can clearly be seen in Fig. 5.27. At the air-fuel ratio of 12:1, Fig. 5.27 (a), there is a small fraction of cycles that finish combustion prior EVO. As the air fuel ratio is increased, the fraction of cycles that complete combustion prior EVO is reduced (13:1), and then for the air-fuel ratio of 14:1, Fig. 5.27 (c), shows that none of the cycles finish combustion prior to EVO. This trend is consistent with the increased COV of IMEP observed at this operating condition.

As the load is increased to 25%, Fig. 5.28, the single-cycle heat release reveals that the fraction of cycles that finish heat release prior EVO has been increased considerably with respect to the 10% load (Fig. 5.27). However, there are still some indications of incomplete combustion. Cylinder 2 shows a higher degree of incomplete combustion than cylinder 1. This difference is more pronounced for the air-fuel ratio of 14:1, where a significant fraction of the cycles do not complete combustion prior to EVO.

At the intermediate load and high speed case (3060 RPM, 25% load), Fig. 5.29, it can be seen that for the majority of the cycles the combustion is finished before EVO, but a few cycles exhibit late combustion. The number of cycles that complete combustion prior EVO has been increased with respect to the same load at 1750 RPM (Fig. 5.28). This observation suggests that the engine speed helps to increase the number of cycles that complete combustion prior EVO. No strong effect of the air-fuel ratio is observed, and both cylinders show roughly the same heat release profile.

For the 50 and 100% load 3060 RPM case, Fig. 5.30-5.31 respectively, all the energy is released significantly before EVO for all of the cycles. This is in full agreement with the observations of the heat release analysis using average pressure, indicating that for these two operating conditions there are not cycles that have incomplete combustion. Thus, for example at the 3060 RPM, 100% load condition, Fig. 5.31, a relatively rapid heat release rate is observed; the CA10 – CA90 duration was on average 27 crank angle degrees. At this operating condition cylinder 2 has a higher peak burning rate. For these two conditions (Fig. 5.30-5.31), it was observed in Fig. 5.16 that the ring pack mechanism was able to fully explain the HC emissions from the engine.

The fact that for the 1750 RPM and 10% load (and in less degree for the 1750 RPM, 25%) load case the majority of the cycles do not complete heat release prior to EVO suggests that incomplete combustion could be contributing to the HC emissions. It has been previously shown by Haugle and Ghandhi [95] that there was a correlation between the observances of higher hydrocarbon concentrations in the exhaust with low-IMEP cycles when the heat release – calculated based on the mean cylinder pressure – extended beyond EVO. Therefore, based on the low load data in Fig. 5.27 it is possible that incomplete combustion is contributing to the HC emissions, which would explain the shortfall in the ring-pack contribution. Also, the isolated slow burn cycles at the 3060 RPM, 25% load case suggests that incomplete combustion may also contribute to the HC emissions at this condition.

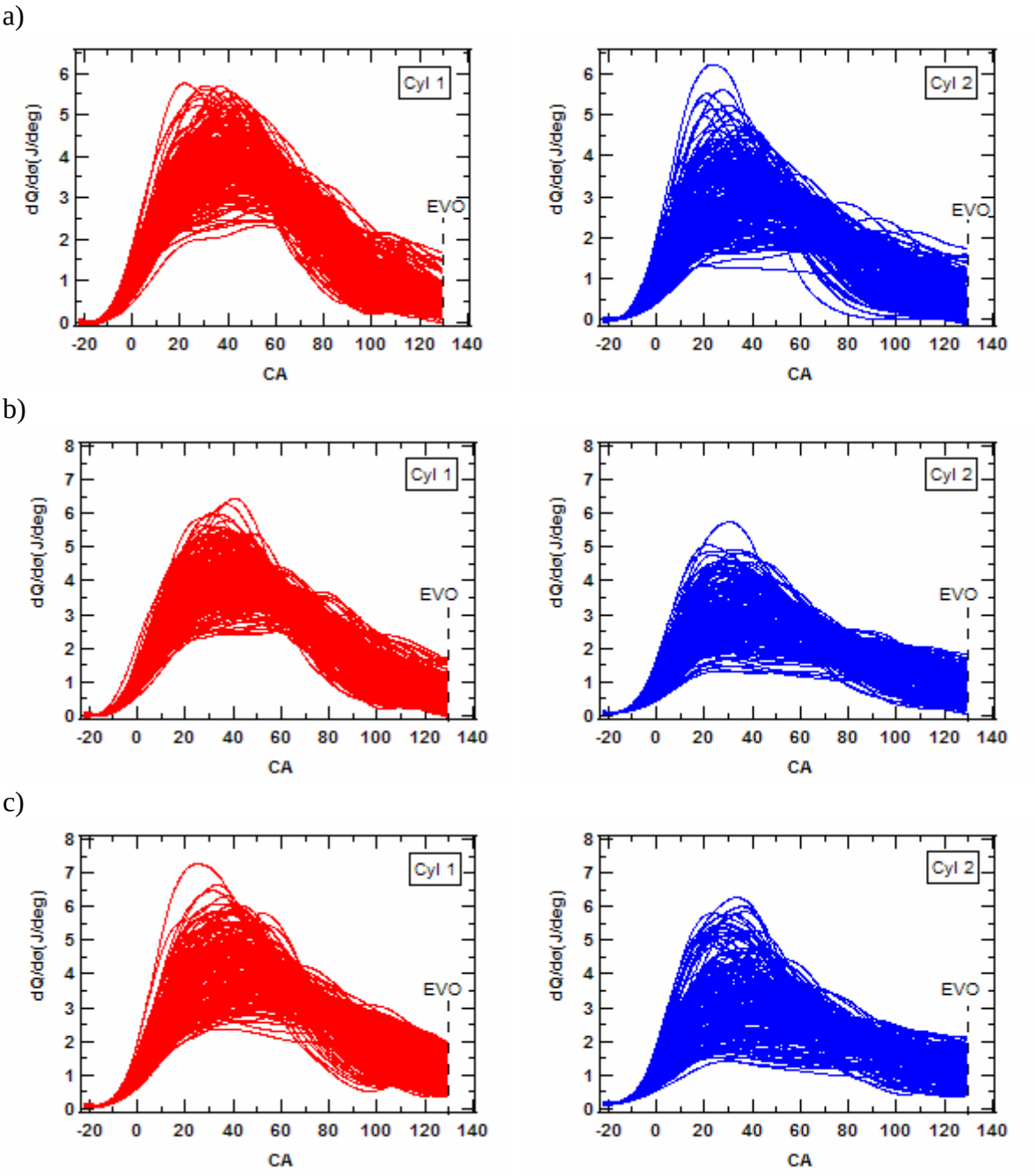

Figure 5.27 Single cycle rate of heat release for 1750 RPM, 10% load, at different air-fuel ratios (a) AF 12:1, (b) AF 13:1, (c) AF 14:1.

a)

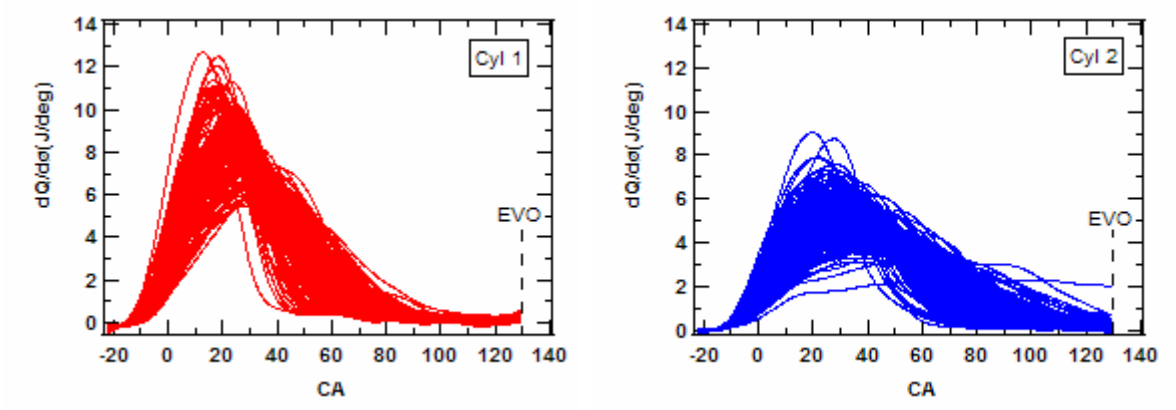

b)

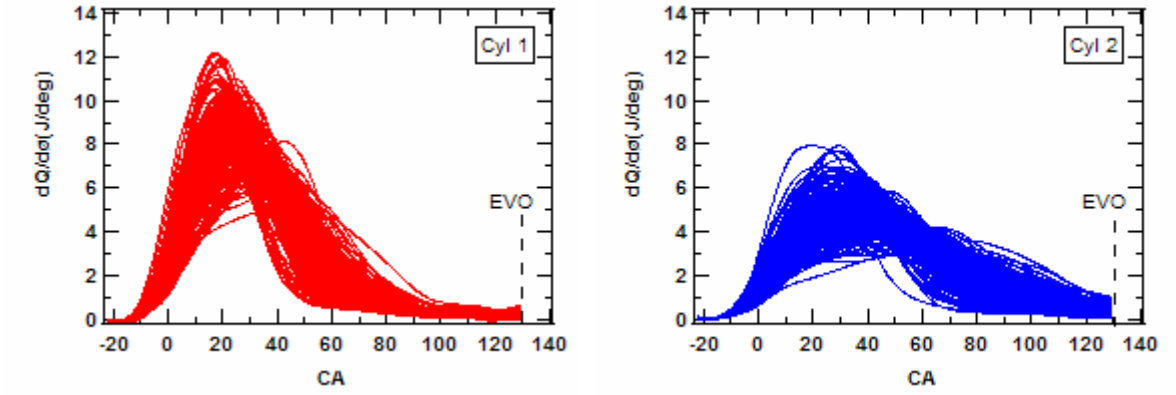

c)

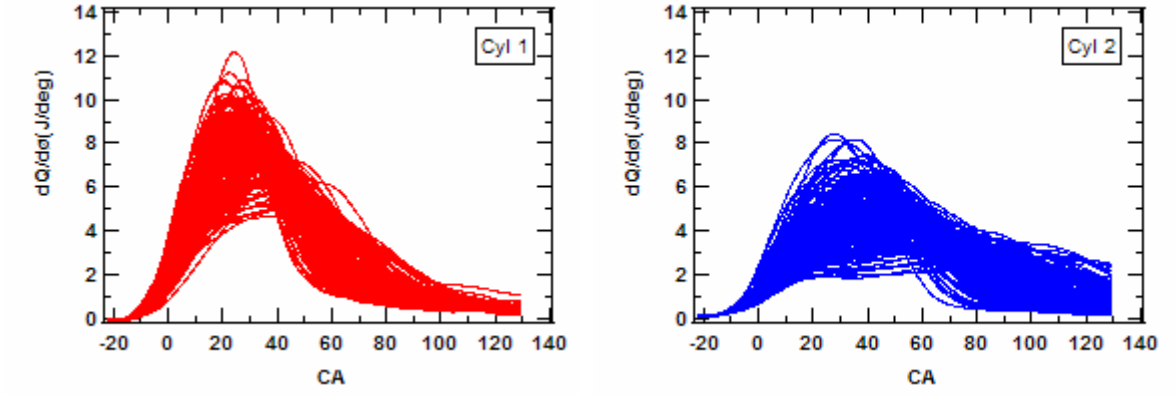

Figure 5.28 Single cycle rate of heat release for 1750 RPM, 25% load, at different air-fuel ratios (a) AF 12:1, (b) AF 13:1, (c) AF 14:1.

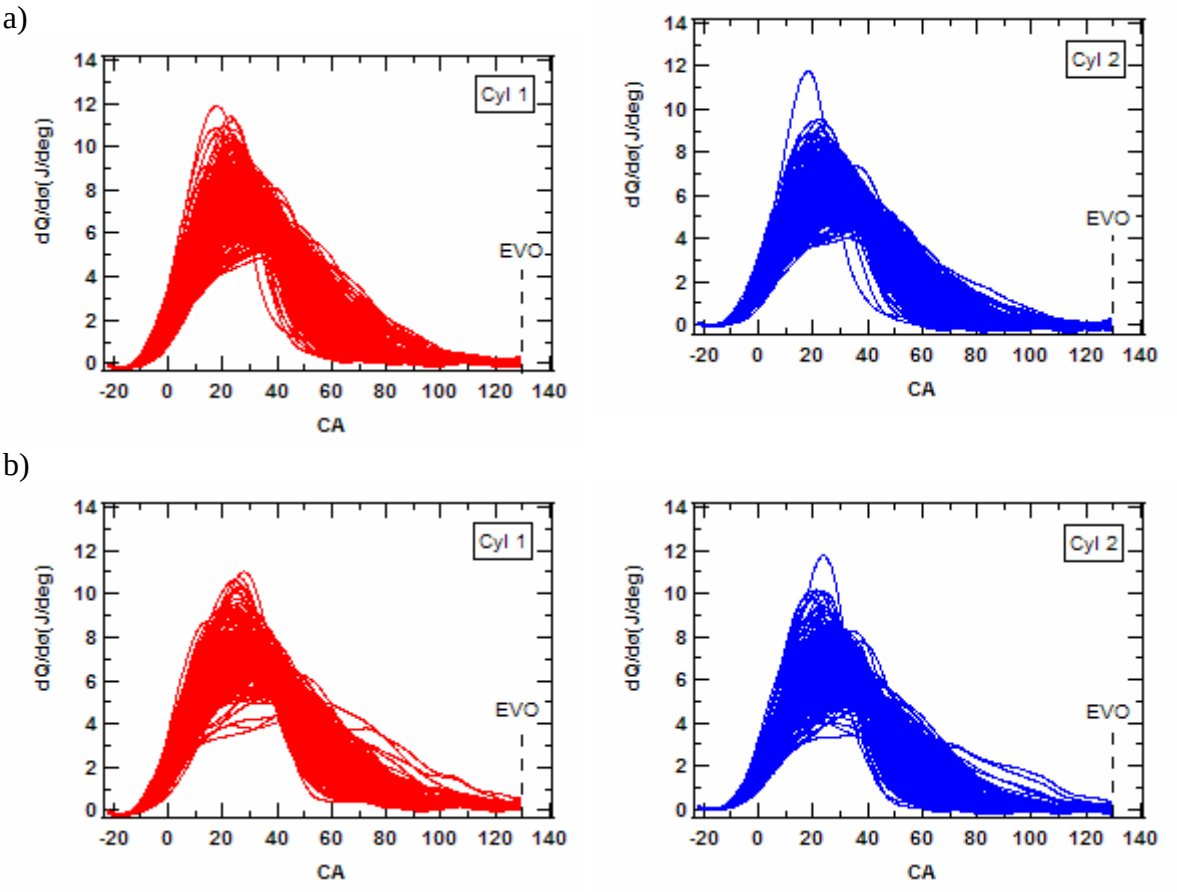

Figure 5.29 Single cycle rate of heat release for 3060 RPM, 25% load, at different air-fuel ratios (a) AF 11:1, (b) AF 12:1.

a)

b)

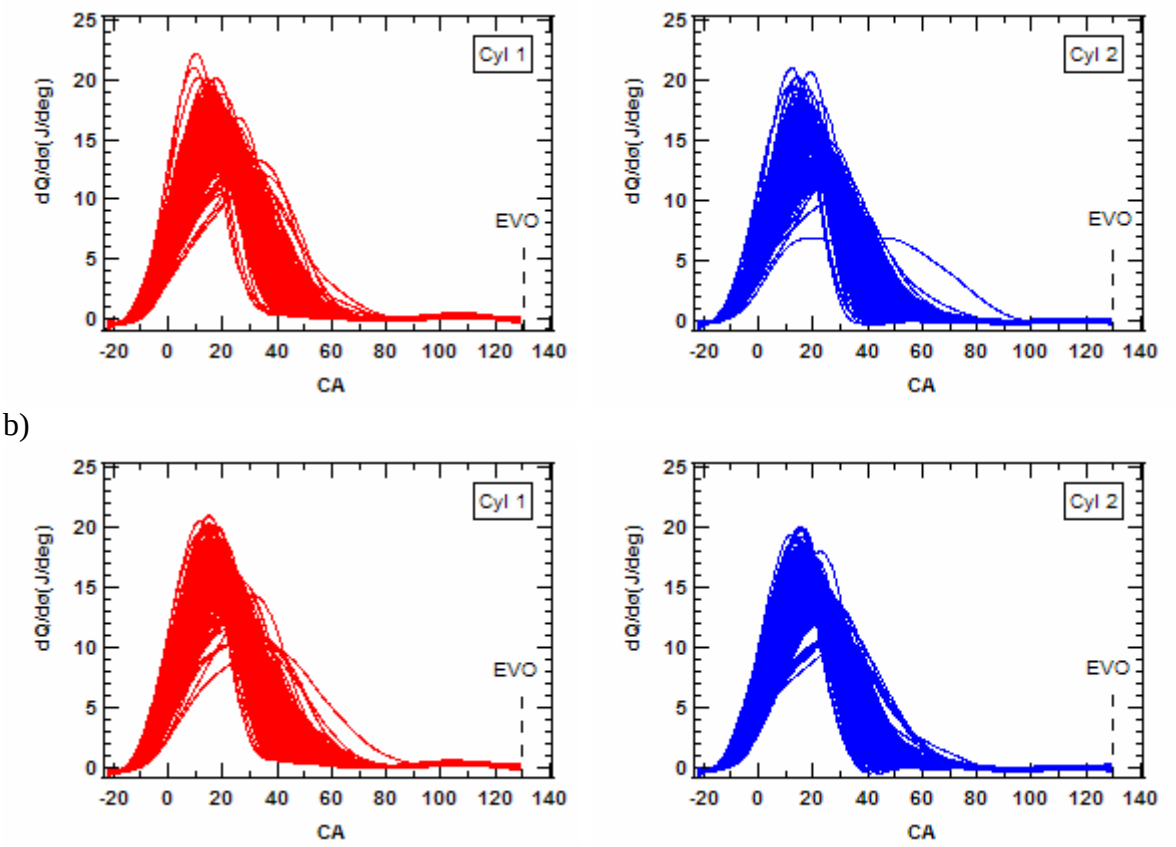

Figure 5.30 Single cycle rate of heat release for 3060 RPM, 50% load, at different air-fuel ratios (a) AF 11:1, (b) AF 12:1.

a)

b)

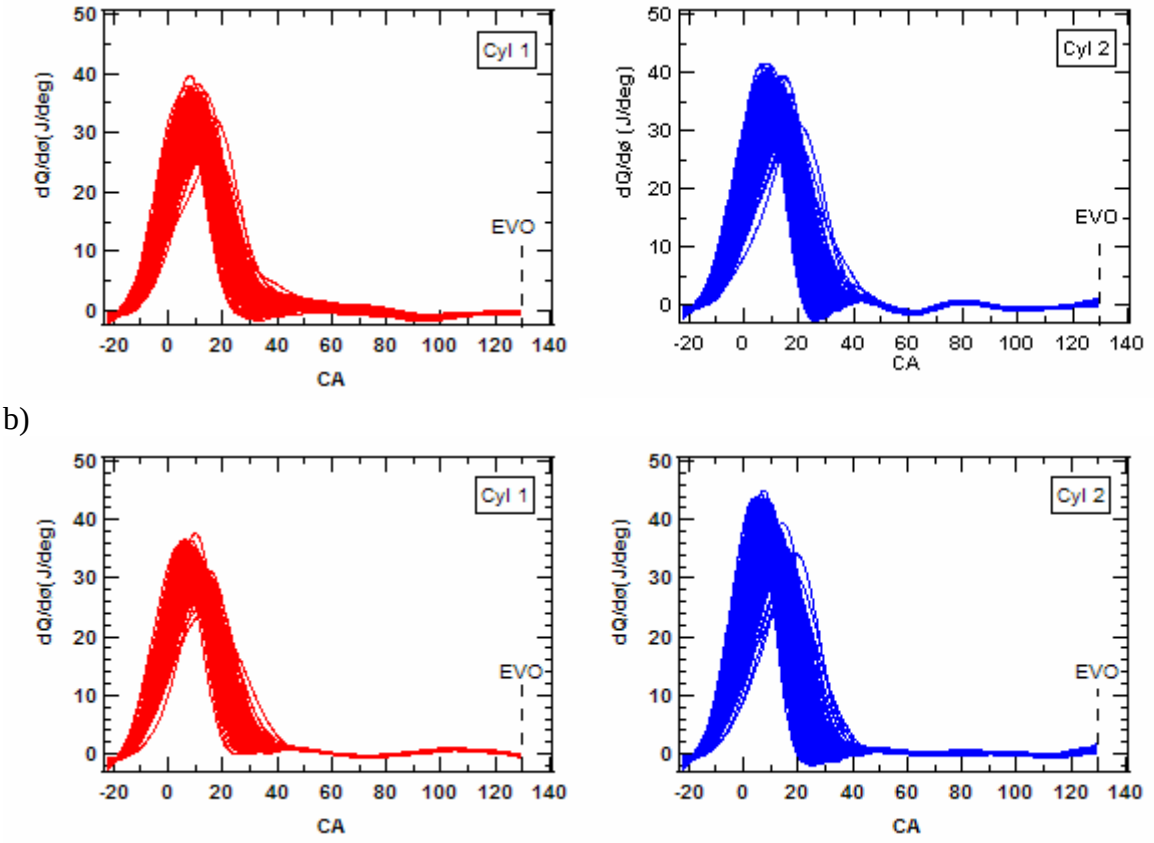

Figure 5.31 Single cycle rate of heat release for 3060 RPM, 100% load, at different air-fuel ratios (a) AF 11:1, (b) AF 12:1.

5.4.2.3 INCOMPLETE COMBUSTION QUANTIFICATION

The contribution of incomplete combustion to HC emissions for the low load cases was investigated further using time-resolved HC measurements performed with the fast FID. Figure 5.32 shows the individual-cycle HC time history for 1750 RPM at 10 and 25% loads; and for the 3060 RPM at 25, 50 and 100% loads for the air-fuel ratio 12:1. The data are shown for cylinder 1 only. The data for cylinder 2 are presented in Appendix XVI. The general shape of the traces is typical of those for spark-ignition

engines, with a slight increase at EVO during blowdown followed by a decrease in concentration during the main part of the exhaust stroke, then an increase near EVC as the roll-up vortex is exhausted. The 3060 RPM data show some cycle-to-cycle variability, but the values typically fall within a band ±15% about the local mean. The low speed, light load condition, however, shows a greater amount of cyclic dispersion, with individual cycles as much as 50% different than the local mean. The higher level of variability does not necessarily imply that there is a link between incomplete combustion and HC emissions. In order to make that connection, in the following sections the HC concentration at a fixed time will be compared to the quality of the combustion event, and then the individual-cycle mass flow of HC will be assessed, and the correlation between the individual-cycle HC mass flow rate and combustion performance will be evaluated.

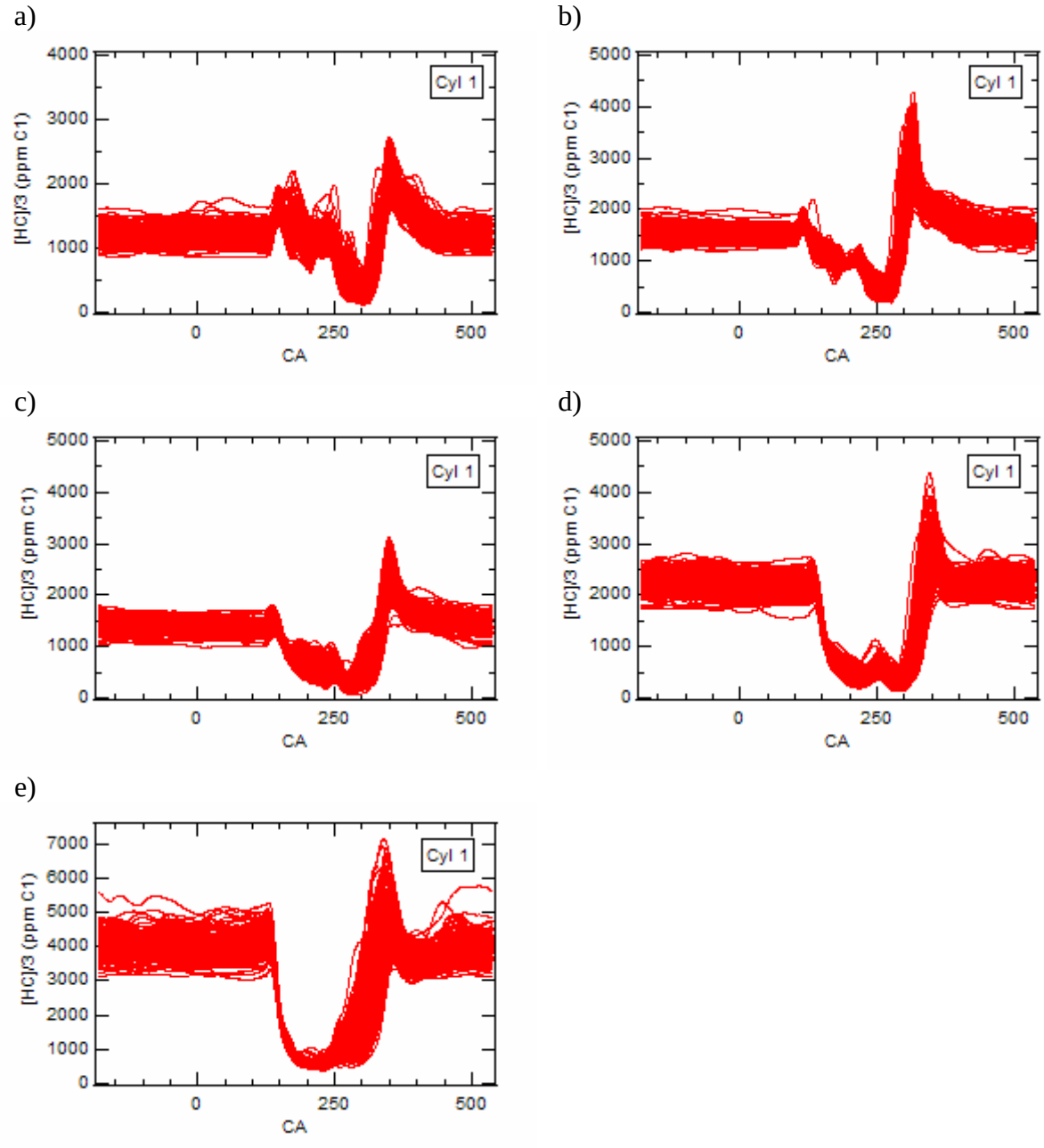

Figure 5.32 Single-cycle resolved HC measurements for cylinder 1 (a) 1750 RPM, 10% load, AF12, (b) 1750 RPM, 25% load, AF 12, (c) 3060 RPM, 25% load, AF12, (d) 3060 RPM, 50% load, AF12, and 3060 RPM, 100% load, AF12.

5.4.2.3.1 CONCENTRATION-BASED CORRELATION

The role of cyclic variations in combustion performance on HC emissions was assessed by relating the HC data from the fast FID with the corresponding IMEP. The HC concentration at a given CA timing in the cycle was compared against the IMEP of the same cycle. Hydrocarbon concentration [HC] values at 160 CA aTDC were chosen because this CA represents the local peak in HC concentration during the blowdown process (see Fig. 5.32). The results of this comparison are presented in Fig. 5.33-5.38

The data at 1750 RPM, 10% load, Fig. 5.33, indicate a correlation between HC concentration at 160 CA aTDC and IMEP. Cycles with low IMEP are seen to have a higher [HC] as would be expected from a partial combustion event. This dependence is more pronounced for cylinder 2, which at the same time shows higher variability in the HC concentration. A linear trend line is shown and appears to adequately represent the data, but does not conclusively suggest a linear correlation. For the 1750 RPM, 25% load, Fig.5.34, a very weak dependence can be seen for all the air fuel ratios except for cylinder 1 at the air-fuel ratios of 12:1 and 13:1 where the dependence is clearer. The 3060 RPM cases (loads 25, 50 and 100 % load), Figs. 5.35-5.37, however, show a nearly random relationship between [HC] at 160 CA aTDC with cycle IMEP. The linear curve fit to the data shown, has a poor quality of the fit. The statistical nature of the fits will be discussed further in the following section.

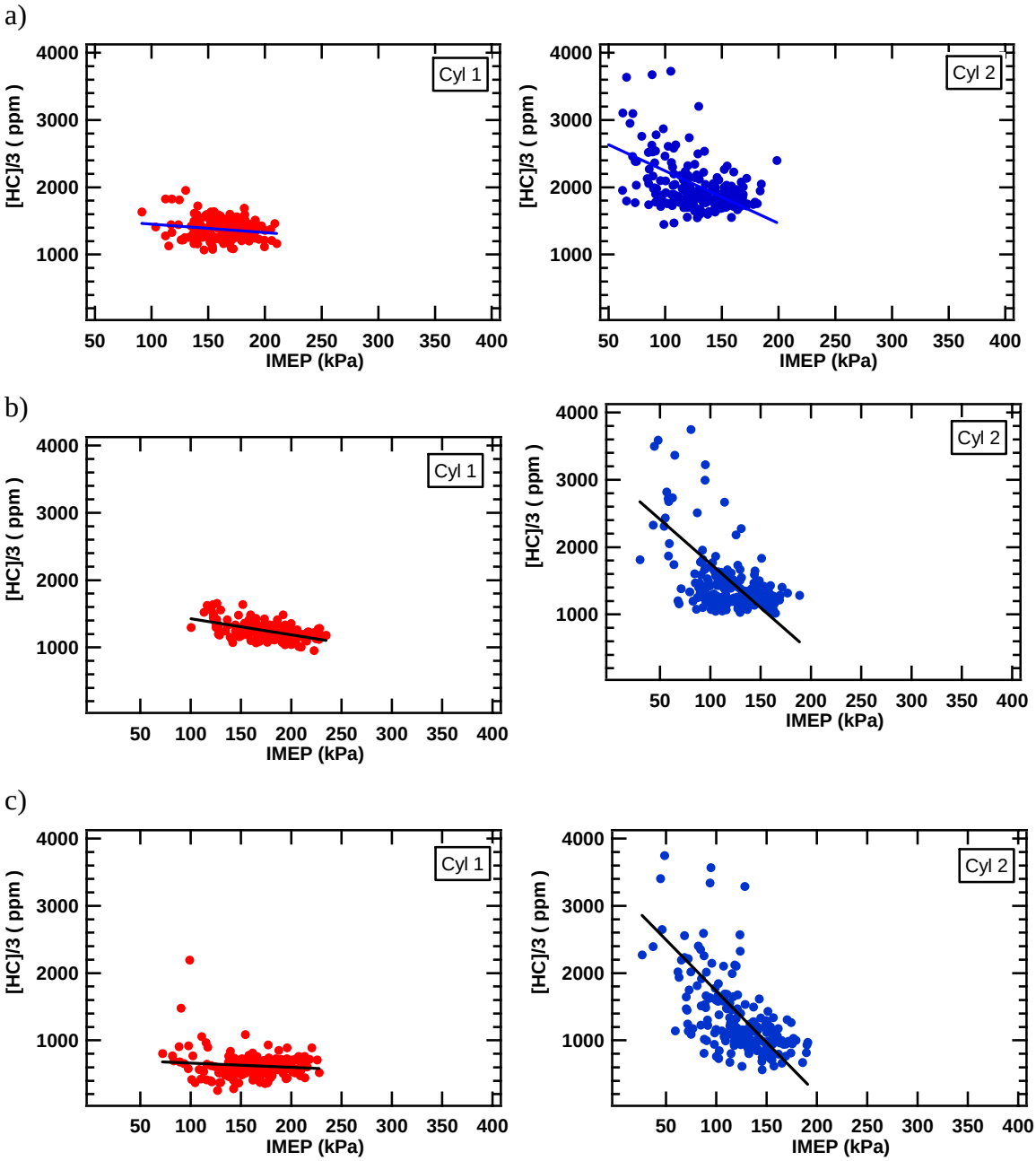

Figure 5.33 HC concentration at 160 CA aTDC vs. IMEP of same cycle for 1750 RPM, 10% load, at different air-fuel ratios (a) AF 12:1, (b) AF 13:1, (c) AF 14:1.

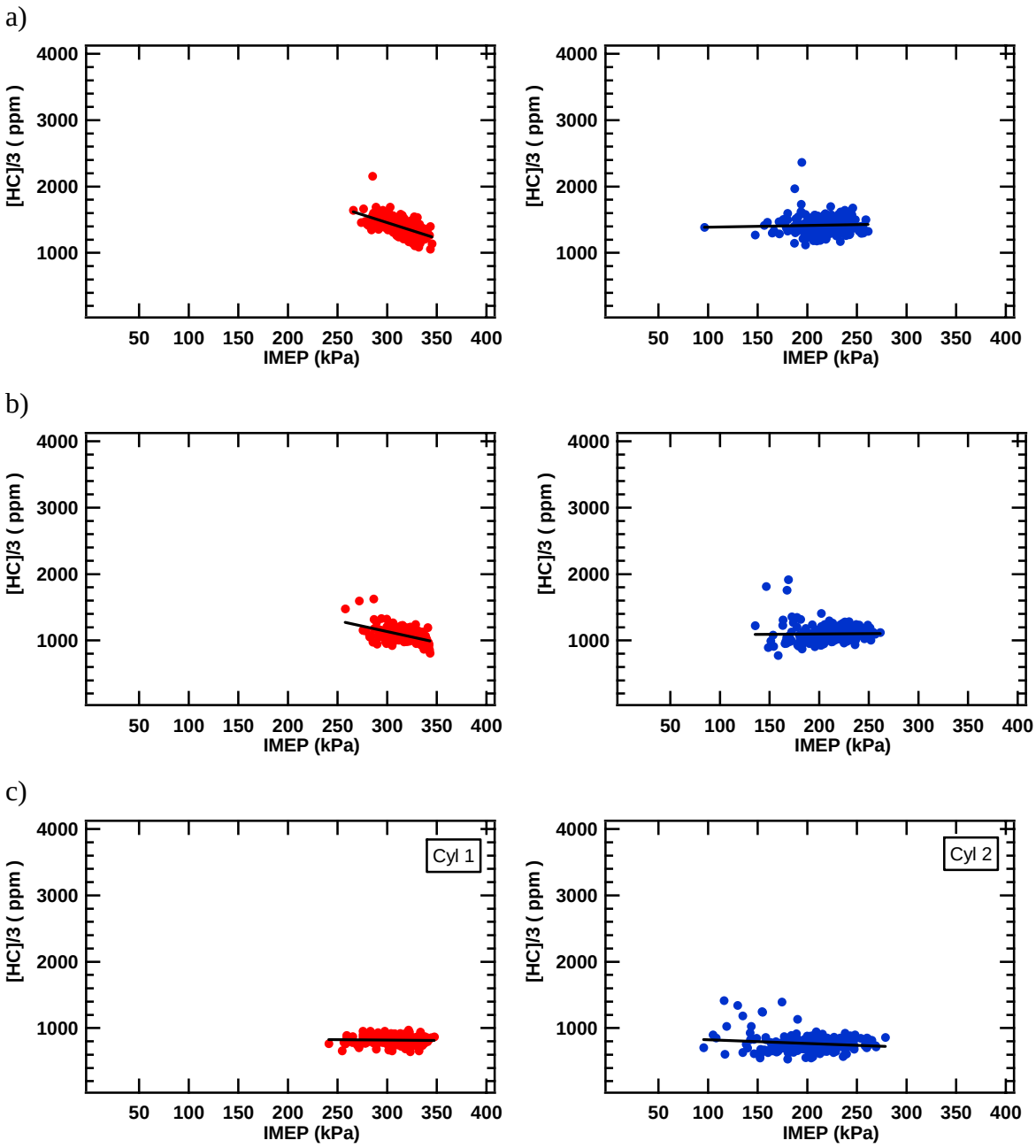

Figure 5.34 HC concentration at 160 CA aTDC vs. IMEP of same cycle for 1750 RPM, 25% load, at different air-fuel ratios (a) AF 12:1, (b) AF 13:1, (c) AF 14:1.

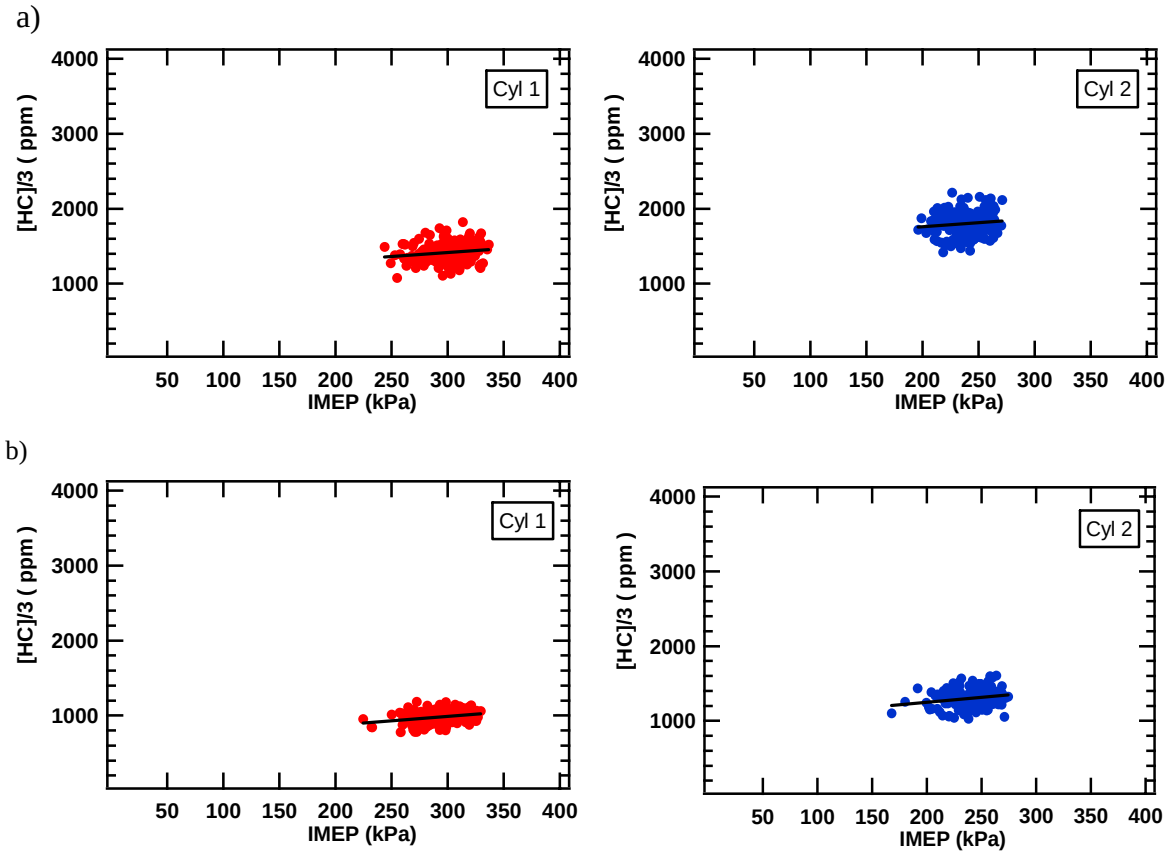

Figure 5.35 HC concentration at 160 CA aTDC vs. IMEP of same cycle for 3060 RPM, 25% load, at different air-fuel ratios (a) AF 11:1, (b) AF 12:1.

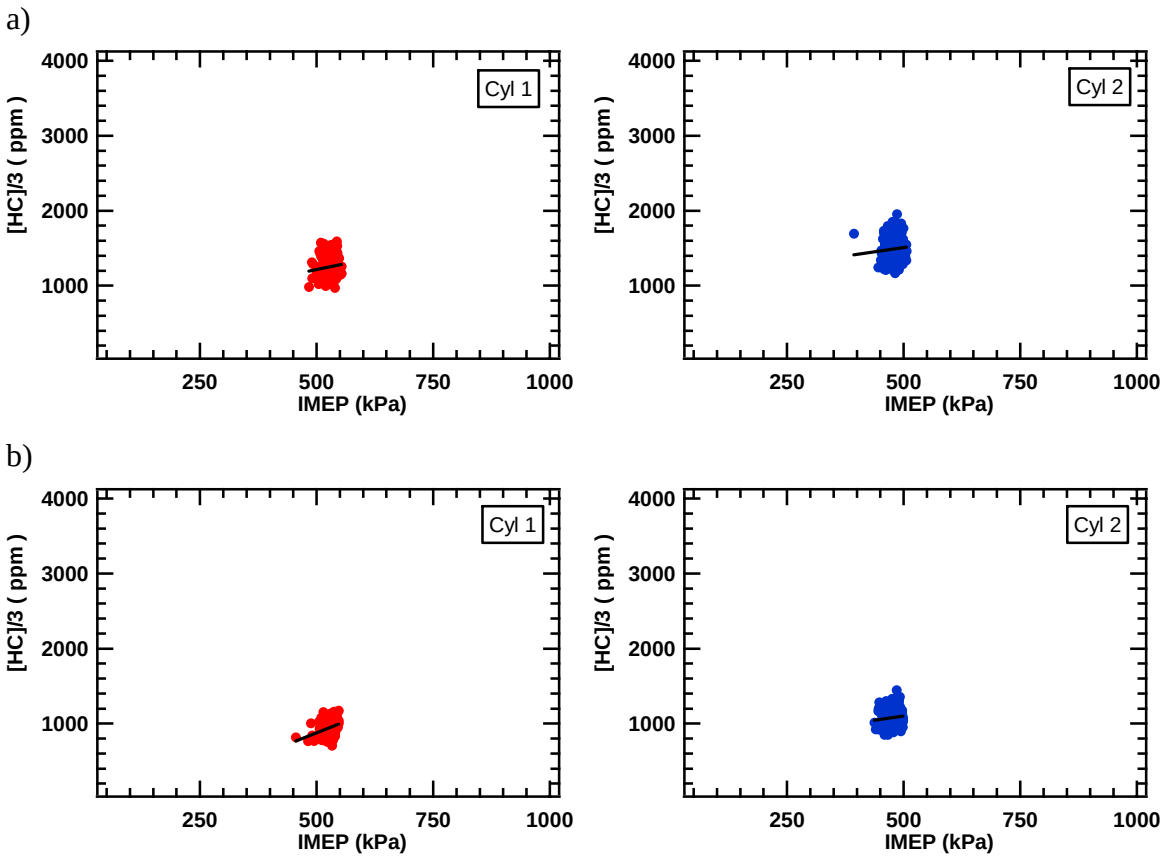

Figure 5.36 HC concentration at 160 CA aTDC vs. IMEP of same cycle for 3060 RPM, 50% load, at different air-fuel ratios (a) AF 11:1, (b) AF 12:1.

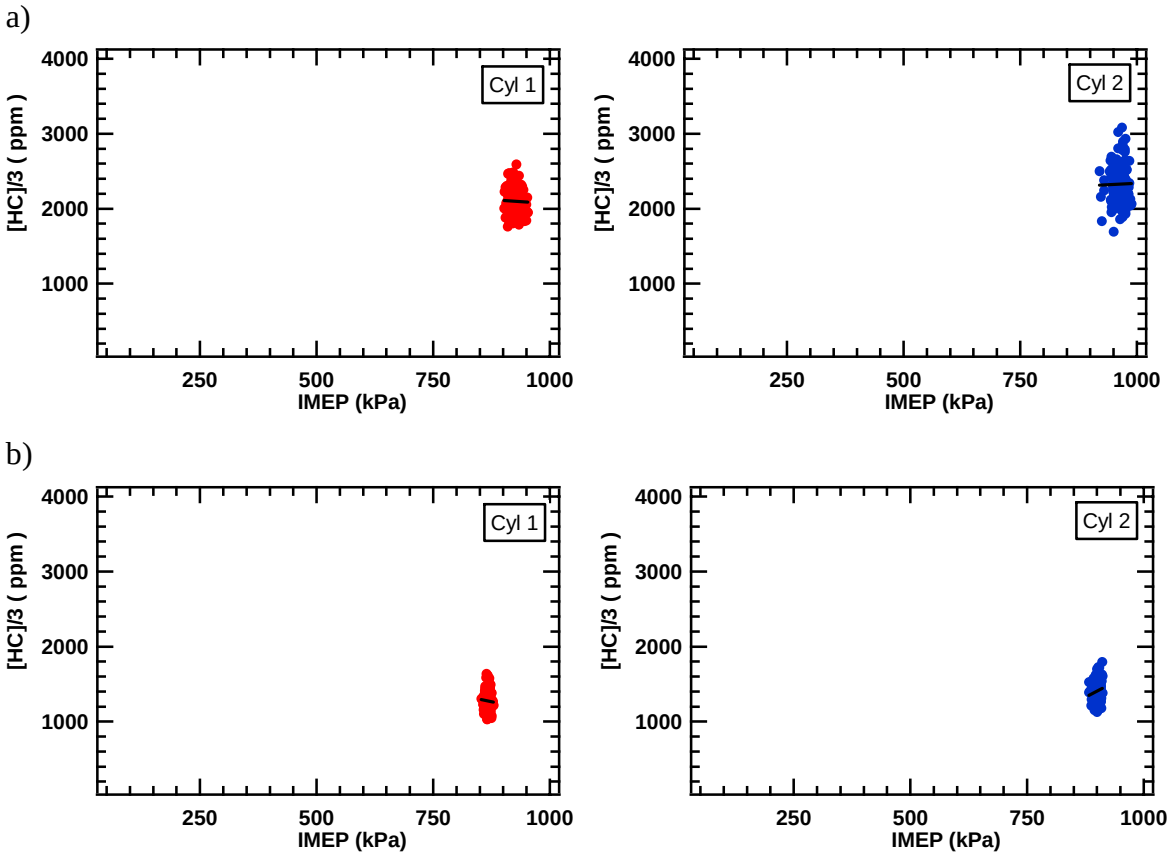

Figure 5.37 HC concentration at 160 CA aTDC vs. IMEP of same cycle for 3060 RPM, 100% load, at different air-fuel ratios (a) AF 11:1, (b) AF 12:1.

5.4.2.3.2 STATISTICAL ANALYSIS

The correlation seen in Fig. 5.33 is not perfect, so it is necessary to statistically investigate whether the correlation truly exists, or if it could be explained by random effects. There are two important metrics that quantify the degree of linear correlation [96]. The linear correlation coefficient, r, which is often reported as r^2, describes the quality of the linear fit to the data. The second metric is the uncorrelation probability, P_c, which gives the probability that a set of random data with the same number of degrees of

freedom could give the same value of r. Only data that concurrently have a large r and a low P_c can be considered to display a true linear correlation.

Tables 5.7 show the value of r and P_c for the linear correlation between the hydrocarbon concentration and IMEP. For the 1750 RPM, 10% load data the correlation between the [HC] with the IMEP is unambiguous. The values of P_c are universally low. This indicates that the observed value of r is statistically meaningful, even though for some conditions r is itself relatively low, *e.g.* at AF of 14. Further, the 3060 RPM, 100% data show low values of r with high values of P_c, indicating that no statistically meaningful correlation is observed. There are isolated cases at the other loads that suggest that a statistically significant correlation exists.

Table 5.7 Linear correlation coefficient, r (upper) and uncorrelation probability Pc in % (lower) for the linear relationship between HC concentration at 160 CA aTDC and the IMEP for the test conditions indicated.

	Speed (RPM) →			1750		3060	
	Cylinder →			1	2	1	2
Load	10%	AF	12	-0.18 1.22	-0.49 0.00		
			13	-0.54 0.00	-0.56 0.00		
			14	-0.11 13.10	-0.63 0.00		
	25%	AF	11			0.16 2.19	0.12 10.25
			12	-0.60 0.00	0.04 53.70	0.28 0.01	0.21 0.36
			13	-0.51 0.00	0.02 80.08		
			14	-0.04 59.15	-0.15 3.39		
	50%	AF	11			0.12 9.02	0.08 24.05
			12			0.31 0.00	0.10 15.56
	100%	AF	11			-0.03 69.23	0.02 81.25
			12			-0.06 43.80	0.02 6.01

5.4.2.3.3 MASS-BASED CORRELATION

In this section the effect of incomplete combustion on HC emissions was characterized by correlating the combustion phasing, IMEP, and ring pack contribution to HC with the integrated exhaust HC mass flow rate on a single-cycle basis. The mass flow rate of HC was calculated on a cycle-by-cycle basis to determine whether

incomplete combustion was contributing to HC emissions at low load where the ring pack crevices cannot fully explain the HC emissions. The methodology to calculate this mass at the exhaust is explained in the next subsection.

5.4.2.3.3.1 INSTANTANEOUS HC MASS FLOW

The instantaneous HC mass flow can be determined from the fast FID data provided that the exhaust mass flow is known during the period when the exhaust valve is open. The instantaneous exhaust mass flow was calculated by considering the flow at the exhaust valve as the flow through a restriction using the compressible flow relations shown in Eq. 5.10.

$$\dot{m}_{exh} = C_D A \rho c \eta \qquad (5.10)$$

where $\dot{m}_{exh}$ is the total exhaust mass flow rate, C_D is the discharge coefficient, A is the instantaneous valve area, c is the speed of sound and η is the compressibility factor [5]. In Eq. 5.10 the restriction area is changing as the valve lift changes; the exhaust valve lift profile was used to calculate the instantaneous area. The discharge coefficient was adapted from [5], which was a function of the valve lift. The adaptation of the discharge coefficient does not have significant impact on the calculated mass flow because the discharge coefficient changes slightly around its mean value making the adaptation a valid and still accurate approximation. Fig. 5.38 shows the discharge coefficient used for the all the calculations as a function of the lift-head diameter ratio (L_v/D_v) (see Fig. 5.39 for the terminology) of the exhaust valve.

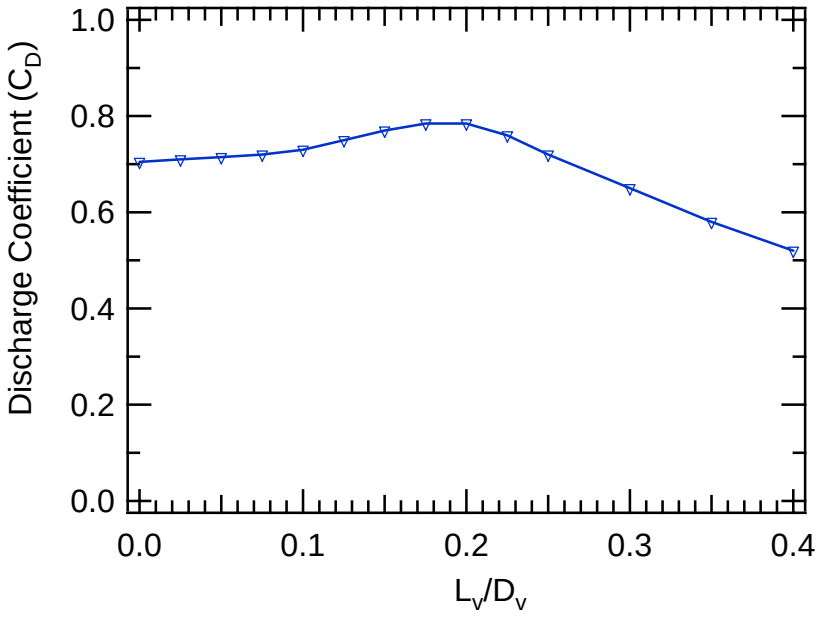

Figure 5.38 Discharge coefficient as a function of the valve lift.

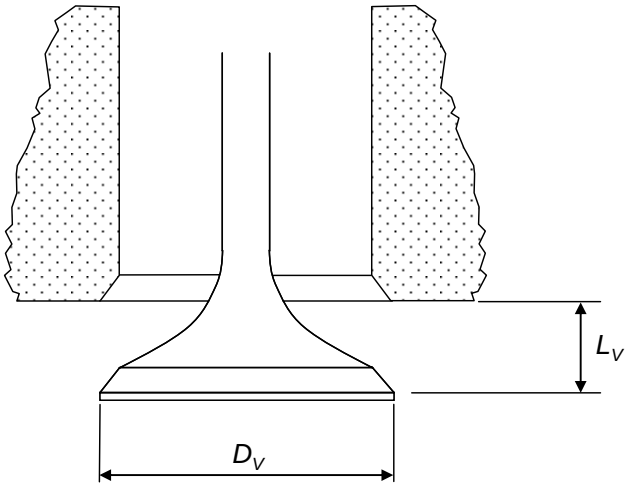

Figure 5.39 Schematic of the exhaust valve at is geometrical parameters.

The molecular weight of the exhaust gas was calculated based on the averaged concentration of the species measured at the exhaust. The gas temperature was

approximated considering that the gas undergoes a polytropic expansion during the blowndown period (Eq. 5.11).

$$T_{exh} = T_{EVO}(\frac{P_{exh}}{P_{EVO}})^{\frac{\gamma}{\gamma-1}} \tag{5.11}$$

The cylinder pressure was pegged to the intake port pressure at BDC of the intake stroke for each cylinder, and the exhaust pressure was measured using an absolute transducer (see § 3.2.9). However, small pressure transducer calibration inaccuracies can lead to significant mass flow rates. To overcome this, the exhaust flow rate was integrated and the exhaust absolute pressure was adjusted by adding a constant to ensure that the integrated mass matched the delivered mass of air and fuel to the engine. Fig. 5.40 shows the pressure before and after the mass conservation as the exhaust was enforced. The integrated HC mass flow was found from

$$m_{exh-HC} = \int_{t_{EVO}}^{t_{EVC}} \dot{m}_{exh} X_{HC} \frac{MW_{HC}}{MW_{exh}} dt \tag{5.12}$$

where X_{HC} is the crank angle-resolved HC concentration obtained from the fast FID, MW_{exh} and MW_{HC} are the molecular weight of the exhaust and fuel on a C1 basis.

a)

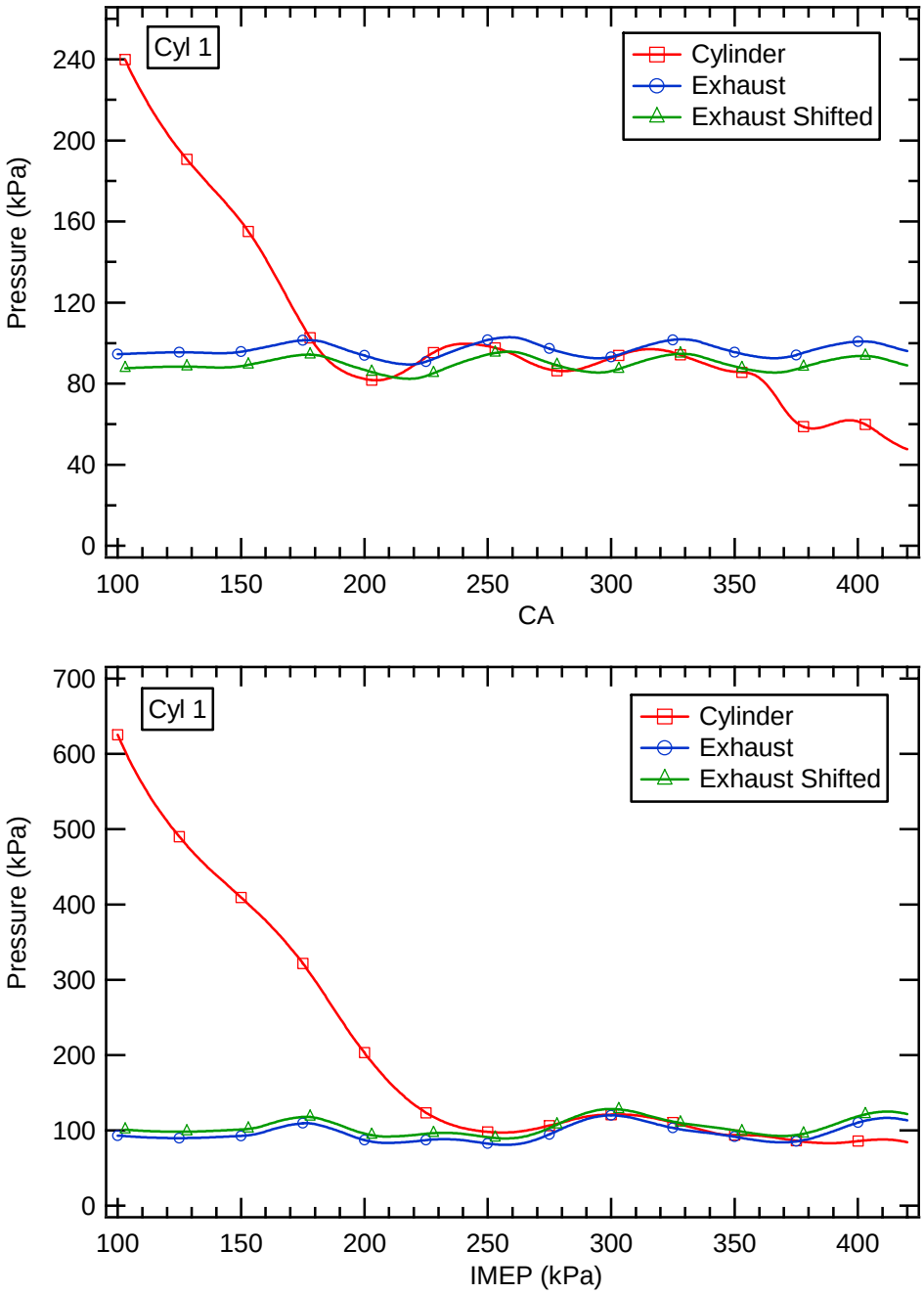

Figure 5.40 Cylinder, exhaust, and exhaust shifted pressures during the period when the exhaust valve is open for (a) 1750 RPM, 10% load, AF 12 and (b) 3060 RPM, 100% load, AF12.

By normalizing the integrated HC mass from Eq. 5.12 with the delivered fuel mass per cycle, one can write the integrated exhaust HC mass as an emission index, which will be referred to as $EIHC_{C,MB}$ from hereafter where the subscript C denotes a calculated quantity and the subscript MB denotes mass balance.

The instantaneous exhaust and HC mass flow during the period when the exhaust valve is open is shown in Figs. 5.41-5.42, for all the loads and speeds with air-fuel ratio of 12:1. These plots show that during the exhaust stroke the flow reverses several times (mass from the exhaust manifold returns to the cylinder). The number of times that the flow reverses is more severe for the low load cases (Fig. 5.41 (a), (b) and Fig. 5.42 (a)). As the load is increased this effect is reduces, and at the 100% load (Fig. 5.42 (c)) the flow reverses only once. It will be shown in the conditional sampling subsection §5.4.3, the peaks observed in the instantaneous mass flow are real and it also appear in the cycle-resolved HC traces. These observations have also been reported in the literature by experimentalists [65, 88].

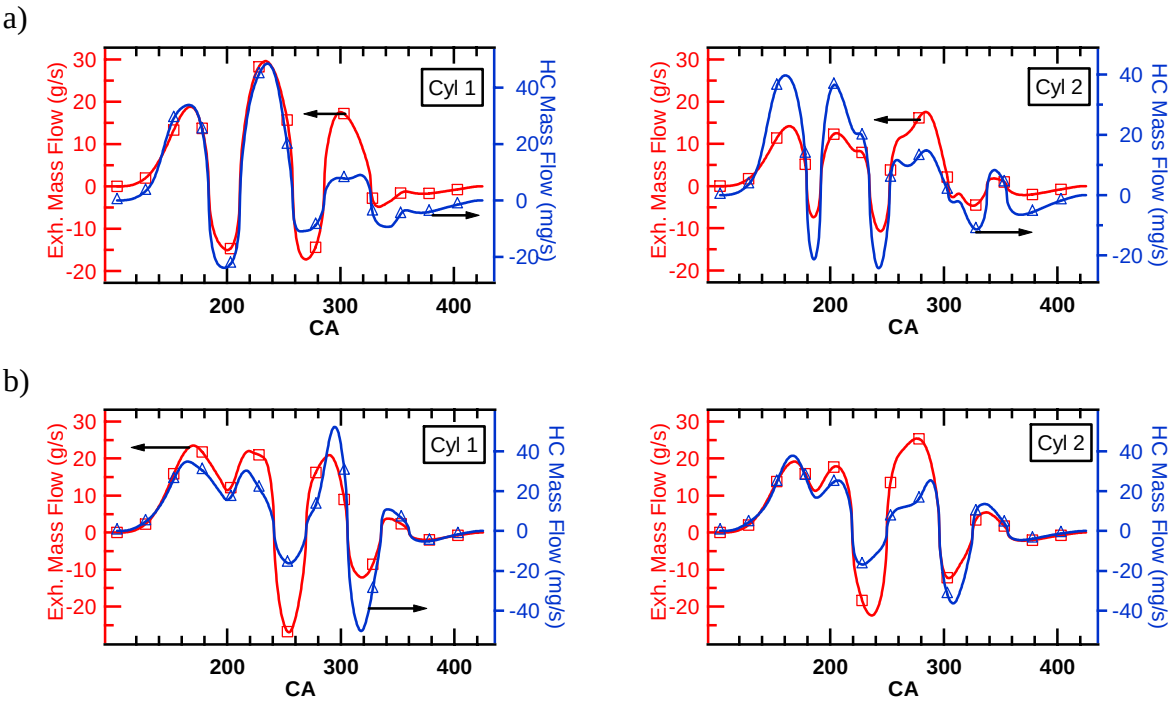

Figure 5.41 Exhaust gas mass flow rate and exhaust HC mass flow rate for (a) 1750 RPM, 10% load, AF12 and (b) 1750 RPM, 25% load, AF12.

Figure 5.43 shows the comparison of the $EIHC_{C,MB}$ with steady state measured values, $EIHC_{M,EXH}$ for all of the operating conditions. The $EIHC_{C,MB}$ was calculated using the ensemble-averaged data. It can be seen in Fig. 5.43 that the ensemble-average integrated exhaust HC mass using the time-resolved HC measurements from the fast FID agree well with the steady state measurements over the entire operating range of the engine in spite of the fact that the measurements were made at a single point and significant processing was performed. This gives confidence in the results and provides confidence in the individual-cycle values. Figures 5.44 and 5.45 show the results, for the individual-cycle data for all the loads and speeds at the air-fuel ratio of 12:1. The horizontal lines represent the steady state values for each cylinder. Of note is the fact that

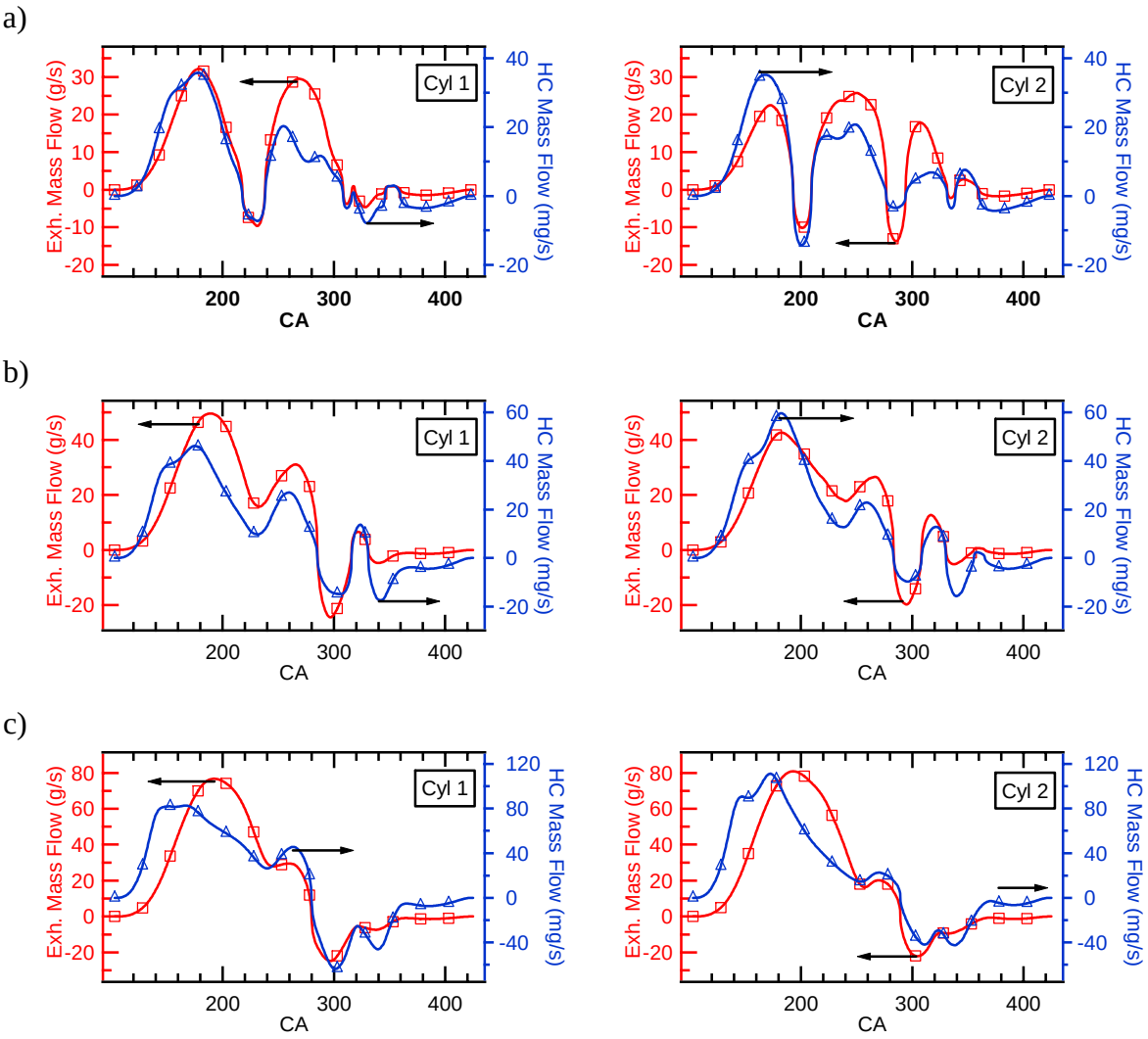

Figure 5.42 Exhaust gas mass flow rate and exhaust HC mass flow rate for (a) 3060 RPM, 25% load, AF12, (b) 3060 RPM, 50% load, AF12 and (c) 3060 RPM, 100% load, AF12.

for the 1750 RPM, 10% load, AF 12 case, Fig. 44 (a), there are individual cycles for cylinder 2 that emit nearly three times the average HC mass per cycle. The relationship of these cycles will be investigated further below.

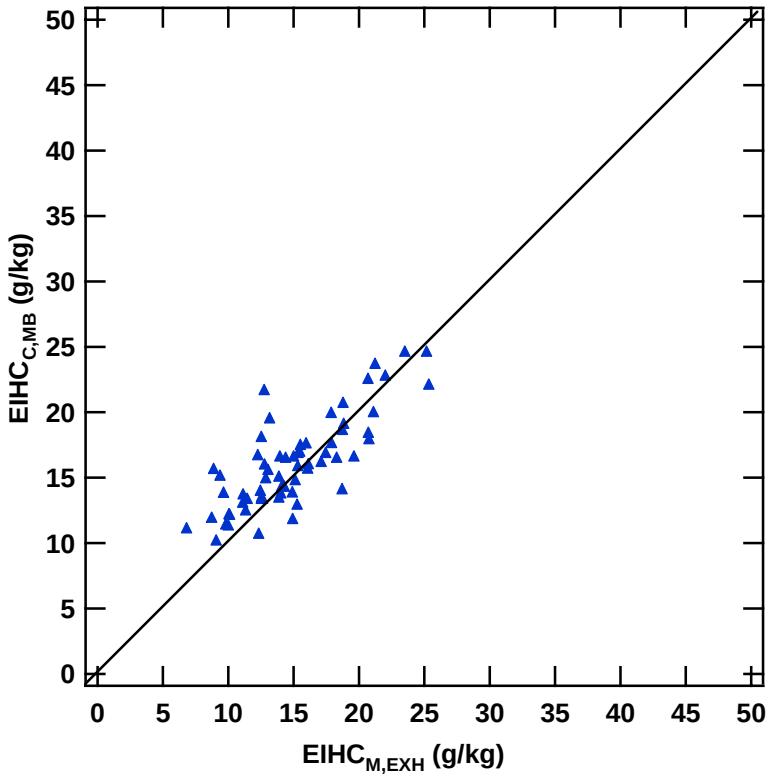

Figure 5.43 Calculated mass of HC vs. the measured HC at the exhaust for the average data fro all the test matrix.

a)

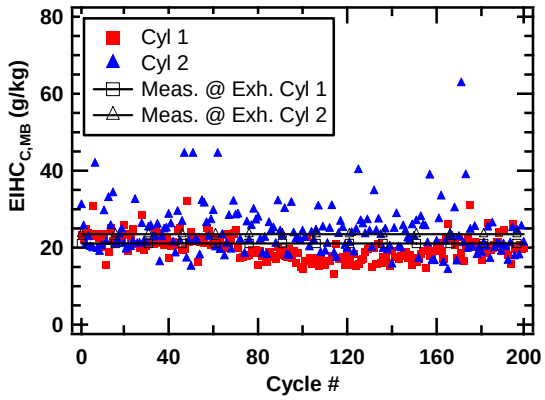

b)

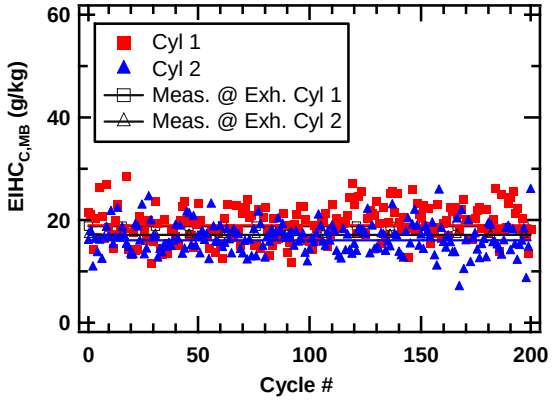

Figure 5.44 Calculated mass of HC vs. the measured HC at the exhaust for the single cycle data for (a) 1750 RPM, 10% load, AF12, and (b) 1750 RPM, 25% load, AF12.

a)

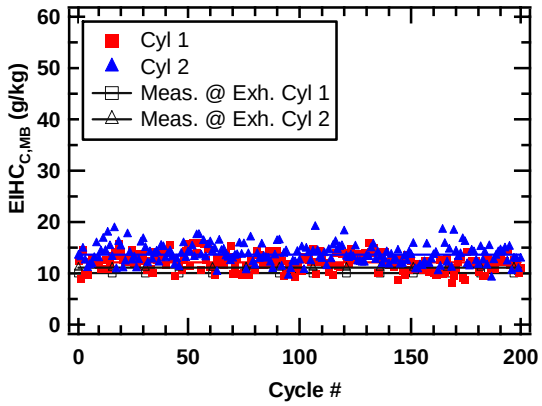

b)

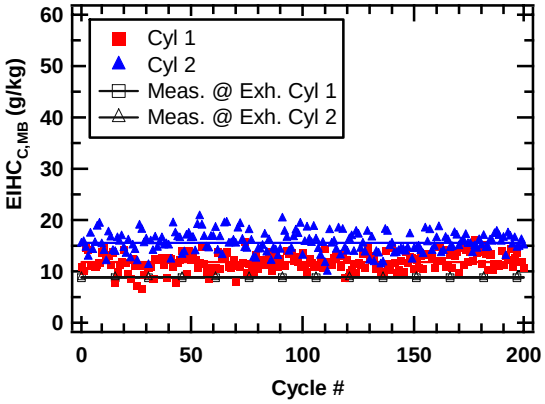

c)

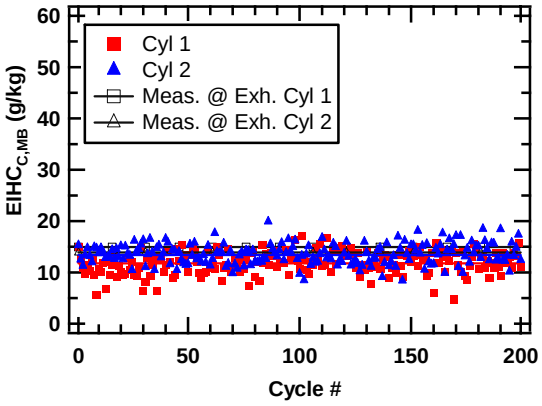

Figure 5.45 Calculated mass of HC vs. the measured HC at the exhaust for the single cycle data for (a) 3060 RPM, 25% load, AF12, (b) 3060 RPM, 50% load, AF12, and (c) 3060 RPM, 100% load, AF12.

5.4.2.3.3.2 COMBUSTION PHASING AND MASS OF HC AT THE EXHAUST

Combustion phasing, usually CA50, is a good indicator the combustion performance. In the present discussion of incomplete combustion, however, the timing of the end of combustion, *e.g.* CA90, is a more appropriate metric. Figures 5.46 to 5.50 show the comparison of the integrate exhaust HC mass with CA90 on a cycle-by-cycle basis. For the 1750 RPM, 10% load case, Fig. 5.46, there is a correlation between CA90 and the integrated exhaust HC mass. As the air fuel ratio is increased this correlation is more visible. The correlation is relatively weak, but still exists, for cycles with early CA90, *i.e.* cycles with late heat release tend to have higher levels of $EIHC_{C,MB}$. It is important to note that there is a direct correlation between highly emitting cycles and very late heat release – all cycles having more than twice the integrated exhaust HC mass have CA90 effectively at EVO. This effect is stronger for the air-fuel ratio 14:1 (Fig. 5.46 (c)) and for cylinder 2, which is in agreement with the concentration results of Fig. 5.33, but because these data take into accounts the mass flow rate variations they are a better indicator that incomplete combustion is a significant contributor to HC emissions. As the load is increased (Fig. 5.47) the combustion phasing is advanced. Thus, for the 1750 RPM, 25% load, AF12 and AF13 (Fig. 5.47 (a)-(b)) all the cycles finish combustion prior EVO. However, for the 1750 RPM, 25% load, AF14 (Fig. 5.47 (c)) there are few cycles that do not complete heat release prior EVO. At this load the correlation between $EIHC_{C,MB}$ and CA90 is weaker than for the 10% load case but still exists. Cylinder 2 still shows more contribution to incomplete combustion.

If the speed is increased as for the 3060 RPM, 25% load case, Fig. 5.48, all the cycles complete combustion prior EVO. Nevertheless, a slight correlation between $EIHC_{C,MB}$ and CA90 is still observed, more pronounced in the case of cylinder 2. A further increase in load at this speed, Fig. 5.49 and 5.50, shows that all the cycles complete energy release relatively early, prior to EVO. For these conditions, there is not a clear correlation between CA90 and the integrated exhaust HC mass and there are not cycles with excessive HC emissions levels.

Overall, the observations above are in agreement with both the single-cycle heat release and the concentration-based results. This suggests that at low load the incomplete combustion could be the source of the high HC levels. To support the weak observations the statistical analysis described in §5.4.2.3.2 was applied, and the results are shown in Table 5.8. Again, the two statistical metrics support the observations that at low load the high levels of HC emissions correlate well with the combustion phasing suggesting that at these conditions the incomplete combustion is the main source of HC emissions.

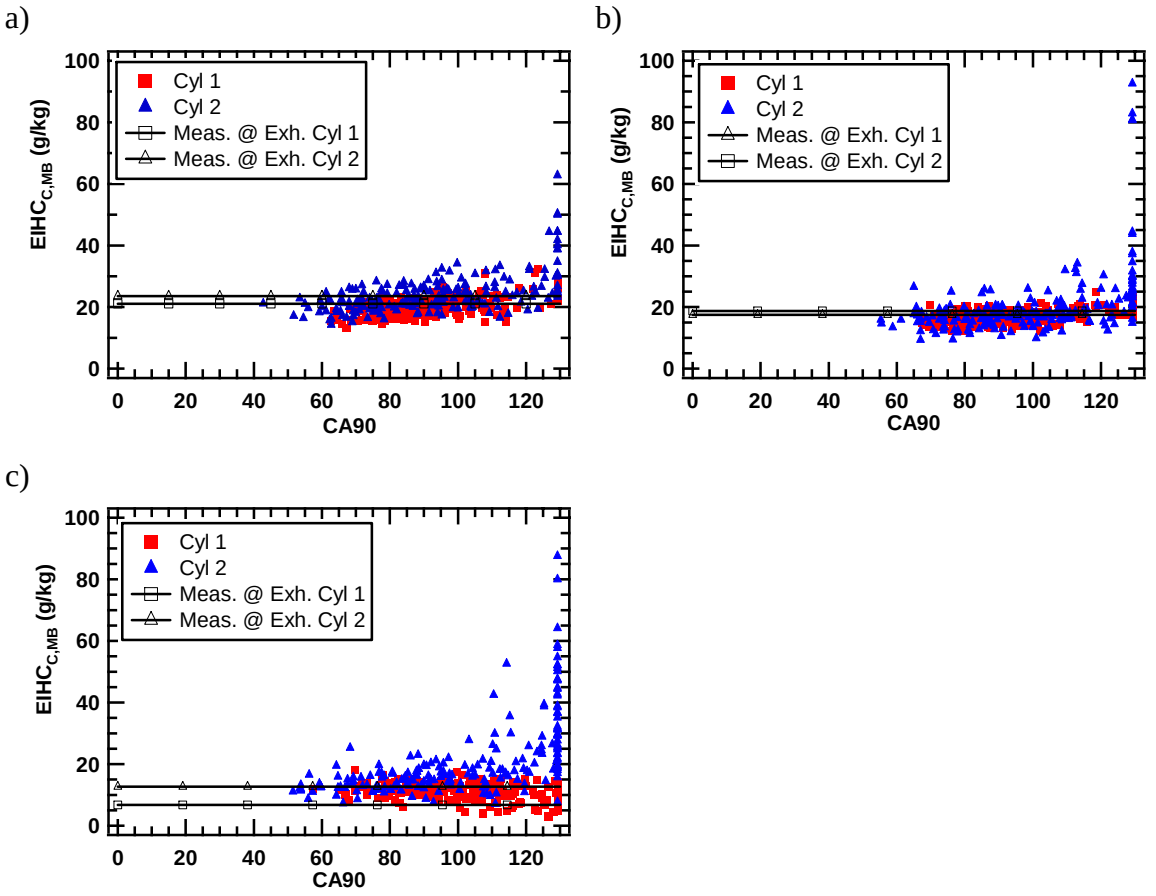

Figure 5.46 Calculated mass of HC vs. CA90 for (a) 1750 RPM, 10% load, AF12, (b) 1750 RPM, 10% load, AF13, and (c) 1750 RPM, 10% load, AF14.

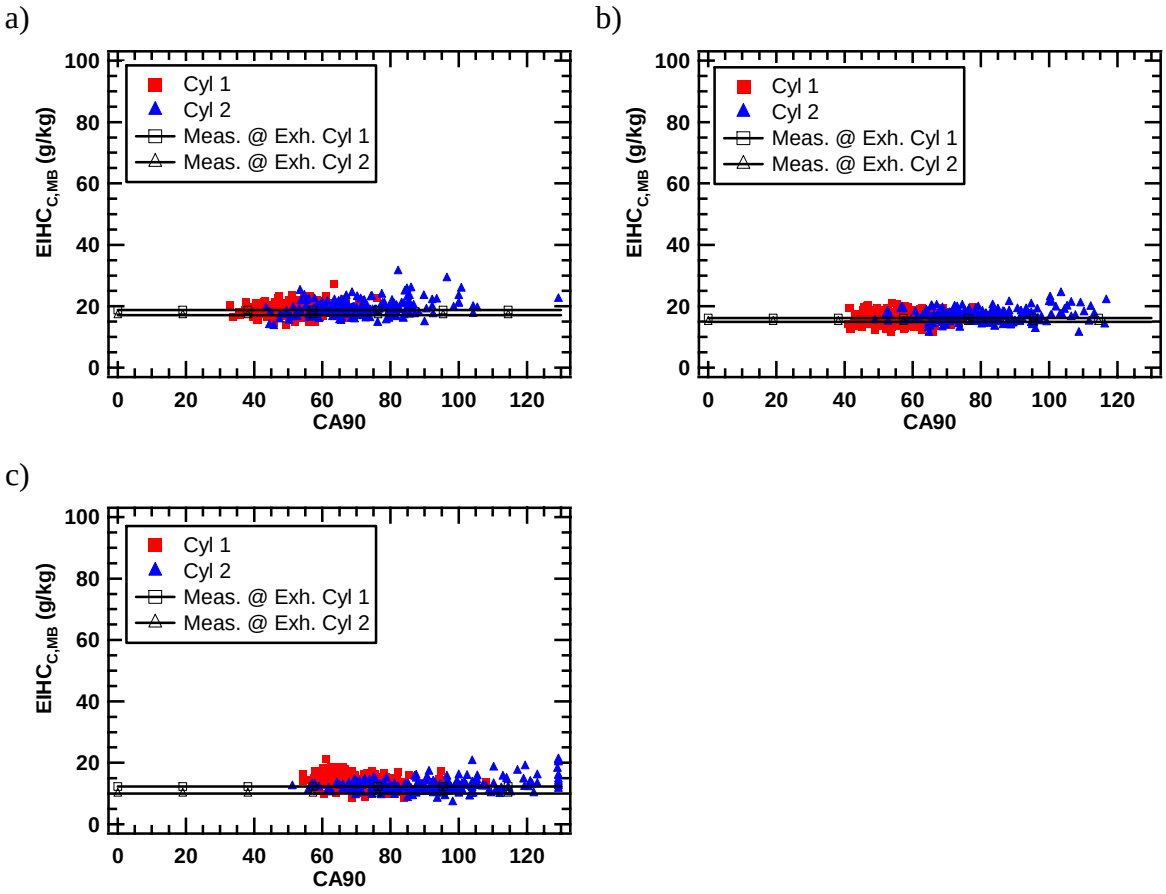

Figure 5.47 Calculated mass of HC vs. CA90 for (a) 1750 RPM, 25% load, AF12, (b) 1750 RPM, 25% load, AF13, and (c) 1750 RPM, 25% load, AF14.

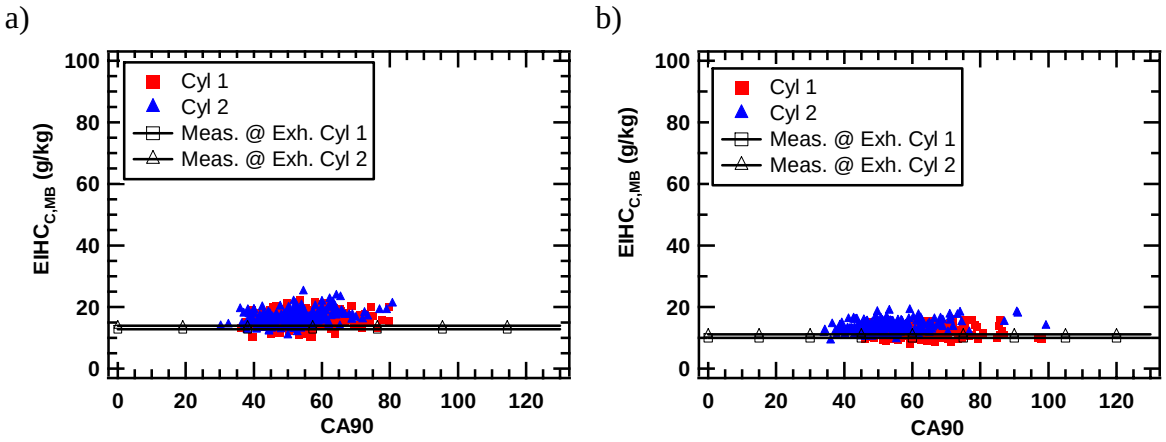

Figure 5.48 Calculated mass of HC vs. CA90 for (a) 3060 RPM, 25% load, AF11, and (b) 3060 RPM, 25% load, AF12.

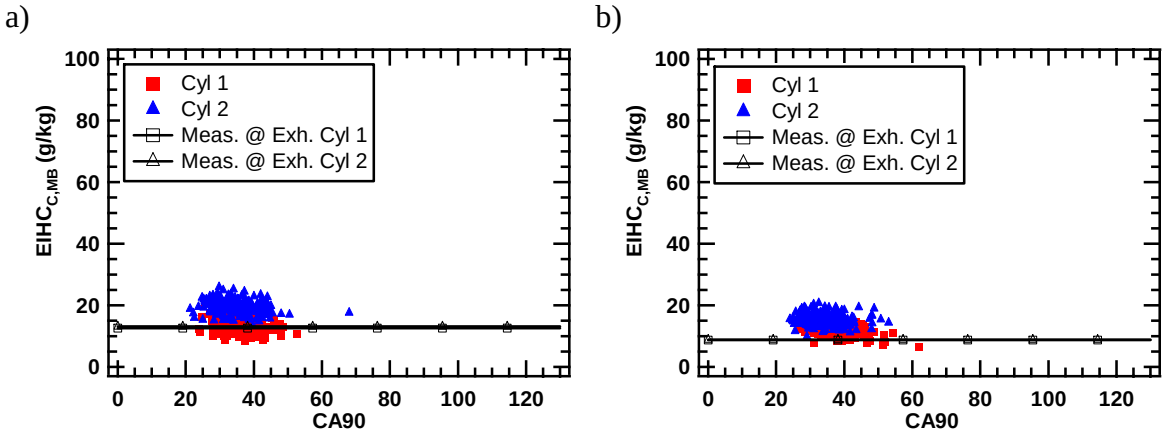

Figure 5.49 Calculated mass of HC vs. CA90 for (a) 3060 RPM, 50% load, AF11, and (b) 3060 RPM, 50% load, AF12.

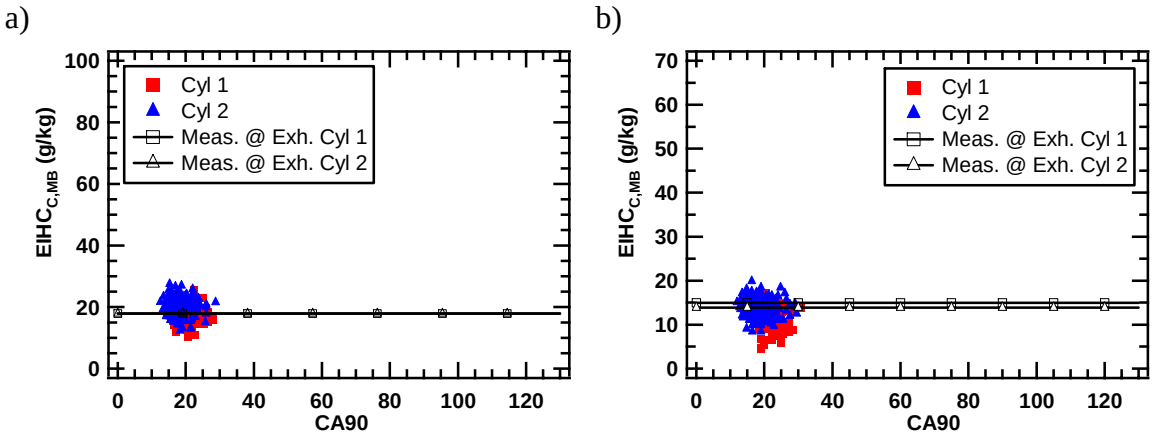

Figure 5.50 Calculated mass of HC vs. CA90 for (a) 3060 RPM, 100% load, AF11, and (b) 3060 RPM, 100% load, AF12.

5.4.2.3.3.3 IMEP AND INTEGRATED EXHAUST HC MASS

Another way to analyze the incomplete combustion at low load is to investigate the dependence of the integrated mass of HC at the exhaust with the *IMEP* (Figs. 5.51-5.55). For the 1750 RPM, 10% load case, the $EIHC_{C,MB}$ correlates very well with the *IMEP* of the same cycle, *i.e.* cycles with low *IMEP* produce high levels of integrated HC mass at the exhaust. This observation is true for both cylinders. Again, cylinder 2 produces higher levels of HC and correspondingly cycles with lower *IMEP*.

For the 1750 RPM, 25% load case, Fig. 5.52, and the 3060 RPM, 25% load case, Fig. 5.53, a slight correlation of the integrated mass of HC and the *IMEP*, is observed especially for cylinder 2. The 3060 RPM, 50 and 100% load cases show that the mass of HC does not correlate with the *IMEP*. It was also shown that for these cases, Fig. 5.49-5.50, there was not correlation between combustion phasing and the mass of HC. Notice that for the 100 % load the relative contribution of each cylinder has been inverted with

respect to the other cases, *i.e.* cylinder 1 is contributing less than cylinder 2 to the HC, and has lower levels of *IMEP*. The statistical analysis explained and applied above was applied to the mass of HC and *IMEP* correlation. The results are shown in Table 5.9, and again they support the theory that the incomplete combustion is likely the main source of HC emissions at low load.

Table 5.8 Linear correlation coefficient, *r* (upper) and uncorrelation probability P_c in % (lower) for the linear relationship between single-cycle integrated exhaust HC mass and the CA90 for all the test matrix.

	Speed (RPM) →			1750		3060	
	Cylinder →			1	2	1	2
Load	10%	AF	12	0.51 0.00	0.57 0.00		
			13	0.48 0.00	0.45 0.00		
			14	-0.32 0.00	0.59 0.00		
	25%	AF	11			0.13 7.44	0.39 0.00
			12	0.17 1.68	0.30 0.00	-0.05 49.18	0.34 0.00
			13	0.02 81.59	0.17 1.61		
			14	-0.24 0.06	0.30 0.00		
	50%	AF	11			-0.30 0.00	-0.17 1.68
			12			-0.38 0.00	-0.15 3.83
	100%	AF	11			-0.10 14.96	-0.05 50.66
			12			-0.10 16.46	-0.08 23.50

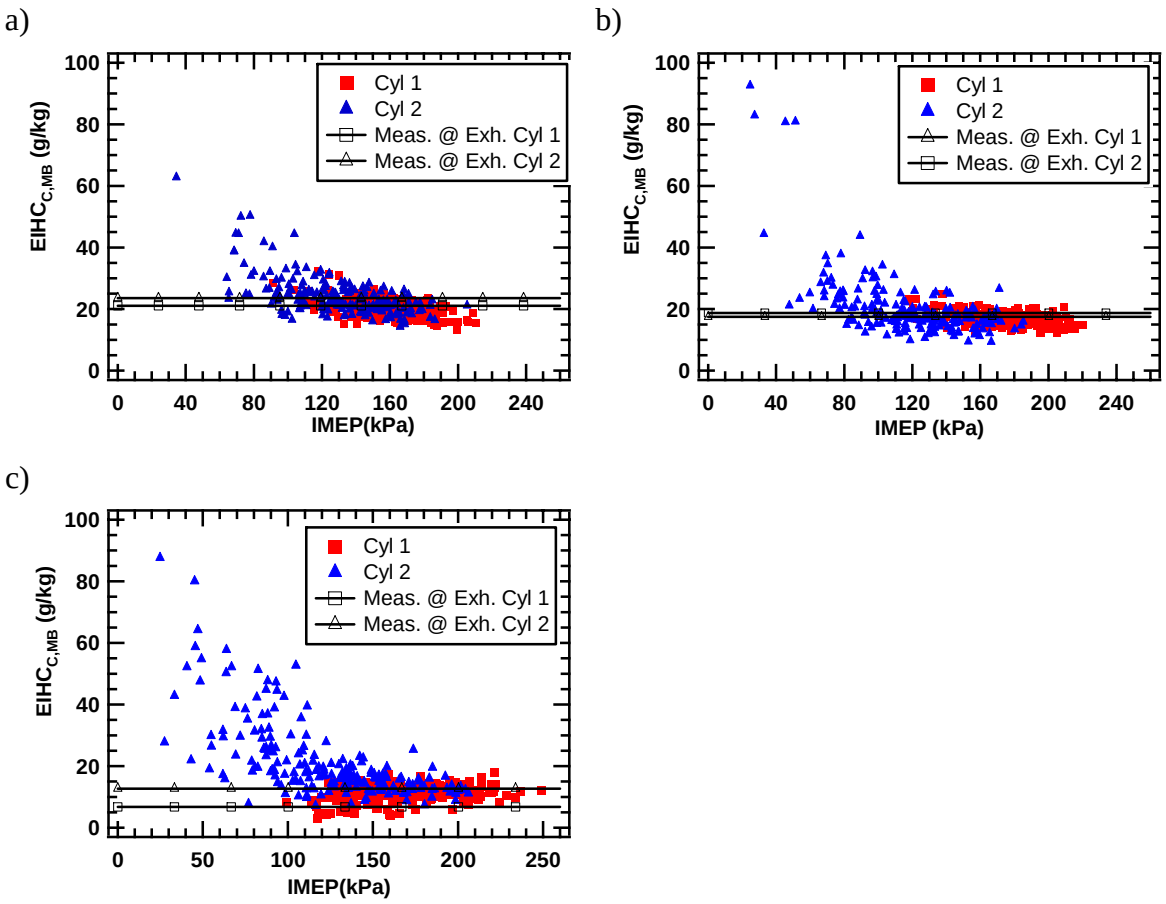

Figure 5.51 IMEP vs. calculated mass of HC for (a) 1750 RPM, 10% load, AF12, (b) 1750 RPM, 10% load, AF13, and (c) 1750 RPM, 10% load, AF14.

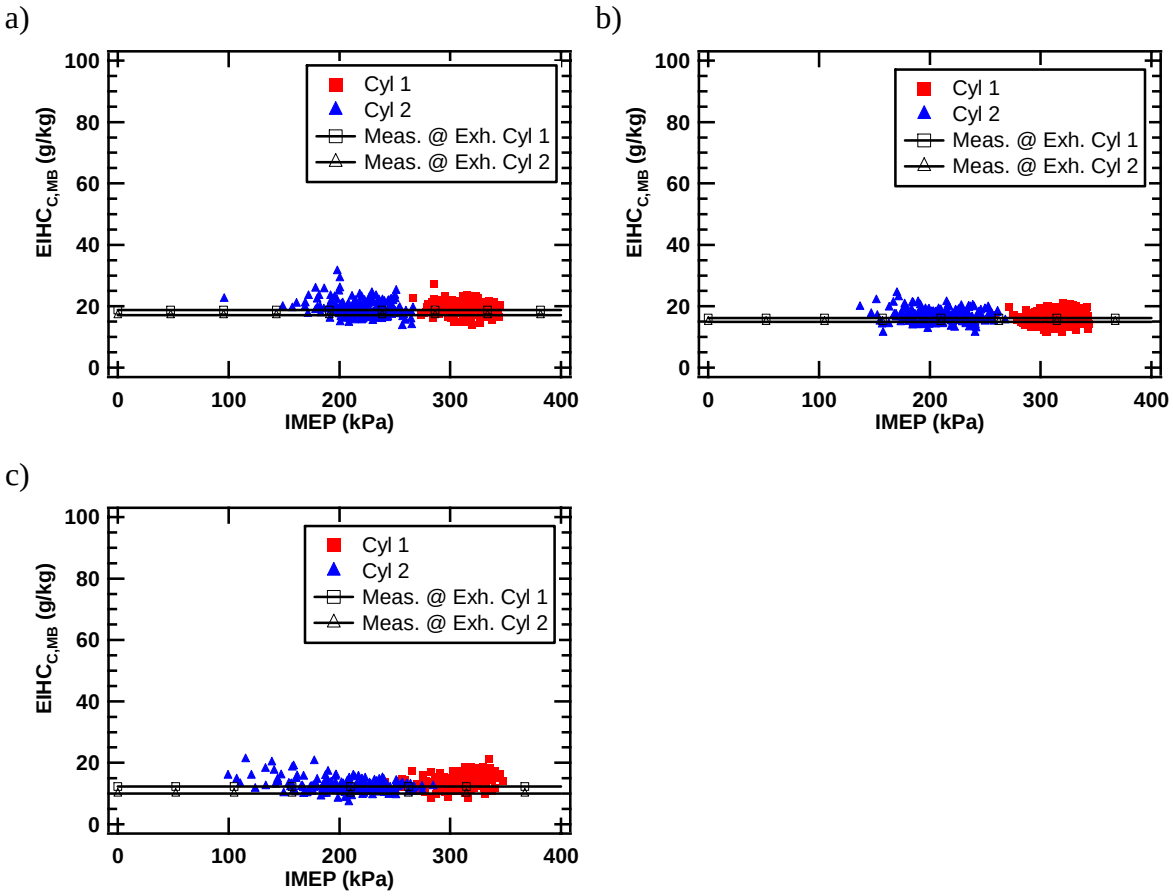

Figure 5.52 IMEP vs. calculated mass of HC for (a) 1750 RPM, 25% load, AF12, (b) 1750 RPM, 25% load, AF13, and (c) 1750 RPM, 25% load, AF14.

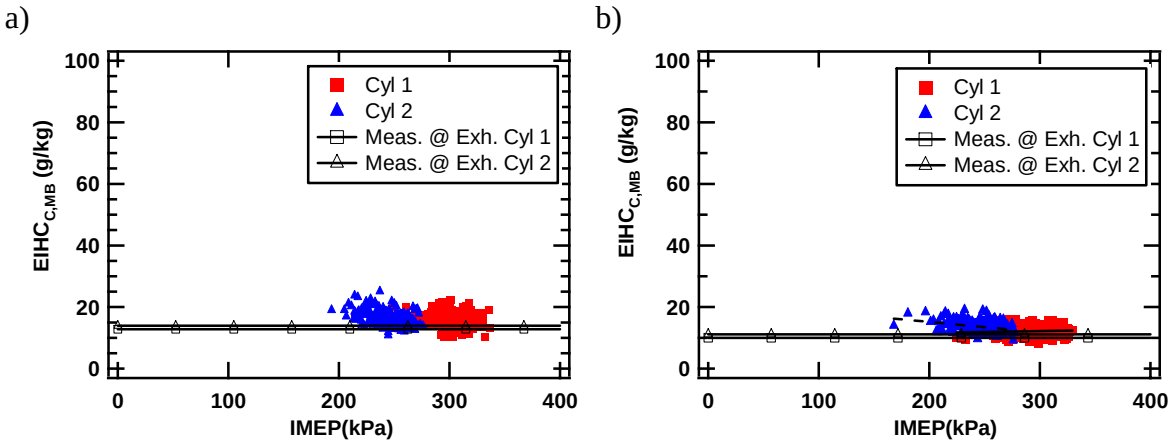

Figure 5.53 IMEP vs. calculated mass of HC for (a) 3060 RPM, 25% load, AF11, and (b) 3060 RPM, 25% load, AF12.

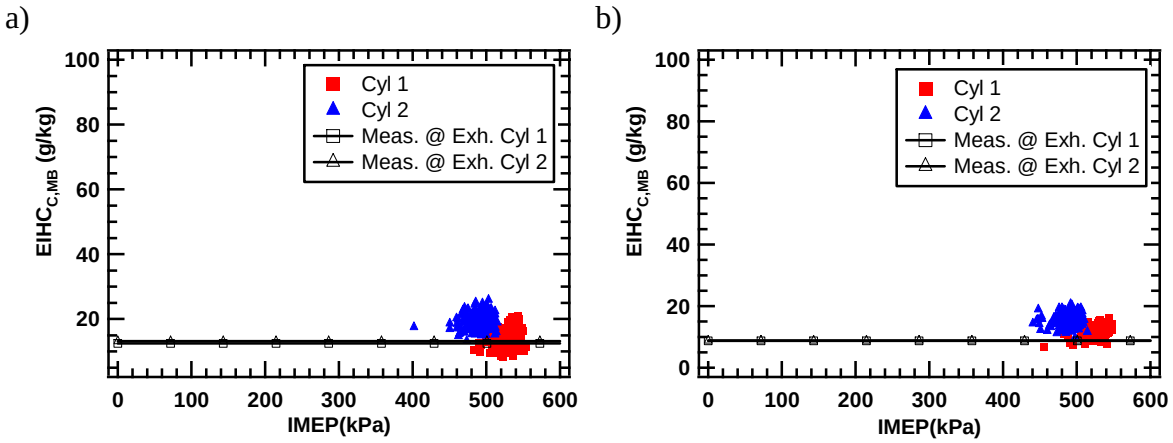

Figure 5.54 IMEP vs. calculated mass of HC for (a) 3060 RPM, 50% load, AF11, and (b) 3060 RPM, 50% load, AF12.

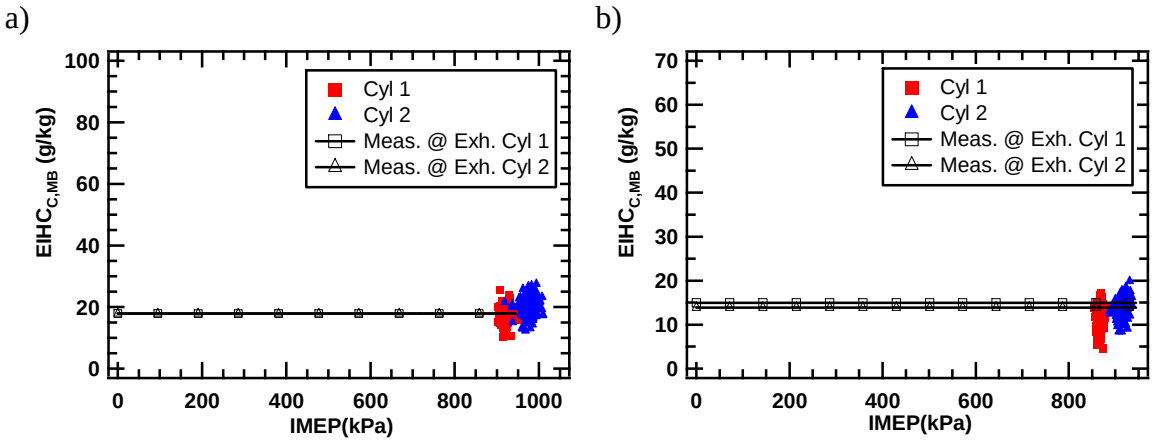

Figure 5.55 IMEP vs. calculated mass of HC for (a) 3060 RPM, 100% load, AF11, and (b) 3060 RPM, 100% load, AF12.

5.4.2.3.3.4 IMEP AND COMBUSTION PHASING (CA90)

The agreement between the results of Figs. 5.46-5.50 and 5.51-5.55 is not surprising given that there is a nearly direct relationship between combustion phasing and cycle work (IMEP). This relationship is seen in Fig. 5.56, where all of the individual-cycle data for the air-fuel ratio 12:1 are shown (similar dependence was observed for the other air-fuel ratios). There is a nearly one-to-one correspondence between CA90 and IMEP. The fact that the integrated exhaust HC mass data correlates better with IMEP is a little surprising given this correspondence between CA90 and IMEP. The choice of CA90 as the correlating parameter in Fig.5.56 was in deference to the ring pack HC model. Figure 5.56 show that there is a strong linear relationship between the CA90 timing and the IMEP, with retarded cycles having low IMEP as would be expected.

Table 5.9 Linear correlation coefficient, r (upper) and uncorrelation probability P_c in % (lower) for the linear relationship between single-cycle IMEP and the integrated mass of HC for all the test matrix.

	Speed (RPM) →			1750		3060	
	Cylinder →			1	2	1	2
Load	10%	AF	12	-0.51 0.00	-0.60 0.00		
			13	-0.49 0.00	-0.58 0.00		
			14	0.32 0.00	-0.66 0.00		
	25%	AF	11			-0.12 9.24	-0.39 0.00
			12	-0.15 3.91	-0.26 0.02	0.07 36.09	-0.32 0.00
			13	-0.01 86.61	-0.15 3.29		
			14	0.27 0.01	-0.34 0.00		
	50%	AF	11			0.28 0.01	0.18 1.31
			12			0.37 0.00	0.09 19.56
	100%	AF	11			0.10 17.94	0.02 79.42
			12			0.09 19.73	-0.03 67.78

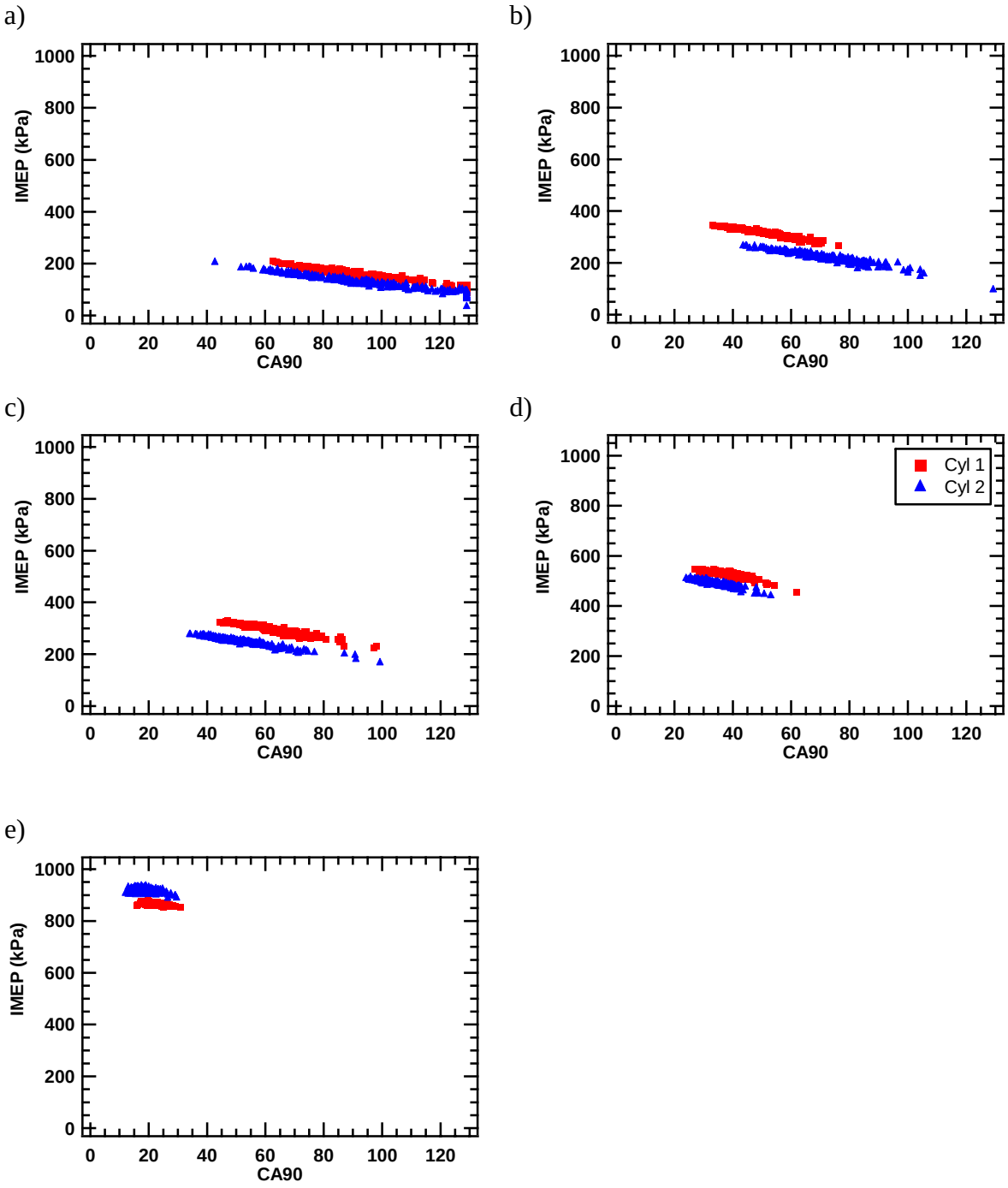

Figure 5.56 CA90 vs. IMEP for (a) 1750 RPM, 10% load, AF12, (b) 1750 RPM, 25% load, AF12, (c) 3060 RPM, 25% load, AF12, (d) 3060 RPM, 50% load, AF12 and (e) 3060 RPM, 100% load, AF12.

5.4.3 CONDITIONAL SAMPLING ANALYSIS

In order to further investigate the role of the ring pack on HC emissions, conditional sampling was performed by dividing the cycles into five groups (0-20%, 20-40%, 40-60%, 60-80% and 80-100%) according to their combustion phasing. The combustion phasing investigated was the CA90 time, and the assignment into groups was made based on where an individual cycle fell in the CA90max - CA90min range; it was not based on an ordinal ranking. Thus, the 0-20% group represents the fastest cycles and those in the 80-100% group are the cycles having the most retarded combustion phasing. It is not a requirement to have the same number of cycles in all groups.

5.4.3.1 HEAT RELEASE - CONDITIONAL SAMPLING ANALYSIS

Figure 5.57 shows the average heat release of each of the five groups for all the conditions of the test matrix with air-fuel ratio of 12:1. For the 1750 RPM, 10% load case, Fig. 5.57 (a), the cycles in the 0-20% group release all their energy before EVO; the cycles in the 20-40% range of CA90 also show that on average combustion completes before EVO (This group represents the largest percentage of the analyzed cycles). The remaining sets of cycles (40-60%, 60-80%, and 80-100%) exhibit heat release that extends beyond EVO. For these cycles, incomplete combustion is expected to contribute to the HC emissions, while the 0-20% and 20-40% cycles may not have an HC contribution from incomplete combustion. As the load is increased to 25%, Fig. 5.57 (b), in the case of cylinder 1 all the groups show complete combustion prior EVO. However, for cylinder 2 there are still some groups that show incomplete combustion. The number

of groups contributing to in complete combustion has been reduced, thus the 40-60% group which finished combustion after EVO at 10% load, for the 25% load shows that completes combustion prior EVO. However, the remaining groups, 60-80% and 80-100%, show incomplete combustion. The 80-100% fraction shows similar profile of heat release than the same group for the 10% load (Fig. 5.57 (a)). This indicates that at this condition there are some cycles that may be contributing to the HC emissions due to incomplete combustion.

At the 3060 RPM, 25% load condition, Fig. 5.58 (a), the majority of the cycles complete combustion before EVO (0-20%, 20-40%, 40-60%, and 60-80%). However, the 80-100% group of cycles shows late combustion, suggesting that for this condition this subgroup of cycles may have incomplete combustion. This shows that although on average the ring pack is the main contributor to the HC emissions, there may be some cycles where the incomplete combustion is present and adversely affecting HC emissions. As the load is increased, as for the 50 and 100% load conditions, Fig. 5.58(b)-(c), none of the groups shows late combustion phasing. For these conditions it is clear that incomplete combustion is not a significant contributor to the engine-out HC emissions, suggesting that the ring pack crevices are the major source of engine-out HC emissions. Similar results were observed for the other air-fuel ratios of the test matrix.

a)

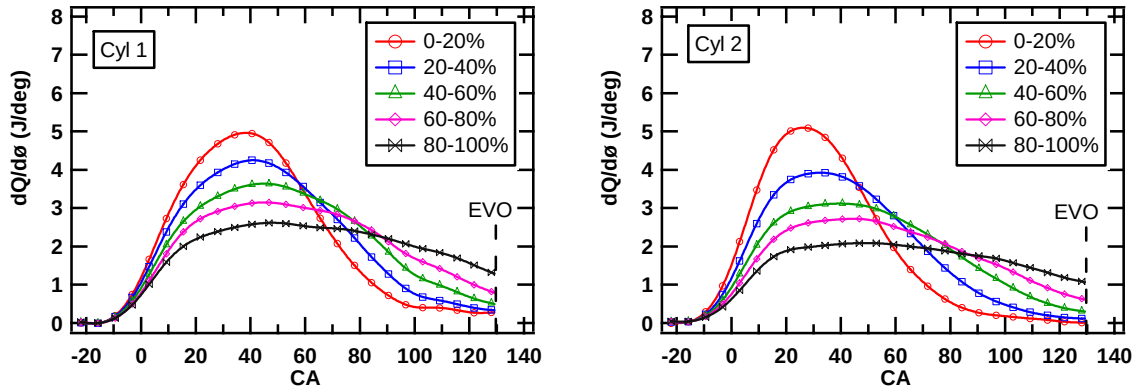

b)

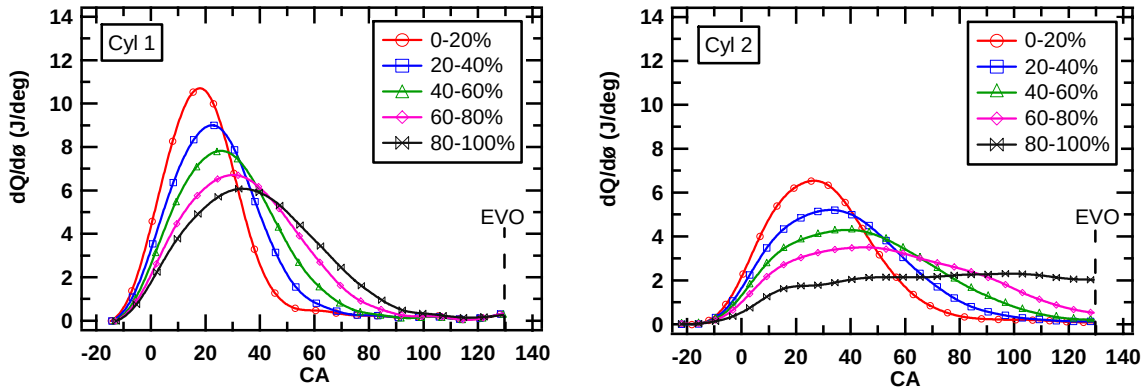

Figure 5.57 Conditional Sampling of the heat release for (a) 1750 RPM, 10% load, AF12, and (b) 1750 RPM, 25% load, AF12.

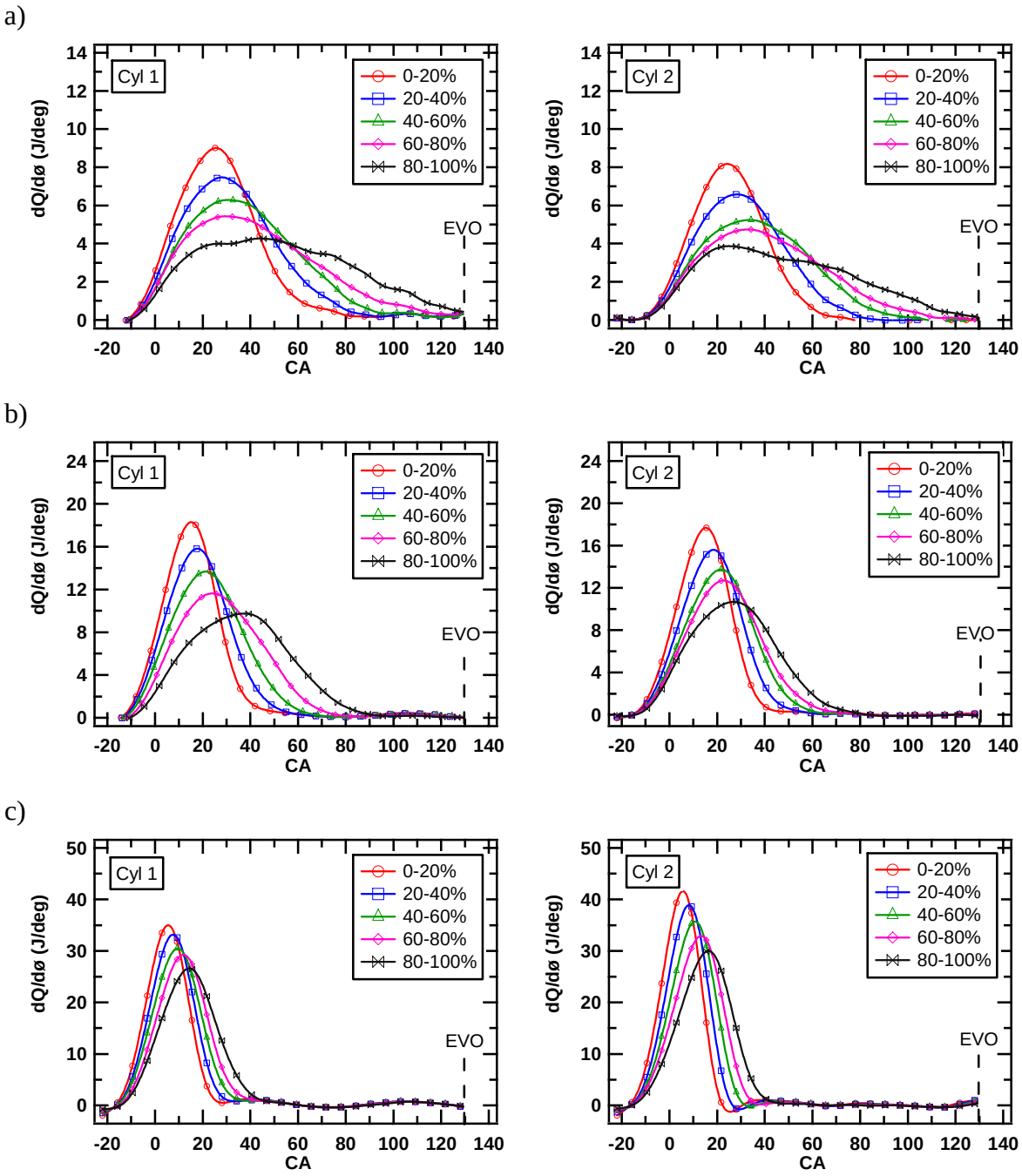

Figure 5.58 Conditional sampling of the heat release for (a) 3060 RPM, 25% load, AF12, (b) 3060 RPM, 50% load, AF12, and (c) 3060 RPM, 100% load, AF12, showing the averages of the intervals under study.

5.4.3.2 RING PACK CONTRIBUTION-CONDITIONAL SAMPLING ANALYSIS

The use of conditional sampling has identified sub-groups within the ensemble of cycles that may fall into different emission regimes. This is further investigated using single-cycle results from the ring pack model and the integrated exhaust HC mass. Figures 5.59-5.60 shows the conditionally sampled results of the $EIHC_{C,RP}$ on the vertical axis and the $EIHC_{C,MB}$ on the horizontal axis, where the symbol color identifies the sub-group. The circular symbol on the 45° line that has vertical and horizontal cross-hairs through it represents the steady state emission value. Cycles above the horizontal cross-hair are expected to have HC emissions largely dominated by the ring pack mechanism. Beginning with the 3060 RPM, 100% load condition, Fig. 5.60 (c), one can see that all of the cycles from each of the sub-groups greatly exceed both the steady state emission value as well as the corresponding single-cycle integrated exhaust HC mass. This confirms that for all of these cycles the previous result that the ring pack dominates the HC emissions remains valid. Similar behavior is observed for the 3060 RPM, 50% load case, Fig. 5.60 (b).

The 1750 RPM, 10% load case, Fig. 5.59 (a), also gives results that are consistent with the previous discussion (§5.4.3.1). Consider the $EIHC_{C,RP}$ using the CA90-EVC integration period. For all of the cycles in all of the subgroups for both cylinders, the $EIHC_{C,RP}$ is less than the steady-state emission value. Further, the $EIHC_{C,RP}$ is less than the $EIHC_{C,MB}$ for almost all of the cycles. Both of these results strongly suggest that the

ring pack, while contributing to the HC emissions, does not dominate the HC emissions at this condition. The wide spread in the $EIHC_{C,MB}$ for the 80-100% group indicates that there are individual cycles that are contributing excess HC. As seen in Figs. 5.46 and 5.51, these cycles are correlated with late-burning, low work-producing cycles, and thus, incomplete combustion in the cylinder. For the 1750 RPM, 25% load case, Fig. 5.59 (b), shows that for cylinder 1 about half of the total number of cycles do not exhibit emissions that are ring-pack dominated. However, for cylinder 2, the majority of the cycles show that $EIHC_{C,RP}$ is less than the $EIHC_{C,MB}$, although the horizontal spreading for the group of cycles with very late combustion (60-80% and 80-100%) has been reduced. The results suggest that for this condition the HC emissions may be highly dominated by the incomplete combustion, especially for cylinder 2.

The 3060 RPM, 25% load condition conditionally sampled results, Fig. 5.60 (a), give indication that the different sub-groups may fall into different emission regimes. Consider again the $EIHC_{C,RP}$ results using the CA90-EVC integration period. For both cylinders, the late combustion cycles – 60-80% and 80-100% – have $EIHC_{C,RP}$ less than the steady state emission level. It is likely that some level of post-oxidation does occur for these conditions, so the fact that these cycles emit an amount of HC that is even close to, let alone less than, the steady state exhaust value strongly suggests that there are other sources of HC contributing to the exhaust measurement. These late-burning cycles also have an $EIHC_{C,MB}$ that is higher than the $EIHC_{C,RP}$, which supports the notion that there are other sources of HC besides the ring pack that are contributing significantly to the HC emissions. As seen in Fig. 5.60 (a), the 80-100% group has a heat release that extends to

EVO, which suggests that incomplete combustion can be contributing to the HC emissions.

a)

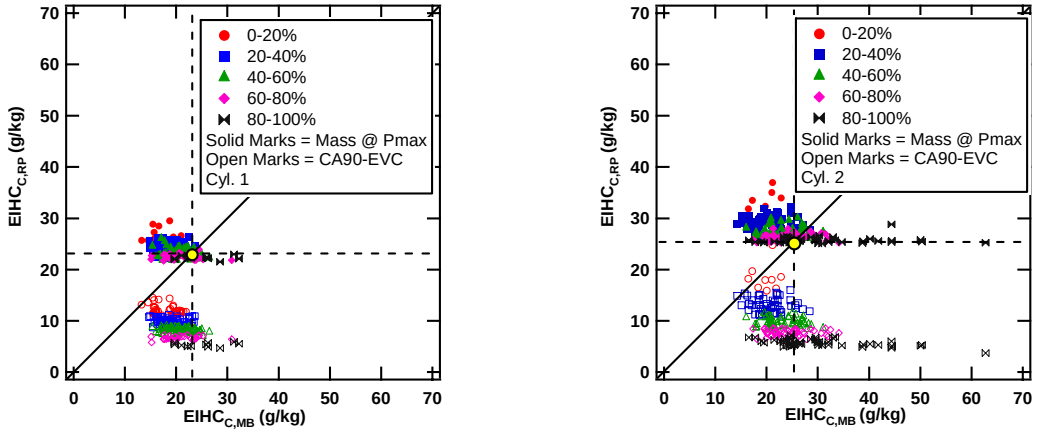

b)

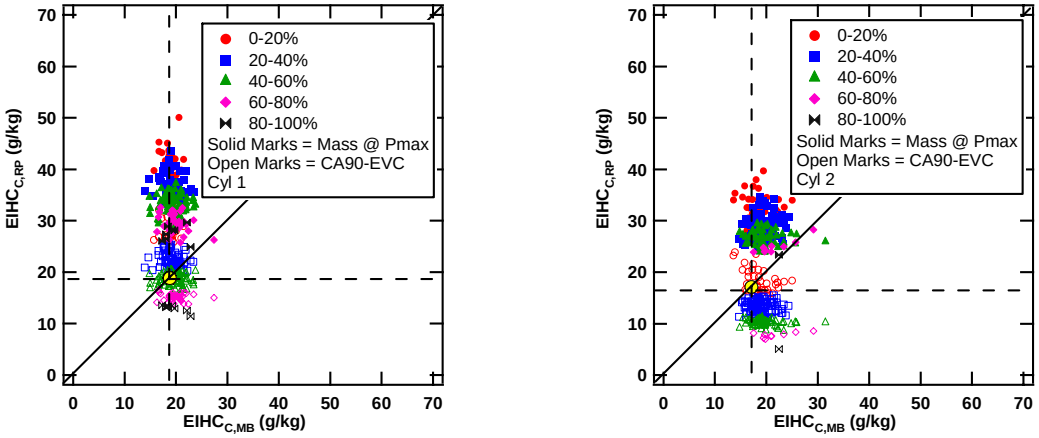

Figure 5.59 Ring pack HC estimation vs. the HC mass at the exhaust for the (a) 1750 RPM, 10% load, AF 12, and (b) 1750 RPM, 25% load, AF12.

a)

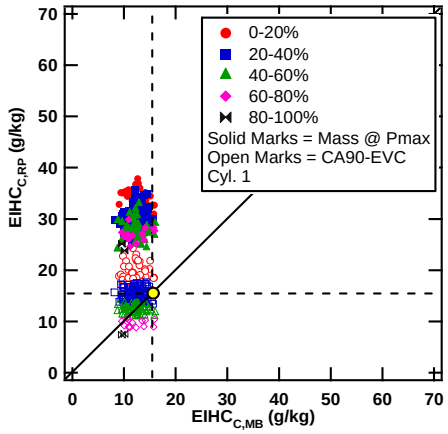

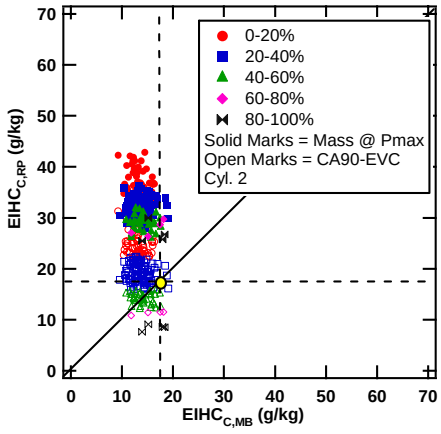

b)

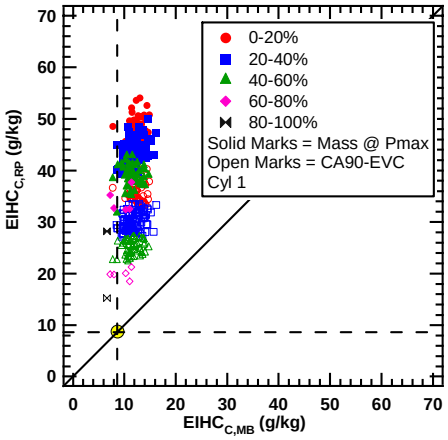

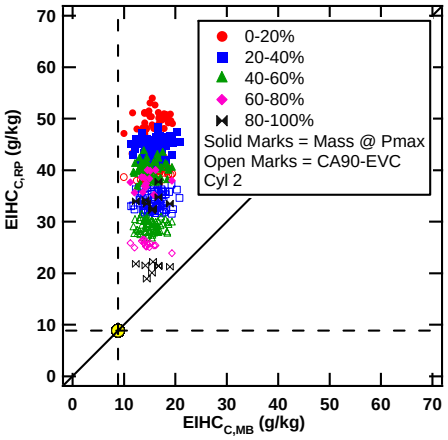

c)

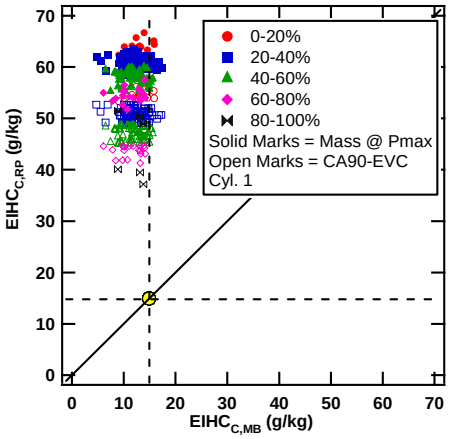

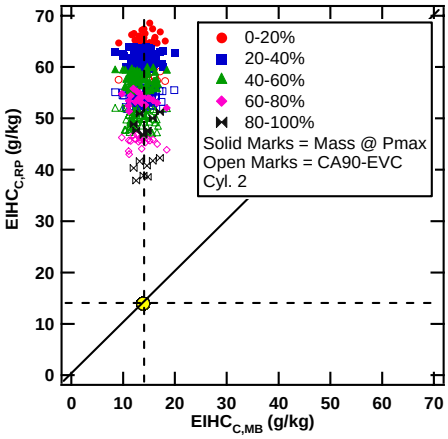

Figure 5.60 Ring pack HC estimation vs. the HC mass at the exhaust for the (a) 3060RPM, 25% load, AF 12, (b) 3060 RPM, 50% load, AF12, and (c) 3060 RPM, 100% load, AF12.

5.4.3.3 CYCLE RESOLVED HC EMISSIONS - CONDITIONAL SAMPLING ANALYSIS

The overall discussion of the sources of HC emissions and the conditional sampling analysis also provide further insight into the interpretation of the time-resolved HC concentrations. Figure 5.61 and 5.62 shows the HC concentrations as a function of crank angle for the conditions discussed above and for each sub-group. The steady state measurements of HC concentration is shown as the horizontal line. Beginning with the 3060 RPM, 100% load condition, where the ring pack dominates the HC emissions, one sees in Fig. 5.62 (c) the typical HC profile observed in the literature, and there is very little effect of the different combustion phasings. At EVO the HC concentration immediately decreases during the blowdown process as the burned cylinder gases escape the cylinder, the HC concentration remains low during most of the exhaust valve open period, then increases near the end of the exhaust stroke as the mass released from the ring pack is pushed out of the cylinder. It is assumed that the main burned gas charge has a very low concentration of HC, and there is a nearly plug-type flow in the port.

The time-resolved HC concentration history for the 1750 RPM, 10% load condition (Fig. 5.61(a)) has a very different character than the 3060 RPM 100% load condition. At the time of EVO the HC concentration increases for all of the sub-groups, but for the late-combustion groups, e.g. the 80-100% group, the increase is larger. The mixture in the port prior to EVO is the mixture left over from the previous cycle. The increase observed at EVO then indicates that the initial burned gases leaving the cylinder have a higher HC content than the last mixture to leave the cylinder. This is consistent

with the notion that incomplete combustion is significantly contributing to HC emissions under these conditions. The oscillations seen in any of the individual traces correlate well with both, the pressure oscillations and the calculated instantaneous mass flow in the exhaust port.

At the high load condition where combustion is complete and the ring pack is dominating the HC emissions, the HC concentration was seen to immediately decrease at EVO, almost at the instrument response rate. However, at the low load condition where there is sufficient evidence provided above that incomplete combustion is a contributor to HC emissions, the HC concentration is seen to increase at EVO. This suggests that the gradient of the HC concentration in the period just after EVO is an indicator of incomplete combustion. It is expected that the first mixture to exit the combustion chamber is burned gas, which has a low HC concentration, causing a sharp decrease in the measured HC concentration. Therefore, a gradient in HC concentration in the early part of the exhaust process that is less steep indicates that there is some incomplete combustion, either in the bulk gas or in mixture trapped in crevices near the head. The data from the 25% load, at 1750 RPM and 3060 RPM conditions provide further confirmation of these observations. At the 3060 PRM, 25% load condition the ring pack contribution to the HC emissions is large, but there is ample evidence that it is not the dominant source of HC. The steady state model results show that the integrated mass from CA90 to EVO is just barely larger than that measured in the exhaust, and the conditionally sampled results in Fig.5.60 (a) indicated that for the most retarded condition

the $EIHC_{C,RP}$ was less than the measured EIHC. Given the possibility that post-oxidation will occur, this suggests that other HC emission mechanisms are contributing.

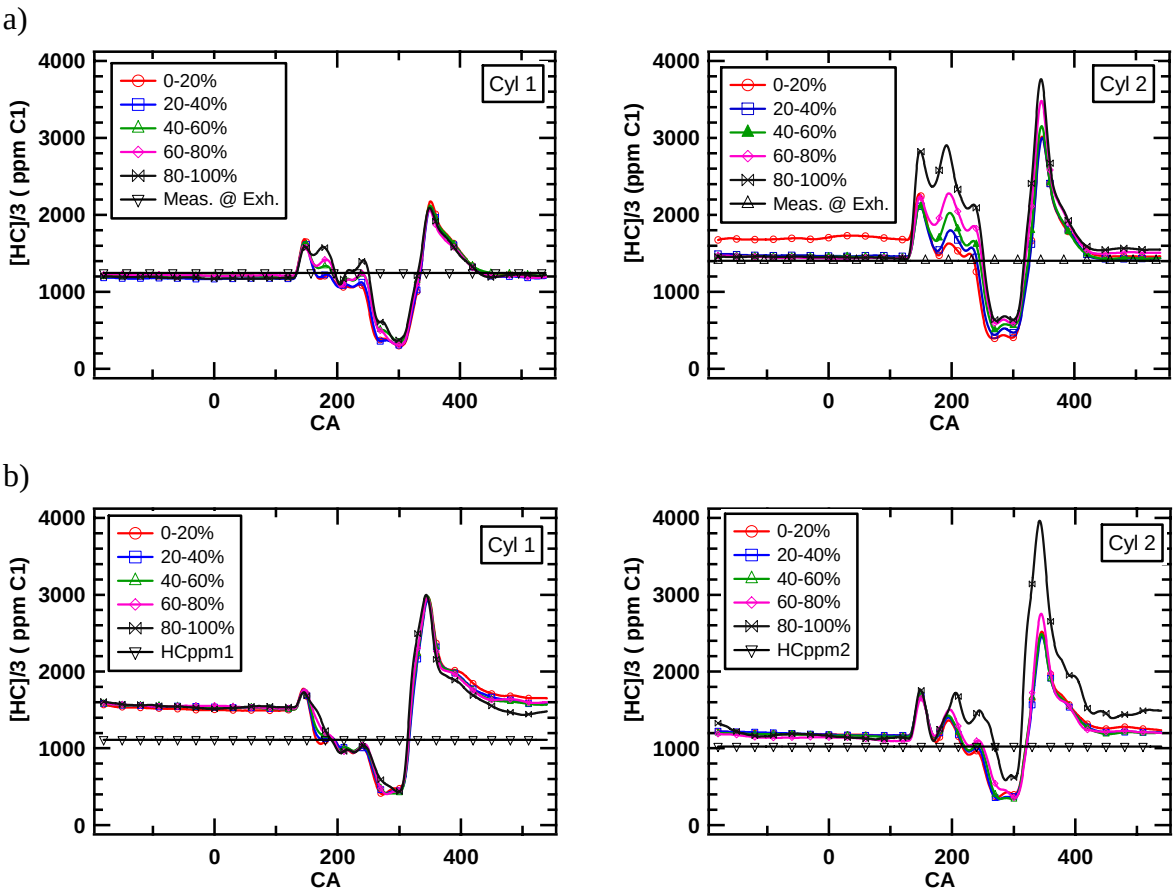

Figure 5.61 Fast FID average traces for the different CA90 sections for (a) 1750 RPM, 10% load, AF12, and (b) 1750 RPM, 25% load, AF12.

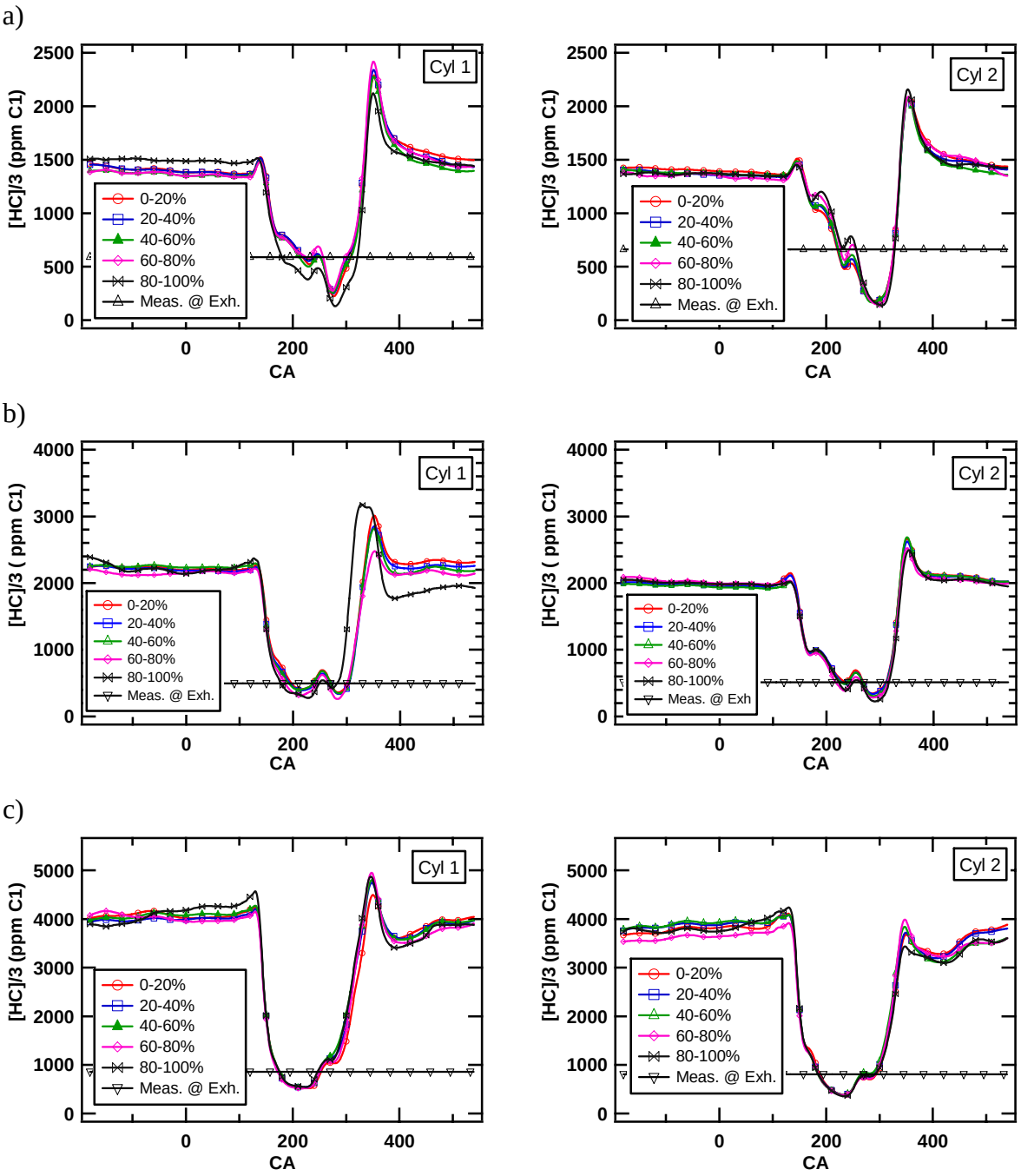

Figure 5.62 Fast FID average traces for the different CA90 sections for (a) 3060 RPM, 25% load, AF12, (b) 3060 RPM, 50% load, AF12, and (b) 3060 RPM, 100% load, AF12.

5.5 SUMMARY

The relative contribution of the ring pack crevices to the HC emissions from a small utility engine was investigated under steady, fully warmed up conditions. The ring pack crevice contribution to HC emissions was evaluated using a simple ring pack filling and discharging model. The model results compared quite favorably to the measured blowby over the full range of conditions tested. The model was used on both an average and single-cycle basis. Two metrics to characterize the emissions were implemented: the mass stored at maximum pressure, and the mass that returns to the combustion chamber from the time when the cumulative burn mass fraction reaches 90 percent to the time when the exhaust valve closes (CA90-EVC). The predictions show that at high load the ring pack is the major contributor to the engine-out HC emissions. However at low load the mass that returns from the ring pack to the cylinder from CA90 to EVC does not account for the measured HC emission at the exhaust, indicating that the ring pack is not the major contributor and that other sources are contributing to the HC emissions. Further analysis on a single-cycle basis showed that at low load incomplete combustion was a likely contributor to the high levels of HC emissions observed. Incomplete combustion was characterized using both concentration- and mass-based correlations. For the concentration-based correlation the cycle-resolved HC concentration at 160 aTDC was correlated with the *IMEP*. At low load the results show a good correlation between the HC concentration and the *IMEP*; cycles with low *IMEP* produce high levels of HC. At high load the results show no correlation. For the HC mass-based correlation, the mass of

HC per cycle leaving the engine was correlated with the combustion phasing and with the *IMEP*. At low load the correlation was significant, however at high load no correlation was observed. A statistical analysis verified that at low load the correlations were meaningful. The results also showed that there is an intermediate load condition where incomplete combustion vanishes and the ring pack starts to be the main HC contributor. For this intermediate condition, although the ensemble-average ring pack model results showed that the mass that returns to the combustion chamber from the top land is slightly higher than the measured HC at the exhaust, the conditional sampling analysis showed that there are some sub-groups of cycles with late combustion where the ring pack contribution is smaller than the measured at the exhaust. It is expected that at this condition there is some in-cylinder post oxidation and the late burning cycles do not contribute excessively to the engine-out HC emission.

CHAPTER VI

FUEL ADSORPTION-DESORPTION IN THE CYLINDER OIL LAYER

6.1 INTRODUCTION

The fuel adsorption and desorption by the oil film mechanism is thought to be one of the main contributors to the engine-out HC emissions [4]. Currently, it is well known that the unburned fuel adsorbs into lubricating oil on the cylinder liner during the intake and compression strokes. Consequently, part of the fuel is hidden from the flame during the main combustion, escaping oxidation. Later, during the expansion and exhaust strokes this stored fuel desorbs, releasing unburned fuel to the cylinder and contributing to the HC emissions. It is important to note that part of the released fuel may be oxidized in the cylinder during the post-flame period [30, 41]. One of the main difficulties in the study of the relative oil film contribution to the HC emission is that it is coupled with the ring pack mechanism. Both HC mechanisms release the fuel to the combustion chamber after the flame arrival for approximately the same period of time. As mentioned before in §2.7, the studies of the oil film relative contribution to the engine-out HC emission are diverse and conflicting, *i.e.* some believe that is a significant contributor [38] and other authors do not [39]. In spite of these differences, it is believed that the oil-fuel adsorption-desorption mechanism does contribute in some degree to the HC emissions.

In the present chapter the effect of the oil-fuel adsorption-desorption problem is studied for a small air-cooled utility engine. The effect of the oil layer on the HC emissions was investigated by running the engine with two different fuels that had different solubility in oil: a research-grade gasoline and propane. Comparison of the steady state HC emissions, cycle-resolved HC emissions, estimation of the ring pack contribution to the HC emissions and the effect of the crankcase pressure were carried out to understand the role of the oil film on the engine-out HC emissions. In addition, the experimental findings were supported with a numerical simulation of the fuel-oil diffusion mechanism.

6.2 TEST CONDITIONS

The engine was tested at various loads, for low and high speeds, and several spark timings at a constant equivalence ratio of 1.2 (Table 6.1). The equivalence ratio of 1.2 corresponds to an air-fuel ratio of 12:1 for gasoline and 12.9:1 for propane. The engine operates at all loads and speeds at this equivalence-ratio; therefore, it was chosen to compare the engine behavior under the two fuels. It is important to mention that the setup for this study was implemented with an arrangement of valves and gages to control the crankcase pressure (see §3.2.7), which allowed the study of the influence of the crankcase pressure on the HC emissions. To estimate the trapped mass in each cylinder spark sweep tests at constant throttle position were performed for the propane tests, as well.

Table 6.1 Test matrix (Equiv. ratio, Φ=1.21)

	LOAD		
SPEED (RPM)	10%	25%	50%
1750	x	x	
3060		x	x

6.3 RESULTS AND DISCUSSION

6.3.1 AVERAGE HC EMISSIONS

In order to isolate the effect of the oil film on the HC emissions the engine was fired at the equivalence ratio (Φ) of 1.21 for the gasoline and propane tests. Figure 6.1 shows the comparison of the average HC emissions for various loads and speeds (cases) for both fuels. Both fuels show similar trends with speed and load; some slight differences in the behavior of cylinder 1 and cylinder 2 can be seen for the 3060 RPM, 25% load, and 3060 RPM, 50% load cases, *i.e.* the cylinder that contributes more to the HC emissions when the engine is fueled with gasoline, contributes less when propane is used to fire the engine. These differences could possibly be attributed to the difference in the combustion process taking place in each cylinder when the fuel is changed. It is important to note that in spite of these slight differences, the measured emissions are very close in magnitude, and follow the same trends in both a qualitative and quantitative manner.

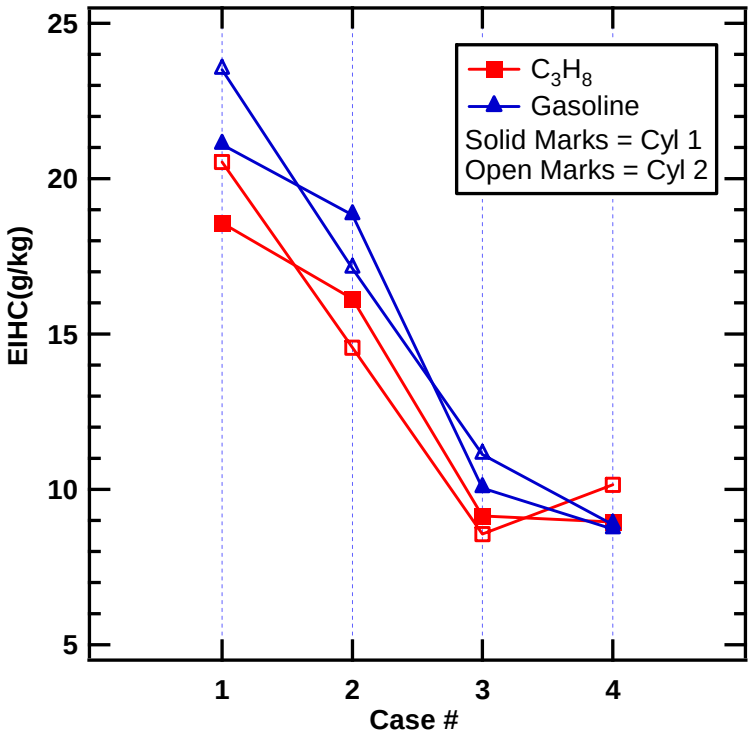

Figure 6.1 Average HC emissions comparison between propane and gasoline for: (case 1), 1750 RPM, 10% load, (case 2) 1750 RPM, 25% load, (case 3) 3060 RPM, 25% load, and (case 4) 3060 RPM, 50% load,. The crankcase pressure for all cases was 101.85 kPa and Φ=1.21.

6.3.2 CRANKCASE PRESSURE EFFECT ON THE AVERAGE HC EMISSIONS

In section §5.2.6 a sensitivity analysis was carried out to investigate how several variables could affect the blowby and the mass flow out of the top land crevice predicted by a simplified ring pack model. One of the variables was the crankcase pressure. The crankcase pressure showed a significant effect on the blowby and a moderate effect on the mass that returns to the cylinder from the ring pack crevices. These predictions were verified during the crankcase pressure tests. Thus, it was observed that the crankcase pressure had a very significant impact on the engine-out HC emissions. This suggested

that controlling the crankcase pressure was necessary to have repeatable HC emission measurements. In addition, a change in the crankcase pressure is expected to affect the ring-pack crevices HC emissions, but not the oil film contribution to the HC emissions. Therefore, fuels of different solubility were expected to yield different trends of the engine-out HC emissions as a function of the crankcase pressure if the fuel-oil adsorption-desorption mechanism is important.

Figure 6.2 shows the change in the engine-out HC emissions when the crankcase pressure was changed from 100.35 kPa to 111.35 kPa for all conditions of interest: 1750 RPM, 10% load, 1750 RPM, 25% load, 3060 RPM, 25% load, and 3060 RPM, 50% load. These correspond to modest load engine running conditions. The atmospheric pressure was approximately 101.35 kPa. From Fig. 6.2 (a), it can be seen that for the 1750 RPM, 10% case a clear increase in the HC emissions is observed as the crankcase pressure is increased. The gasoline and propane tests show the same trend and have approximately the same level of increase. It is interesting to note that the slope $\frac{dEIHC}{dP_{cr}}$ is not the same along the crankcase pressure range. The HC shows a high rate of increase at low crankcase pressures. This increase is observed up to around 106 kPa. Further increases in pressure do not produce a significant increase in the HC emissions. This trend is observed for both cylinders and for the propane tests as well. Increasing the load to 25% for the 1750 RPM speed, a similar trend is observed. However, for the gasoline case the difference in HC contribution between the two cylinders has been reduced. For the propane case the HC contribution of each cylinder has been inverted, i.e. cylinder 1 is

contributing more than cylinder 2. This is observed for the full range of crankcase pressures tested. At higher loads and speeds (the cases of 3060 RPM, 25 and 50% load) it can be observed that the HC emissions increase with increased crankcase pressure, but with lower sensitivity than the 1750 RPM cases. It was observed that at 3060 RPM and 100% load for the gasoline fuel (Fig. 6.3), a change in the crankcase pressure does not produce an appreciable effect on the engine-out HC emissions levels. What is important to note from Fig. 6.2, is that the HC emissions as a function of the crankcase pressure show the same trend for both gasoline and propane tests.

The effect of the crankcase pressure on the HC emissions can be explained by the ring-pack crevice HC transport mechanism. A higher crankcase pressure will result in an increased resistance to the HC flow towards the crankcase; when the flow direction is reversed and the gases are flowing from the ring-pack to the cylinder a higher crankcase pressure will increase the amount of gas that returns to the cylinder, therefore, contributing to higher levels of HC. The increased crankcase pressure acts mainly during the last part of the gas exchange process, when the pressure in the cylinder is close to or below atmospheric. It is important to note that this gas exchange between crankcase and cylinder happens when the cylinder pressure and temperature are very low, which could prevent in-cylinder post oxidation. Therefore, the HC mass that reaches the cylinder by this transport process will directly affect the engine-out emissions.

The decrease of the slope $\frac{dEIHC}{dP_{cr}}$ as the load is increased in Fig. 6.2, can be explained by the fact that the in-cylinder pressure increases as the load is increased,

however the crankcase pressure is kept constant, therefore, there is less driving force for the out-gassing of the mass stored in the ring-pack crevices. Another factor that contributes to the reduction of the crankcase pressure effect on the HC emissions as the load is increased is the fact that at higher load a greater mass of HC is stored in the ring pack. Therefore, more mass returns to the cylinder and this overwhelms the effect of the increase of the crankcase pressure.

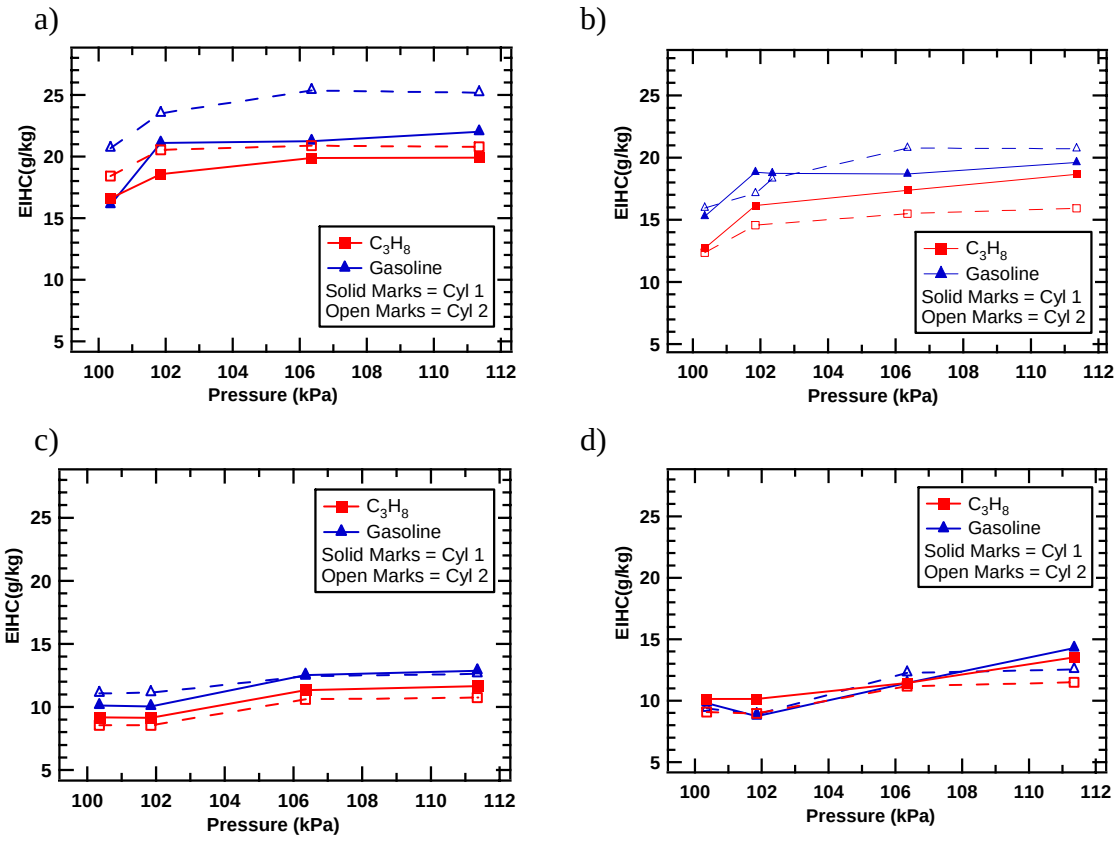

Figure 6.2 Average HC emissions vs. crankcase pressure (a) 1750 RPM, 10% load, (b) 1750 RPM, 25% load, (c) 3060 RPM, 25% load, and (d) 3060 RPM, 50% load.

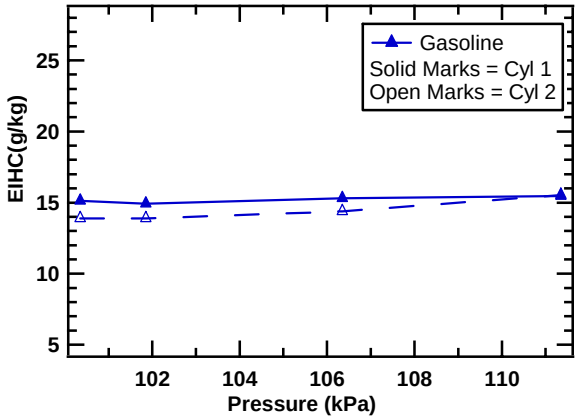

Figure 6.3 Average HC emissions vs. crankcase for gasoline at 3060 RPM, 100% load, and Φ=1.21.

6.3.3 OIL-FUEL ADSORPTION-DESORPTION EFFECT ON THE HC EMISSIONS

6.3.3.1 AVERAGE HC EMISSIONS

The change in HC emissions as a function of the crankcase pressure observed in Fig. 6.2 showed the same trend for both gasoline and propane. This suggests some important implications regarding the role of the fuel-oil adsorption-desorption mechanism. It is important note that the ring-pack crevice flow and the fuel absorption-desorption mechanisms are coupled together with one difference, the ring pack stores an air-fuel mixture while, the oil film stores mainly fuel. Oxygen and nitrogen, practically, do not diffuse in the oil. During the post-flame process the fuel stored in both the ring-pack crevices and the oil film return to the cylinder. Depending of the engine operating conditions part of this unburned fuel may be oxidized during post-flame processes [30, 33, 41]. Then, if the temperature in the exhaust port is high enough, a fraction of the

remaining HC can be oxidized. The remaining HC after post oxidation are the engine-out HC emissions.

The significance of the oil film on the HC emissions should be seen during the crankcase pressure tests. When the crankcase pressure is reduced the ring pack effect is reduced, therefore, if the oil film is a significant contributor to the HC emissions the fuel that has very low solubility in oil should show a different trend of HC emissions as a function of the crankcase pressure. Figure 6.2 shows that the HC emissions follow the same trend for both fuels, below and above the reference (atmospheric) pressure. This suggests that for this engine the oil film may not be a major source of HC emissions, and that the HC emissions are driven by other mechanisms, including the ring pack contribution.

6.3.3.2 HEAT RELEASE ANALYSIS

Heat release analysis gives an indication of the combustion performance, and it was performed with two goals in mind. First, for small engines at low load incomplete combustion [95, chapter 5] has been shown to be a significant contributor to the engine-out HC emissions. Therefore, it is important to avoid this condition if an unbiased comparison is to be made regarding the effect of the oil film on the HC emissions, i.e. for this condition small difference in late-cycle combustion between the two fuels may have a direct impact on HC emissions. The second goal was to evaluate if the combustion event was affected by the type of fuel. Figs. 6.4 and 6.5 shows the comparison of the rate of heat release for both fuels.

The results in Figs. 6.4 and 6.5 shows that the combustion event is not affected significantly when propane was used as a fuel. There are some differences at low load (Fig. 6.4(a)) which indicate that the combustion event is affected slightly, and the effect is not the same in both cylinders. These differences are smaller as the load and speed are increased (Fig. 6.4(b) and 6.5(a)-(b)). From Fig. 6.4(a), it can be seen that with either fuel the heat release is not completed prior to EVO. This suggests that incomplete combustion could contribute to HC at this condition for both fuels. The consequences, as explained in chapter 5, are an increase in HC emissions. For the 1750 RPM, 10% load operating condition, the heat release analysis suggests that the effect of the oil film may be masked by incomplete combustion. In the case of the 25% load for both the 1750 RPM and 3060 RPM speeds, the average heat release shows that the combustion is completed prior EVO. However, as it was shown in the conditional sampling analysis for the gasoline case in § 5.4.3 these two operating conditions still have a fraction of cycles with late heat release. Thus, the HC emissions could be compromised by incomplete combustion at this load, as well. For the 3060 RPM, 50% load case the combustion is finished well before EVO (also supported by conditional sampling in § 5.4.3), therefore, for this conditions the effect of the oil film on the HC emissions, if significant, could be distinguished between the fuels; but no significant effect was observed in Fig. 6.2-(b).

a)

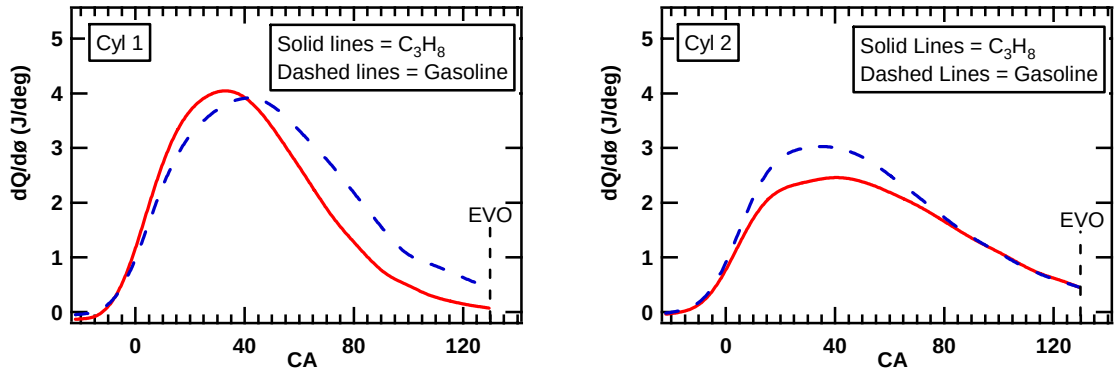

b)

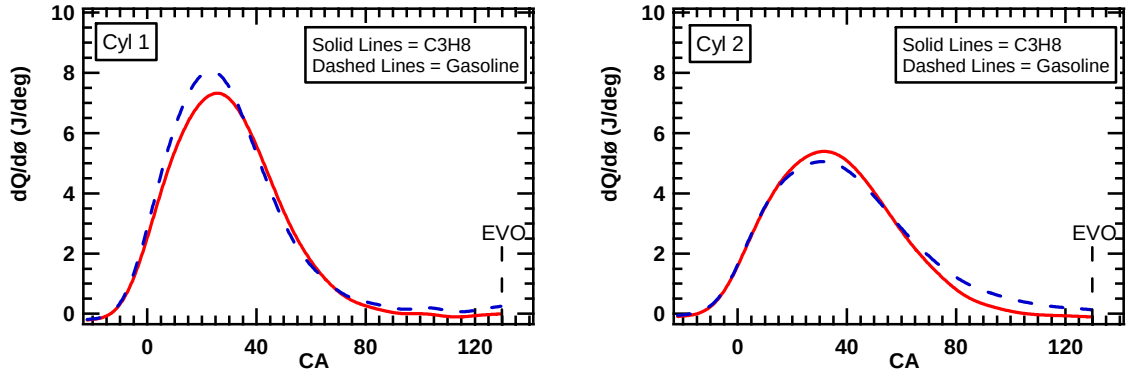

Figure 6.4 Rate of heat release for three different conditions, (a) 1750 RPM, 10% load, and (b) 1750 RPM, 25% load

a)

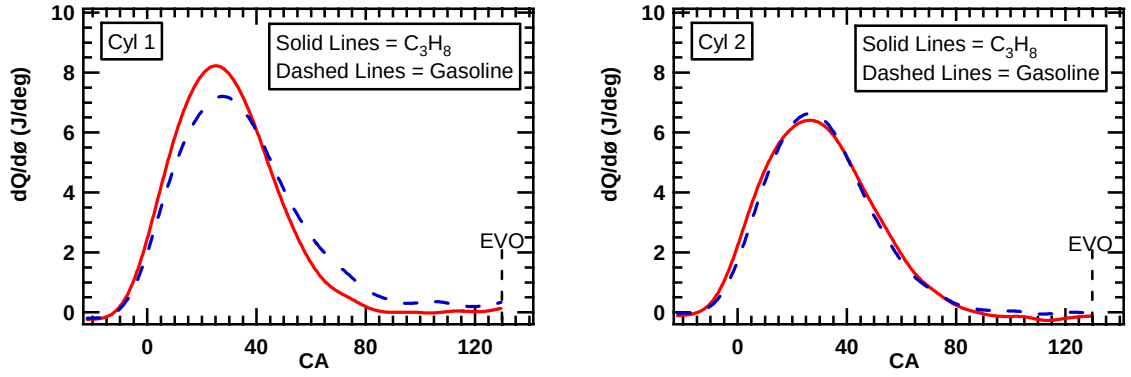

b)

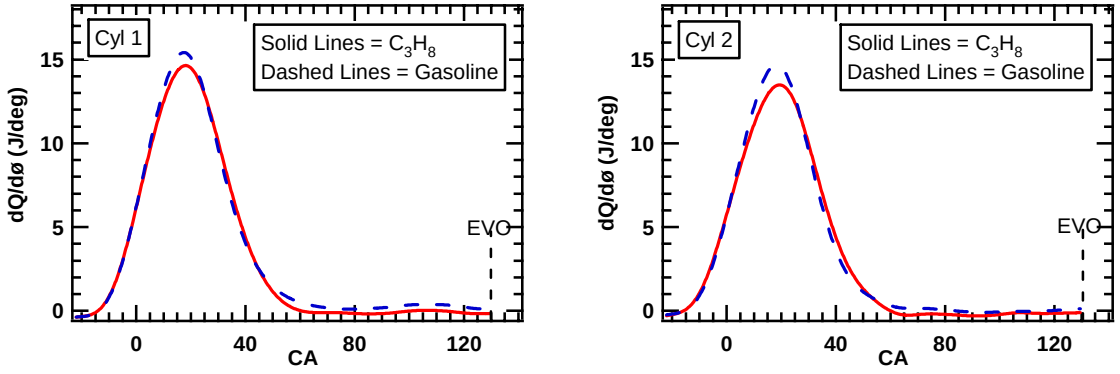

Figure 6.5 Rate of heat release for three different conditions, (a) 3060 RPM, 25% load, and (b) 3060 RPM, 50% load.

6.3.3.3 CYCLE-RESOLVED HC EMISSIONS

Cycle-resolved HC emissions can help to elucidate the HC emissions difference between the two fuels. A comparison of the averaged cycle-resolved FID traces is shown in Fig. 6.6 and 6.7. As mentioned in § 2.7 [41], the oil layer shows its effect on the fast FID traces during the latter part of the exhaust process, when the piston moves up and scrapes the HC wall layer. Therefore, if some influence on the HC emissions due to the oil film is expected it should be seen during the period when the piston scrapes the HC

wall layer at the end of the exhaust stroke; specifically the difference on the fast-FID traces should be observed when the piston is near TDC. During the main blowdown process both the effects of the ring pack and the oil film are overwhelmed by the exhaust of the hot core gases, which have very low HC concentration.

Under low load conditions (Fig. 6.6 (a)-(b)) the comparison can be affected by incomplete combustion [95, chapter 5], but one can note that the propane and gasoline for these conditions show essentially the same basic HC history, although the values are different. This supports the heat release analysis that indicated that incomplete combustion is also present with the propane. Single-cycle analysis of the ring pack contribution and of the heat release for the propane case (not presented here) corroborated this observation.

For the 3060 RPM, 25% load case, Fig. 6.7 (a), no appreciable differences in HC history during the exhaust stage are observed, as well. It was shown in § 5.4.3 that for this condition there are some cycles that have a relatively slow burn rate, however, the majority of the cycles finish combustion before EVO. The fact that no significant differences are observed when the engine is fired with gasoline and propane again suggests that the oil film is not a significant contributor to the engine-out HC emissions.

The most definitive comparison can be made for the 3060 RPM, 50% load case (Fig. 6.7(b)), where all the cycles finish heat release prior EVO. In this case the oil film mechanism should show an influence on the fast FID traces toward the end of the exhaust process when the cylinder approaches TDC. Fig. 6.7(b) shows no appreciable difference

in the history of the cycle-resolved HC emissions for both fuels, suggesting again that the oil film mechanism is not a major contributor to the HC emissions. These observations suggest that for this particular engine the major contributor to HC emissions at high loads are the ring pack crevices; at low loads incomplete combustion also contributes to the engine-out HC emissions.

a)

b)

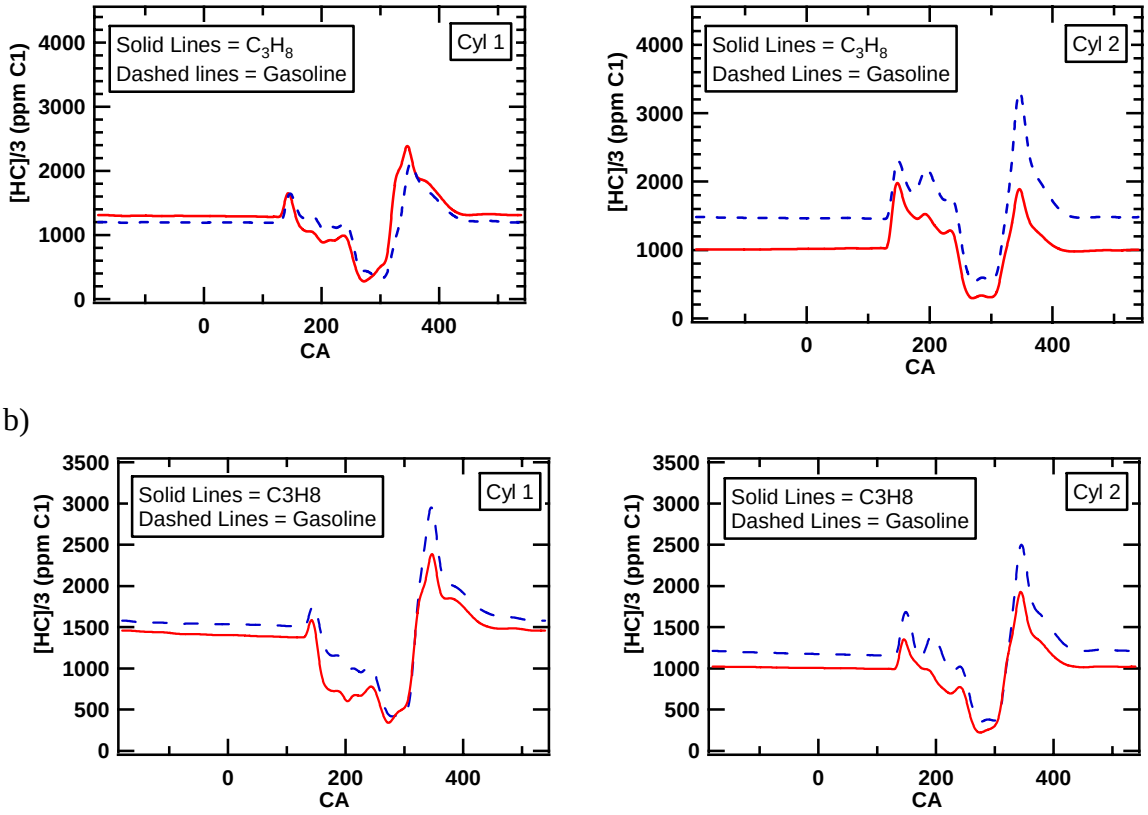

Figure 6.6 Comparison of the cycle-resolved HC emissions for gasoline and propane at: (a) 1750 RPM, 10% load, and (b) 1750 RPM, 25% load.

a)

b)

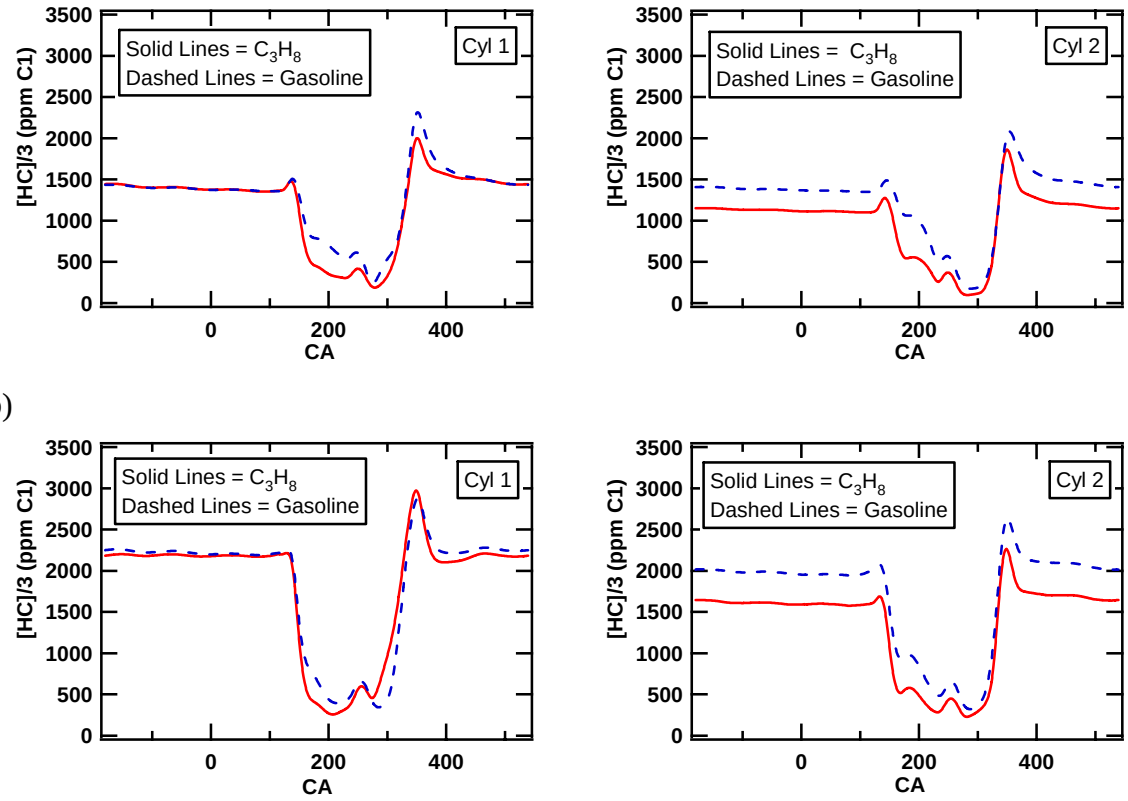

Figure 6.7 Comparison of the cycle-resolved HC emissions for gasoline and propane at: (a) 3060 RPM, 25% load, and (b) 3060 RPM, 50% load

6.3.3.4 THE ROLE OF THE EQUIVALENCE RATIO AND TEMPERATURE IN THE FUEL-OIL DIFFUSION – NUMERICAL SIMULATION

To further understand the role of the oil film on the HC emissions, numerical simulations to estimate the amount of fuel stored in the oil as a function of the wall temperature and mixture equivalence-ratio were performed. A temperature dependence of the fuel solubility in oil has been reported in several studies [35-47] – the fuel solubility in oil is reduced as the temperature is increased. On the other hand, the effect of the

equivalence ratio of the mixture on the fuel-oil solubility is not well documented. As mentioned before there are two particularities of small engines that make the fuel-oil diffusion process different than automotive engines. First, small engines run with rich air-fuel ratio mixtures, and second, small engines are air cooled which makes them operate at higher temperatures. It is, thus, expected that the high operating temperature of a small engine would cause a reduction in the amount of fuel stored in the oil film and reduce its contribution on the HC emissions. The fuel desorption process is directly proportional to the amount of fuel adsorbed in the oil layer. In order to estimate the extent that temperature and air-fuel ratio affects the amount of fuel diffused into the oil film, a simplified analysis was carried out. The details of the simulations are shown in the following subsection.

6.3.3.4.1 PHASE EQUILIBRIUM SIMULATION

The phase equilibrium simulation consisted of calculating the thermodynamic equilibrium composition of the gas-liquid mixture of oil, fuel and air trapped in the cylinder of the engine. In this simulation the piston was static and all trapped components (air-fuel mixture and oil) were allowed to reach equilibrium as show in Fig. 6.8. The dashed line represents the boundary of the closed system under study. The liquid-gas phase equilibria composition was estimated at different temperatures for gasoline and propane with oil using the NIST SUPERTRAPP v3.2 software, which performs phase equilibria calculations of multi-component, multi-phase mixtures and provides as output the composition (mass fractions) and thermophysical properties of all the phases and the feed (initial components). In the analysis, gasoline was substituted by a mixture of

several hydrocarbons having the same formulation as the fuel used by Linna *et al.* [39]. Table 6.2 shows the composition of this synthetic gasoline. N-hexatriacontane ($C_{36}H_{74}$), which has similar properties to mineral base oil [97], was used as a surrogate for the oil.

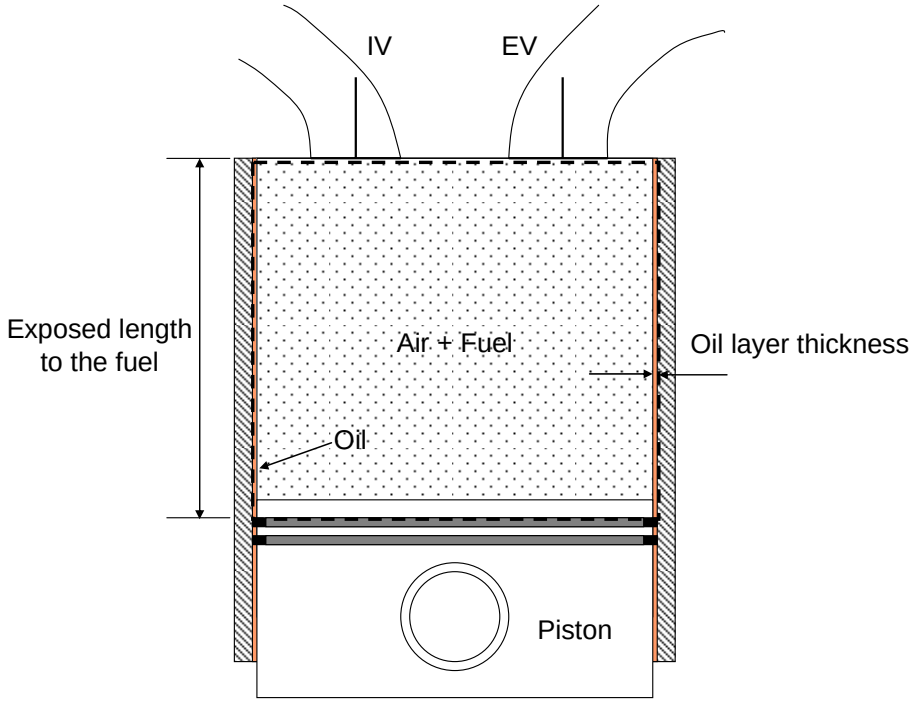

Figure 6.8 Schematic of the system for the static fuel-oil diffusion simulation.

The pressure of the system shown in Fig. 6.8 was constant and equal to 100 kPa. The initial molar fraction of each component was required as input. The mass of oil in the system was estimated by assuming that a constant thickness oil layer of $2\mu m$ covered the cylinder liner. The mass of fuel trapped for a typical medium-load condition was used (10 mg) and the required amount of air for a given equivalence ratio was calculated. The NIST SUPERTRAPP v3.2 software was then used to estimate the maximum amount of fuel stored in the oil layer. The equilibrium adsorbed fuel fraction in the oil as a function

of the temperature and Φ is shown in Fig. 6.9. The software predicts a lower solubility of propane in oil than the gasoline, which is in very good agreement with the literature. At Φ =1.2 the adsorbed gasoline fraction is approximately 10-35 times greater than for propane for the maximum and minimum temperatures studied. It is important to note that for both fuels the amount of fuel diffused into the oil is significantly reduced with elevated temperature for a given equivalence ratio. Figure 6.9 also shows that the mass of propane diffused in oil is less sensitive to temperature than the gasoline.

Table 6.2 Synthetic fuel composition [39]

Compound	Chemical Class	Chemical Formula	% wt
I-Pentane	Saturates	C_5H_{12}	20
3-Methylpentane	Saturates	C_6H_{14}	10
Benzene	Aromatics	C_6H_6	3
n-Heptane	Saturates	C_7H_{16}	5
Toluene	Aromatics	C_7H_8	20
I-Octane	Saturates	C_8H_{18}	15
M,P-Xylene	Aromatics	C_8H_{10}	17
1,2,4-Trimethylbenzene	Aromatics	C_9H_{12}	5
n-Decane	Saturates	$C_{10}H_{22}$	3.5
I-Dodecane	Saturates	$C_{12}H_{26}$	1.5

The reduction in the equilibrium adsorbed fuel fraction seen in Fig. 6.9 suggests that the oil film mechanism of HC emissions should contribute less in small engines than in automotive engines. For automotive engines the maximum operating temperature is limited to some extent by the coolant temperature, which is around 90 °C. The temperature of the combustion chamber side of the liner depends on load and speed; typical values for automotive engines at medium loads are as high as 120 °C [39] and at

full load the temperature can be as high as 220 °C near TDC region [98]. In small air-cooled engines the liner temperature is typically higher; for this particular engine at full load the liner can reach temperatures up to approximately 240 °C, and at low and medium loads the maximum temperatures are around 200 °C. Also, small engines are operated at wide open throttle more than automotive engines. Therefore, based on this simplified equilibrium analysis it is expected that the amount of fuel diffused into the oil in small engines should be smaller than the automotive engines. For automotive engines Linna *et al.* [39] estimate that the maximum contribution of the oil film to the engine-out HC emissions was less than 10%, consequently for small engines it is expected a smaller contribution due to the effect of the high operating temperature.

Figure 6.9, also shows the effect of the equivalence ratio on the fuel solubility in the oil. As the fuel concentration is increased (Φ increases), an approximately exponential increase in the amount of fuel diffused in the oil is observed. This is true for all the temperatures under study. Automotive engines operate at close to stoichiometric while small engines operate with rich equivalence ratios. Typical equivalence ratios for the engine under study are around Φ=1.20, and thus one would expect a larger effect in a small engine than an automotive engine. The contribution of the oil film to the engine-out HC emissions will be result of the competition between the equivalence ratio and temperature effects. Using the results of Fig. 6.9 as a guide, it can be inferred that at full load the difference in the fraction of fuel that diffuses in oil for automotive engines (220 °C, Φ = 1) and for a small engine (240°C, Φ = 1.2) is negligible. This is due to the competition of the higher temperature and relatively high air-fuel ratio in small engines,

and the slightly lower temperature and lower equivalence ratio of the automotive engines. At medium loads the fraction of fuel that diffuses in oil is considerably higher for automotive engines (120°C, $\Phi = 1$) than for small engines (200°C, $\Phi = 1.20$).

This equilibrium analysis supports the previous observations based on the experimental results that the contribution of the oil film to the HC emissions is not significant for small engines. Based on literature estimates for automotive engines [39, 42] the contribution of the oil film to the total engine-out HC emissions is expected to be less than 10% of the total or negligible.

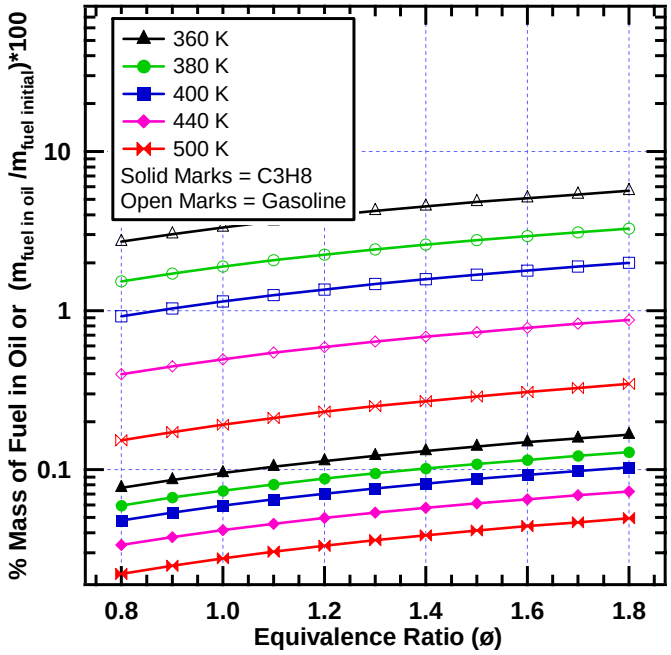

Figure 6.9 Percentage of initial fuel mass adsorbed by the oil (n-hexatriacontane) at equilibrium as a function of the temperature and equivalence ratio Φ.

6.3.3.4.2 CYCLE SIMULATION OF THE FUEL-OIL ADSORPTION-DESORPTION

To supplement the investigation of the role of the fuel-oil diffusion on the engine-out HC emissions a time-resolved numerical simulation of the fuel-oil diffusion process along the cylinder liner was carried out. This simulation provided an estimation of the percent of trapped mass of fuel that returns to the combustion chamber from the oil film after the main combustion. This made possible a comparison between the relative contributions of the oil film and the ring pack. The model assumes a one-dimensional transient diffusion in the radial direction of the oil film as show in the schematic of Fig. 6.10. In Fig. 6.10 the oil thickness is represented by δ, the radial coordinate by x, and the fuel concentration by C.

6.3.3.4.2.1 ASSUMPTIONS

The main assumption in the model is that the diffusion of the fuel components in the oil is the limiting factor in the adsorption-desorption mechanism. This is a reasonable assumption because the diffusivity of the fuel in the oil is of the order 10^4 smaller than in the gas phase [99]. In addition, no information about the flow inside of the combustion chamber is available for this engine. Other assumptions for the calculations include:

a. The fuel flow in the axial direction of the oil film is negligible
b. The temperature of the liner is constant, and the oil temperature is equal to the liner temperature
c. There is no interaction between individual fuel components

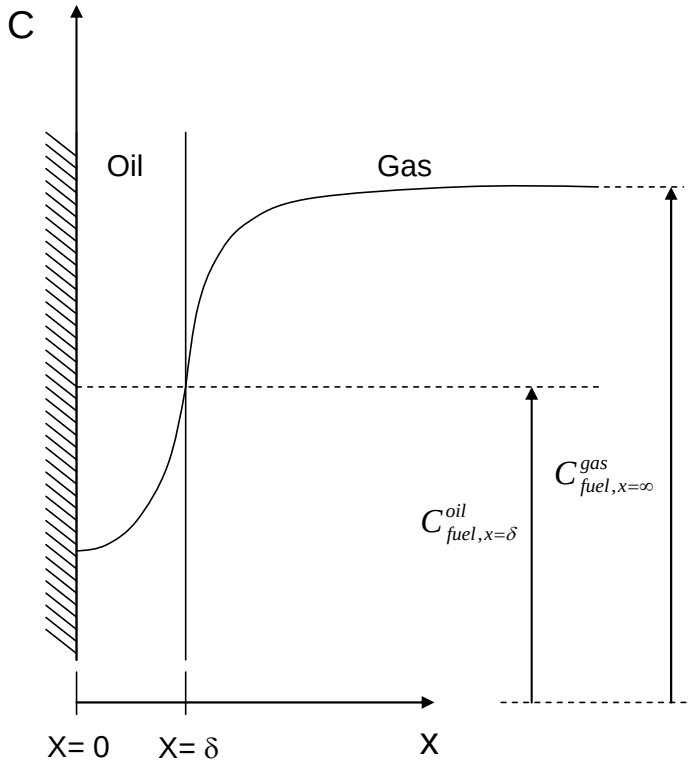

Figure 6.10 Schematic of the fuel concentration in the oil film and in the combustion chamber gas, along with the coordinate system used for the simulation.

d. The fuel is completely vaporized in the gas phase

e. At the end of combustion (CA90), the oil elements above the first ring suddenly and simultaneously became in contact with the burned gases which had zero fuel concentration

f. The oil elements above the first ring were exposed to the chamber gases and those below were exposed to the crankcase gases.

g. The fuel concentration in the vapor-phase in the crankcase was assumed to be approximately 25% of the fuel in the fresh charge [39].

h. The oil thickness is constant along the cylinder liner.

6.3.3.4.2.2 TRANSIENT MASS DIFFUSION EQUATION AND BOUNDARY CONDITIONS

With the above assumptions the fuel-oil adsorption-desorption process can be estimated solving the one-dimensional diffusion equation applied to the oil-film as follows:

$$\frac{\partial C}{\partial t} = D\frac{\partial^2 C}{\partial x^2} \tag{6.1}$$

where the symbols follow the convention of Fig. 6.10, with D being the diffusion coefficient of the fuel component in the oil. The boundary conditions assumed in order to solve Eq. 6.1 were:

$$\frac{\partial C}{\partial x}(0,t) = 0 \tag{6.2}$$

$$C(x = \delta, t) = C_i(t) \tag{6.3}$$

The initial condition was:

$$C(x,0) = 0 \tag{6.4}$$

Equation 6.2 represents the condition at the liner wall, and states that the fuel cannot diffuse into the cylinder liner. The boundary condition at the oil-gas interface was considered to be equal to the liquid-gas phase equilibria composition evaluated at the oil temperature and cylinder pressure, and it was estimated using the NIST SUPERTRAPP

v3.2 software with the same methodology explained in §6.3.3.4.1. The use of this software is more realistic than the approaches used by other researchers [39, 97] where the concentration at the interface was estimated using the Henry's law for single component fuels. SUPPERTRAPP estimates the multi-component concentration of the fuel component at the interface. Therefore, the estimated composition at the oil-gas interface using SUPERTRAPP is believed to be more accurate. It is important to note that the initial condition (Eq. 6.4) was used to start the simulation. However the simulation was carried out until the system reached the steady state condition. It took approximately 10 engine cycles to reach the steady state condition. Again, the oil was considered to be N-hexatriacontane.

Equation 6.1 was solved numerically using the Crank-Nicholson scheme for the time and the second order central-difference scheme for the spatial coordinate. The resulting tri-diagonal system of lineal equations was solved using the Thomas algorithm [100]. The cylinder liner was divided into 40 segments as indicated in Fig. 6.11. The curvature of each segment was neglected since the oil layer thickness is very small compared with the diameter of the cylinder. The length of each segment was equal to the circumference of the cylinder.

The diffusion equation (Eq. 6.1) was applied to each oil film segment (Fig. 6.11) and for each fuel component separately. As mentioned before, it was assumed that the individual fuel components do not interact. A very important parameter in the simulation

is the binary diffusion coefficient of each fuel component in the oil. This was estimated using the Hayduk and Minas correlation [101] as in Eq. 6.5:

$$D_{AB} = 13.3.10^{-8} \frac{T^{1.47} . \mu_B^{(10.2/V_A^{-0.791})}}{V_A^{-0.71}} \qquad (6.5)$$

where D_{AB} is the diffusion coefficient of solute A at a very low concentration in solvent B, in cm^2/s. T is the temperature in K, μ_B is the viscosity of the solvent B in cP (centipoises), and V_A is the molar volume of solute A at its normal boiling temperature in cm^3/mol. The Hayduk and Minas correlation has been shown to predict binary diffusion coefficients with an average deviation of less than 10% [102]. The value for the oil viscosity was obtained from SUPPERTRAPP. The molar volume of each fuel component at its normal boiling point was calculated using the Tyn and Calus method [102] as follows:

$$V_A = 0.285.V_c^{1.048} \qquad (6.6)$$

where V_c is the critical volume and both V_A and V_c are in $cm^3/mole$. This correlation also has been shown the past to provide results within 3-4%.

It is important to mention that the Hayduk and Minas correlation (Eq. 6.5) was developed for paraffin solutions. However, in the present analysis the same correlation was applied to the aromatic fuel components, (see Table. 6.2) as well.

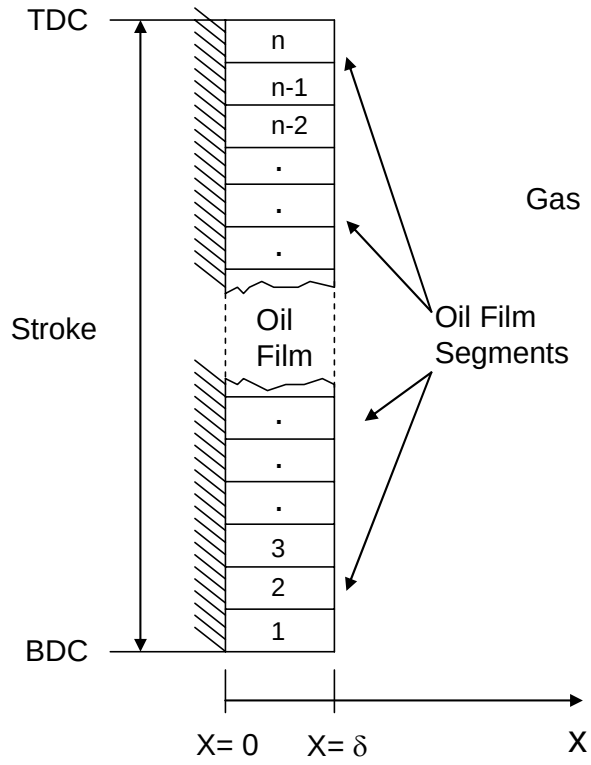

Figure 6.11 Schematic of the oil segments used in the simulation.

6.3.3.4.2.3 NUMERICAL ANALYSIS RESULTS

As mentioned above the model was able to predict the mass of fuel that was adsorbed by the oil layer and the mass of fuel that returned to the combustion chamber after the combustion event ceased. Therefore, these two metrics were studied for all conditions of the text matrix shown in Table 6.1. The influence of the temperature was also studied for the 3060 RPM, 50% load case.

Figure 6.12 show the results for the 1750 RPM, 10 and 25% load cases. For the 10% load case, Fig. 6.12 (a), the simulation shows that up to 0.5% of the mixture escapes

the main combustion due to the oil-film mechanism. The percent of mass that leaves the oil film after the flame reaches the cylinder wall is of approximately 0.45%. The results show that only a small fraction of fuel is desorbed into the crankcase.

a)

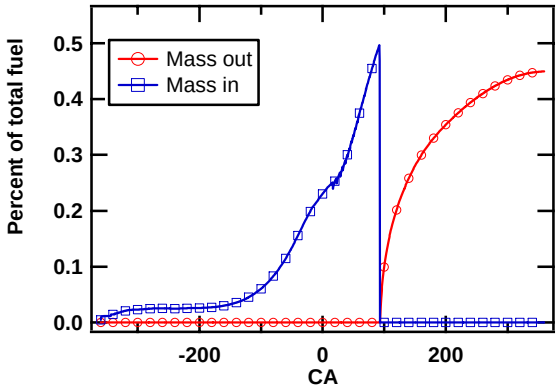

b)

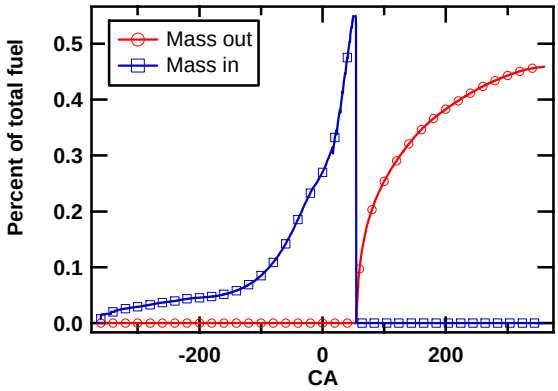

Figure 6.12 Percent of the trapped mass of fuel that is absorbed and desorbed from the oil film for (a) 1750 RPM, 10% load, AF 12, and (b) 1750 RPM, 25% load, AF12. The oil layer thickness was 2 μm and the wall temperature 380 K.

For the 25% load, Fig. 6.12 (b), the percent of mass of fuel that escapes the main combustion has been increased up to approximately 0.56%. The mass of fuel that returns to the combustion chamber has also been increased to about 0.47%. The difference accounts for the mass that is desorbed to the crankcase.

For the 3060 RPM, 25% load case, Fig. 6.13 (a), the results show that the percent of fuel mass that escapes the main combustion due to the oil-film is approximately 0.46%. This is smaller than the same load at 1750 RPM. The explanation to this observation is that the fuel has less time to diffuse into the oil layer. Therefore, less mass is stored in the oil layer. The mass that returns to the combustion chamber has also been reduced to around 0.35%. This is expected because it is proportional to the mass that is stored in the oil film. For this condition a significant part the fuel desorbs in the crankcase (around 0.11%), as well.

As the load is increased to 50%, Fig. 6.13 (b), the simulation shows that the percent of mass of fuel that is trap in the oil film increases. Thus, about 0.50% of the fuel escapes the main combustion. However, the mass that returns to the combustion chamber is almost constant. The increase in mass of fuel that escapes the main combustion due to the oil film as the load is increased is due to the cylinder pressure increase. The concentration of fuel at the oil-gas interfaces increases proportionally with the pressure. Therefore, more fuel diffuses into the oil film. For the 100% load, Fig. 6.13 (c), a further increase in the mass of fuel stored in the oil film is observed. The results for this case indicate that up to 0.55% of the fuel escaped from the main combustion. The normalized mass that returns to the cylinder shows a small reduction. However, a higher HC contribution should be expected at this load because it represents a greater mass of fuel than for the 25 and 50% loads.

a)

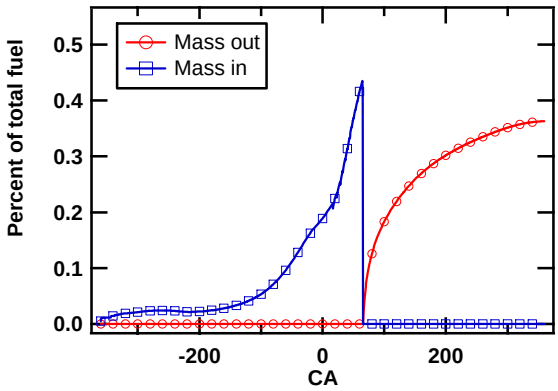

b)

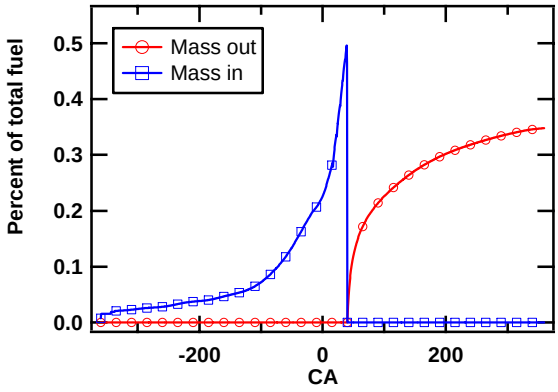

c)

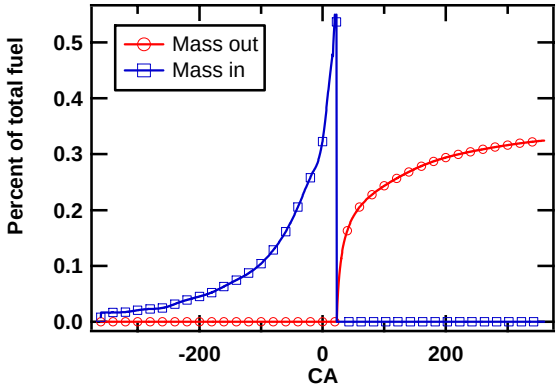

Figure 6.13 Percent of the trapped mass of fuel that is absorbed and desorbed from the oil film for (a) 3060 RPM, 25% load, AF 12, (b) 3060 RPM, 50% load, AF12, and (c) 3060 RPM, 100% load, AF12. The oil layer thickness was 2 μm and the wall temperature 380 K.

From the discussion above, it can be stated that in the worse case up to 0.55% of the fuel mass avoids the main combustion due to the oil film mechanism. The predictions are in very good agreement with other works [39, 103, 104].

Now, considering the 3060 RPM, 50% load case to compare the relative contribution of the oil layer and the ring pack, the following estimation can be made. In §5.2.4 was shown that the mass that returns to the combustion chamber from the top land crevice was approximately 3.57%. This is significantly higher than the mass that desorbs from the oil layer into the combustion chamber (0.35%). The oil film contribution represents approximately 10% of the ring pack contribution. This value is in very good agreement with the estimated contribution of the oil film to the HC emissions reported by Linna et al [39].

To further support the findings in §6.3.3.4.1 and the experimental tests, a simulation with propane for the 3060 RPM, 50% load, AF12 case was performed. The results are show in Fig. 6.14. From Fig. 6.14 it can be seen that the percent of propane stored in the oil layer is of only 0.042%, and the fraction that desorbs into the combustion chamber is around 0.04%. This is considerable smaller than for the normal gasoline case (approximately one order of magnitude). These results are also in good agreement with the phase-equilibria simulations of section §6.3.3.4.1 that indicated that the propane has a very low solubility in oil. The simulation of Fig. 6.14 further supports the findings of the experimental tests with propane and gasoline that indicated that the oil layer is not a significant contributor to the engine-out HC emissions.

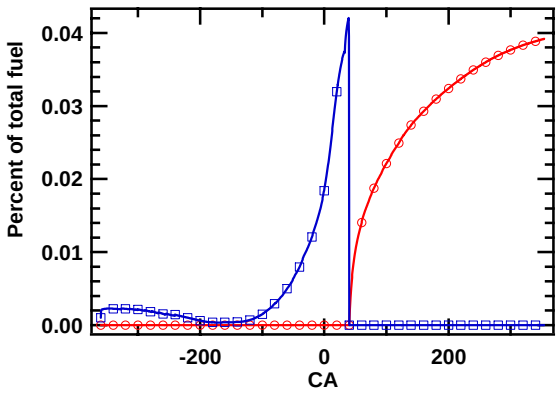

Figure 6.14 Percent of the trapped mass of fuel that is absorbed and desorbed from the oil film at 3060 RPM, 50% load, AF 12. The fuel is propane, the oil layer thickness was 2 µm and the wall temperature 380 K.

As was stated before, small engines run under hot conditions therefore a smaller contribution should be expected for small engines. In order to understand the temperature effect on the oil film contribution, simulations at different cylinder wall temperatures were performed for the 3060 RPM, 50% load case. The results are show in Fig. 6.15.

From Fig. 6.15, it can be seen that as the temperature is increased the mass of fuel that is trapped in the oil layer decreases. The mass of fuel that returns to the combustion chamber has also been reduced by approximately 30% when the temperature was changed from 380K to 500K. As mentioned before at full load typical temperatures in a small engine are of the order of 240°C (513 K). Therefore from Fig. 6.15 it is expected that for the 50% load at 3060 RPM, the mass of fuel that contributes to the HC emissions is below 0.1%.

As mentioned before, not all the fuel mass that returns to the combustion chamber will contribute to the engine-out HC emissions. Part of this fuel will diffuse in the hot

bulk burned gases, and may be oxidized during the post-flame period. The remaining mass will be scraped by the piston during the exhaust stroke and released to the exhaust port where a further post-oxidation may take place. In the cylinder the degree of post oxidation depends mainly of the temperature and on the oxygen availability [30, 41]. The extent of the oxidation of several single-component fuels desorbing from the oil layer has been studied experimentally by Norris and Hochgreb [41]. The results of this work showed that between 50-80% of the desorbed mass is oxidized in the cylinder. Therefore, based on the above results the relative contribution for the 3060 RPM, 50% load case to the engine-out HC emissions could be at most of 0.05% of the total mass trapped in the cylinder, or in emission index notation 0.5 g/kg-fuel. This is within the error of the measurement of the HC emissions (see §4.3.1). This supports the equilibrium simulation and discussion that the oil layer may not be a significant contributor to the engine-out HC emissions in small engines.

a)

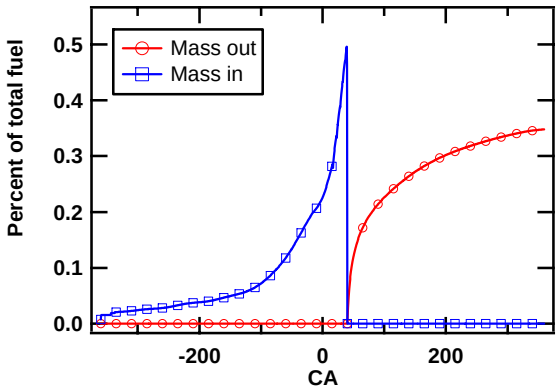

b)

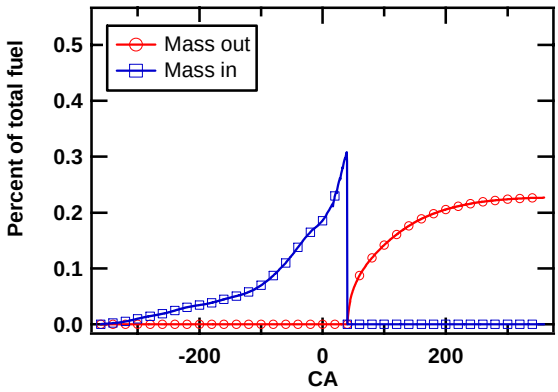

c)

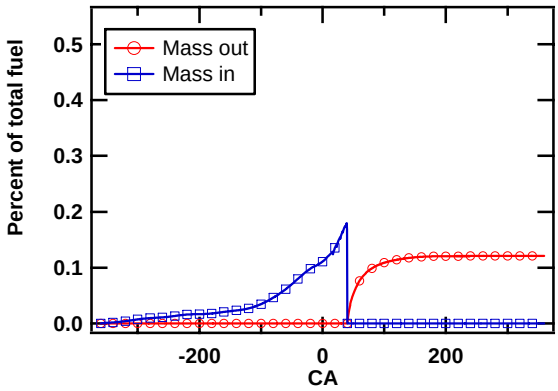

Figure 6.15 Effect of the temperature on the percent of the trapped mass of fuel that is absorbed and desorbed from the oil film for 3060 RPM, 25% load at (a)380K, (b) 440K, and (c) 500K. The oil layer thickness was 2 μm.

6.4 SUMMARY

The role of the oil film on the HC emissions from a small utility engine has been studied experimentally and numerically. The experimental results of the crankcase pressure tests, heat release analysis and cycle-resolved HC emissions show that the oil layer is not a significant contributor to the engine-out HC emissions. Numerical simulations of the fuel absorption supported the experimental findings. The phase equilibrium simulations showed that small engines are favored with respect to the oil-film HC emission contribution due to their high operating temperature. The results of this simulation suggests that a smaller contribution than observed in automotive engines should be expected (less than 10% of the total HC emissions) in small engines. Further analysis of the fuel-oil adsorption-desorption process along the engine cycle showed that at most a contribution of up to 0.05% of the injected mass of fuel could be expected. A comparison with the relative contribution of the ring pack crevice showed that the oil film contribution represents 10% of the ring pack contribution. In conclusion, the experimental and numerical results show that the oil layer mechanism does not contribute significantly to the engine-out HC emissions.

CHAPTER VII

CONCLUSIONS AND RECOMMENDATIONS

7.1 CONCLUSIONS

The main findings of the HC mechanisms study are summarized in the following subsections.

7.1.1 LIQUID FUEL EFFECTS

The effect of fuel mixture preparation system on the combustion and emissions from a small, air-cooled, two-cylinder utility engine was studied. The results from a homogeneous, pre-vaporized mixture were compared to the mixture resulting from a carburetor. Emissions measurements were performed in the standard fashion from an exhaust surge tank, and cycle-resolved HC measurements were performed with a fast FID. The main findings of the liquid fuel effects on the engine-out HC emissions study can be summarized as follows:

a. Stop-injection measurements with a carburetor-mounted low pressure liquid fuel injection system that emulated the carburetor showed that in excess of 60 cycles worth of liquid fuel was held in the intake manifold under the conditions tested.

b. Under steady state operation, the type of fuel system (homogeneous mixture, carburetor or carburetor mounted low pressure liquid fuel injection) did not have a significant effect on the average unburned HC emissions for all the operating conditions and air-fuel ratios tested. Similarly, the CO and NOx emissions were not affected by the fuel mixture preparation system.

c. The cycle-resolved HC emissions showed very small differences between the carburetor and homogeneous mixture system, further suggesting that the air-fuel mixture preparation system does not significantly affect the HC emissions under steady state conditions.

d. The heat release analysis showed that under steady state conditions the combustion event was not affected by the liquid fuel effects for all the tested conditions.

e. The HC emissions results presented, suggest that the presence of the liquid-phase fuel in the intake manifold does not adversely impact the hydrocarbon emissions either in their overall level, or their evolution history. This is in spite of the fact that the engine studied requires the flow to undergo a sharp turn just downstream of the carburetor, which is expected to incur a significant liquid-phase fuel impingement.

7.1.2 RING PACK CREVICES

A comprehensive characterization of the contribution of the ring pack storage mechanism to the HC emissions of both cylinders of a V-twin air-cooled utility engine has been carried out using a phenomenological, simplified ring pack model. The integrated mass leaving the crevices from CA90 to EVC was taken to represent the potential contribution of the ring pack to the overall HC emissions; post-oxidation in the cylinder will consume a fraction of this mass. Time-resolved exhaust HC concentration measurements were also performed, and the instantaneous HC mass flow rate was determined using the measured exhaust and cylinder pressure. The integrated exhaust HC mass was found to, on average, agree well with the steady state measurements, and therefore could be used to provide an indication of an individual cycle's contribution to the overall HC emissions. Several engine performance parameters were correlated with the calculated mass of HC at the exhaust and with the HC concentration at a given CA during the exhaust process. The significance of these correlations was verified carrying out a statistical analysis. Conditional sampling of the data was performed to isolate the contribution of sub-groups of cycles to the HC emissions based on their combustion phasing. Tests were performed for a range of engine load, two engine speeds, varied air-fuel ratio and with a fixed ignition timing using a homogeneous, pre-vaporized fuel mixture system. The major conclusions that can be drawn from this study are:

a. At high load the results indicate that the HC emissions are dominated by the ring pack contribution. The model predicts that the ring pack returns approximately three times as much HC mass to the cylinder as is measured in the exhaust.

Under these conditions the combustion is robust, and isolated late-burning cycles do not behave significantly different than the mean. In addition, for these conditions the temperatures were high enough at the end of combustion to support significant post oxidation, but the chemistry is frozen during exhaust blowdown.

b. At low load conditions (1750 RPM, 10 % load) the ring pack model predicts significantly less mass returning to the cylinder (CA90 – EVC) from the ring pack than is observed in the exhaust, clearly indicating that another HC mechanism is significantly contributing to the exhaust HC emissions.

c. A single-cycle analysis performed at the low load condition showed that including cyclic dispersion in the ring pack model did not allow the shortfall of the ring pack contribution, with respect to the measured HC at the exhaust, to be accounted for.

d. Single-cycle heat release analysis together with conditional sampling indicated that at light load conditions, due to the combustion constraints put on utility-class engines from manufacturing costs, there were a fraction of the cycles that did not complete heat release prior to EVO.

e. At low load the integrated exhaust HC mass was shown to correlate inversely with the IMEP on a cycle-by-cycle basis, which strongly suggest that incomplete combustion is materially contributing to the exhaust HC emissions.

f. A direct analysis was performed using time-resolved HC measurements, and it was shown that cycles with late heat release correlated with high levels of HC mass emissions as well as high levels of HC concentration. The linear correlation coefficients at light load were modest, ~0.18 and 0.49 for cylinder 1 and cylinder 2 respectively, but the probability that an equivalent sample of random data would provide the same level of correlation was effectively zero. Thus, incomplete combustion is a significant contributor to HC emissions at light load in small utility engines.

g. The 3060 RPM, 25% load condition represents the borderline condition between the competition of the incomplete combustion and the ring pack contribution on the HC emissions. The ensemble-average ring pack model results indicate that the mass returned to the cylinder from the ring pack is slightly higher than the amount measured in the exhaust. But, the conditional sampling analysis indicates that there are sub-groups, *i.e.* late-burning cycles, for which this is not true, and the integrated exhaust HC mass, $EIHC_{C,MB}$, for this sub-group of cycles was not considerably lower than the exhaust value. Combined with the fact that there is expected to be some in-cylinder post-oxidation of the ring pack HC mass at this condition, this strongly suggests that there are other mechanisms besides the ring pack that are significantly contributing to the HC emissions at this condition. The most likely mechanism is incomplete combustion.

7.1.3 OIL FILM ADSORPTION-DESORPTION

The influence on engine-out HC emissions of fuel adsorption into the oil layer and its subsequent desorption late in the cycle following combustion was studied by varying the crankcase pressure and fuel composition. Results using a standard full-blend gasoline were compared to those using propane, which has approximately one order of magnitude lower solubility in the oil. Tests were performed for multiple engine speeds and loads, with a fixed equivalence ratio of Φ = 1.21 and a fixed spark timing. The experimental study was supported with a numerical analysis of the liquid-gas phase equilibrium and of the adsorption-desorption process of the fuel in the oil. The following conclusions can be drawn from the study:

a. The steady state emissions for the two fuels were qualitatively and quantitatively in good agreement for all of the operating conditions investigated.

b. The cycle-resolved HC emissions were also in good agreement between the two fuels, most notably during the latter part of the exhaust stroke where the influence of the fuel desorption from the oil is expected to be prominent.

c. The HC emissions were found to be significantly affected by the crankcase pressure at the low speed light load operating condition, but less so at the higher speeds and loads. The cause for the different HC emissions observed with varying crankcase pressure is believed to be the difference in the ring-pack storage. The fact that the relative change in the HC with changes in crankcase pressure was the same for the two fuels, and the lack of a difference in the cycle-

resolved HC emissions strongly suggests that the fuel desorption from the oil film does not have a significant role in the overall HC emissions from small utility engines.

d. A simulation of the liquid-gas phase equilibria of the oil-fuel system indicated the contribution of the oil film to the HC emissions in small engines should be smaller than in automotive engines. This is mainly due to their high operating temperature, in spite of the relatively high equivalence-ratio operation of the small engines. The analysis supported the previous observations based on the experimental results that the contribution of the oil film to the HC emissions is not significant for small engines. Based on literature estimates for automotive engines the contribution of the oil film to the total engine-out HC emissions is expected to be less than 10% of the total or negligible.

e. A numerical analysis of the unsteady adsorption-desorption process along the cycle under steady state conditions predicted that the highest contribution to the HC emissions due to the oil film mechanism should be below 0.05% of the injected mass of fuel. This is lower than the relative contribution of the ring pack (less than 10%). A further reduction due to post oxidation is expected. Therefore, the effect of the oil layer is not a significant contributor in small engines. The effect of the oil layer is expected to be overwhelmed either by the incomplete combustion or the ring pack contribution.

7.2 RECOMMENDATIONS

The following recommendations are considered for future work regarding the HC emission in small engines.

a. For a more accurate calculation of the single-cylinder heat release analysis, a more rigorous estimation of the single-cylinder trapped mass is required. The rate of heat release is affected significantly by the trapped mass of fuel. An over- or under-estimation could affect the analysis of the extent of incomplete combustion contribution. Therefore, the single-cylinder trapped mass should be measured experimentally with enough accuracy. Otherwise, either a single cylinder engine should be used or an even charging should be provided to each cylinder.

b. The piston wall temperature should be measured or predicted with enough accuracy. This could help to improve the accuracy of the predicted contribution of the ring pack. As was mentioned in the sensitivity analysis this parameter has a significant effect on the mass that returns from the top land crevice after the main combustion event.

c. A full characterization of the temperature profile of the cylinder wall should be obtained. The temperature profile will help to improve the prediction of the relative contribution of the oil film to the HC emissions.

d. An estimation of the extent of the in-cylinder and exhaust port oxidation should be performed to characterize the extent of the contribution of the ring pack and oil

film to the engine-out HC emissions. This could help to improve the understanding and the extent of the contribution of each HC mechanism to the engine-out HC emissions. This could be done with a fully threedimensional simulation with chemistry, correlating the measured HC with the mass that escapes combustion due to the ring pack and oil film, as well with experimental tests.

e. Another possible mechanism that could contribute to the engine-out HC emission is the flame quench on the combustion chamber walls. This mechanism was not studied in this thesis. Although, it is expected that its contribution is very small a studied is recommended for the particular operating conditions of small engines.

f. The present study was carried out under steady state conditions. However, under transient conditions some mechanisms such as the liquid fuel could be important. Therefore, the study should be complemented with a transient characterization of the relative contribution of the HC mechanisms.

g. During the ring pack study it was found that the crankcase pressure has a significant effect on the engine out HC emissions. In the present work due to the limitation of the building exhaust vacuum system, the crankcase pressure was reduced only up to 100.35 kPa. It is expected that a further reduction in the crankcase pressure could help to reduce the engine-out HC emissions, especially at low load. Therefore, crankcase pressure tests with significant vacuum levels are suggested.

h. A study to increase the burn rate at the low load condition should be performed. If the combustion is fast at this condition the high levels of HC due to the incomplete combustion could be avoided. It was shown for this engine that by placing flaps in the intake port, the burn rate was increased.

REFERENCES

1. Douglas, R., and Glover, S., "The Feasibility of Meeting CARB/EPA 3 Emission Regulations for Small Engines," SAE Paper 2007-32-0059, 2007

2. EPA Nonroad Engine and Vehicle Emission Study-Report, EPA 460/3-91-02, November 1991

3. US National Transportation Statistics, 2006. US Department of Transportation Report

4. Cheng, W. K., Hamrin, D., Heywood, J. B., Hochgreb, S., Min, K., and, Norris, M., "An Overview of Hydrocarbon Emissions Mechanisms in Spark-Ignition Engines," SAE Paper 932708, 1993

5. Heywood, J. B., "Internal Combustion Engine Fundamentals," McGraw-Hill, 1988

6. O'Sullivan, J. B., Russell, J. A., and Summerson, W. A., "Emission Characteristics of Small Industrial Engines,' SAE Paper 730857, 1973

7. Burrahm, R. W., Carroll, J. N., and White, J. J., "Small Utility Engine Emissions Reduction Using Automotive Technology," SAE Paper 911805, 1991

8. Eccleston, B. H., and Hurn, R. W., "Exhaust Emission from Small, Utility, Internal Combustion Engines," SAE Paper 720197, 1972

9. Hare, C. T., Houtman, W. H., Oliver W. R., and Springer, K. J., "Small Engine Emissions and Their Impact," SAE Paper 730859, 1973

10. Swanson, M., "An Emission Comparison Between a Carburetor and an Electronic Fuel Injection System for Utility Engines," SAE Paper 911806, 1991

11. Angelo, T. G., Borman, G. L., and Martin, J. K., "Emissions and Performance of a Small L-Head Utility Engine Fueled with Homogeneous Propane/Air and Propane/Air/Nitrogen Mixture," SAE Paper 932444, 1993

12. Itano, E., "Characterization of Carburetor Exit Flow," M.S. Thesis, Mechanical Engineering Deparment, University of Wisconsin-Madison, 1996

13. Jehlik, F. A., and Ghandhi, J. B., "Investigation of Intake Port Fuel Films in a Small Engine," SAE Paper 2001-01-1788, 2001

14. Bonneau, B. J., "Development of a Homogeneous Mixture System and Comparison with Carbureted Utility Engine Emissions and Performance," M.S. Thesis, Mechanical Engineering Department, University of Wisconsin-Madison, 1994

15. Boyle, R. J., Boam, D. J., and Finlay, I. C., "Cold Start Performance of an Automotive Engine Using Prevaporized Gasoline," SAE Paper 930710, 1993

16. Meyer, R., Yilmaz, E., and Heywood, J. B., "Liquid Fuel Flow in the Vicinity of the Intake Valve of a Port-Injected SI Engine," SAE paper 982471, 1998

17. Meyer, R., and Heywood, J. B., "Effect of Engine and Fuel Variables on Liquid Fuel Transport into the Cylinder in Port-Injected SI Engines," SAE paper 1999-0l-0563, 1999

18. Takahashi, Y., and Nakase, Y., "Analysis of the Fuel Liquid Film Thickness of a Port Fuel Injection Engine," SAE paper 2006-01-1051, 2006

19. Turns, S. R., "An Introduction to Combustion," McGraw-Hill, 2001

20. Goolsby, A. D., and Haskell, W. W., "Flame-Quench Distance Measurements in a CFR Engine," Combustion and Flame, 26, 105-114, 1976

21. Ishizawa, S., "An Experimental Study on Quenching Crevice Widths in the Combustion Chamber of a Spark-Ignition Engine," Twenty-Sixth Symposium on Combustion, The Combustion Institute, pp. 2605-2611, 1996

22. Alkidas, A.,"Combustion Chamber Crevices: The Major Source of Engine-Out Hydrocarbon Emissions Under Fully Warmed Conditions," Prog. In Energy and Comb. Sci. Vol. 25, pp. 253-273, 1999

23. Wentworth, J. T. "Piston and Ring Variable Affect Exhaust Hydrocarbon Emissions," SAE Paper 680109, 1968

24. Alkidas, A. C., Drews, R. J., Miller, W. F., "Effects of Piston Crevice Geometry on the Steady State Engine Out Hydrocarbon Emissions from an SI Engine," SAE Paper 952537, 1995

25. Bignion, E. and Spicher, U. "Investigation of the Influence of Top Land Crevice Geometry on Hydrocarbon Emissions from SI Engines," SAE Paper 982560, 1998

26. Reitz, R. D. and Kuo, T. "Modeling of HC Emissions Due to Crevice Flows in Premixed-Charge Engines," SAE Paper 892085, 1989

27. Namazian, M. and Heywood, J. B. “Flow in the Piston-Cylinder-Ring Crevices of a Spark-Ignition Engine: Effect on Hydrocarbon Emissions, Efficiency and Power,” SAE Paper 820088, 1982

28. Alkidas, A. C. “The Effects of Head Gasket Geometry on Engine-Out HC Emissions from S.I. Engines,” SAE Paper 1999-01-3580, 1999

29. Green, R. M. and Cloutman, L. D. “Planar LIF Observations of Unburned Fuel Escaping the Upper Ring-Land Crevice in an SI Engine,” SAE Paper 970823, 1997

30. Eng, J. A., Leppard, W. R., Najt, P. M. and Dryer, F. L. “Experimental Hydrocarbon Consumption Rate Correlations From a Spark Ignition Engine,” SAE Paper 972888, 1997

31. Oliveira, I. B. and Hochgreb, S. “Effect of Operating Conditions and Fuel Type on Crevice HC Emissions: Model Results and Comparison with Experiments,” SAE Paper 1999-01-3578, 1999

32. Eng, J. A., Leppard, W. R., Najt, P. M. and Dryer, F. L. “The Interaction Between Nitric Oxide and Hydrocarbon Oxidation Chemistry in a Spark Ignition Engine,” SAE Paper 972889, 1997

33. Kuo-Chun, W. and Hochgreb, S. “Numerical Simulation of Post-Flame Oxidation of Hydrocarbons in Spark Ignition Engines,” SAE Paper 970886, 1997

34. Eng, J. A. “The Effect of Spark Retard on Engine-out Hydrocarbon Emissions,” SAE Paper 2005-01-3867, 2005

35. Kaiser, E. W., Adamczyk, A. A., and Lavoie G. A., “The Effect of Oil Layers on the Hydrocarbon Emissions Generated During Closed Vessel Combustion,” Eighteenth Symposium on Combustion, The Combustion Institute, pp. 1881-1892, 1981

36. Kaiser, E. W., Lorusso, J. A., Lavoie, G. A., and Adamczyk, A. A., “ The Effect of Oil Layers on the Hydrocarbon Emissions from Spark-Ignited Engines,” Combustion Science and Technology, Vol. 28, pp. 69-73, 1982

37. Carrier, G., Fendell, F., and Feldman, P., “Cyclic Absorption/Desorption of Gas in a Liquid Wall Film,” Combustion Science and Technology, Vol. 25, pp. 9-19, 1981

38. Gatellier, B., Trapy, J., Herrier D., Quelin, J. M. and Galliot, F. “Hydrocarbon Emissions of SI Engines as Influenced by Fuel Absorption-Desorption in Oil Films,” SAE Paper 920095, 1992

39. Linna, J., Malberg, H., Bennett, P. J., Palmer, P. J., Tian, T. and Cheng, W. K. "Contribution of Oil Layer Mechanism to the Hydrocarbon Emissions from Spark-Ignition Engines," SAE Paper 972892, 1997

40. Kaiser, E. W., Siegl, W. O. and Russ, S. G. "Effect of Fuel Dissolved in Crankcase Oil on Engine-Out Hydrocarbon Emissions from a Spark-Ignited Engine," SAE Paper 972891, 1997

41. Norris, M. G. and Hochgreb, S. "Extent of Oxidation of Hydrocarbons Desorbing from the Lubricant Oil Layer in Spark-Ignition Engines," SAE Paper 960069, 1996

42. Kaiser, E. W., Siegl, W. O. and Russ, S. G. "Fuel Composition Effects on Hydrocarbon Emissions from a Spark-Ignited Engine – Is Fuel Absorption in Oil Significant?," SAE Paper 952542, 1995

43. Parks, J., Armfield J., Storey, J., Barber, T. and Wachter, E. "In Situ Measurement of Fuel Absorption into the Cylinder Wall Oil Film During Engine Cold Start," SAE Paper 981054, 1998

44. Min, K., and Cheng, W. K., " Oil Layer as Source of Hydrocarbon Emissions In SI Engine," ICE-Vol. 27-4, 1996, Fall Technical Conference, pp. 85-96

45. Yu, S., and Min, K., "Effects of the Oil and Liquid Fuel Film on Hydrocarbon Emissions in Spark Ignition Engines," Proc. Inst. Mech. Engrs. Vol. 216 Part D: Journal of Automotive Engineering, 2002

46. Dent J. C., and Lakshminarayanan, "A model for Absorption and Desorption of Fuel Vapor by Cylinder Lubricating Oil Films and Its Contribution to Hydrocarbon Emissions," SAE Paper 830652, 1983

47. Schramm, J., and Sorenson, S. C., "Solubility of Gasoline Components in Different Lubricants for Combustion Engines Determined by Gas-Liquid Partition Chromatography," Journal of Chromatography, 538, pp. 241-248, 1991

48. Chappelow, C. C., and Prausnitz, J. M., "Solubilities of Gases in High-Boiling Hydrocarbon Solvents," AIChE Journal, Vol. 20, No. 6, 1974

49. Sugiyama, T., Takeuchi, T., and Suzuki, Y., "Thermodynamic Properties of Solute Molecules at Infinite Dilution Determined by Gas-Liquid Chromatography: I. Intermolecular Energies of n-Alkane Solutes in C_{28}-C_{36} n-Alkane Solvents," Journal of Chromatography, 105, pp. 265-272, 1975

50. LoRusso, J. A., Kaiser, E. W., and Lavoie, G. A., "In-Cylinder Measurements of Wall Layer Hydrocarbons in a Spark Ignited Engine," Combustion Science and Technology, Vol. 22, pp. 75-112, 1983

51. Westbrook, C. K., Adamczyk A. A., and Lavoie, G. A., " A Numerical Study of Laminar Flame Wall Quenching," Combustion and Flame, Vol. 40, pp. 81-99, 1981

52. Mercury Service Manual, 200/225 Optimax, Direct Fuel Injection, August 2003

53. Miller, R. W., "Flow Measurement Engineering Handbook," McGraw Hill Publishing Company, 2nd Edition, New York, 1989.

54. Figliola, R. S., and Beasley, D. E., " Theory and Design for Mechanical Measurements," John Wiley & Sons, Inc., Third Edition, New York, 2000

55. MotoTron Corporation, www.mototron.com

56. The MathWorks Inc., www.mathworks.com

57. Green Hills Software Inc., www.ghs.com

58. Electronic Control Unit Data Sheet, ECM model ECM-0565-128-0503, MotoTron Corporation, 2006

59. B&B Electronics Manufacturing Company, www.bb-elec.com

60. Dyne Systems Inc., www.dynesystems.com

61. TB Woods Incorporated, www.tbwoods.com

62. Rexnord Industries LCC, www.rexnord.com

63. Test Procedure for the Measurement of Gaseous Exhaust Emissions from Small Utility Engines, SAE J1088, SAE Recommended Practice, February 1993

64. HRF-500 Fast FID Hydrocarbon Measurement System User Manual version 2.1, Cambustion Inc. 2001.

65. Finlay, I. C., Boam, D. J., Bingham, J. F., and Clark, T. A., "Fast Response FID Measurement of Unburned Hydrocarbons in the Exhaust Port of a Firing Gasoline Engine," SAE paper 902165, 1990

66. Cheng, W. K., Summers, T., and Collings, N., "The Fast-Response Flame Ionization Detector," Progress in Energy and Combustion Science, Vol. 24, pp. 89-124, 1998

67. Dryer Instruments Inc, www.dryer.com

68. Elster American Meter, www.americanmeter.com

69. Kistler Instrumetn Corporation, www.kistler.com

70. National Instruments, www.ni.com

71. HI-Techniques Inc, www.hi-techniques.com

72. BEI Electronics Inc., www.bei.com

73. Johann Haltermann Ltd., a subsidiary of the Dow Chemical Company, www.dow.com

74. Stivender, D. L., "Development of a Fuel-Based Mass Emission Measurement Procedure," SAE Paper 710604, 1971

75. Barrestville Energy Research Center Report, BERC/CP-77/47, 1977

76. Spindt, R. S., "Air-Fuel Ratios from Exhaust Gas Analysis," SAE Paper 650507, 1965

77. Ghandhi, B. J., "Calculation of Engine Mass Emissions and Air-Fuel Ratio from Exhaust Concentration Measurements," Engine Research Center, Technical Report

78. Woschni, G. " A Universally Applicable Equation for the Instantaneous Heat Transfer Coefficient in the Internal Combustion Engine," SAE Paper 670931, 1967

79. Yun, H. J., and Mirsky, W., "Schlieren-Streak Measurements of Instantaneous Exhaust Gas Velocities from a Spark-Ignition Engine," SAE Paper 741015, 1974

80. Brown C.N., Ladommatos N., "The Effects of Mixture Preparation and Trapped Residuals on the Performance of a Spark-Ignition Engine with Air-Shrouded Port Injectors, at low load and low speed," Proceeding of Mechanical Engineers, Part D, Journal of Automobile Engineering, Vol. 205 (D1), pp. 17-30 , 1991

81. Brown C.N., Ladommatos N., "A Numerical Study of Fuel Evaporation and Transportation in the Intake Manifold of a Port-Injected SI Engine," Proceeding of Mechanical Engineers, Journal of Automobile Engineering, Vol. 205 (D3), pp. 161-175, 1991

82. Sher, E. (ed)., "Handbook of Air Pollution from Internal Combustion Engines: Pollutant Formation and Control," Academic Press, Boston, Massachusetts, 1998

83. Lavoie, G. A., Lorusso, J. A., and Adamczyk, A. A., "Hydrocarbon Emission Modelling for Spark Ignition Engines," Combustion Modeling in Reciprocating Engines, pp. 409-445, 1978.

84. Trinker, F. H., Cheng, J., and Davis, G. C., "A Feedgas HC Emission Model for SI Engines Including Partial Burn Effects," SAE Paper 932705, 1993

85. Thompson, N. D., and Wallace, J. S., "Effect of Engine Operating Variables and Piston and Ring Parameters on Crevice Hydrocarbon Emissions," SAE Paper 940480, 1994

86. Daniels, C. H., and Evers, L. W., "The Influence of Mixture Preparation on a Warm 1.9L Ford Engine," SAE Paper 940444, 1994

87. Harrington, J. A., and Shisu, R. C., "A Single-Cylinder Engine Study of the Effects of Fuel Type, Fuel Stoichiometry, and Hydrogen-to-Carbon Ratio and CO, NO, and HC Exhaust Emissions," SAE Paper 730476, 1973

88. Stache, I. and Alkidas, A. C., "The Influence of Mixture Preparation on the HC Concentration Histories from a S.I. Engine Running Under Steady-State Conditions," SAE Paper 972981, 1997

89. Furuhama, S. and Tada, T., "On the Flow of the Gas through the Piston-Rings," (2nd Report, The Character of Gas Leakage) Bulletin of the JSME, Vol. 4., No. 16, pp. 691-698, 1961

90. Kuo, T.W., Sellnau, M. C., Theobald, M. A., and Jones, J. D., "Calculation of the Flow in the Piston-Cylinder-Ring Crevices of a Homogeneous-Charge Engine and Comparison with Experiment," SAE Paper 890838, 1989

91. Furuhama, S. and Tada, T., "On the Flow of the Gas through the Piston-Rings," (1st Report, The Discharge Coefficient and Temperature of Leakage) Bulletin of the JSME, Vol. 4., No. 16, pp. 684-690, 1961

92. Roberts, C. E., and Matthews, R. D., "Development and Application of an Improved Ring Pack Model for Hydrocarbon Emissions Studies," SAE Paper 961966, 1996

93. Kim, C. G., Bae, C. S., and Choi, S. M., "Importance of the Inter-Ring Crevice Volume as a Source of Unburned Hydrocarbon Emissions-Numerical Considerations," Proceedings of the Institute of Mechanical Engineers, Vol 214, part D, pp 395-403, 2000

94. Kuo, K. K., "Principles of Combustion," John Wiley & Sons, Inc., Second Edition, New Jersey, 2005

95. Haugle, N. J., and Ghandhi, J. B., “The Effects of Exhaust Gas Recirculation in Utility Engines,” SAE Paper 2006-32-0116, 2006

96. Bevington, P. R., “ Data Reduction and Error Analysis for the Physical Sciences,” McGraw-Hill, 1969

97. Linna, J. R., and Hochgreb, S., “Analytical Scaling Model for Hydrocarbon Emissions From Fuel Absorption in Oil Layers in Spark Ignition Engines,” Combustion Science and Technology, Vol. 109, pp.205-226, 1995

98. Cipollone, R., “On the Thermal Fields of I.C.E. Cylinder Liners,” SAE paper 900455, 1990

99. Schramm, J. and Sorenson, S. C., “A Model for Hydrocarbon Emissions form SI Engines,” SAE Paper 902169, 1990

100. Tannehill, J. C., Anderson, D. A., and Plectcher, R. H., “Computational Fluid Mechanics and Heat Transfer,” Taylor & Francis Ltd., 1997

101. Hayduk, W. and Minas, B. S., “Correlations for Prediction of Molecular Diffusivities in Liquids,” *Can. J. Chem. Eng.*, 60, 295-299, 1982

102. Poling, B., Prausnitz, J., and Poling, B. E., “The Properties of Gases and Liquids,” McGraw Hill, New York, 2001

103. Trinker, F. H., Cheng, J., Davis, G. C., “ A Feedgas HC Emission Model for SI Engines Including Partial Burn Effects,” SAE Paper 932705, 1993

104. Min, K. and Yu, S. “Effects of the Oil and Liquid Fuel Film on Hydrocarbon Emissions in Spark Ignition Engines,” Proceedings of the Institute of Mechanical Engineers, Vol 216, part D, pp 759-771, 2002

105. Fluid Meters, Theory and Applications, 6th Ed., American Society of Mechanical Engineers, New York, 1971

106. Doebelin, E. O., “Measurement Systems: Applications and Design,” McGraw-Hill Publishing Company, Fourth Edition, New York, 1990

107. Gatowsky, J. A., Balles, E. N., Chun, K. M., Nelson, F. E., Ekchian, J. A., and Heywood, J. B., 1994, “Heat Release Analysis of Engine Pressure Data,” SAE Paper 841359, 1984

108. Cheung, H., and Heywood, J. B., “Evaluation of a One-Zone Burn-Rate Analysis Procedure Using Production SI Engine Pressure Data,” SAE Paper 93274, 1993

109. Lanzafame, R., and Messina, M., "ICE Gross Heat Release Strongly Influenced by Specific Heat Ratio Values," International Journal of Automotive Technology, Vol. 4, No. 3, pp. 125-13, 2003

APPENDIX I - MICROMOTION FLOWMETER CALIBRATION

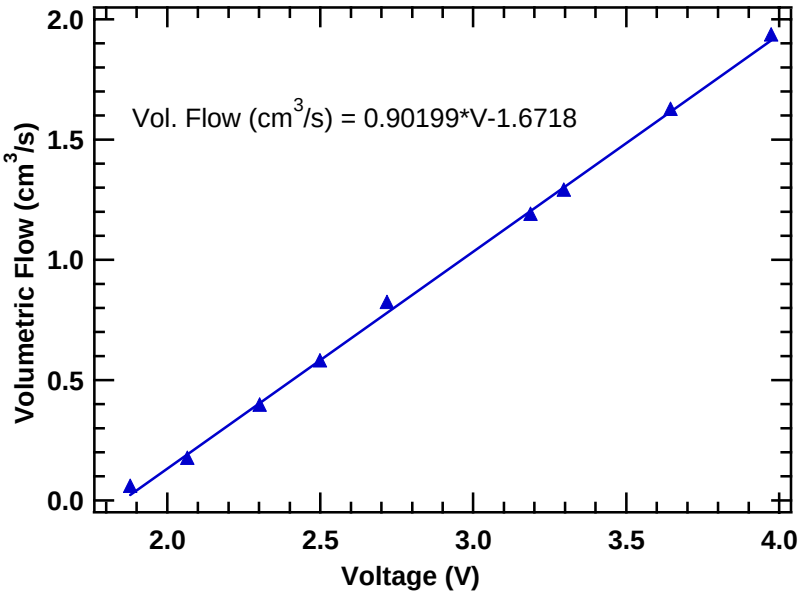

Figure A1.1 Volumetric flow vs Voltage output of the transmitter of the Micromotion flowmeter.

APPENDIX II - CALIBRATION OF THE ORIFICES PLATES

The calibration of the orifice plates was performed using a bellows meter as indicated in Fig. A2.1. The bellows meter measures volumetric flow rate, which was converted to mass flow rate considering ideal gas behavior. Under choked flow conditions through the orifice plate, a direct relationship exists between the mass flow and the upstream density or pressure when isothermal [53, 54, 105]. Figure A2.2 shows the measured data for all the orifice plates used in the experiments. The pressure drop through the bellows meter is very small (around 0.5 in of water) and was neglected in all the mass flow calculations. It is important to mention that the humidity was not taken in account during the calibration or the tests; however it is expected a very small influence in the results because the compressed air is partially dried.

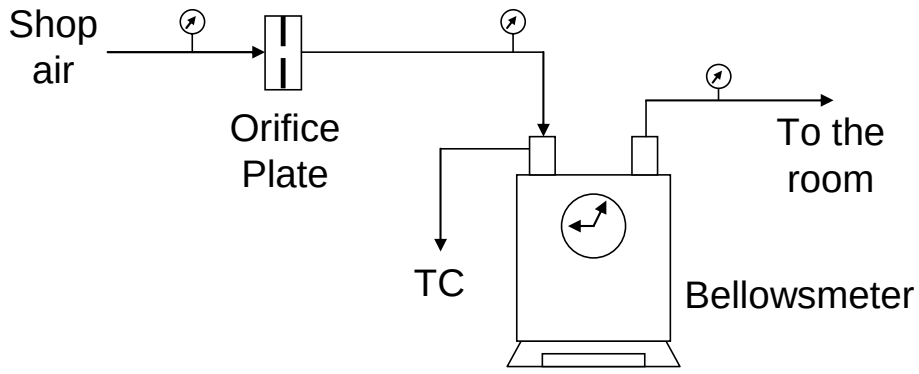

Figure A2.1 Schematic for the calibration process of the orifice plates to measure the air mass flow rate

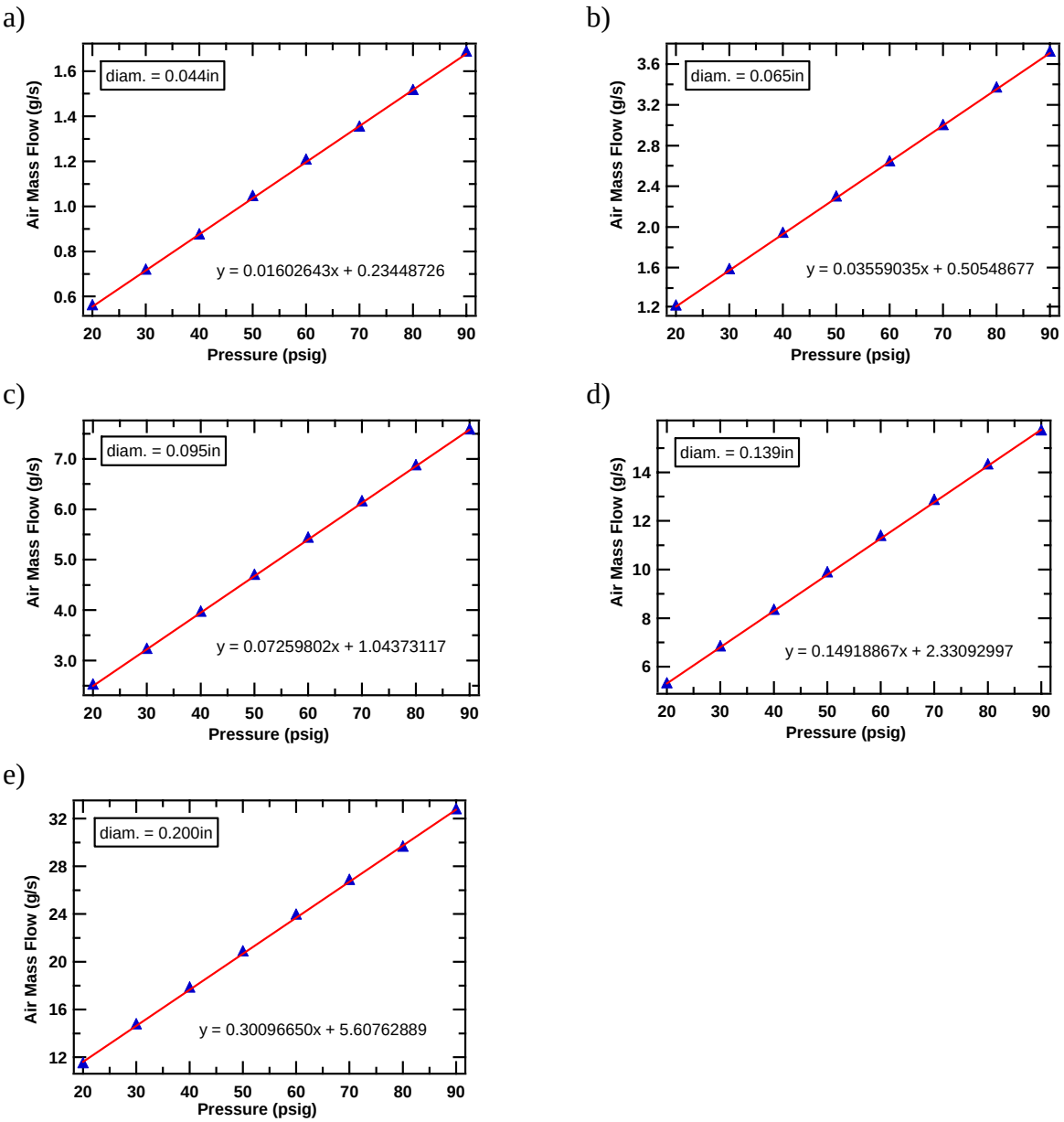

Figure A2.2 Calibration curves of the orifice plates used to measure the air mass flow.

APPENDIX III - CYLINDER PRESSURE TRANSDUCER CALIBRATION

The calibration of the pressure transducers was carried using a dead weight tester and the calibration curves for the sensors of both cylinders are shown in Fig. A3.1.

a)

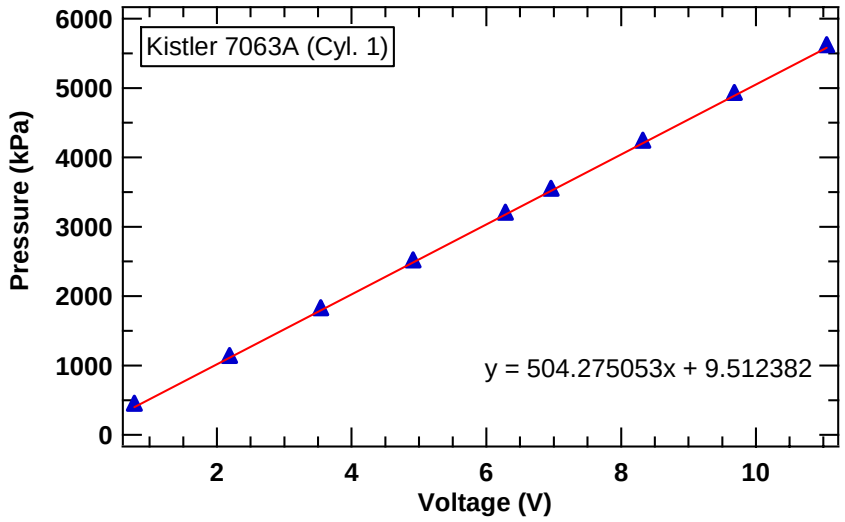

b)

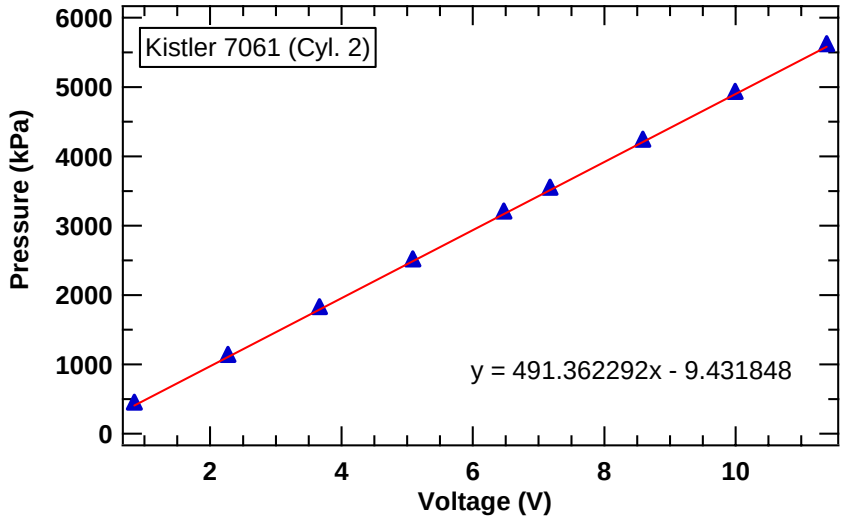

Figure A3.1 Calibration curves of the piezoelectric pressure transducers for the cylinder pressure measurements.

APPENDIX IV - CORRECTION OF THE MAP PRESSURE TRACES

The MAP sensors (from MotoTron) used to measure the dynamic intake and exhaust pressures are low cost and intended to measure static pressures or dynamic signals of very low frequency. Therefore, in order to measure the cycle-resolved pressures with these sensors a first order dynamic correction as the following was necessary [54, 106]:

$$\tau.\frac{dP_{slow}}{dt} + P_{slow} = K.P_{fast} \qquad \text{(A4.1)}$$

where τ and K are the time constant and the static sensitivity of the slow sensor (MAP). P_{slow} and P_{fast} are the pressure output of the slow and fast sensor respectively. The objective was to obtain pressure traces similar to P_{fast} based on P_{slow} traces. Therefore, the values of τ and K were needed. These values were obtained using the equation A4.1 and simultaneously measuring the pressure traces using a fast sensor (Piezoelectric) and the slow sensor (MAP). The schematic of the setup used for this purpose is indicated in Fig. A4.1.

The two sensors were mounted in a tee and exposed to the same time-averaging pressure waves from the engine. Both pressure traces were recorded with the HiTechniques data acquisition system. Figure A4.2, shows both pressure traces without any correction. It can be seen that, the MAP pressure trace is lagging the piezoelectric sensor.

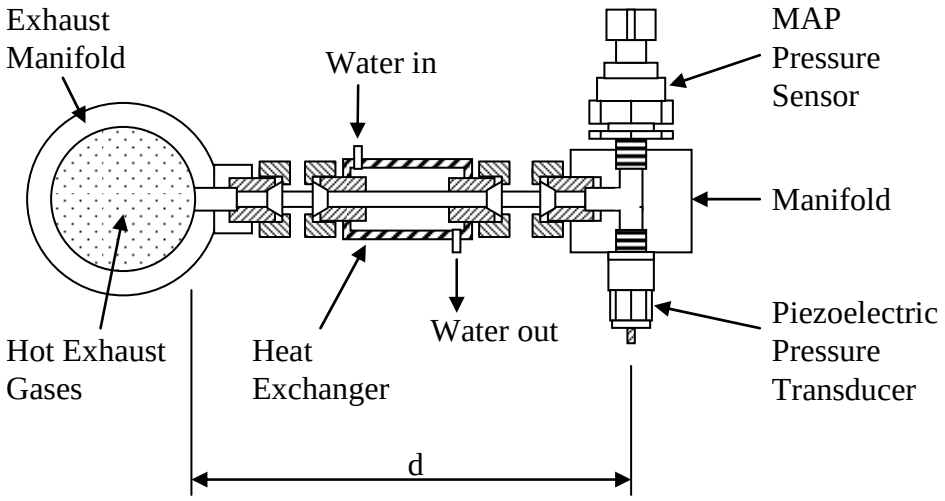

Figure A4.1 Schematic of the Pressure configuration to correct the slow MAP sensor response.

Using Eq. A4.1, the constants τ and K were adjusted until the difference between the corrected trace and the fast trace reached a minimum. This process was repeated for several sets of pressure traces for motored and fired conditions at different speeds and loads. Then, the average value for all the runs of τ and K was calculated giving the following values:

$$\tau = 0.87 \pm 0.2ms$$

$$K = 0.029 \pm 0.015$$

Using the values of the constants τ and K, the corrected pressure traces was determined as follows:

$$P_{corr-slow} = \tau . \frac{dP_{slow}}{dt} + P_{slow} \qquad \text{(A4.2)}$$

The corrected slow pressure trace obtained using Eq. A4.2, and the fast pressure trace from the piezoelectric are shown in Figure A4.3

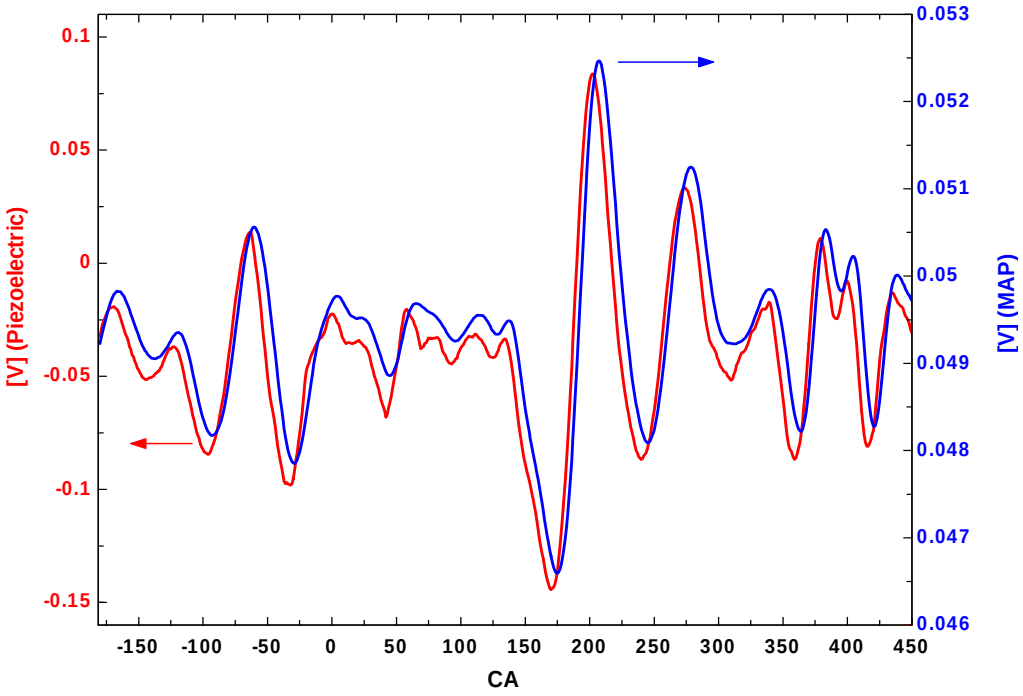

Figure A4.2 Signals from the piezoelectric and MAP (strain gage) sensors for 1000 RPM, 25% load, motored.

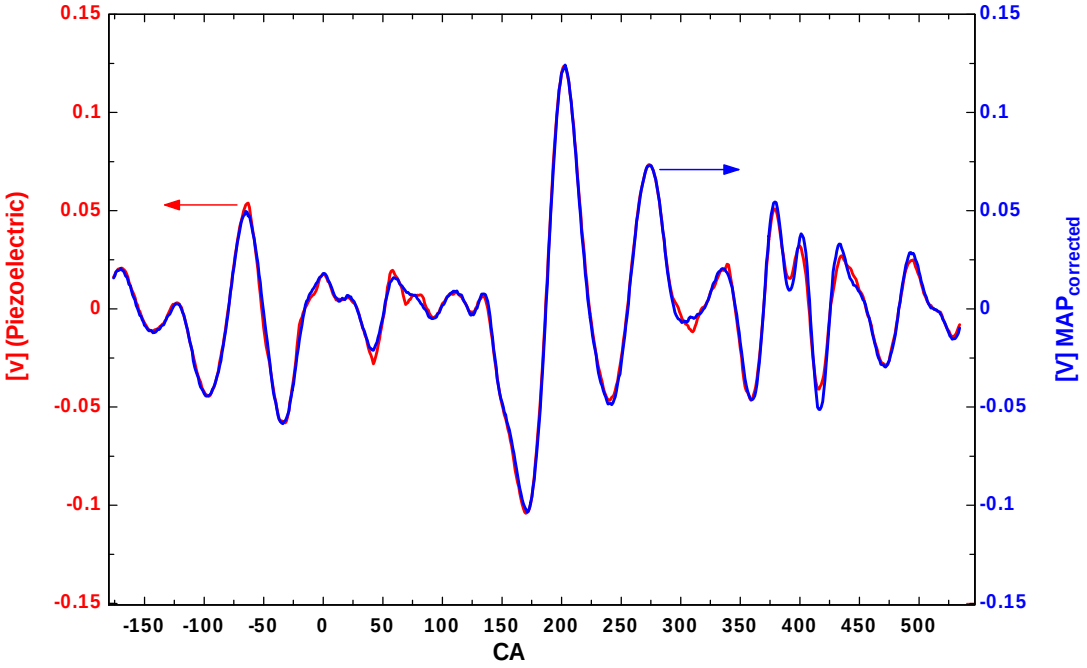

Figure A4.3 Traces from the piezoelectric and corrected MAP sensors for 1000 RPM, 25% load, motored.

APPENDIX V - LABVIEW EQUATIONS FOR EMISSIONS CALCULATIONS

The equations used to calculate the combustion efficiency, emissions index, air mass flow rate are given below.

```
//------Equations used by the Emission Bench LabView program. Written by Victor M. Salazar

float rho_air, R_air, B,S,MW_air,m_air,m_air_cyc,m_fuel_cyc, MW_CO2, MW_CO, MW_NO2, MW_fuel, N, H2O, H2,    MW_H2, MW_HC, MW_O2, MW_N2, QHV_CO, QHV_H2, HC_C1, NOx, NO2,N2, MW_NOx,MW_exh,F_c, R, Q, F_b,  AF_stoic, N_air, Y_HC, Y_CO, Y_H2, N_exh, m_CO, m_HC, m_NO, V_act, V_dis;

// KNOWN PARAMETERS

MW_air=28.97; // Air molecular weigth
MW_CO2=44.01;  //CO2 molecular weigth
MW_CO=28.01;  //  CO molecular weigth
MW_NO2=46.01;  // NO2 molecular weigth
MW_H2=2.016;  // H2 molecular weigth
MW_O2=31.999;  // O2 molecular weigth
MW_N2=28.013;  // N2 molecular weig th
MW_NOx=MW_NO2;  // NOx assumed as NO2
QHV_CO=10100;  // Lower heating value of CO (kJ/kg)
QHV_H2=120000;  // Lower heating value of H2 (kJ/kg)
R_air=0.28703; // Air constant gas (kJ/kg)

MW_fuel=12.01+1.008*y;   // Molecular weight of fuel in a 1 mole of fuel basis
MW_HC=MW_fuel;  //Molecular weight of hydrocarbons assumed to be the same as fuel
rho_air=P_atm/(R_air*(273.15+T))*6.89476;    // Air density (kg/m^3)

// ENGINE PARAMETERS

B=0.08;  // Cylinder bore (m)
S=0.067;  // Stroke (m)
m_air=V_air*rho_air;    // Mass air flow (kg/s)
m_air_cyc=m_air/RPM*120000;    //Mass of air per cycle (mg/cycle)
V_act=V_air/RPM*120;   // Actual of air in the cylinder per cycle (m^3/ cycle)
V_dis=2*3.141593*(B/2)*(B/2)*S;  //Displacement volume (m^3/cycle)
eff_Vol=V_act/V_dis;  //Volumetric efficiency
```

```
POWER=RPM*TQ*3.141593/30000;  //Engine power (kW)


//CALCULATED CONCENTRATION OF SPECIES

HC_C1=3*HC/10000;   //Concentration of HC in C1 measured in dry basis (%)
NOx=NO/10000;  // NO concentration in (%)

// *******AIR FUEL RATIO CALCULATIONS **********

//GM AF CALCULATION METHOD

N = 100/(HC_C1 + CO2 + CO);
H2O = ((y/2*100/N) -((3*y)/2)*(HC_C1/3))/((CO /(3.8*CO2)) +1);
H2 = (y/2)*(100/N) - H2O - ((3*y)/2)*(HC_C1/3);

        //== N2 and MWexh CALCULATION==

N2=100-(CO + CO2 + O2 +NOx + HC_C1 + H2);  // N2 concentration in dry basis (%)
MW_exh=1/100*(CO*MW_CO + CO2*MW_CO2 + O2*MW_O2 + NOx*MW_NOx +
HC_C1*MW_HC + H2*MW_H2 + N2*MW_N2);   // Molecular weight of the exhaust
gases (kg/kmol)

        //=======================

AF_C = (MW_air/MW_fuel)*((N/100)*(100+(3/2)*H2O+(((3*y)/2)-1)*(HC_C1/3) -
(1/2)*CO)-y/2);
AF_O = 4.76*(MW_air/MW_fuel)*((N/100)*(CO2 + CO/2 + H2O/2 + NOx/2 + O2));

        // OXYGEN (%) INDIRECT CALCULATION

O2_Calc = AF_C*(MW_fuel/MW_air)*(100/(N*4.76))-(CO2+CO/2+H2O/2+NOx/2);

 // SPINDT AF CALCULATION METHOD

F_c=12.01/(12.01+y);
R=CO/CO2;
Q=O2/CO2;
F_b=(CO+CO2)/(CO+CO2+HC_C1);

AF_Spindt=F_b*(11.492*F_c*(1+R/2+Q)/(1+R)+120*(1-F_c)/(3.5+R));
```

```
//BARTLESVILLE AF CALCULATION METHOD

AF_stoic=4.76*(1+y/4)*MW_air/MW_fuel;
AF_Bartlesville=(AF_stoic/(2+y/2))*((1+y/2)*CO+(2+y/2)*CO2+2*O2+NOx-
H2)/(CO+CO2+HC_C1);


// JAAL B. GHANDHI AF CALCULATION METHOD

N_air=N/100*(CO2+0.5*CO-0.5*H2-0.25*y*HC_C1+O2+0.5*NOx)+0.25*y;
AF_Jaal=4.76*N_air*MW_air/MW_fuel;

// MASS FRACTIONS OF THE SPECIES AT THE EXHAUST

H2=0.25*y*CO;  // Used Only for eff_comb calculation

Y_HC=HC_C1/100*(MW_HC/MW_exh);  // HC mass fraction in the exhaust in dry
basis

Y_CO=CO/100*(MW_CO/MW_exh);    // CO mass fraction in the exhaust in dry basis

Y_H2=H2/100*(MW_H2/MW_exh);    // H2 mass fraction in the exhaust in dry basis

m_fuel= m_air/AF_O;    // fuel mass flow obtained from the air fuel ratio (kg/s)
m_fuel_cyc = m_fuel/RPM*120000;   // Mass of fuel per cycle (mg/cycle)

// COMBUSTION EFFICIENCY

eff_comb=1- (Y_HC*QHV_HC + Y_CO*QHV_CO +
Y_H2*QHV_H2)/(m_fuel*QHV_HC/(m_fuel+m_air));  // Combustion efficiency,
according to: Internal Combustion Engines Fundamentals by Heywood, eqn. 4.69, pg 154

// MASS FLOW OF THE EXHAUST EMISSIONS

N_exh=100/(CO+CO2+HC_C1);    // Number of moles in the exhaust air
m_CO= CO/100*N_exh*(MW_CO/MW_fuel)*m_fuel;    //  Mass flow of CO (kg/hr)
m_HC= HC_C1/100*N_exh*m_fuel;    // Mass flow of HC (kg/hr)
m_NO=NOx/100*N_exh*(MW_NOx/MW_fuel)*m_fuel;  // Mass flow of NO (kg/hr)

// BREAK SPECIFIC CALCULATIONS

BSFC= m_fuel/POWER*3600000;    //Brake specific fuel consumption (g/kW-hr)
BSCO= m_CO/POWER*3600000;    // Brake specific CO emission (g/kW-hr)
BSHC= m_HC/POWER*3600000;     // Brake specific HC emission (g/kW-hr)
```

```
BSNO= m_NO/POWER*3600000;     // Brake specific NO emission (g/kW-hr)
BSHCNO= BSHC + BSNO;          // Breke specific NO + HC   (g/kW-hr)

// EMISSIONS INDEX

EICO=m_CO*1000/m_fuel;   // Emissions index of CO ( g CO/kg fuel)
EINO=m_NO*1000/m_fuel;   // Emissions index of NO (g NO/ kg fuel)
EIHC=m_HC*1000/m_fuel;   // Emissions index of HC (g HC/ kg fuel)
```

APPENDIX VI - AIR-FUEL RATIO CALCULATION

The air-fuel ratio was calculated starting from the following equation (adapted from Stivender [74]):

$$CH_y + a\,(O_2 + 3.76\,N_2) \rightarrow b\,CO_2 + c\,CO + \ldots$$
$$\ldots + d\,H_2O + e\,C_3H_8 + f\,NO + g\,H_2 + h\,O_2 + i\,N_2 \qquad \text{(A6.1)}$$

where the hydrocarbons are represented by propane ($[C_3H_8]=[HC_{C3}]$). Performing a mass balance for the different atomic components we have the following equations:

C: $1 = b + c + 3e$ (A6.2)

H: $y = 2d + 8e + 2g$ (A6.3)

O: $2a = 2b + c + d + f + 2h$ (A6.4)

N: $3.76\,a * 2 = f + 2i$ (A6.5)

The total number of moles of products gases, N_P, per mol of fuel is:

$$N_P = b + c + d + e + f + g + h + i \qquad \text{(A6.6)}$$

From the definition of air-fuel ratio and from Eq. A6.1:

$$AF = \frac{N_{air}}{N_{fuel}} * \frac{MW_{air}}{MW_{fuel}}, \text{ or}$$

$$AF = 4.76a * \frac{MW_{air}}{MW_{fuel}} \quad \text{(A6.7)}$$

Also from the carbon balance dividing by the number of moles of products:

$$\frac{1}{N_P} = \frac{b}{N_P} + \frac{c}{N_P} + 3\frac{e}{N_P} \quad \text{(A6.8)}$$

This is equivalent to:

$\frac{1}{N_P} = X_{CO} + X_{CO_2} + 3X_{HC_{C3}}$, or converting the molar fractions to percent:

$$\frac{1}{N_P} = \frac{1}{100}([CO](\%) + [CO_2](\%) + 3[HC_{C3}](\%))$$

where [CO](%), [CO_2](%) and [HC_{C3}](%) are the measured concentration of the gases at the exhaust in percent. Rrearranging,

$$N_P = \frac{100}{([CO](\%) + [CO_2](\%) + 3[HC_{C3}](\%))} \quad \text{(A6.9)}$$

6.1 CARBON BALANCE AF CALCULATION

For this method is necessary express N_P in Eq. A6.6 as a function of the moles of *CO*, CO_2, and H_2. Rearranging Eqs. A6.2-5:

C: $b = 1 - c - 3\,e$ (A6.10)

H: $g = y/2 - d - 4\,e$ (A6.11)

O: $h = a - b - c/2 - d/2 - f/2$ (A6.12)

N: $i = 3.76\ a - f/2$ (A6.13)

Replacing Eqs. A6.8-11 in A6.6, and rearranging:

$$N_P = 4.76a - 3e + c/2 - d/2 + y/2 \quad \text{(A6.12)}$$

Rearranging Eq. A6.12 in terms of the *a* coefficient:

$$4.76a = N_P + 3e - c/2 + d/2 - y/2 \quad \text{(A6.13)}$$

Substituting Eq. A6.13 in A6.7:

$$AF_C = \frac{MW_{air}}{MW_{fuel}}(N_P + 3e - c/2 + d/2 - y/2) \quad \text{(A6.14)}$$

In order to use the concentrations measured at the exhaust in Eq. A6.14 it is necessary of express the number of moles: *e*, *c*, and *d* as mole fractions or percent. The following conversion factor (unity) is introduced in Eq. A6.14:

$$AF_C = \frac{MW_{air}}{MW_{fuel}}(N_P + (\frac{N_P}{100}.\frac{100}{N_P}).\{3e - c/2 + d/2\} - y/2), \text{ or}$$

$$AF_C = \frac{MW_{air}}{MW_{fuel}}(N_P + \frac{N_P}{100}.\{3[HC_{C3}](\%) - [CO](\%)/2 + [H_2O](\%)/2\} - y/2) \ldots$$

$$\ldots \quad \text{(A6.14)}$$

In this equation the concentration of water at the exhaust is required. This is obtained from the water-shift reaction equilibrium:

$$K = 3.8 = \frac{[CO](\%)[H_2O](\%)}{[CO_2](\%)[H_2](\%)} \qquad \text{(A6.15)}$$

The hydrogen concentration in Eq. A6.15 is obtained from the hydrogen balance Eq. A6.11 and introducing the conversion factor:

$$\left(\frac{100}{N_P}\frac{N_P}{100}\right) g = y/2 - (d + 4e)\left(\frac{100}{N_P}\frac{N_P}{100}\right), \text{ rearranging}$$

$$[H_2](\%)\frac{N_P}{100} = y/2 - \{[H_2O](\%) + 4[HC_{C3}](\%)\}\frac{N_P}{100}, \text{ or}$$

$$[H_2](\%) = y/2\frac{100}{N_P} - \{[H_2O](\%) + 4[HC_{C3}](\%)\} \qquad \text{(A6.16)}$$

Finally from Eq. A6.15 and A6.16 the concentration of water is:

$$[H_2O](\%) = \frac{y/2\dfrac{100}{N_P} - 4[HC_{C3}](\%)}{\dfrac{[CO](\%)}{K[CO_2](\%)} + 1} \qquad \text{(A6.17)}$$

In the calculation of the *AF* carbon based method the N_P from Eq. A6.9 and $[H_2O]$ from A.6.17 must be calculated and then substituted in Eq. A6.14. The HC molecular weight (MW_{HC}) was considered equal to the molecular weight of the fuel in C1 basis (MW_{fuel_C1}).

6.2 OXYGEN BALANCE AF CALCULATION

In the oxygen balance method, the equation for the hydrogen balance (Eq. A6.4) can be recast as follows:

$$a = b + c/2 + d/2 + f/2 + h$$

Introducing the conversion factor (unity) as before:

$$a = \left(\frac{N_P}{100}\frac{100}{N_P}\right)(b + c/2 + d/2 + h) \text{ ,or rearranging}$$

$$a = \frac{N_P}{100}\left\{[CO_2](\%) + [CO](\%)/2 + [H_2O](\%)/2 + [O_2](\%)\right\} \qquad \text{(A6.18)}$$

Replacing Eq. A6.9 (the expression for N_P) in Eq. A6.18:

$$a = \frac{\left\{[CO_2](\%) + [CO](\%)/2 + [H_2O](\%)/2 + [O_2](\%)\right\}}{[CO_2](\%) + [CO](\%) + 3[HC_{C3}](\%)} \qquad \text{(A6.19)}$$

Finally replacing the value of *a* in Eq. A6.7:

$$AF_{O_2} = 4.76\frac{MW_{air}}{MW_{fuel}}\frac{\left\{[CO_2](\%) + [CO](\%)/2 + [H_2O](\%)/2 + [O_2](\%)\right\}}{[CO_2](\%) + [CO](\%) + 3[HC_{C3}](\%)} \ldots$$

$$\ldots \qquad \text{(A6.20)}$$

where the value of the water concentration is obtained from Eq. A6.17.

6.3 SPINDT METHOD

The method is documented in [76] as it is calculated as follows:

$$AF_{Spindt} = F_b.\left[11.492.F_c\left(\frac{1+R/2+Q}{1+R}\right)+\left(\frac{120.(1-F_c}{3.5+R}\right)\right] \quad \text{(A6.21)}$$

where:

$$F_c = \frac{12.01}{12.01+y} \quad \text{(A6.22)}$$

$$R = \frac{[CO](\%)}{[CO_2](\%)} \quad \text{(A6.23)}$$

$$Q = \frac{[O_2](\%)}{[CO_2](\%)} \quad \text{(A6.24)}$$

$$F_b = \frac{[CO](\%)+[CO2](\%)}{[CO](\%)+[CO2](\%)+3[HC_{C3}](\%)} \quad \text{(A6.25)}$$

6.4 BARTLESVILLE METHOD

For this method the following expression was used [75]:

$$AF_{Bartlesville} = \frac{AF_{stoic}}{2+y/2}\ldots$$

$$\ldots\frac{\{(1+y/2).[CO](\%)+(2+y/2)[CO_2](\%)+2[O2]+[NOx]-[H2]\}}{[CO](\%)+[CO2]+3[HC_{C3}](\%)}\ldots$$

... (A6.26)

where:

$$AF_{stoic} = 4.76 \frac{MW_{air}}{MW_{fuel}} (1 + y/4) \quad \text{(A6.27)}$$

6.5 ERC METHOD

This method was developed by Jaal B. Ghandhi [77] and it is calculated as follows:

$$AF_{Jaal} = 4.76 N_{air} \frac{MW_{air}}{MW_{fuel}}$$

where:

$$N_{air} = \frac{N_P}{100} \{[CO_2](\%) + [CO](\%)/2 - [H_2](\%)/2 - 3.y.[HC_{C3}](\%) + ...$$

$$... + [O_2](\%) + [NO_x](\%)\} + y/4 \quad \text{... (A6.28)}$$

In Eq. A6.28 N_P is calculated from Eq. A6.9.

APPENDIX VII - FUEL SPECIFICATIONS

Certificate 2861052 Haltermann Products Page 1

Date: 02/14/2006 Certificate of Analysis

Quality Assurance
UNIVERSITY OF WISCONSIN SYSTEM Fax:
1500 ENGINEERING DR
MADISON WI 53706-0000 UNITED STATES

Cust P.O.: Verbal Victor Salzar 02/13/06 Dlvy Note: 64023557 10
Cust Ref: Order No.: 21024832

Material: EEE, EPA Tier II
55 GALLON STEEL DRUM GMID: 207000
Cust Mtl:
Batch: UA1621LS10

Dlvy Qty:DR 1
Vehicle:

Ship from: JOHANN HALTERMANN LTD CHANNELVIEW TX UNITED STATES

Feature	Units		Results UA1621LS10	Limits Minimum	Maximum	Method
Distillation-IBP	degC		31	24	35	ASTM D86
Distillation-5%	degC		46	----	----	ASTM D86
Distillation-10%	degC		52	49	57	ASTM D86
Distillation-20%	degC		63	----	----	ASTM D86
Distillation-30%	degC		77	----	----	ASTM D86
Distillation-40%	degC		93	----	----	ASTM D86
Distillation-50%	degC		106	93	110	ASTM D86
Distillation-60%	degC		112	----	----	ASTM D86
Distillation-70%	degC		118	----	----	ASTM D86
Distillation-80%	degC		129	----	----	ASTM D86
Distillation-90%	degC		161	149	163	ASTM D86
Distillation-95%	degC		169	----	----	ASTM D86
Distillation-EP	degC		202	----	213	ASTM D86
Recovery	% vol		98.1	----	----	ASTM D86
Residue	% vol		1.0	----	----	ASTM D86
Loss	% vol		0.9	----	----	ASTM D86
Gravity, API	-		59.0	58.7	61.2	ASTM D4052
Density	kg/L		0.743	0.734	0.744	ASTM D4052
Reid Vapor Pressure	psi		9.0	8.7	9.2	ASTM D5191
Reid Vapor Pressure	psi		9.0	----	----	ASTM D5191
Oxygen	% wt	<	0.01	----	0.05	ASTM D4815
Sulfur	% wt		0.0027	0.0015	0.0080	ASTM D5453
Lead	g/gal	<	0.010	----	0.010	ASTM D3237
Phosphorous	g/gal	<	0.005	----	0.005	ASTM D3231
Aromatics	% vol		28.3	----	35.0	ASTM D1319
Olefins	% vol		0.6	----	10.0	ASTM D1319
Saturates	% vol		71.1	----	----	ASTM D1319

Certificate 2861052 Haltermann Products Page 2

Date: 02/14/2006 Certificate of Analysis

Quality Assurance
UNIVERSITY OF WISCONSIN SYSTEM Fax:
1500 ENGINEERING DR
MADISON WI 53706-0000 UNITED STATES

Cust P.O.: Verbal Victor Salzar 02/13/06 Dlvy Note: 64023557 10
Cust Ref: Order No.: 21024832

Material: EEE, EPA Tier II
55 GALLON STEEL DRUM GMID: 207000
Cust Mtl:

Dlvy Qty:DR 1
Vehicle:

Ship from: JOHANN HALTERMANN LTD CHANNELVIEW TX UNITED STATES

Feature	Units		Results UA1621LS10	Limits Minimum	Maximum	Method
Carbon weight fraction	% wt		0.8650	----	----	ASTM D3343
Carbon weight fraction	% wt		0.8629	----	----	ASTM E191
Hydrogen weight fraction	% wt		0.1332	----	----	ASTM E191
H2/Carbon, mol/mol	-		1.840	----	----	ASTM E191
Fuel Econ. Numer.	-		2,431	2,401	2,441	ASTM E191
C Factor	-		1.002	----	----	ASTM E191
Particulate Matter	mg/L		0.6	----	1.0	ASTM D5452
Oxidation Stability	min	>	1,000	240	----	ASTM D525
Corrosion - Copper		1A				ASTM D130
Washed Gum	mg/100	<	1	----	5	ASTM D381
RON	-		97.4	93.0	----	ASTM D2699
MON	-		89.2	----	----	ASTM D2700
Sensitivity	-		8.2	7.5	----	ASTM D2699/D2700
Color clear, bright, homogeneous			Passes			Visual
Net Heating Value	Btu/lb		18,482	----	----	[redacted]
Net Heating Value	Btu/lb		18,375	----	----	ASTM D240

Business Quality Leader
Dow Haltermann

For inquiries please contact Customer Service or local sales.

APPENDIX VIII - STOP FUEL INJECTION TESTS

A8.1 EQUATIONS

The following analysis was done in order to quantify the amount of fuel in the intake manifold. After the injection was stopped, the mixture at the exhaust was considered to be a mixture of air and fuel.

From the mass balance at the exhaust:

$$Y_{fuel} + Y_{air} = 1 \tag{A8.1}$$

or in molar basis,

$$X_{fuel} + X_{air} = 1 \tag{A8.2}$$

In Eqs. A8.1-2 X and Y are the molar and mass fractions respectively.The mass fraction Y is defined as:

$$Y_{fuel} = \frac{\dot{m}_{fuel}}{\dot{m}_{total}} \tag{A8.3}$$

$$Y_{air} = \frac{\dot{m}_{air}}{\dot{m}_{total}} \tag{A8.4}$$

where $\dot{m}_{fuel}$ and $\dot{m}_{air}$ are the mass flow rate of fuel and air (measured) respectively. $\dot{m}_{total}$ represents the total mass flow rate. Similarly the molar fraction X is defined by:

$$X_{fuel} = \frac{\dot{N}_{fuel}}{\dot{N}_{total}} \tag{A8.5}$$

$$X_{air} = \frac{\dot{N}_{air}}{\dot{N}_{total}} \tag{A8.6}$$

where $\dot{N}_{fuel}$ and $\dot{N}_{air}$ are the molar flow rate of fuel and air respectively. $\dot{N}_{total}$ represents the total molar flow rate. The total mass flow is given by the following expression:

$$\dot{m}_{total} = \dot{m}_{air} + \dot{m}_{fuel} \tag{A8.7}$$

or in molar basis,

$$\dot{N}_{total} = \dot{N}_{air} + \dot{N}_{fuel} \tag{A8.8}$$

Now, from equation (A8.3) and (A8.4) we have:

$$\frac{Y_{fuel}}{Y_{air}} = \frac{\dot{m}_{fuel}}{\dot{m}_{air}} \tag{A8.9}$$

Rearranging Eq. A8.9 the mass of fuel is given by:

$$\dot{m}_{fuel} = \dot{m}_{air} \frac{Y_{fuel}}{Y_{air}} \tag{A8.10}$$

Using Eq. (A8.2) in (A8.10)

$$\dot{m}_{fuel} = \dot{m}_{air} \frac{Y_{fuel}}{1 - Y_{fuel}} \tag{A8.11}$$

Rearranging,

$$\dot{m}_{fuel} = \dot{m}_{air} \frac{1}{(1/Y_{fuel} - 1)} \tag{A8.12}$$

From the relation between mass fraction and molar fraction we have:

$$Y_{fuel} = X_{fuel} . \frac{MW_{fuel}}{MW_{mix}} \tag{A8.13}$$

where MW_{fuel} and MW_{mix} are the molecular weight of the fuel and the air-fuel mixture respectively. Replacing Eq. (A8.13) in (A8.12):

$$\dot{m}_{fuel} = \dot{m}_{air} . \frac{1}{(X_{fuel} . MW_{fuel} / MW_{mix})^{-1} - 1} \tag{A8.14}$$

Rearranging:

$$\dot{m}_{fuel} = \dot{m}_{air} . \frac{X_{fuel} . MW_{fuel}}{MW_{mix} - X_{fuel} . MW_{fuel}} \tag{A8.15}$$

From the definition of the molecular weight of the mixture:

$$MW_{mix} = X_{fuel} . MW_{fuel} + X_{air} . MW_{air} \tag{A8.16}$$

Replacing Eq. (A8.16) into (A8.15) and rearranging, the following relationship is obtained:

$$\dot{m}_{fuel} = \dot{m}_{air} . \frac{X_{fuel} . MW_{fuel}}{(1 - X_{fuel}) . MW_{air}} \tag{A8.17}$$

which is the equation that allows conversion of the mass fraction, $X_{fuel,}$ (measured by the FFID) into mass of fuel in *mg* per cycle.

In equation (A8.17) the molecular weight of the fuel is the molecular weight on a C1 basis, and it is calculated as follows:

$$MW_{fuel} = MW_C + y.MW_H \qquad \text{(A8.18)}$$

where $MW_C = 12.0011$ is atomic weight of the carbon, $MW_H = 1.0079$ is the atomic weight of the hydrogen and *y* is the hydrogen to carbon ratio of the fuel per mol of C1:

$$y = H/C \text{ ratio of the fuel} \qquad \text{(A8.19)}$$

The fuel molar concentration must be provided in molar fraction. Therefore the concentration of the fuel being read by the FFID in ppm must be converted to molar fraction by using the following conversion:

$$X_{fuel} = 3.X_{fuelC3}/10^6 \qquad \text{(A8.20)}$$

where X_{fuelC3} is the concentration of the fuel in a *C3* base (because propane was used to calibrate the fast-FID).

A8.2 Program

```
%Program to extract the data from the Hi-Techniques data acquisition
%and to calculate the amount of fuel present in the intake manifold
%Written by: Victor M. Salazar, ERC-UW Madison
%August 28th, 2006.
%The program uses as inputs the engine parameters and the file name to
%be processed which are stored in the text file "FolderList.txt"

close all
clc
clear
tic
% Filename and input values search in FolderList.txt file
FName = fopen('FoldersList.txt','r');
i=1;
while (~feof(FName))
 C(i)=textscan(FName, '%s',1,'commentStyle', '//');
 i=i+1;
end
 [F,f]=size(C);
for j=1:1:f
 c{j}=cell2mat(C{j});
end
fclose(FName);
% Values from FolderList.txt input file
y=str2num(c{1});                % Crank radius to road length ratio
m_air_cycle=str2num(c{2});      % Clearance volume
m_fuel_cycle_e=str2num(c{3});   % Mass of fuel per engine cycle firing
nch=str2num(c{4});              % Number of Channels to be processed
npeg=str2num(c{5});             % Chanel with the pegging location
shift=str2num(c{6});            % Time shift for the FFID (not used)
theta_peg=-180;                 % Angle for the pegging location

% Getting the RPM value
% This part of the program opens the file ERESULTA.arg of the HI
% Techniques output file and looks for the speed (RPM)
for r=7:1:f
 RPMc{r-6}=strcat(c{r},'/ERESULTA.arg');
 FRPM = fopen(RPMc{r-6},'r');
 for j=1:1:81
  RPMf(j)=textscan(FRPM, '%s',1,'delimiter','/n');
 end
  fclose(FRPM);
  a=cell2mat(RPMf{81}); [ro,co]=size(a); b=a(16:co);
  RPM(r-6) = str2num(b);  % RPM value from ERESULTA.arg file
end
% Reading the binary data of each channel of the file
for k=7:1:f
 for n=1:1:nch
  nc=num2str(n);
  pth{n}=strcat(c{k},'/ACH00',nc,'01.dat');
 end
 for p=1:1:nch
```

```
  fid1=fopen(pth{p});  % Extracting the data - by Jaal B. Ghandhi
  [A1,count] = fread(fid1,35,'uchar');
  % Reading first values
  [B1,count] = fgets(fid1,15);  value1(1)=str2double(B1);
  % Scaling factor
  [C1,count] = fgets(fid1,15);  value1(2)=str2double(C1);
  % Data offset
  [D1,count] = fgets(fid1,15);  value1(3)=str2double(D1);
  % Shaft encoder resolution in CAD
  [E1,count] = fgets(fid1,15);  value1(4)=str2double(E1);
  % Array start - not used
  [F1,count] = fgets(fid1,10);  value1(5)=str2double(F1);
  % Number of points
  [A1,count] = fgets(fid1,1);
  % Empty space
  [G1,count] = fgets(fid1,10);  offset1=str2double(G1);
  % Start of data location
  status1 = fseek(fid1,2*offset1+256+2*(540/value1(3)),'bof');
  ndpc=720/value1(3); % Number of data points per cycle
  ncycles1=floor((value1(5)-offset1)/ndpc);  % Number of cycles
  data1=zeros(ndpc,ncycles1-2);
  low(1:ndpc*(ncycles1-2))=fread(fid1,ndpc*(ncycles1-2),'uchar',1); %
Low byte
  status = fseek(fid1,2*offset1+256+2*(540/value1(3)),'bof');
  l=fread(fid1,1,'schar');
  high(1:ndpc*(ncycles1-2))=fread(fid1,ndpc*(ncycles1-2),'schar',1); %
High byte
  for j=1:ncycles1-2
   n=j-1;
   for i=1:ndpc
data1(i,j)=value1(1)*(256*double(high(i+ndpc*n))+double(low(i+ndpc*n)))
-value1(2);
   end
  end
  alldata{p}=data1;
  AD=cell2mat(alldata);      % Matrix with all the data
  datamean1{p} = mean (data1,2);
 end
 M=cell2mat(datamean1);      % Conversion of datamean to a matrix
 fclose (fid1);
% Start of the stored mass of fuel calculation
 CA=-180:value1(3):540-value1(3);  % Crank Angle Vector
% known parameters:
 MW_air = 28.9;
 MW_C= 12.011;
 MW_H=1.0079;
 MW_fuel= 12.011 + 1.0079*y;     % Fuel Molecular weight in C1 base
 ncp= ncycles1-2;                % Number of cycles
 ndp=720/value1(3);              % Number of points per cycle
 t=1;                            % Initialization of the variable that
counts the cycles after stop Injection
 m_fuel_cum =0;                  % Initialization variable to calculate
the cumulative mass of fuel
```

```
 m=0;                                % Initialization for the variable
that indicates when the fuel was stopped
% Conversion of the HC mass fraction to mass of fuel per cylce
    for j=1:1:ncp;
     FI_max(j)=max(AD(:,2*ncp+j)); % Looking at the maximum value of
the fuel injecton pulse
     if FI_max(j)<0.1              % Looking for the cycle when the
injection has been stopped.
      m=m+1;
      if m==1                      % Condition to plot the FFID and the
Injector signal at the moment the injector is stop
      p=j;
       for j=p-3:1:p+3;            % Plot cycles before and after the
injection has been stopped
        figure
        hold on
        axis on; box on;
        [AX,H1,H2] = plotyy(CA,AD(:,ncp+j),CA,AD(:,2*ncp+j),'plot');
        set(get(AX(1),'Ylabel'),'String','HC/3 (ppm)')
        set(get(AX(2),'Ylabel'),'String','Fuel Injector Signal
(Volts)')
        set(AX(2),'YLim',[0 1])
        set(AX(1),'XLim',[-180 540])
        set(AX(2),'XLim',[-180 540])
        t1=title(['HC and Fuel Injector Signal at @ ',num2str(j),'
cycles']);
        xlabel('CA');
       end
      end
      HC_mean(t)=3/1000000*mean(AD(:,ncp+j));% Mean HC concentration
during a cycle in molar fraction
      m_fuel_cycle(t)=HC_mean(t)*MW_fuel/((1-
HC_mean(t))*MW_air)*m_air_cycle;    % Mass of fuel per cycle in
mg/cycle
      m_fuel_cum=m_fuel_cum+ m_fuel_cycle(t);% Cumulative mass of fuel
      m_fuel_cum_p(t)=m_fuel_cum;            % Vector with the
cumulative mass of fuel
      m_fuel_cum_nor(t)=m_fuel_cum_p(t)/m_fuel_cycle_e; % Normalized
cumulative mass of fuel
      t=t+1;
      end
     end
% Output files
js{k}=strcat('O_',c{k},'.txt');
fidO=fopen(js{k},'wt');
fprintf(fidO, 'Cyc_'); fprintf(fidO, c{k}); fprintf(fidO, '\t');
fprintf(fidO, 'm_fuel_'); fprintf(fidO, c{k}); fprintf(fidO, '\t');
fprintf(fidO, 'm_fuel_cum_'); fprintf(fidO, c{k}); fprintf(fidO, '\t');
fprintf(fidO, 'm_fuel_cum_nor_'); fprintf(fidO, c{k});
fprintf(fidO, '\t');
fprintf(fidO, '\n');
for v=1:t-1
 fprintf(fidO, '%3.1f\t\t', v);  fprintf(fidO, '%g\t\t',
m_fuel_cycle(v));  fprintf(fidO, '%g\t\t', m_fuel_cum_p(v));
```

```
 fprintf(fidO, '%g\t\t', m_fuel_cum_nor(v));   fprintf(fidO, '\n');
end
fclose(fidO);
end
toc % time that takes to run the program
disp(['Elapsed time in minutes:']);disp(toc/60);
```

APPENDIX IX - HITECHNIQUES PRESSURE CODE

```
%Program to extract the binary data from the HiTechniques data
%acquisition and to correct the time delay of the MAP sensors and the
%FFID traces. The inputs and file names were provided through a GUI.

%Beginning of Main Code - Pressure Data Processing
%Getting the Engine Parameters
R = handles.metricdata.lrdata ;            % Crank radius to road
length ratio
Vc = handles.metricdata.Vcdata ;           % Clearance volume
Vdisp = handles.metricdata.Vddata ;        % Displacement volume
theta_peg = - 180 ;                        % Angle for the pegging
location
ncyl = numofcylinders_index ;              % Number of cylinders
chcyl2 = get(handles.chancyl2, 'Value')+1; % Channel with the cyl 2
phacyl = handles.metricdata.anglecyl ;     % Angle between cyls in CA
% End Getting the Engine Parameters
fc = handles.metricdata.FilterConst ;
%Getting the Engine Filter Constant
peg1Option = manualpegging_index;          % Pegg. Cyl. 1, if manual:
peg1Option = 1, if MAP(or Ch.): peg1Option = 2
peg2Option = manualpch2_index;             % Pegg. Cyl. 1, if manual:
peg2Option = 1, if MAP(or Ch.): peg2Option = 2
P_m_peg1 = ppegging1;                      % Pressure for the manual
pegging Cyl.1, in kPa
P_m_peg2 = ppegging2;                      % Pressure for the manual
pegging Cyl.2, in kPa
nch_peg1 = channel1MAP;                    % Channel with pressure data
for pegging Cyl. 1
nch_peg2 = channel2MAP;                    % Channel with pressure data
for pegging Cyl. 2
% Phase Shift for MAP Sensors-Mototron SENSPRESS001H00
if correction1_index == 1  % MAP Cyl. 1
 cpeg1 = 1;                                % Phase Shift, MAP Cyl 1
else
 cpeg1 = 0;                                % No Phase Shift, MAP Cyl 1
end
if correction2_index == 1  %---MAP Cyl. 2---
 cpeg2 = 1 ;                               % Phase Shift, MAP Cyl 2
else
 cpeg2 = 0 ;                               % No Phase Shift, MAP Cyl 2
end
% Other Channels with MAP data for Phase Shift (Maximum of 2 chnls
if othercorrection_index == 1
 omapch = 1 ;                % There are more channels for Phase Shift
elseif othercorrection_index == 2
 omapch = 0 ;                % No more channels for Phase Shift
end
nomapch = numchannels4map ;  % Number of other channels for correction
chomap1 = chomap1_index ;    % Channel for the first other MAP sensor
chomap2 = chomap2_index ;    % Channel for the second other MAP sensor
```

```
% End of Phase Shift for MAP Sensors-Mototron SENSPRESS001H00
nchfid = ffidchannels_index-1 ;            % Channels for fast FID
chfid1 = chffid1_index ;                   % 1st Channel with FFID Data
chfid2 = chffid2_index ;                   % 2nd Channel with FFID Data
shfid1 = handles.metricdata.timeffid1v ;   % Time shift for the fid1
shfid2 = handles.metricdata.timeffid2v ;   % Time shift for the fid2
% Getting the Engine Speed (RPM) from the ERESULTA.arg file
er = 0;
err = 0;
for r = 1 : 1 : sbdata
 RPMc{r} = strcat( bdata( r ) , '/ERESULTA.arg' ) ;
 FRPM = fopen( RPMc{r}, 'r' ) ;
 if FRPM == -1
  errordlg('File ERESULTA.arg could not be found or accessed under
specified folder.  Check Folder Names table or file
availability.','Error');
  er = 1;
  else
   for j = 1 : 1 : 81
    RPMf( j ) = textscan( FRPM, '%s', 1, 'delimiter' , '/n');    %
Storage of the lines of:... /ERESULTA.arg
   end
   fclose(FRPM);
   a = cell2mat( RPMf{ 81 } ) ; % Row with the RPM value
   [ ro, co] = size( a ) ;      % RPM line size
   b = a( 16: co ) ;            % RPM value
   RPM(r) = str2num(b);         % RPM value from ERESULTA.arg file
  end
end
if er==0
 if outfiles_index == 1
  fida = fopen('HT_ADD_AVG_INFO.txt','wt') ;
  fprintf(fida, 'FileName'); fprintf(fida, '\t');
  fprintf(fida, 'CA_Pmax1'); fprintf(fida, '\t');
  fprintf(fida, 'Pmax1(kPa)'); fprintf(fida, '\t');
  fprintf(fida, 'IMEP1 (kPa)'); fprintf(fida, '\t');
  fprintf(fida, 'Ppeg1 (kPa)'); fprintf(fida, '\t');
  fprintf(fida, 'COV_1'); fprintf(fida, '\t');
  fprintf(fida, 'CA_Pmax2'); fprintf(fida, '\t');
  fprintf(fida, 'Pmax2(kPa)'); fprintf(fida, '\t');
  fprintf(fida, 'IMEP2 (kPa)'); fprintf(fida, '\t');
  fprintf(fida, 'Ppeg2 (kPa)'); fprintf(fida, '\t');
  fprintf(fida, 'COV_2'); fprintf(fida, '\t');
  fprintf(fida, '\n');
 end
% Start Data File and Channel Reading
 f = sbdata ;    % Number of Pressure Data Files or Folders
 nump = 1 ;
 for k = 1 : 1 : f
  for p = 1 : 1 : numofchannels_index
   fid1 = fopen( folderpath{nump} ) ; % Reading of binary file
   if fid1 == -1
    errordlg('File ACH00x01.dat could not be found or
accessed','Error');
```

```
    err=1;
   else
    [A1,count] = fread(fid1,35,'uchar');
    [B1,count] = fgets(fid1,15);  value1(1)=str2double(B1);   % data
scaling factor
    [C1,count] = fgets(fid1,15);  value1(2)=str2double(C1);   % data
offset
    [D1,count] = fgets(fid1,15);  value1(3)=str2double(D1);   % shaft
encoder resolution in CAD
     [E1,count] = fgets(fid1,15);  value1(4)=str2double(E1);   % array
start - not used
     [F1,count] = fgets(fid1,10);  value1(5)=str2double(F1);   % number
of points
     [A1,count] = fgets(fid1,1);                               % empty
space
     [G1,count] = fgets(fid1,10);  offset1=str2double(G1);     % start
of data location
% Move pointer to where the data start in the file
% the factor of 2 arises from the fact that the data are 2 bytes in
length
% the factor of 256 accounts the file header
% the 540/value(3) is necessary to get the data at BDC of compression
     status1 = fseek( fid1 , 2 * offset1 + 256 + 2 * ( 540 / value1 ( 3
) ) , 'bof' ) ;
     ndpc = 720 / value1 ( 3 ) ; % Number of data points per cycle
     ncycles1 = floor( ( value1( 5 ) - offset1 ) / ndpc ) ;  % Number
of cycles
     data1 = zeros( ndpc , ncycles1 - 2 ) ; % Data initialization
     low( 1 : ndpc * ( ncycles1 - 2 ) ) = fread( fid1 , ndpc * (
ncycles1 - 2 ) , 'uchar' , 1 ) ; % Low byte
     status = fseek( fid1 , 2 * offset1 + 256 + 2 * ( 540 / value1( 3 )
) , 'bof' ) ; % Moving pointer back to the bof
     l = fread( fid1 , 1 , 'schar' ) ; % Move pointer 1 byte for
optimization purpose
     high( 1 : ndpc * ( ncycles1 - 2 ) ) = fread( fid1 , ndpc * (
ncycles1 - 2 ) , 'schar' , 1 ) ;         % High byte that includes sign
% Data Storing in the "data1" matrix
     for j = 1 : ncycles1 - 2
      n = j - 1;
      for i = 1 : ndpc
       data1( i , j ) = value1( 1 ) * (256 * double( high( i + ndpc * n
) ) + double( low( i + ndpc * n ) )) - value1( 2 ) ;
      end
     end
     alldata{ p } = data1 ;
     datamean1{ p } = mean ( data1 , 2 );
     nump = nump + 1 ;
    end
   end
   if err==1
    err=0;
   else
    AD = cell2mat( alldata ) ;    % Main Matrix with All data
    M = cell2mat( datamean1 ) ;   % Conversion of datamean to matrix
```

```
    fclose (fid1);
   end
   chcount = zeros (1,numofchannels_index);
% Parameters Calculation (Only once per file)
% Cyl. 1
   CA = -180 : value1(3) : 540-value1(3) ;
   for i = 1 : 720 / value1(3)
    Vol ( i ) = Vc + (Vdisp / 2) * ( R + 1 - cos ( CA ( i ) * pi / 180
) - sqrt ( R * R - ( sin ( CA ( i ) * pi / 180 ) ) ^ 2 ) ) ;
    dV_dtetha ( i ) = Vdisp / 2 * ( sin ( CA ( i ) * pi / 180 ) + ( sin
( CA ( i ) * pi / 180 ) * cos ( CA ( i ) * pi / 180 ) ) / ( sqrt ( R ^
2 - ( sin ( CA ( i ) * pi / 180 ) ) ^ 2 ) ) ) ;
     end
% IMEP Calculation
     ncp = ncycles1 - 2 ;           % Number of cycles stored
     ndp = 720 / value1( 3 ) ;      % Number of data points per cycle
     P_1_sumi = zeros( 1 , 720 / value1( 3 ) ) ;
     P_2_sumi = zeros( 1 , 720 / value1( 3 ) ) ;
%-----------------------Cylinder 1-------------------------
     chcount(1) = 1 ;
     for j = 1 : ncycles1 - 2
      Pmax1( j ) = 0 ;
      if peg1Option == 1      % 1=Manual Pegging, 2= Pegging from
pressure trace-channel
       P_MAP_peg1 = P_m_peg1 ;
       elseif peg1Option == 2  % 1=Manual Pegging,  2= Pegging  from
pressure trace-channel
        chcount(nch_peg1) = 1 ;
        if j == 1           % Asigning all the data to a matrix
         AllMAP = AD(:, ncp * ( nch_peg1 -1 ) + 1 : ncp * ( nch_peg1 -1
) + ncp );
         AllMAP1D = AllMAP( : ) ;
         CAfict = ( 1 : 1 : ncp * ndp )';
         AllMAP1D =  csaps ( CAfict , AllMAP1D , fc , CAfict ) ;
% MAP Correction for all the cycles in Cylinder 1
         dt = 1000 * value1( 3 ) / ( 6 * RPM( k ) ) ;         % Time
step calculation
         if cpeg1 == 1  % phase shift of pegging pressure
          MAP_R_CORR( 1 ) = 1 / K1 * ( AllMAP1D( 1 ) + tau1 * ( (
AllMAP1D( 2 ) - AllMAP1D( ncp*ndp ) ) / ( 2 * dt ) ) ) ;
          MAP_R_CORR( 2 ) = 1 / K1 * ( AllMAP1D( 2 ) + tau1 * ((
AllMAP1D( 3 ) - AllMAP1D( 1 )) / ( 2 * dt ) ) ) ;
          MAP_R_CORR( ncp*ndp - 1 ) = 1 / K1 * ( AllMAP1D( ncp*ndp ) +
tau1 * ( ( AllMAP1D( ncp*ndp ) - AllMAP1D( ncp*ndp - 2 ) ) / ( 2 * dt )
) ) ;
          MAP_R_CORR(ncp*ndp) = 1 / K1 * ( AllMAP1D( 1 ) + tau1 * ( (
AllMAP1D( 1 ) - AllMAP1D( ncp*ndp - 1 ) ) / ( 2 * dt ) ) ) ;
          for i = 3 : 1 : ncp*ndp-2
           MAP_R_CORR( i ) = 1 / K1 * ( AllMAP1D( i ) + tau1 * ( (
AllMAP1D( i + 1 ) - AllMAP1D( i - 1 ) ) / ( 2 * dt ) ) ) ;
          end
         end
% Conversion of Vector to Matrix
         AllfMAP_R_CORR  =  reshape(MAP_R_CORR , ndp , ncp);
```

```
        end
% MAP Pressure Corrrected for cycle j
        fMAP_R_CORR = AllfMAP_R_CORR ( : , j ) ;
% Average over the 5 CA degrees - MAP pegging pressure Cyl. 1
        nwp = floor ( 2.5 / value1 ( 3 ) ) ;  % Number of points in the
5 CA window
        meanMAP1r = mean ( fMAP_R_CORR ( ( theta_peg + 180 ) / value1 (
3 ) + 1 : nwp ) ) ;
        meanMAP1l = mean ( fMAP_R_CORR ( 720 / value1 ( 3 ) - ( (
theta_peg + 180 ) / value1 ( 3 ) + nwp ) + 1 : 720 / value1 ( 3 ) ) ) ;
        P_MAP_peg1 = ( meanMAP1r + meanMAP1l ) / 2 ;
% Pressure of the MAP sensor for pegging in Cyl. 1
       end
% Average over the 5 CA degrees Pegging Process for the Cyl 1 Press
       nwp = floor ( 2.5 / value1 ( 3 ) ) ;
        meanP1r = mean ( AD ( ( theta_peg + 180 ) / value1 ( 3 ) + 1 :
nwp , j ) ) ;
        meanP1l = mean ( AD ( 720 / value1 ( 3 ) - ( ( theta_peg + 180
) / value1 ( 3 ) + nwp ) + 1 : 720 / value1 ( 3 ),j) );
        P_1peg = ( meanP1r + meanP1l ) / 2 ;  % Raw pressure of the
Cyl. 1 for pegging in Cyl. 1
% Pegging of Cylinder Pressure 1
        for i = 1 : 720 / value1 ( 3 )
         P_1 ( i ) = P_MAP_peg1 + ( AD (i , j) - P_1peg) ;
         P_1_sum ( i ) = P_1_sumi ( i ) + P_1 ( i ) ;
        end
% Cylinder 1 Parameters
        P_1_sumi = P_1_sum;
        [ Pmax1( j ) , i1max( j ) ] = max ( P_1 ) ;   %Max. Pressure of
the single cycle j
        tetha1max ( j ) = CA ( i1max ( j ) ) ;        %Location of Max.
Pressure of the single cycle j
        allP_1{j} = P_1' ;                            % Cell with all
the Cylinder 1 Pressure Data
        for i = 1 : 720 / value1 ( 3 ) - 1
         dw1 ( i ) = pi / 180 * (P_1 ( i ) * dV_dtetha ( i ) + P_1 ( i
+ 1 ) * dV_dtetha ( i + 1 ) ) / 2 * value1 ( 3 ) ; % Work for the main
cylinder
        end
        imep1 ( j ) = sum ( dw1 ) / Vdisp ;        % IMEP of the single
cycle j
       end
       P_1 = P_1_sum / ( ncycles1 - 2 ) ;          % Averaged Cylinder
1 Pressure (main cylinder)
       [ Pmax1_avg , i1max_avg ] = max ( P_1 ) ;   % Max. Pressure Avg.
Cyl. 1
       tetha1max_avg  = CA ( i1max_avg ) ;         % Location of Avg.
Peak Pressure Cyl. 1
       mimep1 = mean ( imep1 ) ;                    % Mean IMEP
       cov1 = std ( imep1 ) / mimep1 ; % COV of Avg. IMEP Cyl. 1
% All Pressure Cylinder 1
       AP_1 = cell2mat ( allP_1 ) ;         % Matrix with all the data
of the Cyl. 1 Pressure
       AllP1D1 = AP_1( : ); % Vector with all the Pcyl2 data
```

```
       CAfictP1 = ( 1 : 1 : ncp*ndp )';  % Fictituous CA for filteting
pourposes
       AllP1D1_f =  csaps ( CAfictP1 , AllP1D1 , fc , CAfictP1 ) ; %
Filtering process
       AP_1  =  reshape( AllP1D1_f , ndp , ncp ) ;  % Conversion of 1-D
to 2-D
       if peg1Option == 2  % 1=Manual Pegging,  2= Pegging  from
pressure trace-channel
        meanAllfMAP_R_CORR =  mean (  AllfMAP_R_CORR, 2) ;
        OCH( : , nch_peg1 ) =  csaps ( CA , meanAllfMAP_R_CORR , fc ,
CA ) ; % Averaged MAP1 Corrected Pressure ( main cylinder)
        channelnfig{nch_peg1}= 'MAP Cyl.1 Pres.(kPa)' ;
       end
% De-noising of the Cylineder Pressure datamean
       fP_1 = csaps ( CA , P_1 , fc , CA ) ;     % Cyl 1 Pressure-
filtered
       OCH( : , 1 ) = fP_1 ;                     % Assigning the Cyl.1
pressure to the OCH matrix that has all the data
         channelnfig{1}= 'Cyl.1 Pres.(kPa)' ;
% This version puts in phase Cyl.2 with Cyl.1
         if ncyl == 2 ;
          chcount(chcyl2) = 1 ;
% Second cylinder data shifting by phacyl = 270 CA
          ns_phcyl2 = phacyl / value1 ( 3 ) ;
          AllP2 = AD( : , ncp * ( chcyl2 -1 ) + 1 : ncp * ( chcyl2 -1 )
+ ncp );                      % Matrix with all the Pcyl2 data
          AllP2D1 = AllP2( : ); % Vector with all the Pcyl2 data
% Shifting of the data
          AllP2D1_s ( 1: ncp*ndp - ns_phcyl2 + 1 ,1) = AllP2D1 (
ns_phcyl2 : ncp*ndp , 1 );
          AllP2D1_s ( ncp*ndp - ns_phcyl2 + 2 : ncp*ndp , 1 ) = AllP2D1
( 1 : ns_phcyl2 -1 , 1 );
          CAfictP2 = ( 1 : 1 : ncp*ndp )';  % Fictituous CA for
filteting pourposes
          AllP2D1_sf =  csaps ( CAfictP2 , AllP2D1_s , fc , CAfictP2 )
; % Filtering process
          AllP2_s  =  reshape( AllP2D1_sf , ndp , ncp ) ;
% Conversion of 1-D to 2-D
          AD( : , ncp * ( chcyl2 -1 ) + 1 : ncp * ( chcyl2 -1 ) + ncp )
= AllP2_s ;
% End of Second cylinder data shifting
          for j = 1 : ncycles1 - 2
           Pmax2(j) = 0 ;
           if peg2Option == 1  % 1=Manual Pegging, 2= Pegging from
pressure trace-channel
            P_MAP_peg2 = P_m_peg2 ;
           elseif peg2Option == 2  % 1=Manual Pegging, 2= Pegging from
pressure trace-channel
% MAP Correction for each Cycle in Cylinder 2
            chcount(nch_peg2) = 1 ;
            if j == 1  % Asigning all data to a matrix
             AllMAP2 = AD( : , ncp * ( nch_peg2 -1 ) + 1 : ncp * (
nch_peg2 -1 ) + ncp );
             AllMAP1D2 = AllMAP2( : );
```

```
% Shifting of the MAP2 data by phacyl 270CA
             AllMAP1D2_s ( 1: ncp*ndp - ns_phcyl2 + 1 ,1) = AllMAP1D2 (
ns_phcyl2 : ncp*ndp , 1 );
             AllMAP1D2_s ( ncp*ndp - ns_phcyl2 + 2 : ncp*ndp , 1 ) =
AllMAP1D2 ( 1 : ns_phcyl2 -1 , 1 );
             CAfict2 = ( 1 : 1 : ncp*ndp )';
% Fictituous CA for smoothing
             AllMAP1D2 =  csaps ( CAfict2 , AllMAP1D2_s , fc , CAfict2
) ;  % Smoothing of data
% MAP Correction for all the cycles in Cylinder 1
             dt = 1000 * value1( 3 ) / ( 6 * RPM( k ) ) ; % Time step
calculation
             if cpeg1 == 1  % phase shift of pegging pressure
              MAP_R_CORR2( 1 ) = 1 / K2 * ( AllMAP1D2( 1 ) + tau2 * ( (
AllMAP1D2( 2 ) - AllMAP1D2( ncp*ndp ) ) / ( 2 * dt ) ) ) ;
              MAP_R_CORR2( 2 ) = 1 / K2 * ( AllMAP1D2( 2 ) + tau2 * ((
AllMAP1D2( 3 ) - AllMAP1D2( 1 )) / ( 2 * dt ) ) ) ;
              MAP_R_CORR2( ncp*ndp - 1 ) = 1 / K2 * ( AllMAP1D2(
ncp*ndp ) + tau2 * ( ( AllMAP1D2( ncp*ndp ) - AllMAP1D2( ncp*ndp - 2 )
) / ( 2 * dt ) ) ) ;
               MAP_R_CORR2(ncp*ndp) = 1 / K2 * ( AllMAP1D2( 1 ) + tau2
* ( ( AllMAP1D2( 1 ) - AllMAP1D2( ncp*ndp - 1 ) ) / ( 2 * dt ) ) ) ;
               for i = 3 : 1 : ncp*ndp-2
                MAP_R_CORR2( i ) = 1 / K2 * ( AllMAP1D2( i ) + tau2 * (
( AllMAP1D2( i + 1 ) - AllMAP1D2( i - 1 ) ) / ( 2 * dt ) ) ) ;
               end
              end
              MAP_R_CORR2f =  csaps ( CAfict2 , MAP_R_CORR2 , fc ,
CAfict2 ) ;
              AllfMAP_R_CORR2  =  reshape( MAP_R_CORR2f , ndp , ncp ) ;
% Conversion of Vector to Matrix
             end
% MAP Pressure Corrrected for cycle j
             fMAP_R_CORR2 = AllfMAP_R_CORR2 ( : , j ) ;
% Average over the 5 CA degrees -MAP pegging pressure Cyl. 2
             nwp2 = floor ( 2.5 / value1 ( 3 ) ) ;
             meanMAP2r = mean ( fMAP_R_CORR2 ( ( theta_peg + 180 ) /
value1 ( 3 ) + 1 : nwp2 ) ) ;
             meanMAP2l = mean ( fMAP_R_CORR2 ( ( 720 / value1 ( 3 ) - (
( theta_peg + 180 ) / value1 ( 3 ) + nwp2 ) + 1 : 720 / value1 ( 3 ) )
)) ;
             P_MAP_peg2 = ( meanMAP2r + meanMAP2l ) / 2 ;
% Pressure of the MAP sensor for pegging in Cyl. 2
            end
% Average over the 5 CA degrees Pegging Process for the Cyl 2 Pressure
            nwp2 = floor ( 2.5 / value1 ( 3 ) ) ;
            meanP2r = mean ( AD ( ( theta_peg + 180 ) / value1 ( 3 ) +
1 : nwp2 , ncp * ( chcyl2 -1 ) + j ) ) ;
            meanP2l = mean ( AD (  720 / value1 ( 3 ) - ( ( theta_peg +
180 ) / value1 ( 3 ) + nwp2 ) + 1 : 720 / value1 ( 3 ) ,  ncp * (
chcyl2 -1 ) + j ) ) ;
            P_2peg = ( meanP2r + meanP2l ) / 2 ;    % Raw pressure of
the Cyl. 2 for pegging in Cyl. 2
% Pegging of Cylinder Pressure 2
```

```
            for i = 1 : 720 / value1 ( 3 )
             P_2 ( i ) = P_MAP_peg2 + ( AD ( i , ncp * ( chcyl2 -1 ) +
j ) - P_2peg ) ;
             P_2_sum ( i ) = P_2_sumi ( i ) + P_2 ( i );
            end
% Cylinder 2 Parameters
            P_2_sumi = P_2_sum ;
            [ Pmax2( j ) , i2max( j ) ] = max ( P_2 ) ;  % Max.
Pressure of the single cycle j
            tetha2max ( j ) = CA ( i2max ( j ) ) ;       %Location of
Max. Pressure of the single cycle j
            allP_2{j} = P_2' ;                           % Cell with
all the Cylinder 1 Pressure Data
            for i = 1 : 720 / value1 ( 3 ) - 1
             dw2 ( i ) = pi / 180 * ( P_2 ( i ) * dV_dtetha ( i ) + P_2
( i + 1 ) * dV_dtetha ( i + 1 ) ) / 2 * value1 ( 3 ) ;  % Work for the
second cylinder
            end
            imep2 ( j ) = sum ( dw2 ) / Vdisp ;     % IMEP of the
single cycle j
           end
           P_2 = P_2_sum / ( ncycles1 - 2 ) ;       % Averaged second
Cylinder Pressure
            [ Pmax2_avg , i2max_avg ] = max ( P_2 ) ;%Max. Pressure
Avg. Cyl. 2
            tetha2max_avg  = CA ( i2max_avg ) ;      %Location of Avg.
Peak Pressure Cyl. 2
            mimep2 = mean ( imep2 ) ;                % Mean IMEP
            cov2 = std ( imep2 ) / mimep2 ;          % COV of Avg. IMEP
Cyl. 2
            AP_2 = cell2mat ( allP_2 ) ;             % Matrix with all
the data of the Cyl. 2 Pressure
            AllP_1D2 = AP_2( : );                    % Vector with all
the Pcyl2 data
            CAfict_P2 = ( 1 : 1 : ncp*ndp )';        % Fictituous CA
for filteting pourposes
            AllP_1D2_f =  csaps ( CAfict_P2 , AllP_1D2 , fc , CAfict_P2
) ;                                                  % Filtering process
            AP_2 = reshape( AllP_1D2_f , ndp , ncp ) ;  % Conversion of
1-D to 2-D
            if peg2Option == 2                       % 1=Manual Pegging,
2= Pegging  from pressure trace-channel
             meanAllfMAP_R_CORR2 =  mean (  AllfMAP_R_CORR2, 2) ;
             if nch_peg2 == nch_peg1
              OCH( : , nch_peg2 ) = OCH( : , nch_peg1 ) ;
              channelnfig{nch_peg2}= 'MAP Cyl.1 Pres.(kPa)' ;
             else
              OCH( : , nch_peg2 ) =  csaps ( CA , meanAllfMAP_R_CORR2 ,
fc , CA ) ; % Averaged MAP2 Corrected Pressure ( main cylinder)
              channelnfig{nch_peg2}= 'MAP Cyl.2 Pres.(kPa)' ;
             end
            end
% De-noising of the Cylineder Pressure datamean
            fP_2 = csaps ( CA , P_2 , fc , CA ) ;
```

```
            OCH( : , chcyl2 ) = fP_2 ;
            channelnfig{chcyl2}= 'Cyl.2 Pres.(kPa)' ;
        end
% Other  MAP Channels for Phase Shift (Maximum of Two channels)
     if omapch==1;    % Phase shift of the first additional channel
      chcount(chomap1) = 1 ;
      AllMAP3 = AD( : , ncp * ( chomap1 -1 ) + 1 : ncp * ( chomap1 -1 )
+ ncp ); % Asigning all data to a matrix
      AllMAP1D3 = AllMAP3( : ) ;
      CAfict3 = ( 1 : 1 : ncp*ndp )';
      AllMAP1D3 =  csaps (CAfict3 , AllMAP1D3 , fc , CAfict3);
      dt = 1000 * value1( 3 ) / ( 6 * RPM( k ) ) ; % Time step calc.
% Start of phase shift
      MAP_R_CORR3( 1 ) = 1 / K3 * ( AllMAP1D3( 1 ) + tau3 * ( (
AllMAP1D3( 2 ) - AllMAP1D3( ncp*ndp ) ) / ( 2 * dt ) ) ) ;
      MAP_R_CORR3( 2 ) = 1 / K3 * ( AllMAP1D3( 2 ) + tau3 * ((
AllMAP1D3( 3 ) - AllMAP1D3( 1 )) / ( 2 * dt ) ) ) ;
      MAP_R_CORR3( ncp*ndp - 1 ) = 1 / K3 * ( AllMAP1D3( ncp*ndp ) +
tau3 * ( ( AllMAP1D3( ncp*ndp ) - AllMAP1D3( ncp*ndp - 2 ) ) / ( 2 * dt
) ) ) ;
      MAP_R_CORR3(ncp*ndp) = 1 / K3 * ( AllMAP1D3( 1 ) + tau3 * ( (
AllMAP1D3( 1 ) - AllMAP1D3( ncp*ndp - 1 ) ) / ( 2 * dt ) ) ) ;
      for i = 3 : 1 : ncp*ndp - 2
       MAP_R_CORR3( i ) = 1 / K3 * ( AllMAP1D3( i ) + tau3 * ( (
AllMAP1D3( i + 1 ) - AllMAP1D3( i - 1 ) ) / ( 2 * dt ) ) ) ;
      end
% Conversion of shifted Vector to Matrix
       AllfMAP_R_CORR3  =  reshape(MAP_R_CORR3 , ndp , ncp) ;
% Average of all the shifted traces
       meanAllfMAP_R_CORR3 =  mean (  AllfMAP_R_CORR3, 2) ;
% Filtering of the Corrected Exhaust MAP pressure
       OCH( : , chomap1 ) =  meanAllfMAP_R_CORR3 ;
       channelnfig{chomap1}= 'Other MAP1 Pres.(kPa)' ;
       if nomapch==2 % Phase shift of the second additional channel
        chcount(chomap2) = 1 ;
        AllMAP4 = AD( : , ncp * ( chomap2 -1 ) + 1 : ncp * ( chomap2 -1
) + ncp ) ; % Asigning all data to a matrix
        AllMAP1D4 = AllMAP4( : ) ;
% Shifting of the MAP2 data by phacyl 270CA
        AllMAP4D2_s ( 1: ncp*ndp - ns_phcyl2 + 1 ,1) = AllMAP1D4 (
ns_phcyl2 : ncp*ndp , 1 );
        AllMAP4D2_s ( ncp*ndp - ns_phcyl2 + 2 : ncp*ndp , 1 ) =
AllMAP1D4 ( 1 : ns_phcyl2 -1 , 1 );
% End of Shifting
        CAfict4 = ( 1 : 1 : ncp*ndp )';             % Fictituous CA for
smoothing
        AllMAP1D4 =  csaps ( CAfict2 , AllMAP4D2_s , fc , CAfict4 ) ;
% Smoothing of data
        dt = 1000 * value1( 3 ) / ( 6 * RPM( k ) ) ;% Time step
% Start of phase shift
        MAP_R_CORR4( 1 ) = 1 / K3 * ( AllMAP1D4( 1 ) + tau3 * ( (
AllMAP1D4( 2 ) - AllMAP1D4( ncp*ndp ) ) / ( 2 * dt ) ) ) ;
        MAP_R_CORR4( 2 ) = 1 / K3 * ( AllMAP1D4( 2 ) + tau3 * ((
AllMAP1D4( 3 ) - AllMAP1D4( 1 )) / ( 2 * dt ) ) ) ;
```

```
        MAP_R_CORR4( ncp*ndp - 1 ) = 1 / K3 * ( AllMAP1D4( ncp*ndp ) +
tau3 * ( ( AllMAP1D4( ncp*ndp ) - AllMAP1D4( ncp*ndp - 2 ) ) / ( 2 * dt
) ) ) ;
        MAP_R_CORR4(ncp*ndp) = 1 / K3 * ( AllMAP1D4( 1 ) + tau3 * ( (
AllMAP1D4( 1 ) - AllMAP1D4( ncp*ndp - 1 ) ) / ( 2 * dt ) ) ) ;
        for i = 3 : 1 : ncp*ndp-2
         MAP_R_CORR4( i ) = 1 / K3 * ( AllMAP1D4( i ) + tau3 * ( (
AllMAP1D4( i + 1 ) - AllMAP1D4( i - 1 ) ) / ( 2 * dt ) ) ) ;
        end
% Conversion of shifted Vector to Matrix
        AllfMAP_R_CORR4  =  reshape( MAP_R_CORR4 , ndp , ncp ) ;
% Average of all the shifted traces
        meanAllfMAP_R_CORR4 =  mean (  AllfMAP_R_CORR4 , 2) ;
% Filtering of the Corrected Exhaust MAP pressure
        OCH( : , chomap2 ) =   meanAllfMAP_R_CORR4 ;
        channelnfig{chomap2}= 'Other MAP2 Pres.(kPa)' ;
       end
     end
     if nchfid >=1  % FFID Channels Shifting
      chcount( chfid1 )= 1 ;
      ns1(k) = floor(6*RPM(k) / (value1(3) * 1e3) * shfid1); % Number
of data points to be shifted
      Allfid1 = AD( : , ncp * ( chfid1 -1 ) + 1 : ncp * ( chfid1 -1 ) +
ncp );                              % Matrix with FFID1 data
      Allfid1D1 = Allfid1( : );   % Vector with all the FFID1 data
      CAfictfid1 = ( 1 : 1 : ncp*ndp )';  % Fictitouos CA for filtering
purposes
% Shifting Process
      Allfid1D1_s ( 1: ncp*ndp - ns1( k ) + 1 ,1) = Allfid1D1 ( ns1( k
): ncp*ndp , 1 );
      Allfid1D1_s ( ncp*ndp - ns1( k ) + 2 : ncp*ndp , 1 ) = Allfid1D1
( 1 : ns1( k ) -1 , 1 );
%  End of Shifting
      Allfid1D1_sf =  csaps ( CAfictfid1 , Allfid1D1_s , fc ,
CAfictfid1 ) ; % Filtering of all the data
      Allfid1_s  =  reshape( Allfid1D1_sf , ndp , ncp ) ;
% Conversion of 1-D to 2-D
      FFID_s1 = mean ( Allfid1_s , 2 ) ;  % Averaging of the traces for
all the cycles
      OCH( : , chfid1 ) = FFID_s1 ;       % Data for writing and
ploting
      channelnfig{chfid1}= 'Fast FID1 HC (ppm/3)' ;
      if nchfid==2  % if there is a second channel with FFID data
       chcount ( chfid2 )  = 1 ;
       ns2( k ) = floor( 6 * RPM( k ) / (value1( 3 ) * 1e3 ) * shfid2);
% Number of data points to be shifted
       Allfid2 = AD( : , ncp * ( chfid2 -1 ) + 1 : ncp * ( chfid2 -1 )
+ ncp );          % Matrix with all the FFID2 data
       Allfid1D2 = Allfid2( : ); % Vector with all FFID2 data
       CAfictfid2 = ( 1 : 1 : ncp*ndp )';  % Fictituous CA for
filteting purposes
% Shifting Process
       Allfid1D2_s ( 1: ncp*ndp - ns2( k ) - ns_phcyl2 + 1 ,1) =
Allfid1D2 ( ns2( k ) + ns_phcyl2 : ncp*ndp , 1 );
```

```
       Allfid1D2_s ( ncp*ndp - ns2( k ) - ns_phcyl2 + 2 : ncp*ndp , 1 )
= Allfid1D2 ( 1 : ns2( k ) + ns_phcyl2 -1 , 1 );
% End of Shifting
       Allfid1D2_sf =  csaps ( CAfictfid2 , Allfid1D2_s , fc ,
CAfictfid2 ) ;                              % Filtering process
       Allfid2_s  =  reshape( Allfid1D2_sf , ndp , ncp ) ; % Conversion
of 1-D to 2-D
       FFID_s2 = mean ( Allfid2_s , 2 ) ;                  % Averaging
of the traces for all the cycles
       OCH( : , chfid2 ) = FFID_s2 (:,1) ;                 % Data for
writing and ploting
       channelnfig{chfid2}= 'Fast FID2 HC (ppm/3)' ;
      end
      figure
      plot(CA, FFID_s1,CA, FFID_s2)
     end
% Looking for other Channels to be in the output file
    for i = 1: numofchannels_index
      if chcount(i) == 0
       FData = csaps ( CA , M( : , i ) , fc , CA ) ;
       OCH( : , i ) = FData;
       channelnfig{i}= channeln{i};
      end
    end
%---------------- Filtering Crankcase Pressure data -------------------
    chPcr = 8 ;           % Channel with the crankcase pressure data
    ns_phcyl2 = phacyl / value1 ( 3 ) ; % Number of points to shift for
the second cyl. (270 CA)
    AllPcr = AD( : , ncp * ( chPcr -1 ) + 1 : ncp * ( chPcr -1 ) + ncp
);                                        % Matrix with all the Pcr data
      AllPcrD1 = AllPcr( : );             % Vector with all the Pcr data
        CAfictPcr = ( 1 : 1 : ncp*ndp )';
% Fictituous CA for filteting purposes
       AllPcrD1_f =  csaps ( CAfictPcr , AllPcrD1 , fc , CAfictPcr ) ;
% Filtering process
       AllPcr_f  =  reshape( AllPcrD1_f , ndp , ncp ) ;
% Conversion of 1-D to 2-D, this is used for the exhuast
% Second cylinder Crankcase Pressure data shifting by phacyl = 270 CA-
       AllPcr2D1_s ( 1: ncp*ndp - ns_phcyl2 + 1 ,1) = AllPcrD1 (
ns_phcyl2 : ncp*ndp , 1 );
       AllPcr2D1_s ( ncp*ndp - ns_phcyl2 + 2 : ncp*ndp , 1 ) =
AllPcrD1 ( 1 : ns_phcyl2 -1 , 1 );
       AllPcr2D1_fs =  csaps ( CAfictPcr , AllPcr2D1_s , fc ,
CAfictPcr ) ;                                       % Filtering process
       AllPcr2_fs  =  reshape( AllPcr2D1_fs , ndp , ncp ) ; %
Conversion of 1-D to 2-D, crankcase pressure cyl.2
%--------------------------Output files-------------------------
    if outfiles_index == 1 % Header of Main Output File
     js{k}=strcat('O_',foldname{k},'.txt');
     fidO=fopen(js{k},'wt');
     fprintf(fidO, 'CA_'); fprintf(fidO,foldname{k}); fprintf(fidO,
'\t\t');
     fprintf(fidO, 'Vol_'); fprintf(fidO,foldname{k}); fprintf(fidO,
'\t\t');
```

```
     fprintf(fidO, 'P1_'); fprintf(fidO,foldname{k}); fprintf(fidO,
'\t\t');
     if ncyl==2;
      fprintf(fidO, 'P2_'); fprintf(fidO,foldname{k}); fprintf(fidO,
'\t\t');
      if numofchannels_index > 2
       for namch = 2 : 1 : numofchannels_index
        if namch ~= chcyl2
         fprintf(fidO, channeln{namch}); fprintf(fidO,'_');
         fprintf(fidO,foldname{k}); fprintf(fidO, '\t\t');
        end
       end
      end
      else
       if numofchannels_index > 2
        for namch = 2:1: numofchannels_index
         fprintf(fidO, channeln{namch});
fprintf(fidO,'_');fprintf(fidO,foldname{k}); fprintf(fidO, '\t\t');
        end
       end
      end
      fprintf(fidO, '\n');
%------------------Data-Main Output File-------------------
      for v=1:720/value1(3)
       fprintf(fidO, '%3.1f\t\t', CA(v));
       fprintf(fidO, '%g\t\t', Vol(v));
       fprintf(fidO, '%g\t\t', fP_1(v));
       if ncyl==2;
        fprintf(fidO, '%g\t\t', fP_2(v));
        if numofchannels_index > 2
         for namch = 2 : 1 : numofchannels_index
          if namch ~= chcyl2
           fprintf(fidO, '%g\t\t', OCH( v , namch ));
          end
           end
          end
          else
           if numofchannels_index > 2
            for namch = 2 : 1 : numofchannels_index
             fprintf(fidO, '%g\t\t', OCH( v , namch ));
            end
           end
          end
          fprintf(fidO, '\n');
       end
       fclose(fidO);
%-----Output Files for Exhaust HC mass flow Calculation Avg. ------
       demhc = 1 ;   % Indicator if output file for the AVG exhaust hc
mass calc.
       if demhc == 1 % Output File for Cyl. 1 , P_1
        om{k}=strcat('O1_', foldname{k}, '.txt');
        fidm=fopen(om{k}, 'wt');
        fprintf(fidm, 'CA_'); fprintf(fidm,foldname{k}); fprintf(fidm,
'\t\t');
```

```
        fprintf(fidm, 'Vol_'); fprintf(fidm,foldname{k}); fprintf(fidm,
'\t\t');
        fprintf(fidm, 'P1_'); fprintf(fidm,foldname{k}); fprintf(fidm,
'\t\t');
        fprintf(fidm, 'ExMAP1_'); fprintf(fidm,foldname{k});
fprintf(fidm, '\t\t');
        fprintf(fidm, 'HCFFID1_'); fprintf(fidm,foldname{k});
fprintf(fidm, '\t\t');
        fprintf(fidm, '\n');
        for m1=1:720/value1(3)
         fprintf(fidm, '%3.1f\t\t', CA(m1));
         fprintf(fidm, '%g\t\t', Vol(m1));
         fprintf(fidm, '%g\t\t', fP_1(m1));
         fprintf(fidm, '%g\t\t', OCH( m1 , chomap1 ) ) ;
         fprintf(fidm, '%g\t\t', OCH( m1 , chfid1 ) ) ;
         fprintf(fidm, '\n');
        end
        fclose(fidm);
        if ncyl==2; % Output File for Cyl. 2 , P_2
         om1{k}=strcat('O2_', foldname{k}, '.txt');
         fidm1=fopen(om1{k}, 'wt');
         fprintf(fidm1, 'CA2_'); fprintf(fidm1,foldname{k});
fprintf(fidm1, '\t\t');
         fprintf(fidm1, 'Vol2_'); fprintf(fidm1,foldname{k});
fprintf(fidm1, '\t\t');
         fprintf(fidm1, 'P2_'); fprintf(fidm1,foldname{k});
fprintf(fidm1, '\t\t');
         fprintf(fidm1, 'ExMAP2_'); fprintf(fidm1,foldname{k});
fprintf(fidm1, '\t\t');
         fprintf(fidm1, 'HCFFID2_'); fprintf(fidm1,foldname{k});
fprintf(fidm1, '\t\t');
         fprintf(fidm1, '\n');
         for m1=1:720/value1(3)
          fprintf(fidm1, '%3.1f\t\t', CA(m1));
          fprintf(fidm1, '%g\t\t', Vol(m1));
          fprintf(fidm1, '%g\t\t', fP_2(m1));
          fprintf(fidm1, '%g\t\t', OCH( m1 , chomap2 ) ) ;
            fprintf(fidm1, '%g\t\t', OCH( m1 , chfid2 ) ) ;
            fprintf(fidm1, '\n');
           end
           fclose(fidm1);
          end
        end
% Output Files for Single Cycle Ring Pack and Exhaust Mass Calculation
dallscyc = 1 ;   % Indicator if output files for single cylce calc
        if  dallscyc == 1
% LookUp File for All pressure cylinder 1, A_P1
         up1{k}=strcat('A_P1_', foldname{k}, '.txt');
         fidup1=fopen(up1{k}, 'wt');
         fprintf(fidup1, 'CA'); fprintf(fidup1, '\t');
         fprintf(fidup1, 'A_P1 [kPa]'); fprintf(fidup1, '\n');
         for v=1:720/value1(3)
          fprintf(fidup1, '%3.1f\t', CA(v));
          fprintf(fidup1, '%g\t', Vol(v));
```

```
          for r=1: ncycles1 - 2
           fprintf(fidup1, '%g\t', AP_1(v,r));
% Cylinder Pressure
          end
          fprintf(fidup1, '\n');
         end
         fclose(fidup1);
% LookUp File for All pressure cylinder 1, A_EP1
         up3{k}=strcat('A_EP1_', foldname{k}, '.txt');
         fidup3=fopen(up3{k}, 'wt');
         fprintf(fidup3, 'CA'); fprintf(fidup3, '\t');
         fprintf(fidup3, 'ExhP_1 [kPa]'); fprintf(fidup3, '\n');
         for v=1:720/value1(3)
          fprintf(fidup3, '%3.1f\t', CA(v));
          for r=1: ncycles1 - 2
           fprintf(fidup3, '%g\t', AllfMAP_R_CORR3(v,r));
          end
          fprintf(fidup3, '\n');
         end
         fclose(fidup3);
% LookUp File for all FFID Data
         up4{k}=strcat('A_HC1_', foldname{k}, '.txt');
         fidup4=fopen(up4{k}, 'wt');
         fprintf(fidup4, 'CA'); fprintf(fidup4, '\t');
         fprintf(fidup4, 'AHC_1 [ppm/3]'); fprintf(fidup4, '\n');
         for v=1:720/value1(3)
          fprintf(fidup4, '%3.1f\t', CA(v));
          for r=1: ncycles1 - 2
           fprintf(fidup4, '%g\t', Allfid1_s (v,r));
          end
          fprintf(fidup4, '\n');
         end
         fclose(fidup4);
% LookUp File for all Crankcase Pressure Data
         up2{k}=strcat('A_Pcr1_', foldname{k}, '.txt');
         fidup2=fopen(up2{k}, 'wt');
         fprintf(fidup2, 'CA'); fprintf(fidup2, '\t');
         fprintf(fidup2, 'Pcr_1 [kPa]'); fprintf(fidup2, '\n');
         for v=1:720/value1(3)
          fprintf(fidup2, '%3.1f\t', CA(v));
          for r=1: ncycles1 - 2
           fprintf(fidup2, '%g\t', AllPcr_f (v,r));
          end
          fprintf(fidup2, '\n');
         end
         fclose(fidup2);
         if ncyl==2;
% LookUp File for All pressure cylinder 1, A_P1
          up5{k}=strcat('A_P2_', foldname{k}, '.txt');
          fidup5=fopen(up5{k}, 'wt');
          fprintf(fidup5, 'CA'); fprintf(fidup5, '\t');
          fprintf(fidup5, 'A_P2 [kPa]'); fprintf(fidup5, '\n');
          for v=1:720/value1(3)
           fprintf(fidup5, '%3.1f\t', CA(v));
```

```
            fprintf(fidup5, '%g\t', Vol(v));
            for r=1: ncycles1 - 2
             fprintf(fidup5, '%g\t', AP_2(v,r)); % Cylinder Pressure
            end
            fprintf(fidup5, '\n');
           end
           fclose(fidup5);
% LookUp File for All pressure cylinder 1, A_EP1
           up6{k}=strcat('A_EP2_', foldname{k}, '.txt');
           fidup6=fopen(up6{k}, 'wt');
           fprintf(fidup6, 'CA'); fprintf(fidup6, '\t');
           fprintf(fidup6, 'ExhP_2 [kPa]'); fprintf(fidup6, '\n');
           for v=1:720/value1(3)
            fprintf(fidup6, '%3.1f\t', CA(v));
            for r=1: ncycles1 - 2
             fprintf(fidup6, '%g\t', AllfMAP_R_CORR4(v,r));
            end
            fprintf(fidup6, '\n');
           end
           fclose(fidup6);
% LookUp File for all FFID Data
           up7{k}=strcat('A_HC2_', foldname{k}, '.txt');
           fidup7=fopen(up7{k}, 'wt');
           fprintf(fidup7, 'CA'); fprintf(fidup7, '\t');
           fprintf(fidup7, 'AHC_2 [ppm/3]'); fprintf(fidup7, '\n');
           for v=1:720/value1(3)
            fprintf(fidup7, '%3.1f\t', CA(v));
            for r=1: ncycles1 - 2
             fprintf(fidup7, '%g\t', Allfid2_s (v,r));
            end
            fprintf(fidup7, '\n');
           end
           fclose(fidup7);
% LookUp File for all Crankcase Pressure Data
           up8{k}=strcat('A_Pcr2_', foldname{k}, '.txt');
           fidup8=fopen(up8{k}, 'wt');
           fprintf(fidup8, 'CA'); fprintf(fidup8, '\t');
           fprintf(fidup8, 'Pcr_2 [kPa]'); fprintf(fidup8, '\n');
           for v=1:720/value1(3)
            fprintf(fidup8, '%3.1f\t', CA(v));
            for r=1: ncycles1 - 2
             fprintf(fidup8, '%g\t', AllPcr2_fs (v,r));
            end
            fprintf(fidup8, '\n');
           end
           fclose(fidup8);
          end
        end
% Lookup File for P_1
        ln{k}=strcat('lu1_', foldname{k}, '.txt');
        fidl=fopen(ln{k}, 'wt');
        fprintf(fidl, '720'); fprintf(fidl, '\t');
        fprintf(fidl, '-'); fprintf(fidl, '5');
        fprintf(fidl, '\n');
```

```
        fprintf(fidl, 'F1 theta'); fprintf(fidl, '\n');
        fprintf(fidl, 'F3 pressure [kPa]'); fprintf(fidl, '\n');
        fprintf(fidl, 'F8 volume [m^3]'); fprintf(fidl, '\n');
        fprintf(fidl, 'F3 fpressure [kPa]'); fprintf(fidl, '\n');
        fprintf(fidl, 'F3 fCr_pressure [kPa]'); fprintf(fidl, '\n');
        for v=1:720/value1(3)
         fprintf(fidl, '%3.1f\t\t', CA(v));
         fprintf(fidl, '%g\t\t', P_1(v));
         fprintf(fidl, '%g\t\t', Vol(v));
         fprintf(fidl, '%g\t\t', fP_1(v));
         fprintf(fidl, '%g\t\t', OCH( v , 8 ) ) ;
         fprintf(fidl, '\n');
        end
        fclose(fidl);
        if ncyl==2;
% LookUp File for P_2
         ln1{k}=strcat('lu2_', foldname{k}, '.txt');
         fidn=fopen(ln1{k}, 'wt');
         fprintf(fidn, '%g\t\t',720/value1(3)); fprintf(fidn, '\t');
         fprintf(fidn, '-'); fprintf(fidn,'5');
         fprintf(fidn, '\n');
         fprintf(fidn, 'F1 theta'); fprintf(fidn, '\n');
         fprintf(fidn, 'F3 pressure [kPa]'); fprintf(fidn, '\n');
         fprintf(fidn, 'F8 volume [m^3]'); fprintf(fidn, '\n');
         fprintf(fidn, 'F3 fpressure [kPa]'); fprintf(fidn, '\n');
         fprintf(fidn, 'F3 fCr_pressure [kPa]'); fprintf(fidn, '\n');
         for v=1:720/value1(3)
          fprintf(fidn, '%3.1f\t\t', CA(v));
          fprintf(fidn, '%g\t\t', P_2(v));
          fprintf(fidn, '%g\t\t', Vol(v));
          fprintf(fidn, '%g\t\t', fP_2(v));
          fprintf(fidn, '%g\t\t', OCH( v , 8 ) ) ;
          fprintf(fidn, '\n');
         end
         fclose(fidn);
        end
%---------------------SP Files--------------------
        sp1{k}=strcat('sp1_', foldname{k}, '.txt');
        fids1=fopen(sp1{k}, 'wt');
        fprintf(fids1, '\t');
        fprintf(fids1, '%g\t\t', mimep1);
        fprintf(fids1, '%g\t\t', cov1);
        fprintf(fids1, '\n');
        fprintf(fids1, 'imep1'); fprintf(fids1, foldname{k});
fprintf(fids1, '\t\t');
        fprintf(fids1, 'Pmax1'); fprintf(fids1, foldname{k});
fprintf(fids1, '\t\t');
        fprintf(fids1, 'theta1max'); fprintf(fids1, foldname{k});
fprintf(fids1, '\t\t');
        fprintf(fids1, '\n');
        for s1=1:ncycles1-2
             fprintf(fids1, '%g\t\t', imep1(s1));
             fprintf(fids1, '%g\t\t', Pmax1(s1));
             fprintf(fids1, '%g\t\t', tetha1max(s1));
```

```
            fprintf(fids1, '\n');
        end
         fclose(fids1);
         if ncyl==2;
          sp2{k}=strcat('sp2_', foldname{k}, '.txt');
          fids2=fopen(sp2{k}, 'wt');
          fprintf(fids2, '\t');
          fprintf(fids2, '%g\t\t', mimep2);
          fprintf(fids2, '%g\t\t', cov2);
          fprintf(fids2, '\n');
          fprintf(fids2, 'imep2'); fprintf(fids2, foldname{k});
fprintf(fids2, '\t\t');
          fprintf(fids2, 'Pmax2'); fprintf(fids2, foldname{k});
fprintf(fids2, '\t\t');
          fprintf(fids2, 'theta2max'); fprintf(fids2, foldname{k});
fprintf(fids2, '\t\t');
          fprintf(fids2, '\n');
          for s2=1:ncycles1-2
               fprintf(fids2, '%g\t\t', imep2(s2));
               fprintf(fids2, '%g\t\t', Pmax2(s2));
               fprintf(fids2, '%g\t\t', tetha2max(s2));
               fprintf(fids2, '\n');
          end
          fclose(fids2);
         end
     else
      output='No output files generated at this time';
     end
% HT Additional Info file data
if outfiles_index == 1
         fprintf(fida,foldname{k});
         fprintf(fida, '\t');
         fprintf(fida, '%g\t', tetha1max_avg);
         fprintf(fida, '%g\t', Pmax1_avg);
         fprintf(fida, '%g\t', mimep1);
         fprintf(fida, '%g\t', P_MAP_peg1);
         fprintf(fida, '%g\t', cov1);
         if ncyl==2;
             fprintf(fida, '%g\t', tetha2max_avg);
             fprintf(fida, '%g\t', Pmax2_avg);
             fprintf(fida, '%g\t', mimep2);
             fprintf(fida, '%g\t', P_MAP_peg2);
             fprintf(fida, '%g\t', cov2);
         end
         fprintf(fida, '\n');
end
%----------Plots----------
if plot_index==1
% Plot of the two cylinder pressure traces
   if ncyl == 2
      figure('Name', foldname{k});                % Cylinder Pressure
      axis on; grid on; box on;
      plot(CA, OCH( : , 1 ),'r', CA, OCH( : , chcyl2 ),'b');
      legend('Pre. Right Cyl.1','Pre. Left Cyl.2');
```

```
      set(gca,'fontsize',14);
      t1=title([' Right and Left Cylinders Pressure at ',foldname{k}]);
      xlabel('CA');ylabel('P (kPa)');
   end
% Plots for every channel
   for pin = 1 : 1 : numofchannels_index
       figure('Name', foldname{k});              % Cylinder Pressure
       axis on; grid on; box on;
       plot(CA, OCH( : , pin ),'b');
       legend(channelnfig{pin});
       set(gca,'fontsize',14);
       t1=title([channelnfig{pin}, '@', foldname{k}]);
       xlabel('CA');ylabel(channelnfig{pin});
    end
% Plots of the IMEP, Pmax as a function of the CA
    figure('Name', foldname{k});                 % Pmax Rigth Cylinder
    axis on; grid on; box on;
    plot(tetha1max,Pmax1,'r*');
    legend('Pmax-Rigth Cyl.');
    set(gca,'fontsize',14);
    t1=title([' Rigth Cyl. Maximum Pressure vs. CA  @ ',foldname{k}]);
    xlabel('CA');ylabel('Pmax(kPa)');
    if ncyl == 2
       figure('Name', foldname{k});              %Pmax Left Cylinder
       axis on; grid on; box on;
       plot(tetha2max,Pmax2,'b*');
       legend('Pmax-Left Cyl.');
       set(gca,'fontsize',14);
       t1=title([' Left Cyl. Maximum Pressure vs. CA @ ',foldname{k}]);
       xlabel('CA');ylabel('Pmax (kPa)');
    end
    figure('Name', foldname{k});                 %imep Rigth Cylinder
    axis on; grid on; box on;
    plot(tetha1max,imep1,'r*');
    legend('IMEP-Rigth Cyl.');
    set(gca,'fontsize',14);
    t1=title([' Rigth Cyl. IMEP vs. CA  @ ',foldname{k}]);
    xlabel('CA');ylabel('IMEP(kPa)');
    if ncyl == 2
       figure('Name', foldname{k});              %imep Left Cylinder
       axis on; grid on; box on;
       plot(tetha2max,imep2,'b*');
       legend('IMEP-Left Cyl.');
       set(gca,'fontsize',14);
       t1=title([' Left Cyl. IMEP vs. CA  @ ',foldname{k}]);
       xlabel('CA');ylabel('IMEP (kPa)');
    end
    else
        result='No Plots generated at this time';
    end
    end
    end
else
    errordlg('Folder Names table must be filled correctly','Error');
```

```
end
toc
set(handles.processingtime, 'String', toc-0.029);
set(handles.calculate, 'Enable', 'on');
%========END OF DATA PROCESSING========
```

APPENDIX X - EMISSIONS INDEX CALCULATION

The emission index was calculated starting from the following equation:

$$CH_y + a\,(O_2 + 3.76\,N_2) \rightarrow b\,CO_2 + c\,CO + \ldots$$
$$\ldots + d\,H_2O + e\,C_3H_8 + f\,NO + g\,H_2 + h\,O_2 + i\,N_2 \qquad \text{(A10.1)}$$

where the hydrocarbons are represented by propane ($[C_3H_8]=[HC_{C3}]$). Applying the definition of emissions index (see §3.6.3) for the CO:

$$EICO = \frac{\#moles - CO}{\#moles - fuel} \qquad \text{(A10.2)}$$

From Eq. A10.1 this is equal to:

$$EICO = \frac{c}{1} \qquad \text{(A10.3)}$$

In Eq. A10.3 the numbers of moles of CO at the exhaust, *c*, are unknown; however, what it is known from the emissions bench is the molar fraction of CO. In addition, from Eq.A10.1 (from the carbon mass balance) the number of moles of fuel is also equal to:

$$\#moles\text{-}fuel = 1 = b + c + 3\,e \qquad \text{(A10.4)}$$

Therefore from Eq. A10.4 in Eq. A10.3:

$$EICO = \frac{c}{b + c + 3e} \tag{A10.5}$$

Dividing by the total number of moles of the exhaust the following relationship is obtained:

$$EICO = \frac{X_{CO}}{X_{CO2} + X_{CO} + 3X_{HC}} \tag{A10.6}$$

where X_i is the molar fraction of species i, or converting the mole fraction to percent:

$$EICO = \frac{[CO](\%)}{[CO_2](\%) + [CO](\%) + 3[HC_{C3}](\%)} \tag{A10.7}$$

where [CO](%), [CO_2](%) and [HC](%) are the measured concentration of the gases at the exhaust in percent. To convert the emission index in molar units to mass units the following conversion is needed:

$$EICO = \frac{[CO](\%)}{[CO_2](\%) + [CO](\%) + 3[HC_{C3}](\%)} \cdot \frac{MW_{CO}}{MW_{fuel}} \tag{A10.8}$$

Where MW_i is the molecular weight of species i. The same procedure is applied to the other species of interest:

$$EINO_x = \frac{[NO_x](\%)}{[CO_2](\%) + [CO](\%) + 3[HC_{C3}](\%)} \cdot \frac{MW_{NO_2}}{MW_{fuel}} \tag{A10.9}$$

$$EIHC = \frac{3[HC](\%)}{[CO_2](\%) + [CO](\%) + 3[HC_{C3}](\%)} \cdot \frac{MW_{HC}}{MW_{fuel}} \tag{A10.10}$$

It is important to mention that in Eq. A10.6-10.10, the concentration of hydrocarbons is in C3 basis ($[C_3H_8]$), and the HC molecular weight (MW_{HC}) was considered equal to the molecular weight of the fuel in C1 basis (MW_{fuel_C1}).

APPENDIX XI - COMBUSTION EFFICIENCY

The combustion efficiency was calculated based in the methodology of the combustion inefficiency [5] as follows:

$$1-\eta_c = \frac{Y_{CO}.Q_{HV_{CO}} + Y_{H_2}.Q_{HV_{H_2}} + Y_{HC}Q_{HV_{HC}}}{\left[\dot{m}_{fuel}/(\dot{m}_{fuel}+\dot{m}_a)\right]Q_{HV_{HC}}} \qquad \text{(A11.1)}$$

Where η_c is the combustion efficiency; Y_{CO}, Y_{H_2}, and Y_{HC} are the mass fractions of *CO*, H_2 and the hydrocarbons respectively; $\dot{m}_{fuel}$ and $\dot{m}_a$ are the mass flow of fuel and air respectively; and $Q_{HV_{CO}}$, $Q_{HV_{H_2}}$ and $Q_{HV_{HC}}$ are the lower heating value of the CO (10.1 MJ/kg), H_2 (120 MJ/kg) and the hydrocarbons respectively (the heating value was consider the same as the fuel).

The mass flow of air, $\dot{m}_a$, was measured experimentally and the mass of fuel was estimated based in the air-fuel ratio using the oxygen balance method.

$$\dot{m}_{fuel} = \dot{m}_{air} / AF \qquad \text{(A11.2)}$$

The mass fractions for each *i* component were estimated as follows:

$$Y_i = X_i.MW_i / MW_{exh} \qquad \text{(A11.3)}$$

where MW_i is the molecular weight of the *i* component and the MW_{exh} is the molecular weight of the mixture calculated as follows:

$$MW_{exh} = \frac{1}{100}([CO](\%).MW_{CO} + [CO_2](\%).MW_{CO_2} + [O_2].MW_{O_2} + [NO_x](\%).MW_{NO_2} + \ldots$$

$$\ldots + [HC_{C1}](\%).MW_{HC_{C1}} + [H_2](\%).MW_{H_2} + [N_2](\%).MW_{N_2}]) \qquad \text{(A11.4)}$$

APPENDIX XII - HEAT RELEASE ANALYSIS

A12.1 HEAT RELEASE ANALYSIS EQUATIONS

ENERGY CONSERVATION EQUATION

The heat release program performs a single-zone heat release analysis [107, 108] having as an input the in-cylinder pressure trace. The analysis consists in an energy balance in the combustion chamber which is considered as a closed system. The first law of the thermodynamics for the closed system is:

$$dU_s = dQ + dW \tag{A12.1}$$

where *Us* represents the internal energy, *Q* the heat transfer, and *W* the work. The calculation and approximation of each term in Eq. (A12.1) is described below.

WORK TERM

The work transfer term is calculated as:

$$dW = -PdV \tag{A12.2}$$

where *P* is the in cylinder pressure and *V* is the volume of the combustion chamber.

INTERNAL ENERGY TERM

The change in internal energy of the system is given by:

$$dU_s = mc_v(T)dT \qquad \text{(A12.3)}$$

where m is the mass of the air-fuel mixture, c_v the specific heat at constant volume, and T the temperature of the mixture. From the ideal gas law the dT term is: $dT = d(PV)/mR$, and assuming that the gas constant R does not change the following relation is obtained: $R/c_v(T) = k(T) - 1$; where *k(T)* represents the specific heat ratio and it was calculated following the correlation form suggested by Cheung and Heywood [108]: $k(T) = a + bT$, with a = 1.392, and b = - 0.000075.

HEAT TRANSFER TERM

The heat transfer term in Eq. (A12.1) was considered to be equal to the energy released by the fuel less the heat transfer trough the walls of the system.

$$dQ = dQ_{hr} - dQ_w \qquad \text{(A12.4)}$$

The heat transfer through the cylinder wall dQ_w in Eq. (A12.4) was calculated using the Woschni correlation for the heat transfer coefficient [78]:

$$h_c = 3.26 C_1 B^{b-1}.P.T^{0.75-1.62b} w^b \quad [\text{W/(m}^2\text{K)}] \qquad \text{(A12.5)}$$

Following the heat transfer correlation for turbulent flow in a pipe [78]: $Nu = C.\text{Re}^{0.8}$, the coefficient b in Eq. (A12.5) is set to $b = 0.8$. The constant C_1 is a scaling factor and it has a particular value for each engine, B represents a characteristic length and in the case of an engine is given by the bore of the cylinder in meters, P is the in-cylinder pressure in

kPa, T is the temperature in K, and w represents the parameter that accounts for the gas movement in the cylinder due to piston motion and due to the velocity assumed to result from expansion of the gases during the combustion stage, having the following form:

$$w = 2.28u_p + 3.24\times10^{-3}C_2\frac{V_{disp}}{p_{ivc}V_{ivc}}(P - P_m)T_{ivc} \qquad \text{(A12.6)}$$

In Eq. (A12.6) u_p is the piston mean velocity in *m/s*, V_{disp} is the displacement volume. The subscript *ivc* stands for intake valve closing. The term P_m is the pressure that the engine could have if it were being motored at the same crank angle. This term is calculated as follows:

$$P_m = P_{ivc}\left(\frac{V_{ivc}}{V}\right)^n \qquad \text{(A12.7)}$$

The value of the polytropic exponent in Eq. (A12.7) was calculated from the pressure data as:

$$n = \ln(P_{30CA,bTDC} / P_{ivc+5}) / \ln(V_{ivc+5} / V_{30CA,bTDC}) \qquad \text{(A12.8)}$$

The constant C_2 has a particular value for each engine. Its value is usually chosen so that negative heat release is avoided, i.e. to have a normalized cumulative heat release greater than 1 [107-109].

Finally rearranging Eq. (A12.1) and substituting the assumptions for each term the final energy balance equation is obtained:

$$dQ_{hr} = \frac{k(T)}{k(T)-1} PdV + \frac{1}{k(T)-1} VdP + dQ_w \qquad \text{(A12.9)}$$

or in the friendly form:

$$\frac{dQ_{hr}}{d\theta} = \frac{k(T)}{k(T)-1} P\frac{dV}{d\theta} + \frac{1}{k(T)-1} V\frac{dP}{d\theta} + \frac{dQ_w}{d\theta} \qquad \text{(A12.10)}$$

The equation (A12.10) was integrated along the period where the heat release was taking place.

CALCULATION OF THE CONSTANT C_1 OR HEAT TRANSFER MULTIPLIER *HT* IN THE HEAT RELEASE PROGRAM (C_1 = *HT*)

The integration of the equation (A12.10) gives the following equation:

$$Q_{hr} = \int_{\theta_{start}}^{\theta_{end}} \frac{k(T)}{k(T)-1} P\frac{dV}{d\theta} d\theta + \int_{\theta_{start}}^{\theta_{end}} \frac{1}{k(T)-1} V\frac{dP}{d\theta} d\theta + Q_w \qquad \text{(A12.11)}$$

In Eq. (A12.8) the first two terms of the right hand side can be calculated from the pressure traces. The total heat release (left hand side term) can be calculated as well from: $Q_{hr} = m_{fuel}.LHV.\eta_c$; where m_{fuel} is the mass of fuel, *LHV* represents the lower heating value of the fuel, and η_c is the combustion efficiency calculated from the measured emissions concentration [5, Appendix XI]. Thus, from Eq. (A12.11) the total heat transfer to the walls Q_w can be calculated, which at the same time must match the following integral:

$$Q_w = \int_{\theta_{start}}^{\theta_{end}} h_c.A.(T - Tw)d\theta \qquad \text{(A12.12)}$$

In this equation A represents the instantaneous heat transfer area, T the in cylinder bulk temperature, T_w is the wall temperature, and h_c a scaling heat transfer coefficient to satisfy Eq. (A12.12). The only unknown in Eq. (A12.12) is the constant C_1 of the heat transfer coefficient (h_c). The value of C_1 must be one such that Eq. (A12.9) is satisfied. The value of C_1 can be determined doing the following substitution:

$$h_c = C_1 h_c^{'} \qquad \text{(A12.13)}$$

where :

$$h_c^{'} = 3.26B^{b-1}.P.T^{0.75-1.62b}w^b \qquad [\text{W/(m}^2\text{K)}] \qquad \text{(A12.14)}$$

Thus:

$$C_1 = \frac{Q_w}{\int_{\theta_{start}}^{\theta_{end}} h^{'}.A.(T - Tw)d\theta} \qquad \text{(A12.15)}$$

With this constant at hand the instantaneous heat release and the instantaneous heat transfer to the wall can be calculated. As it can be notice the choice of the wall temperature is not relevant, because the constant C_1 will take care of it when balancing the total heat released through the wall.

A12.2 PROGRAM

```
% All the inputs for this program were provided via a GUI
% BEGGINNING OF DATA PROCESSING
tic
% Known Parameters
    resolution_index = get(handles.eresolution, 'Value');
    pressured_index = get(handles.pressured, 'Value');
    C2 = handles.metricdata.e_velocity; % Expansion Velocity in the
Heat Transfer Coefficient
    if resolution_index == 1            % Encoder Resolution
        enc_res = 1;
    elseif resolution_index == 2
        enc_res = 0.5;
    elseif resolution_index == 3
        enc_res = 0.25;
    end
    istep=0.25;                         %Integration Step
% Additional Info Header
    fida = fopen('HR_ADDITIONAL_INFO.txt','wt') ;
    fprintf(fida, 'FileName'); fprintf(fida, '\t');
    fprintf(fida, 'Qtot (J)'); fprintf(fida, '\t');
    fprintf(fida, 'Qht (J)'); fprintf(fida, '\t');
    fprintf(fida, 'Q_hr (J)'); fprintf(fida, '\t');
    fprintf(fida, 'Yres'); fprintf(fida, '\t');
    fprintf(fida, 'Yres,int'); fprintf(fida, '\t');
    fprintf(fida, 'HT'); fprintf(fida, '\t');
    fprintf(fida, 'CA10'); fprintf(fida, '\t');
    fprintf(fida, 'CA50'); fprintf(fida, '\t');
    fprintf(fida, 'CA90'); fprintf(fida, '\t');
    fprintf(fida, 'CA_evc'); fprintf(fida, '\t');
    fprintf(fida, 'CA_pmax'); fprintf(fida, '\t');
    fprintf(fida, 'Pmax(kPa)'); fprintf(fida, '\t');
    fprintf(fida, 'Pevc (kPa)'); fprintf(fida, '\t');
    fprintf(fida, 'Tmax (K)'); fprintf(fida, '\t');
    fprintf(fida, '\n');
    for nf = 1 : nlines
        DT = TData{ nf } ;
        for dd = 1 : 8
          comp1( dd ) = strcmp( DT ( dd ) , str ) ;
        end
        if  comp1(1) == 0 & comp1(2) == 0 & comp1(3) == 0 & comp1(4) ==
0 & comp1(5) == 0 & comp1(6) == 0 & comp1(7) == 0 & comp1(8) == 0
            tx = DT( 1 ) ;
            tstart = handles.metricdata.sangle ;    % Start Angle
            tend = handles.metricdata.eangle ;      % End Angle
            tivc = handles.metricdata.ivcv ;        % IVC timing - aTDC
            tevo = handles.metricdata.evov ;        % EVO timing - aTDC
            tevc = handles.metricdata.evcv ;        % EVC timing
            LHV = handles.metricdata.lhvv ;         % LHV(kJ/kg)
            D = handles.metricdata.borev ;          % Bore(m)
            stroke = handles.metricdata.strokev ;   % Stroke(m)
            T_wall = handles.metricdata.twallv ;    % T_wall(° K)
```

```
            tn_2 = -30 ;                                % CA of the second
point to calcualte the polytropic index n
% Cylinder two @ tcyl2 = 270
            if tx(3)=='2'
                tcyl2 = 270 ;                           % timing second
cylinder, this is very particular for the CH23 Kohler Engine.
                tstart = tcyl2 +  tstart ;              % Start Angle
                tend = tcyl2 + tend ;                   % End Angle
                tivc = tcyl2 + tivc ;                   % IVC timing - aTDC
                tevo = tcyl2 + tevo ;                   % EVO timing - aTDC
                tevc = tcyl2 + tevc ;                   % EVC timing
                if tevc > 540
                    tevc = ( tevc - 540 ) -180 ;
                end
                tn_2 = tcyl2 - 30 ;                     % CA of the second
point to calcualte the polytropic index n
            end
            fid = fopen( tx ) ;                         % Data Table files
            if fid == -1
                errordlg('File name entered could not be found or
accessed','Error');
            else
                line = '';
                while isempty( findstr( line , 'F3 fpressure [kPa]' ) )
                    line = fgetl( fid ) ;
                end
                d = fscanf( fid , '%f' , [ 4 , inf ] )' ;  % Extracting
the data of the look Up file
                [ Nd , f ] = size( d ) ;
                fclose( fid ) ;
                eta = str2num( DT( 2 ) ) ;          % eff._comb
                m_air = str2num( DT( 3 ) ) ;        % mass_air(kg/cycle)
                m_fuel = str2num( DT( 4 ) ) ;       % mass_fuel(kg/cycle)
                RPM = str2num( DT( 5 ) ) ;          % RPM
                T_exh = str2num( DT( 6 ) ) ;        % T_exhaust (°K)
                T_int = str2num( DT( 7 ) ) ;        % T_intake(  °K)
                EGR = str2num( DT( 8 ) ) ;          % EGR
% Checking the GUI table inputs
                ee = isempty( eta );  mm = isempty( m_air );  mf =
isempty( m_fuel );  tin = isempty( T_int );
                rpp = isempty( RPM );  tex = isempty( T_exh );  egr1 =
isempty( EGR);
                if ee == 0 & mm == 0 & mf == 0 & tin == 0 &rpp == 0 &
tex == 0 & egr1 == 0
% Constants
                    Ru=8.314;           % Universal Gas Constant
                    MW_air=28.90;       % Air molar mass
                    R=Ru/MW_air;        % Air constant
% Vectors with data from the Look UP file
                    CA=d(:,1);          % Crank angle vector
                    P=d(:,2);           % Cylinder Pressure
                    V=d(:,3);           % Volume data
                    fP=d(:,4);          % Filtered Pressure
```

```
                    enc_res = d(2,1)-d(1,1); % Encoder resolution from
the input data file
% Selection between filtered (1) or not filtered (2) pressure
                    if pressured_index == 2
                        fP = P;
                    end
                    Vdisp= interp1(CA,V,-180,'spline')-
interp1(CA,V,0,'spline');              % Displacement Volume
                    V_ivc=interp1(CA,V,tivc,'spline');
                    V_evo=interp1(CA,V,tevo,'spline');
                    V_evc=interp1(CA,V,tevc,'spline');
                    P_evo=interp1(CA,fP,tevo,'spline');
                    P_ivc=interp1(CA,fP,tivc,'spline');
                    P_evc=interp1(CA,fP,tevc,'spline');
% Pressures and Volumes to calculate the compression politropic
coefficient
                    P_1=interp1(CA,fP,tivc+5,'spline');
                    P_2=interp1(CA,fP,tn_2,'spline');
                    V_1=interp1(CA,V,tivc+5,'spline');
                    V_2=interp1(CA,V,tn_2,'spline');
                    n_comp=log(P_2/P_1)/log(V_1/V_2);
% Residual Mass Calculation
                    y_res_int=(V_evc/V_evo)*(P_evc/P_evo)^(1/n_comp);
% Calcualtion of the mass trapped
                    m_trapped = (m_air + m_fuel)*(1+(EGR/100)/(1-
EGR/100))/(1-y_res_int);
                    m_res_int = y_res_int*m_trapped;
                    m_res_ext = m_trapped - m_res_int - (m_air +
m_fuel);
                    m_res = m_res_int + m_res_ext;
                    y_res = m_res/m_trapped;
                    T_ivc=P_ivc*((V_ivc/R)/(m_air + m_fuel + m_res));
                    Q=m_fuel*LHV*eta;
                    speed=60/(RPM*360);
                    time=60/RPM;
                    Vp=2*stroke/time;
% Setting the CA, P, and V according to the integration step
                    CAi = ( tstart : istep : tend ) ;
                    [ ri , Ni ] = size ( CAi ) ;
                    for i = 1 : 1 : Ni
                        Vi(i) = interp1(CA , V , CAi( i ) , 'spline');
                        Pi(i) = interp1(CA , fP , CAi( i ) , 'spline');
                    end
% Pressure and Volume Derivatives
                    for i = 1 : 1 : Ni-1 ;
                        dP( i ) = ( Pi( i + 1 ) - Pi( i ) ) / istep ;
                        dV( i ) = ( Vi( i + 1 ) - Vi( i ) ) / istep ;
                    end
                    for i = 1 : 1 : Ni - 1
                        T( i ) = Pi( i ) * ( Vi( i ) / R ) / ( m_air +
m_fuel + m_res ) ;
                        gamma( i ) = 1.392 - 0.000075 * T( i ) ;
                        W( i ) = 2.28 *( Vp + C2 * 0.0136 * Vdisp /
V_ivc * ( Pi( i ) /P_ivc -( V_ivc / Vi( i ) ) ^ n_comp ) * T_ivc ) ;
```

```
                    h1( i ) = 0.131 * D ^ 0.2 * ( Pi( i ) / 101.3 )
^ 0.8 / ( T( i ) ^ 0.53 ) * W( i ) ^ 0.8 ;
                    AREA( i ) = 2 * pi * D ^ 2 / 4 + pi * D * Vi( i
) / ( pi * D ^ 2 / 4 ) ;
                    dI_ht( i ) = h1( i ) * AREA( i ) * ( T( i ) -
T_wall ) * speed ;
                    dI_hr( i ) = ( Vi( i ) / ( gamma( i ) -1 ) ) *
dP( i ) + gamma( i ) / ( gamma( i ) - 1 ) * Pi( i ) * dV( i ) ;
                end
% Integration to find I_tot_ht, I_tot_hr, and HT
                for i=1:1:Ni-2
                    I_hr ( i ) = 1 / 2 * ( dI_hr ( i ) + dI_hr ( i
+ 1 ) ) * istep ;
                    I_ht ( i ) = 1 / 2 * ( dI_ht ( i ) + dI_ht ( i
+ 1 ) ) * istep ;
                end
                I_tot_ht = sum ( I_ht ) ;
                I_tot_hr = sum ( I_hr ) ;
                HT = ( Q - I_tot_hr ) / ( I_tot_ht ) ;
% Calculation of dQ_ht,dQ_hr, and Q_hr_cum using the calculated scaling
factor HT
                for i = 1 : 1 : Ni-1
                    dQ_ht ( i ) = HT * h1 ( i ) * AREA ( i ) * ( T
( i ) - T_wall ) * speed ;
                    dQ_hr ( i ) = dQ_ht ( i ) + ( Vi ( i ) / (
gamma ( i ) - 1 ) ) * dP ( i ) + gamma ( i ) / ( gamma ( i ) - 1) * Pi
( i ) * dV ( i );
                end
% Filtering of the Heat release
                filter = get( handles.filteronoff , 'Value' );  % 0
= OFF 1 = ON
                if filter == 1
                   dQ_hr = csaps ( CAi(1:Ni-1),dQ_hr(1:Ni-1) ,
0.005 , CAi(1:Ni-1)) ;
                end
                cum = 0 ;
                for i = 1 : 1 : Ni - 2
                    Q_hr( i ) = 1 / 2 * ( dQ_hr( i ) + dQ_hr( i + 1
) ) * istep ;
                    Q_ht( i ) = 1 / 2 * ( dQ_ht( i ) + dQ_ht( i + 1
) ) * istep ;
                    cum = cum + Q_hr( i ) ;
                    Q_hr_cum( i ) = cum / Q ;
                end
% Conversion to J (1000 factor)
                dQ_hr = 1000 * dQ_hr ;              % Heat release
                dQ_ht = 1000 * dQ_ht ;              % Heat transfer
                Q_tot_ht = 1000 * sum( Q_ht ) ;     % Total heat
transfer
                Q_tot_hr = 1000 * sum( Q_hr ) ;     % Total heat
release
                Diff =( Q * 1000 - Q_tot_hr ) ;
% Heat Release at 10%, 50%, 90%
                for i = 1 : 1 : Ni - 3
```

```
                        if Q_hr_cum( i ) <= 0.1 && Q_hr_cum( i + 1 ) >
0.1
                           CA_10 = CAi( i )
                           Q_hr_cum_10 = Q_hr_cum( i )
                        elseif Q_hr_cum( i ) <= 0.5 && Q_hr_cum( i + 1
) > 0.5
                           CA_50 = CAi( i )
                           Q_hr_cum_50 = Q_hr_cum( i )
                        elseif Q_hr_cum( i ) <= 0.9 && Q_hr_cum( i + 1
) > 0.9
                           CA_90 = CAi( i )
                           Q_hr_cum_90 = Q_hr_cum( i )
                        end
                    end
            [ P_max , imax ] = max ( P ) ;   %Peak Pressure
            CA_pmax  = CA ( imax ) ;         %Location of Peak Pressure
            CA_evc = tevc ;    % CA of exhaust valve closing
            CA_evo = tevo ;    % CA of exhaust valve opening
% In Cylinder Temperature Calculation
            R_b = R ;          % Burned gases constant equal to the air
constant in kJ/kg-K
            for i = 1 : Nd
                Tm ( i ) = P ( i ) * V ( i ) / ( R_b * ( m_air + m_fuel
+ m_res ) ) ;                  % Pressure in kPa
            end
            T_max = max ( Tm ) % Maximun temperature in the cyl. in K
%--------------------------Output files ------------------------
% Output File Heat Release
OHR{nf}=strcat('hr_',tx);
fidO=fopen(OHR{nf},'wt');
[qlr,qlc]=size(tx);
TX=tx(3:(qlc-4));
fprintf(fidO, 'CA_hr_'); fprintf(fidO, TX); fprintf(fidO, '\t\t');
fprintf(fidO, 'dQ_hr_'); fprintf(fidO, TX); fprintf(fidO, '\t\t\t');
fprintf(fidO, 'dQ_ht_'); fprintf(fidO, TX); fprintf(fidO, '\t\t\t');
fprintf(fidO, 'Q_hr_cum_'); fprintf(fidO, TX);
fprintf(fidO, '\n');
for v=1:Ni-2
  fprintf(fidO, '%3.3f\t\t\t', CAi(v));
  fprintf(fidO, '%g\t\t\t', dQ_hr(v));
  fprintf(fidO, '%g\t\t\t', dQ_ht(v));
  fprintf(fidO, '%g\t\t\t', Q_hr_cum(v));
    fprintf(fidO, '\n');
end
    fclose(fidO);
% HR_ADDITIONAL_INFO.txt
    fprintf(fida, tx);
    fprintf(fida, '\t');
    fprintf(fida, '%g\t', Q*1000);
    fprintf(fida, '%g\t', Q_tot_ht);
    fprintf(fida, '%g\t', Q_tot_hr);
    fprintf(fida, '%g\t', y_res);
    fprintf(fida, '%g\t', y_res_int);
    fprintf(fida, '%g\t', HT);
```

```
    fprintf(fida, '%g\t', CA_10);
    fprintf(fida, '%g\t', CA_50);
    fprintf(fida, '%g\t', CA_90);
    fprintf(fida, '%g\t', CA_evc);
    fprintf(fida, '%g\t', CA_pmax);
    fprintf(fida, '%g\t', P_max);
    fprintf(fida, '%g\t', P_evc);
    fprintf(fida, '%g\t', T_max);
    fprintf(fida, '\n');
 %---------------------- Plots ---------------------------------
    figure       % Heat Release,Cum. Heat Release,Heat Transfer
    hold on
    axis on; grid on; box on; % Axis image;
    [AX,H1,H2] = plotyy(CAi(1:Ni-1),dQ_hr(1:Ni-1),CAi(1:Ni-
2),Q_hr_cum(1:Ni-2),'plot');
    set(get(AX(1),'Ylabel'),'String','dQ-hr')
    set(get(AX(2),'Ylabel'),'String','Q-hr-cum (J/J/deg)')
    t1=title(['Heat Release and Heat Transfer   @  ',TX]);
    xlabel('CA');ylabel('dQ-ht , dQ-ht  (J/deg)');
    hold on
    plot(CAi(1:Ni-1),dQ_ht(1:Ni-1),'Color',[0 0.5 0]);
    plot(CAi(1:Ni-1),dQ_ht(1:Ni-1),'r');
    legend('dQ-hr','Q-hr-cum','dQ-ht');
   else
   errordlg('Parameters must be numeric','Error');
   end
   end
   else
    errordlg('Table should be filled correcty','Error');
   end
  end
  fclose(fida);
else
  errordlg('Table should be filled','Error');
end
toc
set(handles.text36, 'String', toc);
set(handles.calculate, 'Enable', 'on');
set(handles.reset, 'Enable', 'on');
%==========END OF DATA PROCESSING==========
```

APPENDIX XIII - RING PACK PROGRAM

```
%The ring pack program was a function called by the Ring-Pack-Heat-
%Release program (see next appendix). The dimensions of the ring pack
%were provided by the function RPVol, shown at the bottom of this
appendix.

%RING PACK MODEL function
%This program models the flow in the ring pack crevices and provides
%as output their contribution to the HC emissions
function  [ m1out_CA90_to_CA_evc , m1out_CA90_to_CA_evo ,
m1stored_CA_pmax , m1out , m1in , m_s_blowby ] = RP2CR_GCR ( CA_90 ,
CA_evc , CA_evo, CA_pmax , d , tx , RPM )
% Known Parameters
Cd = 0.85;                  % Discharge Coefficient
gamma = 1.4;                % Specific Heat Ratio
T = 385;                    % Wall Temperature in °K
R = 287;                    % Air constant J/kg-K
[Vi , Vii , Viii , Viv , A1L , A1U , A2L , A2U ] = RPvol; % from the
RPvol function - Ring Pack Volumes and Ring End Gap Areas
[ Nd , f ] = size ( d ) ;
CA = d ( : , 1 );           % CA vector from the reading vector
P1 = 1000 * d ( : , 4 ) ;   % Cylinder pressure data vector, Pa
Pc = 1000 * d ( : , 5 ) ;   % Crankcase pressure vector, Pa
[ r , c ] = size ( P1 ) ;   % Size of the cylinder pressure vector
dCA=CA(2,1)-CA(1,1);        % CA step integration, in Crank Angle units
dt=dCA/(6*RPM);             % Integration time step in sec for each
file changes with the velocity
Ps = csaps(CA,P1,0.005,CA); % Smoothing of the Cylinder Pressure data
P1 = Ps ;                   % Pressure 1 equal to the smooth cyl. press
% Differentiation of the Pressure data: dP/dt
for i=1:1:r-1;
        dP(i)=(Ps(i+1)-Ps(i))/dt;
end
dP(1440)=(Ps(1)-Ps(r))/dt;  % Derivative of the last point
% Initial Pressure in the Ring Pack Crevices Volumes
P2(1)=53;                   % Initial Pressure in the Volume 2, a guess
% WHILE LOOP for the convergency of P2(1)= P2(r)=last point press
differ = 1;                 % Criteria to stop the while loop
N = 0;
while abs(differ) >10e-5
  for i=1:r-1               % Integration of the eq around the cyc
      P3(i)=Pc(i);          % Cranckcase Pressure
  if P1(i)>=P2(i)           % Mass balance in the first volume
      if P2(i)/P1(i) < 0.52
          eta1=(2/(gamma+1))^((gamma+1)/(2*(gamma-1)));
      else
          eta1=(2/(gamma-1)*((P2(i)/P1(i))^(2/gamma)-
(P2(i)/P1(i))^((gamma+1)/gamma)))^0.5;
      end
      A1 = A1L ;       % Ring seating at the bottom part of the groove
```

```
        m2(i)=Cd*A1*(sqrt(gamma/(R*T))*P1(i))*eta1;
        V1 ( i ) = Vi + Vii ;% Crevice volume over the first ring
  else
  if P1(i)/P2(i) < 0.52
        eta2i=(2/(gamma+1))^((gamma+1)/(2*(gamma-1)));
  else
        eta2i=(2/(gamma-1)*((P1(i)/P2(i))^(2/gamma)-
(P1(i)/P2(i))^((gamma+1)/gamma)))^0.5;
  end
  A1 = A1U ;              % Ring seating at the upper partof the groove
  m2(i)=-Cd*A1*(sqrt(gamma/(R*T))*P2(i))*eta2i;
  V1 ( i ) = Vi ;         % Crevice volume over the first ring
  end
  m1 ( i ) = m2 ( i ) + V1 ( i ) / ( R * T ) * dP ( i ) ;
  m1stored ( i ) = P1 ( i ) * V1 ( i ) / ( R * T ) ;
  V1stored ( i ) = V1 ( i ) ;
  if P2(i)>=P3(i)         % Mass balance in the second  volume
        if P3(i)/P2(i) < 0.52
            eta2=(2/(gamma+1))^((gamma+1)/(2*(gamma-1)));
        else
            eta2=(2/(gamma-1)*((P3(i)/P2(i))^(2/gamma)-
(P3(i)/P2(i))^((gamma+1)/gamma)))^0.5;
        end
        A2 = A2L; % Second ring seating on the bottom part of the groove
        m3(i)=Cd*A2*(sqrt(gamma/(R*T))*P2(i))*eta2;
  elseif P2(i)/P3(i) < 0.52
        eta3i=(2/(gamma+1))^((gamma+1)/(2*(gamma-1)));
  else
        eta3i=(2/(gamma-1)*((P2(i)/P3(i))^(2/gamma)-
(P2(i)/P3(i))^((gamma+1)/gamma)))^0.5;
  end
  A2 = A2U ;     % Second ring seating at the upper part of the groove
  m3(i)=-Cd*A2*(sqrt(gamma/(R*T))*P3(i))*eta3i;
  end
  if P1(i)>=P2(i) && P2(i)>=P3(i) % Crevice Vol. between 1st and 2nd
ring
        V2 ( i ) = Viii + Viv;
  elseif P1(i)>=P2(i) && P2(i)<P3(i)
        V2 ( i ) = Viii;
  elseif P1(i)<P2(i) && P2(i)<P3(i)
        V2 ( i ) = Vii + Viii;
  elseif P1(i)<P2(i) && P2(i)>P3(i)
        V2 ( i ) = Vii + Viii + Viv;
  end
        P2 ( i + 1 ) = P2 ( i ) + ( ( m2 ( i ) -  m3 ( i ) ) *  R * T /
V2 ( i ) ) * dt ;                % Pressure in the volume V2
        m2stored ( i ) = P2 ( i ) * V2 ( i ) / ( R * T ) ;
        V2stored ( i ) = V2 ( i ) ;
  end
% Difference in Pressure at the end and the start of the cycle
  deltaP2(N+1)=P2(1)-P2(r);
  differ = deltaP2(N+1);
  N = N + 1;
  P2(1)=P2(r); % Reasigment of the inital press in the crevices volume
```

```
end
% Blowby Calculation
for i=1:r-2
    dm3(i)=(m3(i)+m3(i+1))/2*dt;
end
m3total=sum(dm3);            % Total mass due to blowby
m_blowby_cyc = m3total;      % Blowby mass per cycle
m1ini = 0 ;                  % Cummulative Mass In and Out Calculation
m1outi = 0 ;
m2ini = 0 ;
m2outi = 0 ;
m3ini = 0 ;
m3outi = 0 ;
for i = 1 : r - 2 ;
    if  m1 ( i ) >= 0        % For Volume 1
        dm1in ( i ) = ( m1 ( i ) + m1 ( i + 1 ) ) / 2 * dt ;
        m1in ( i ) = m1ini + dm1in ( i ) ;
        m1ini = m1in ( i ) ;
        m1out ( i ) = m1outi + 0 ;
    else
        dm1out ( i ) = ( m1 ( i ) + m1 ( i + 1 ) ) / 2 * dt ;
        m1out ( i ) = m1outi + dm1out ( i ) ;
        m1outi = m1out ( i ) ;
        m1in ( i ) = m1ini + 0 ;
    end
    if  m2 ( i ) >= 0        % For Volume 2
        dm2in ( i ) = ( m2 ( i ) + m2 ( i + 1 ) ) / 2 * dt ;
        m2in ( i ) = m2ini + dm2in ( i ) ;
        m2ini = m2in ( i ) ;
        m2out ( i ) = m2outi + 0 ;
    else
        dm2out ( i ) = ( m2 ( i ) + m2 ( i + 1 ) ) / 2 * dt ;
        m2out ( i ) = m2outi + dm2out ( i ) ;
        m2outi = m2out ( i ) ;
        m2in ( i ) = m2ini + 0 ;
    end
    if  m3 ( i ) >= 0        % For Volume 3
        dm3in ( i ) = ( m3 ( i ) + m3 ( i + 1 ) ) / 2 * dt ;
        m3in ( i ) = m3ini + dm3in ( i ) ;
        m3ini = m3in ( i ) ;
        m3out ( i ) = m3outi + 0 ;
    else
        dm3out ( i ) = ( m3 ( i ) + m3 ( i + 1 ) ) / 2 * dt ;
        m3out ( i ) = m3outi + dm3out ( i ) ;
        m3outi = m3out ( i ) ;
        m3in ( i ) = m3ini + 0 ;
    end
end
P3(1440)=Pc(1440);           % Last point crankcase pressure
m1out = - m1out ;            % Mass out with possitive sign in kg
m2out = - m2out ;            % Mass out with possitive sign in kg
m3out = - m3out ;            % Mass out with possitive sign in kg
m3blowby = m3in - m3out ;    % Blowby cummulative mass in kg
m1outi = m1out ;             % Mass for integration
```

```
m1out_CA90_to_CA_evc = 0 ;   % Mass Out from CA_90 to EVC
m1out_CA90 = 0 ;
m1out_CA_evc = 0 ;
m1out_CA_evo = 0;
for i = 1 : r - 2
    if CA ( i ) >= CA_90 && CA ( i ) < ( CA_90 + dCA )
        m1out_CA90 = m1outi(i);
    end
    if CA ( i ) >= CA_evc && CA ( i ) < ( CA_evc + dCA )
        m1out_CA_evc = m1outi(i);
    end
    if CA ( i ) >= CA_evo && CA ( i ) < ( CA_evo + dCA )
        m1out_CA_evo = m1outi(i);
    end
    if CA ( i ) >= CA_pmax && CA ( i ) < ( CA_pmax + dCA )
        m1stored_CA_pmax = m1stored(i);
    end
end
m1out_CA90_to_CA_evc = ( m1out_CA_evc - m1out_CA90 ) ; % in kg
m1out_CA90_to_CA_evo = ( m1out_CA_evo - m1out_CA90 ) ; % in kg
m1stored_CA_pmax = ( 0 + m1stored_CA_pmax ) ;          % in kg
%-------------------------Unit Conversion-------------------------
P1 = P1 / 1000 ;              % kPa
P2 = P2 / 1000 ;              % kPa
P3 = P3 / 1000 ;              % kPa
Pc = Pc / 1000 ;              % kPa
m1 = m1 * 1000 ;              % grams/sec
m2 = m2 * 1000 ;              % grams/sec
m3 = m3 * 1000 ;              % grams/sec
m1stored = m1stored * 1000 ;  % grams
m2stored = m2stored * 1000 ;  % grams
m_blowby_cyc = m_blowby_cyc * 1000 ; % grams/cycle
m1in = 1000 * m1in ;          % Mass 1 in with possitive sign in g
m2in = 1000 * m2in ;          % Mass 2 in with possitive sign in g
m3in = 1000 * m3in ;          % Mass 3 in with possitive sign in g
m1out = 1000 * m1out ;        % Mass 1 out with possitive sign in g
m2out = 1000 * m2out ;        % Mass 2 out with possitive sign in g
m3out = 1000 * m3out ;        % Mass 3 out with possitive sign in g
m3blowby = 1000 * m3blowby ;  % Blowby cummulative mass in g
%-------------Steady State Blowby Mass Flow----------------------------
% (to be compared with the measured by the bells meter)
m_s_blowby = m_blowby_cyc * RPM / 120  ; % (g/s)
%-----------------------------Plots-----------------------------------
figure
plot(CA,P1,CA,P2, CA, P3)
legend('P1','P2','Pc')
xlabel('CA');ylabel('Pressure(kPa)');
figure
plot(CA(1:r-1),m1,CA(1:r-1),m2,CA(1:r-1),m3)
legend('m1','m2','m3')
xlabel('CA');ylabel('Mass Flow (g/s)');
figure
plot(CA(1:r-2),m1in,CA(1:r-2),m2in,CA(1:r-2),m3in)
legend('m1in','m2in','m3in')
```

```
xlabel('CA');ylabel('Mass In of the Crevices (g)');
figure
plot(CA(1:r-2),m1out,CA(1:r-2),m2out,CA(1:r-2),m3out)
legend('m1out','m2out','m3out')
xlabel('CA');ylabel('Mass Out of the Crevices (g)');
figure
plot(CA(1:r-2),m3blowby)
legend('Mass Blowby')
xlabel('CA');ylabel('Total mass to the crankcase (g)');
%---------------------------Output files-------------------------------
js=strcat('ORPap_',tx) ;  fidO=fopen(js,'wt');
[qlr,qlc]=size(tx);       tx1=tx(3:(qlc-4));
fprintf(fidO,'CA');       fprintf(fidO, tx1); fprintf(fidO, '\t');
fprintf(fidO,'P1(kPa)');  fprintf(fidO, tx1); fprintf(fidO, '\t');
fprintf(fidO,'P2(kPa)');  fprintf(fidO, tx1); fprintf(fidO, '\t');
fprintf(fidO,'m1(g/s)');  fprintf(fidO, tx1); fprintf(fidO, '\t');
fprintf(fidO,'m2(g/s)');  fprintf(fidO, tx1); fprintf(fidO, '\t');
fprintf(fidO,'m3(g/s)');  fprintf(fidO, tx1); fprintf(fidO, '\t');
fprintf(fidO,'m_c_cum(g)');fprintf(fidO, tx1); fprintf(fidO, '\t');
fprintf(fidO,'m1_in(g)'); fprintf(fidO, tx1); fprintf(fidO, '\t');
fprintf(fidO,'m2_in(g)'); fprintf(fidO, tx1); fprintf(fidO, '\t');
fprintf(fidO,'m3_in(g)'); fprintf(fidO, tx1); fprintf(fidO, '\t');
fprintf(fidO,'m1_out(g)');fprintf(fidO, tx1); fprintf(fidO, '\t');
fprintf(fidO,'m2_out(g)');fprintf(fidO, tx1); fprintf(fidO, '\t');
fprintf(fidO,'m3_out(g)');fprintf(fidO, tx1); fprintf(fidO, '\t\t');
fprintf(fidO, '\n');
for v=1:r-2
    fprintf(fidO, '%3.1f\t', CA(v));
    fprintf(fidO, '%g\t', P1(v));
    fprintf(fidO, '%g\t', P2(v));
    fprintf(fidO, '%g\t', m1(v));
    fprintf(fidO, '%g\t', m2(v));
    fprintf(fidO, '%g\t', m3(v));
    fprintf(fidO, '%g\t', m3blowby(v));
    fprintf(fidO, '%g\t', m1in(v));
    fprintf(fidO, '%g\t', m2in(v));
    fprintf(fidO, '%g\t', m3in(v));
    fprintf(fidO, '%g\t', m1out(v));
    fprintf(fidO, '%g\t', m2out(v));
    fprintf(fidO, '%g\t', m3out(v));
    fprintf(fidO, '\n');
end
fclose(fidO);

%   RING PACK VOLUMES (GEOMETRY) CALCULATION function
%   Dimension provided below are not real dimensions they are used only
%   for illustration purposes
function [V1,V2,V3,V4,A1L,A1U,A2L,A2U] = RPvol ;
%   All dimensions are in millimeters (mm)
%   Written by Victor M. Salazar
%   Engine Research Center
%   University of Wisconsin - Madison
%   February 24th, 2007 version
%--------------------Volume V1------------------------
```

```
dcyl = 82;
h1 = 5.2 ;
d1L = 78.5;
d1U = 79.0;
r1L = d1L/2;
r1U = d1U/2;
Ve1 = pi / 4 * dcyl ^ 2 * h1;  % External Volume Ve1
Vi1 = 1 / 3 * pi * h1 * ( r1L ^ 2 + r1U ^ 2 + r1L * r1U ); % Internal
Volume
V1 = Ve1 - Vi1;
h2 = 1.7 + 0.01;
di2 = 72.0 ;
diRI = 75 ;
hRI = 1.7 ;
Ve2 = pi / 4 * dcyl ^ 2 * h2 ; % External Volume
Vi2 = pi / 4 * di2 ^ 2 * h2 ;  % Internal Volume
VRI = pi / 4 * ( dcyl ^ 2 - diRI ^ 2) * hRI ;    % Ring Volume
V2 = Ve2 - Vi2 - VRI;
h3 = 4.0 ;
d3L = 80.01 ;
d3U = 79.01 ;
r3L = d3L / 2 ;
r3U = d3U / 2 ;
Ve3 = pi / 4 * dcyl ^ 2 * h3 ;  % External Volume
Vi3 = 1 / 3 * pi * h3 * ( r3L ^ 2 + r3U ^ 2 + r3L * r3U ) ; % Internal
Volume
V3 = Ve3 - Vi3;
h4 = 1.7 ;
di4 = 72 ;
diRII = 72.48 ;
hRII = 1.8 ;
Ve4 = pi / 4 * dcyl ^ 2 * h4 ;  % External Volume
Vi4 = pi / 4 * di4 ^ 2 * h4 ;   % Internal Volume
VRII = pi / 4 * ( dcyl ^ 2 - diRII ^ 2 ) * hRII ; % Ring Volume
V4 = Ve4 - Vi4 - VRII;
% Units conversion from mm^3 to m^3
V1 = V1 * 1e-9;                 % m^3
V2 = V2 * 1e-9;                 % m^3
V3 = V3 * 1e-9;                 % m^3
V4 = V4 * 1e-9;                 % m^3
% End Gap Ring I  Area
EGRI = 0.60;
A1L = EGRI * ( dcyl - d3U ) ;
A1U = EGRI * ( dcyl - d1L ) ;
% End Gap Ring II  Area
EGRII = 0.80;
d5U = 79.682 ;
A2L = EGRII * ( dcyl - d5U ) ;
A2U = EGRII * ( dcyl - d3L ) ;
% Units conversion from mm^2 to m^2
A1L = A1L * 1e-6 ;
A1U = A1U * 1e-6 ;
A2L = A2L * 1e-6 ;
A2U = A2U * 1e-6 ;
```

APPENDIX XIV - RING PACK-HEAT RELEASE PROGRAM

```
% All the inputs to this program were provided by a GUI

% BEGGINNING OF DATA PROCESSING
tic
    resolution_index = get(handles.eresolution, 'Value');
    pressured_index = get(handles.pressured, 'Value');
    C2 = handles.metricdata.e_velocity;      % Expansion Velocity in
the Heat Transfer Coefficient
    if resolution_index == 1                 % Encoder Resolution
        enc_res = 1;
    elseif resolution_index == 2
        enc_res = 0.5;
    elseif resolution_index == 3
        enc_res = 0.25;
    end
    istep=0.25;                              % Integration Step
    fida = fopen('RINGPACK_AVG_PH_ADD_INFO.txt','wt') ;
    fprintf(fida, 'FileName'); fprintf(fida, '\t');
    fprintf(fida, 'Qtot (J)'); fprintf(fida, '\t');
    fprintf(fida, 'Qht (J)'); fprintf(fida, '\t');
    fprintf(fida, 'Q_hr (J)'); fprintf(fida, '\t');
    fprintf(fida, 'Yres'); fprintf(fida, '\t');
    fprintf(fida, 'Yres,int'); fprintf(fida, '\t');
    fprintf(fida, 'HT'); fprintf(fida, '\t');
    fprintf(fida, 'CA10'); fprintf(fida, '\t');
    fprintf(fida, 'CA50'); fprintf(fida, '\t');
    fprintf(fida, 'CA90'); fprintf(fida, '\t');
    fprintf(fida, 'CA_evc'); fprintf(fida, '\t');
    fprintf(fida, 'CA_pmax'); fprintf(fida, '\t');
    fprintf(fida, 'EIHC_exh (g/kg)'); fprintf(fida, '\t');
    fprintf(fida, 'EIHC_crev_CA90_evc (g/kg)'); fprintf(fida, '\t');
    fprintf(fida, 'EIHC_crev_CA90_evo (g/kg)'); fprintf(fida, '\t');
    fprintf(fida, 'EIHC_crev_sto_pmax (g/kg)'); fprintf(fida, '\t');
    fprintf(fida, 'Pmax(kPa)'); fprintf(fida, '\t');
    fprintf(fida, 'Pevc (kPa)'); fprintf(fida, '\t');
    fprintf(fida, 'Tmax (K)'); fprintf(fida, '\t');
    fprintf(fida, 'Tau_CA90_evc (s)'); fprintf(fida, '\t');
    fprintf(fida, 'Tau_CA90_evo (s)'); fprintf(fida, '\t');
    fprintf(fida, 'Tau_pmax_evo (s)'); fprintf(fida, '\t');
    fprintf(fida, 'X_02'); fprintf(fida, '\t');
    fprintf(fida, 'X_02_calc'); fprintf(fida, '\t');
    fprintf(fida, 'm_blowby (g/s)'); fprintf(fida, '\t');
    fprintf(fida, '\n');
    for nf = 1 : nlines
        DT = TData{ nf } ;
        for dd = 1 : 13
          comp1( dd ) = strcmp( DT ( dd ) , str ) ;
        end
        if  comp1(1) == 0 & comp1(2) == 0 & comp1(3) == 0 & comp1(4) ==
0 & comp1(5) == 0 & comp1(6) == 0 & comp1(7) == 0 & comp1(8) == 0 &
```

```
comp1(9) == 0 & comp1(10) == 0 & comp1(11) == 0 & comp1(12) == 0&
comp1(13) == 0
            tx = DT( 1 ) ;
            tstart = handles.metricdata.sangle ;   % Start Angle
            tend = handles.metricdata.eangle ;     % End Angle
            tivc = handles.metricdata.ivcv ;       % IVC timing - aTDC
            tevo = handles.metricdata.evov ;       % EVO timing - aTDC
            tevc = handles.metricdata.evcv ;       % EVC timing
            LHV = handles.metricdata.lhvv ;        % LHV(kJ/kg)
            D = handles.metricdata.borev ;         % Bore(m)
            stroke = handles.metricdata.strokev ;  % Stroke(m)
            T_wall = handles.metricdata.twallv ;   % T_wall(° K)
            tn_2 = -30 ;                           % CA of the second
point to calcualte the polytropic index n
            tevc_tau = tevc ;                      % Tau
            fid = fopen( tx ) ;                    % Data Table files
open
            if fid == -1
                errordlg('File name entered could not be found or
accessed','Error');
            else
                line = '';
                while isempty(findstr(line , 'F3 fCr_pressure [kPa]'))
                    line = fgetl( fid ) ;
                end
                d = fscanf( fid , '%f' , [ 5 , inf ] )' ;  % Extracting
data of the look Up file
                [ Nd , f ] = size( d ) ;
                fclose( fid ) ;
                eta = str2num( DT( 2 ) ) ;         % eff._comb
                m_air = str2num( DT( 3 ) ) ;       % mass_air(kg/cycle)
                m_fuel = str2num( DT( 4 ) ) ;      % mass_fuel(kg/cycle)
                RPM = str2num( DT( 5 ) ) ;         % RPM
                T_exh = str2num( DT( 6 ) ) ;       % T_exhaust (°K)
                T_int = str2num( DT( 7 ) ) ;       % T_intake(  °K)
                X_O2_calc = str2num( DT( 8 ));     % Molar fraction O2
calc
                EIHC_exh = str2num(DT( 9 ));       % Emissions index HC
(g/kg)
                MW_exh = str2num( DT( 10 ) ) ;     % Molecular weight
                AF = str2num(DT(11));              % Air fuel ratio (kg
air / kg fuel)
                X_O2 = str2num( DT( 12 ) ) ;       % Oxygen mole
fraction
                EGR = str2num( DT( 13 ) ) ;        % EGR concentration
% Checking the GUI table inputs
                ee = isempty( eta );  mm = isempty( m_air );  mf =
isempty( m_fuel );  tin = isempty( T_int );
                rpp = isempty( RPM );  tex = isempty( T_exh );  mfocalc
= isempty( X_O2_calc );  eihcex = isempty( EIHC_exh );
                mwex = isempty( MW_exh );  afm = isempty( AF );  mfo =
isempty( X_O2 ); egr1 = isempty( EGR);
```

```
                if ee == 0 & mm == 0 & mf == 0 &rpp == 0 & tex == 0 &
mfocalc == 0 & eihcex == 0 & tin == 0 & mwex == 0 & afm == 0 & mfo == 0
& egr1 == 0
% Constants
                    Ru=8.314;                       % Universal Gas
Constant
                    MW_air=28.90;                   % Air molar mass
                    R=Ru/MW_air;                    % Air constant
% Vectors with data from the Look UP file
                    CA=d(:,1);                      % Crank angle vector
                    P=d(:,2);                       % Cylinder Pressure
                    V=d(:,3);                       % Volume data
                    fP=d(:,4);                      % Filtered Pressure
                    enc_res = d(2,1)-d(1,1);        % Encoder resolution
% Selection between filtered (1) or not filtered (2) pressure
                    if pressured_index == 2
                        fP = P;
                    end
                    Vdisp= interp1(CA,V,-180,'spline')-
interp1(CA,V,0,'spline');                           % Displacement Volume
                    V_ivc=interp1(CA,V,tivc,'spline');
                    V_evo=interp1(CA,V,tevo,'spline');
                    V_evc=interp1(CA,V,tevc,'spline');
                    P_evo=interp1(CA,fP,tevo,'spline');
                    P_ivc=interp1(CA,fP,tivc,'spline');
                    P_evc=interp1(CA,fP,tevc,'spline');
% Pressures and Volumes to calculate the compression politropic
coefficient
                    P_1=interp1(CA,fP,tivc+5,'spline');
                    P_2=interp1(CA,fP,tn_2,'spline');
                    V_1=interp1(CA,V,tivc+5,'spline');
                    V_2=interp1(CA,V,tn_2,'spline');
                    n_comp=log(P_2/P_1)/log(V_1/V_2);
% Residual Mass Calculation
                    y_res_int=(V_evc/V_evo)*(P_evc/P_evo)^(1/n_comp);
                    m_trapped = (m_air + m_fuel)*(1+(EGR/100)/(1-
EGR/100))/(1-y_res_int); % Calcualtion of the mass trapped
                    m_res_int = y_res_int*m_trapped;
                    m_res_ext = m_trapped - m_res_int - (m_air +
m_fuel);
                    m_res = m_res_int + m_res_ext;
                    y_res = m_res/m_trapped;
                    T_ivc=P_ivc*((V_ivc/R)/(m_air + m_fuel + m_res));
                    Q=m_fuel*LHV*eta;
                    speed=60/(RPM*360);
                    time=60/RPM;
                    Vp=2*stroke/time;
% Setting the CA, P, and V according to the integration step
                    CAi = ( tstart : istep : tend ) ;
                    [ ri , Ni ] = size ( CAi ) ;
                    for i = 1 : 1 : Ni
                        Vi(i) = interp1( CA , V , CAi( i ), 'spline');
                        Pi(i) = interp1( CA , fP , CAi( i ), 'spline');
                    end
```

```
% Pressure and Volume Derivatives
                    for i = 1 : 1 : Ni-1 ;
                        dP( i ) = ( Pi( i + 1 ) - Pi( i ) ) / istep ;
                        dV( i ) = ( Vi( i + 1 ) - Vi( i ) ) / istep ;
                    end
                    for i = 1 : 1 : Ni - 1
                        T(i) = Pi(i)*(Vi(i)/R)/(m_air+m_fuel+m_res);
                        gamma( i ) = 1.392 - 0.000075 * T( i ) ;
                        W( i ) = 2.28 *( Vp + C2 * 0.0136 * Vdisp /
V_ivc * ( Pi( i ) /P_ivc -( V_ivc / Vi( i ) ) ^ n_comp ) * T_ivc ) ;
                        h1( i ) = 0.131 * D ^ 0.2 * ( Pi( i ) / 101.3 )
^ 0.8 / ( T( i ) ^ 0.53 ) * W( i ) ^ 0.8 ;
                        AREA( i ) = 2 * pi * D ^ 2 / 4 + pi * D * Vi( i
) / ( pi * D ^ 2 / 4 ) ;
                        dI_ht( i ) = h1( i ) * AREA( i ) * ( T( i ) -
T_wall ) * speed ;
                        dI_hr( i ) = ( Vi( i ) / ( gamma( i ) -1 ) ) *
dP( i ) + gamma( i ) / ( gamma( i ) - 1 ) * Pi( i ) * dV( i ) ;
                    end
% Integration to find I_tot_ht, I_tot_hr, and HT
                    for i=1:1:Ni-2
                        I_hr ( i ) = 1 / 2 * ( dI_hr ( i ) + dI_hr ( i
+ 1 ) ) * istep ;
                        I_ht ( i ) = 1 / 2 * ( dI_ht ( i ) + dI_ht ( i
+ 1 ) ) * istep ;
                    end
                    I_tot_ht = sum ( I_ht ) ;
                    I_tot_hr = sum ( I_hr ) ;
                    HT = ( Q - I_tot_hr ) / ( I_tot_ht ) ;
% Calculation of dQ_ht,dQ_hr, and Q_hr_cum using the calculated scaling
factor HT
                    for i = 1 : 1 : Ni-1
                        dQ_ht ( i ) = HT * h1 ( i ) * AREA ( i ) * ( T
( i ) - T_wall ) * speed ;
                        dQ_hr ( i ) = dQ_ht ( i ) + ( Vi ( i ) / (
gamma ( i ) - 1 ) ) * dP ( i ) + gamma ( i ) / ( gamma ( i ) - 1) * Pi
( i ) * dV ( i );
                    end
       filter = get( handles.filteronoff , 'Value' );  % 0 = OFF 1 = ON
                     if filter == 1
                         dQ_hr = csaps ( CAi(1:Ni-1),dQ_hr(1:Ni-1) ,
0.005 , CAi(1:Ni-1)) ;
                     end
                    cum = 0 ;
                    for i = 1 : 1 : Ni - 2
                        Q_hr( i ) = 1 / 2 * ( dQ_hr( i ) + dQ_hr( i + 1
) ) * istep ;
                         Q_ht( i ) = 1 / 2 * ( dQ_ht( i ) + dQ_ht( i +
1 ) ) * istep ;
                        cum = cum + Q_hr( i ) ;
                        Q_hr_cum( i ) = cum / Q ;
                    End
% Conversion to J (1000 factor)
                    dQ_hr = 1000 * dQ_hr ;        % Heat release
```

```
                    dQ_ht = 1000 * dQ_ht ;        % Heat transfer
                    Q_tot_ht = 1000*sum( Q_ht );  % Total heat transfer
                    Q_tot_hr = 1000 * sum( Q_hr );% Total heat release
                    Diff =( Q * 1000 - Q_tot_hr ) ;
% Heat Release at 10%, 50%, %90
                    for i = 1 : 1 : Ni - 3
                        if Q_hr_cum(i) <= 0.1 && Q_hr_cum(i + 1) > 0.1
                            CA_10 = CAi( i ) ;
                            Q_hr_cum_10 = Q_hr_cum( i ) ;
                        elseif Q_hr_cum(i)<= 0.5 && Q_hr_cum(i + 1)>0.5
                            CA_50 = CAi( i ) ;
                            Q_hr_cum_50 = Q_hr_cum( i ) ;
                        elseif Q_hr_cum(i)<=0.9 && Q_hr_cum(i + 1)>0.9
                            CA_90 = CAi( i ) ;
                            Q_hr_cum_90 = Q_hr_cum( i ) ;
                        end
                    end
% EIHCcrev CALCULATION
% Mass stored in the top land ring pack crevices
             [ P_max , imax ] = max ( P );% Peak Pressure
             CA_pmax  = CA ( imax ) ;     % Location of Peak Pressure
             CA_evc = tevc ;              % CA of exhaust valve closing
             CA_evo = tevo ;              % CA of exhaust valve opening
% Calling the RP2CR_GCR function
             [ m_out_CA90_evc , m_out_CA90_evo , m_stored_pmax ,  m_out
, m_in , m_blowby ] = RP2CR_GCR ( CA_90 , CA_evc , CA_evo, CA_pmax , d
, tx , RPM );
% Calling the RP2CR_GCR function
% Crevice emission index for each method of Calc.
             EIHC_crev_CA90_evc = m_out_CA90_evc / ( ( 1 + AF ) * m_fuel
) * 1000 ;                                    % in g/kg
             EIHC_crev_CA90_evo = m_out_CA90_evo / ( ( 1 + AF ) * m_fuel
) * 1000 ;                                    % in g/kg
             EIHC_crev_sto_pmax = m_stored_pmax / ( ( 1 + AF ) * m_fuel
) * 1000 ;                                    % in g/kg
% Time constant Tau for each method of Calc
             CA_tau_CA90_evc=tevc_tau-CA_90;% in degrees CA_evc=tevc_tau
             CA_tau_CA90_evo = tevo - CA_90;% in degrees CA_evo = tevc
             CA_tau_sto_pmax = tevo-CA_pmax;% in degrees CA_evo = tevo
             Tau_CA90_evc = CA_tau_CA90_evc / ( 6 * RPM ) ; % in seconds
             Tau_CA90_evo = CA_tau_CA90_evo / ( 6 * RPM ) ; % in seconds
             Tau_sto_pmax_evo = CA_tau_sto_pmax / ( 6 * RPM ) ; % in sec
% Maximun Temperature Calculation
             R_b = Ru / MW_exh ;           % Burned gases constant in
kJ/kg-K
             for i = 1 : Nd
                 Tm ( i ) = P ( i ) * V ( i ) / ( R_b * ( m_air + m_fuel
+ m_res ) ) ;               % Pressure in kPa
             end
             T_max = max(Tm); % Maximun temperature in the cylinder in K
% Piston mean speed
             Sp = 2 * stroke * RPM / 60 ;     % m/s
% Oxigen concentration at the exhaust calculated
             X_O2_calc = X_O2_calc ;
```

```
%------------------------------Output files ------------------------
            OHR{nf}=strcat('hr_',tx);
            fidO=fopen(OHR{nf},'wt');
            [qlr,qlc]=size(tx);
            TX=tx(3:(qlc-4));
            fprintf(fidO, 'CA_hr_'); fprintf(fidO, TX); fprintf(fidO,
'\t\t');
            fprintf(fidO, 'dQ_hr_'); fprintf(fidO, TX); fprintf(fidO,
'\t\t\t');
            fprintf(fidO, 'dQ_ht_'); fprintf(fidO, TX); fprintf(fidO,
'\t\t\t');
            fprintf(fidO, 'Q_hr_cum_'); fprintf(fidO, TX);
            fprintf(fidO, '\n');
            for v=1:Ni-2
                fprintf(fidO, '%3.3f\t\t\t', CAi(v));
                fprintf(fidO, '%g\t\t\t', dQ_hr(v));
                fprintf(fidO, '%g\t\t\t', dQ_ht(v));
                fprintf(fidO, '%g\t\t\t', Q_hr_cum(v));
                fprintf(fidO, '\n');
            end
            fclose(fidO);
            fprintf(fida, tx);   fprintf(fida, '\t');
            fprintf(fida, '%g\t', Q*1000);
            fprintf(fida, '%g\t', Q_tot_ht);
            fprintf(fida, '%g\t', Q_tot_hr);
            fprintf(fida, '%g\t', y_res);
            fprintf(fida, '%g\t', y_res_int);
            fprintf(fida, '%g\t', HT);
            fprintf(fida, '%g\t', CA_10);
            fprintf(fida, '%g\t', CA_50);
            fprintf(fida, '%g\t', CA_90);
            fprintf(fida, '%g\t', CA_evc);
            fprintf(fida, '%g\t', CA_pmax);
            fprintf(fida, '%g\t', EIHC_exh);
            fprintf(fida, '%g\t', EIHC_crev_CA90_evc);
            fprintf(fida, '%g\t', EIHC_crev_CA90_evo);
            fprintf(fida, '%g\t', EIHC_crev_sto_pmax);
            fprintf(fida, '%g\t', P_max);
            fprintf(fida, '%g\t', P_evc);
            fprintf(fida, '%g\t', T_max);
            fprintf(fida, '%g\t', Tau_CA90_evc);
            fprintf(fida, '%g\t', Tau_CA90_evo);
            fprintf(fida, '%g\t', Tau_sto_pmax_evo);
            fprintf(fida, '%g\t', X_O2);
            fprintf(fida, '%g\t', X_O2_calc);
            fprintf(fida, '%g\t', m_blowby);
            fprintf(fida, '\n');
%---------------------- Plots ---------------------
           figure        % Heat Release,Cum. Heat Release,Heat Transfer
           hold on; axis on; grid on; box on;
           [AX,H1,H2] = plotyy(CAi(1:Ni-1),dQ_hr(1:Ni-1),CAi(1:Ni-
2),Q_hr_cum(1:Ni-2),'plot');
           set(get(AX(1),'Ylabel'),'String','dQ-hr')
           set(get(AX(2),'Ylabel'),'String','Q-hr-cum (J/J/deg)')
```

```
            t1=title(['Heat Release and Heat Transfer @ ',TX]);
            xlabel('CA');ylabel('dQ-ht , dQ-ht  (J/deg)');
            hold on
            plot(CAi(1:Ni-1),dQ_ht(1:Ni-1),'Color',[0 0.5 0]);
            plot(CAi(1:Ni-1),dQ_ht(1:Ni-1),'r');
            legend('dQ-hr','Q-hr-cum','dQ-ht');
            else
                 errordlg('Parameters must be numeric','Error');
            end
            end
        else
             errordlg('Table should be filled correcty','Error');
        end
    end
    fclose(fida);
else
    errordlg('Table should be filled','Error');
end
toc
set(handles.text36, 'String', toc);
set(handles.calculate, 'Enable', 'on');
set(handles.reset, 'Enable', 'on');
%========END OF DATA PROCESSING========
```

APPENDIX XV - SINGLE CYCLE RING PACK CONTRIBUTION

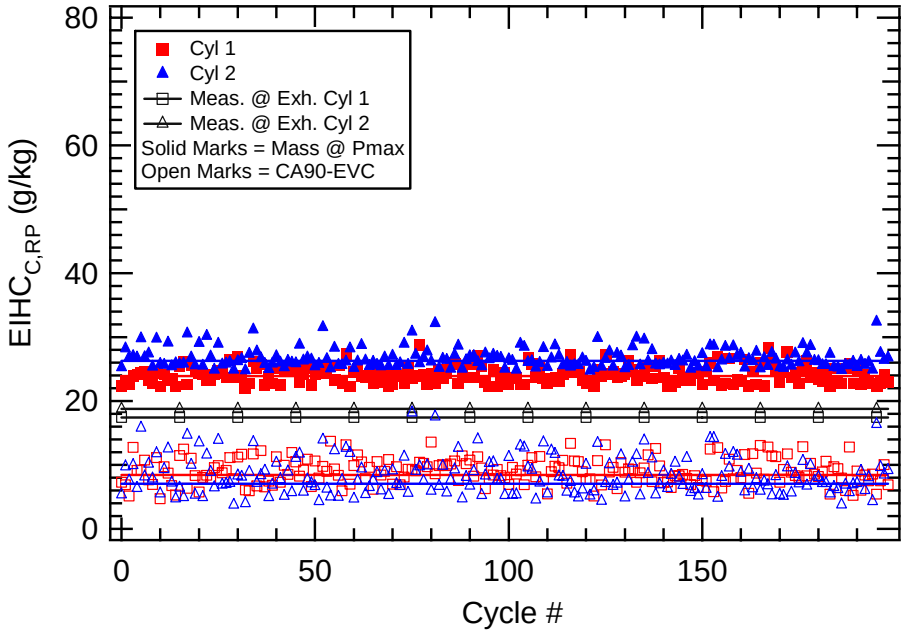

Figure A15.1 EIHC predicted by the ring pack model from single cycle analysis for 1750 RPM, 10% load, AF13

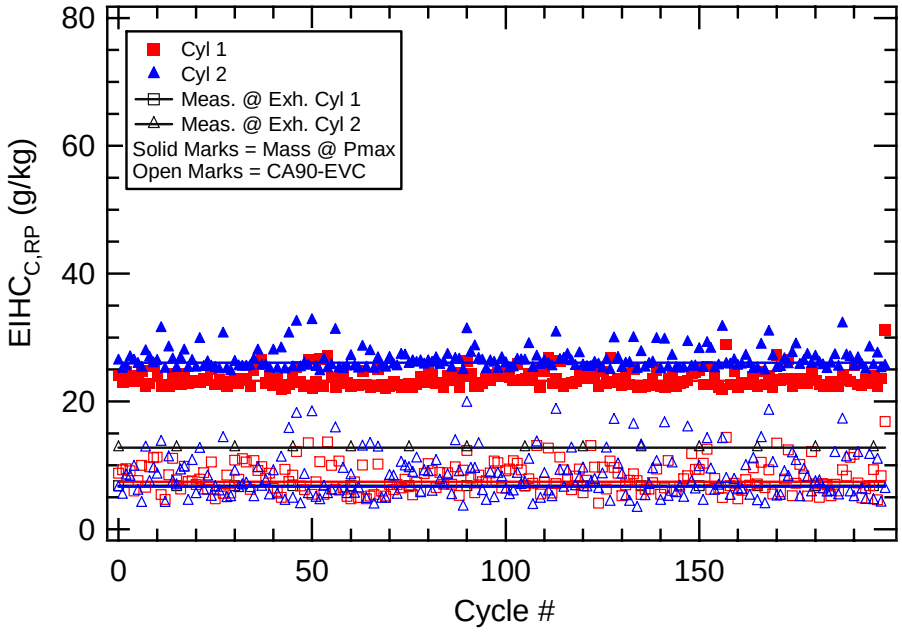

Figure A15.2 EIHC predicted by the ring pack model from single cycle analysis for 1750 RPM, 10% load, AF14

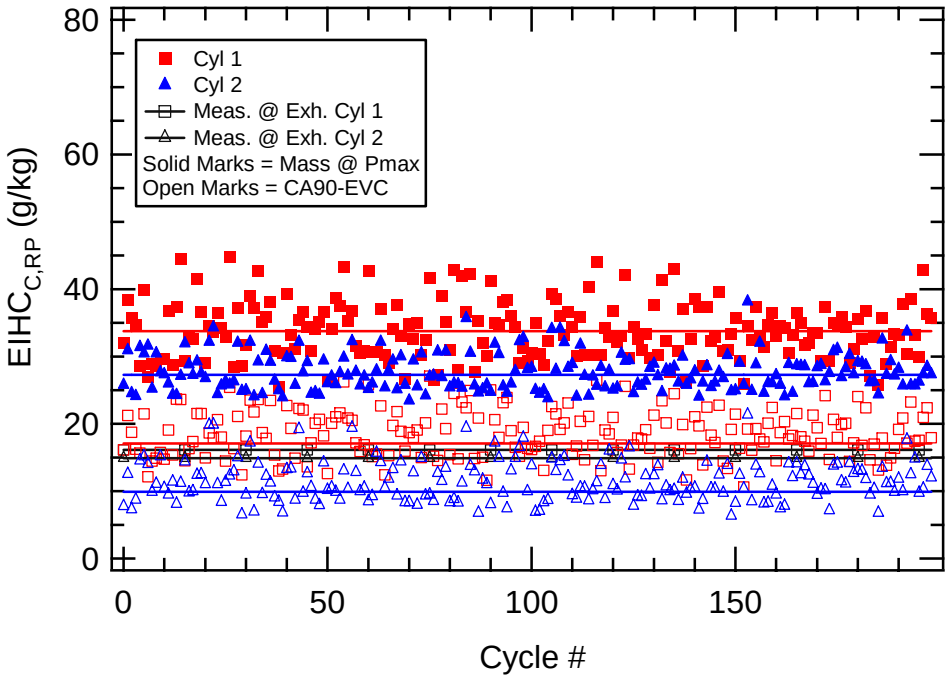

Figure A15.3 EIHC predicted by the ring pack model from single cycle analysis for 1750 RPM, 25% load, AF13

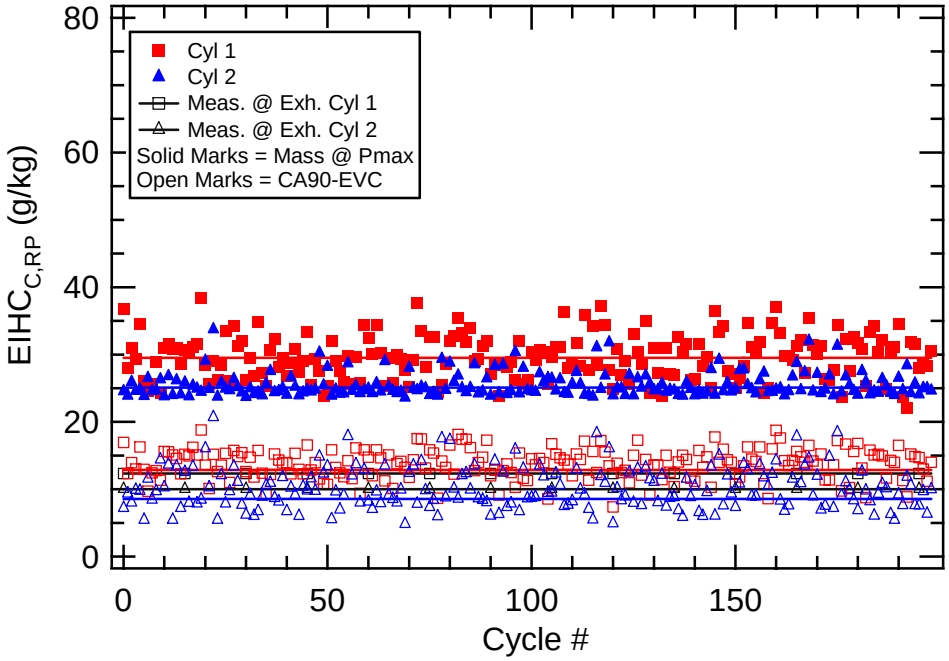

Figure A15.4 EIHC predicted by the ring pack model from single cycle analysis for 1750 RPM, 25% load, AF14

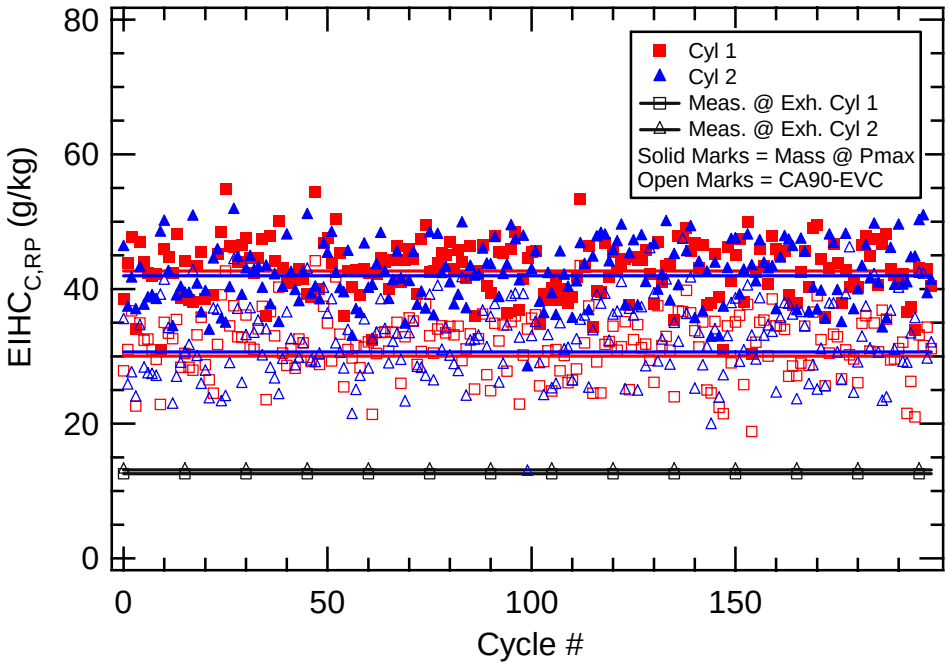

Figure A15.5 EIHC predicted by the ring pack model from single cycle analysis for 3060 RPM, 25% load, AF11

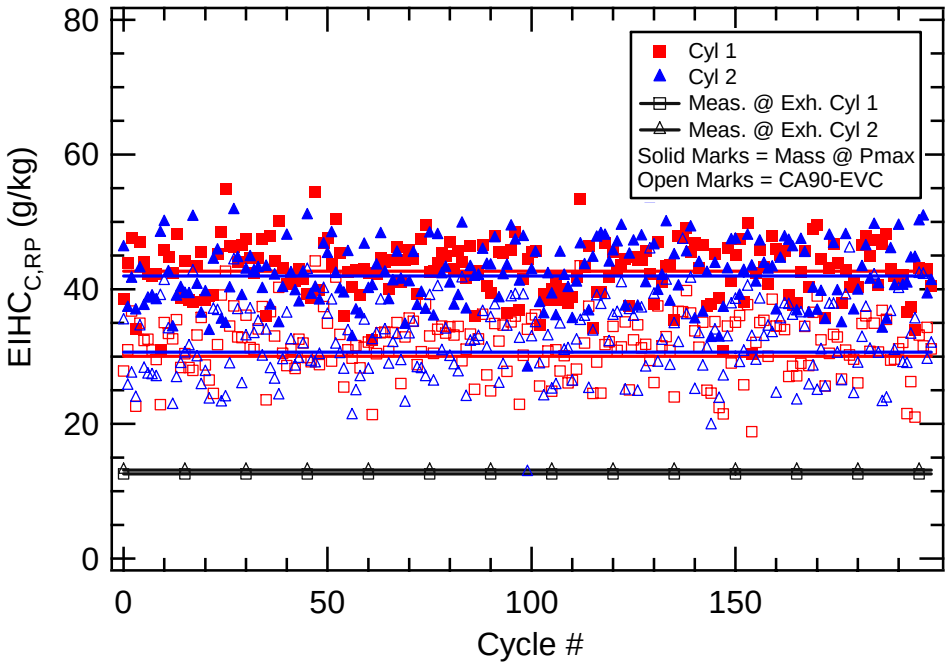

Figure A15.6 EIHC predicted by the ring pack model from single cycle analysis for 3060 RPM, 50% load, AF11

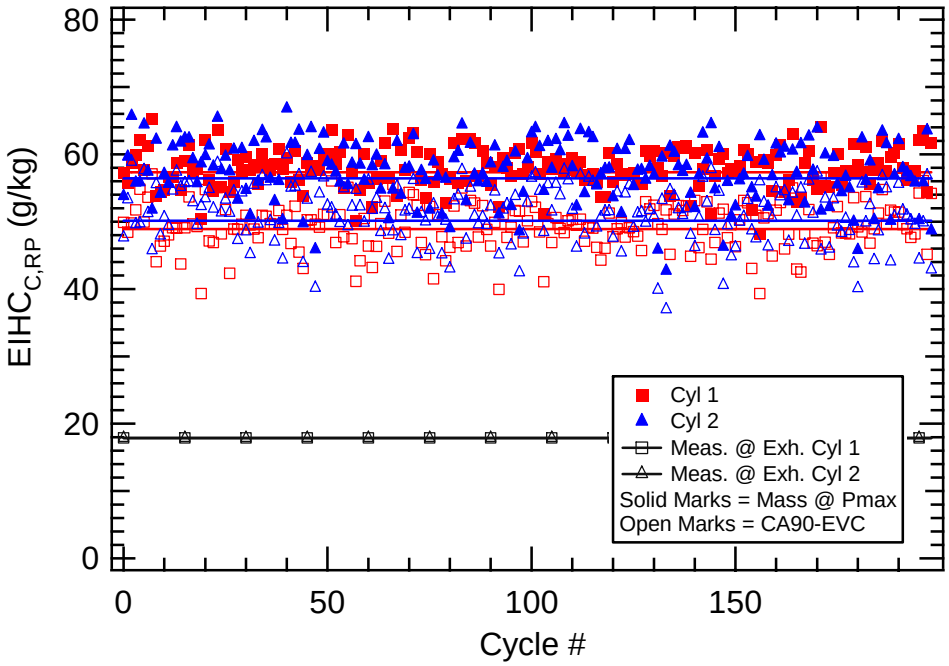

Figure A15.7 EIHC predicted by the ring pack model from single cycle analysis for 3060 RPM,100% load, AF11

APPENDIX XVI - SINGLE CYCLE RESOLVED HC EMISSIONS

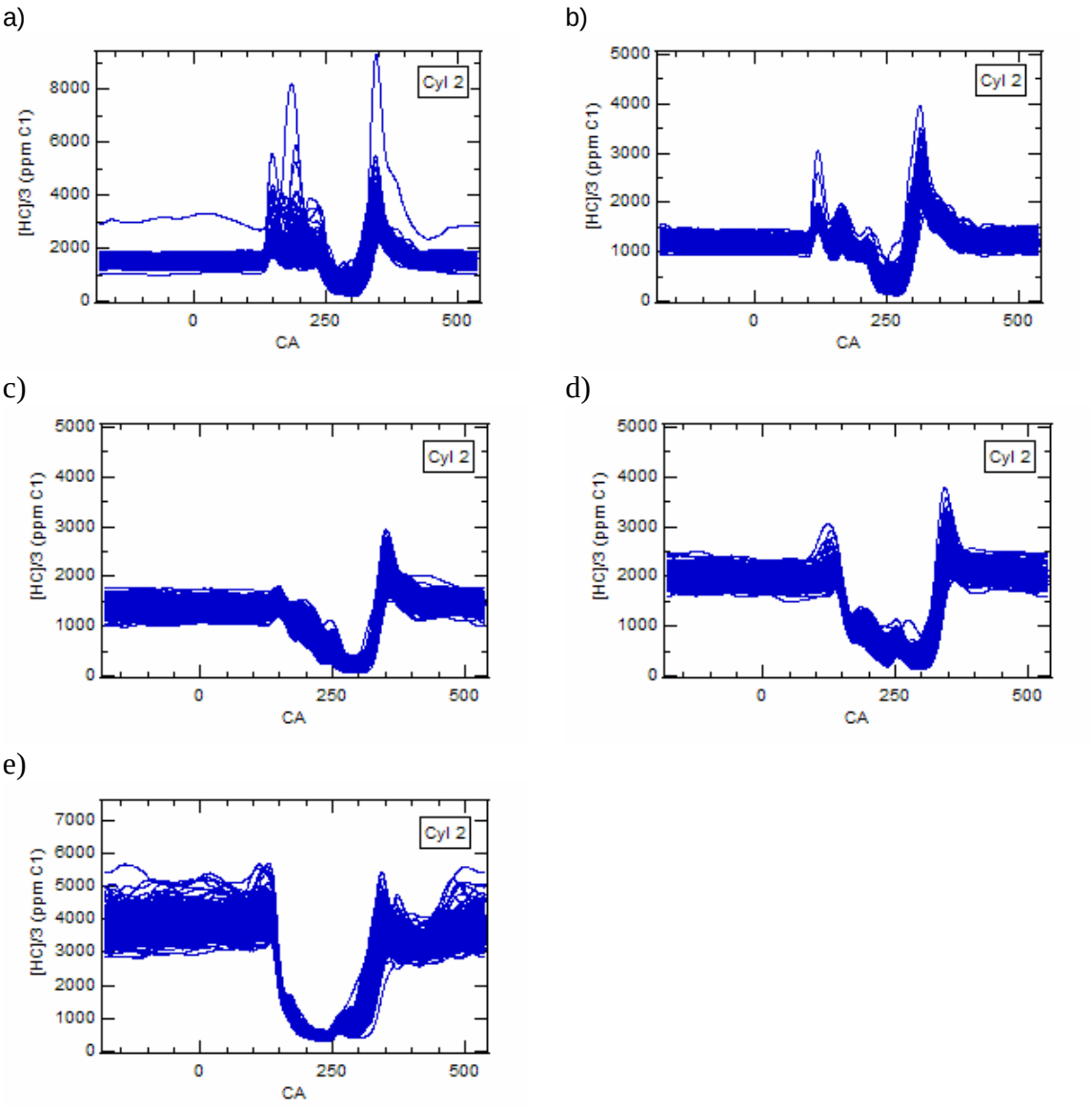

Figure A16.1 Single-cycle resolved HC measurements for cylinder 2 at (a) 1750 RPM, 10% load, AF13, (b) 1750 RPM, 25% load, AF 13, (c) 3060 RPM, 25% load, AF13, (d) 3060 RPM, 50% load, AF13, and 3060 RPM, 100% load, AF13

APPENDIX XVII – MASS BALANCE AT THE EXHUAST

```
% The input parameters for this program were provided via a GUI
% BEGGINNING OF DATA PROCESSING
% Known Parameters
    resolution_index = get(handles.eresolution, 'Value');
    pressured_index = get(handles.pressured, 'Value');
    C2 = handles.metricdata.e_velocity;     % Expansion Velocity in the
Heat Transfer Coefficient
    if resolution_index == 1                % Encoder Resolution
        enc_res = 1;
    elseif resolution_index == 2
        enc_res = 0.5;
    elseif resolution_index == 3
        enc_res = 0.25;
    end
    istep=0.25;                             % Integration Step
 % Header of the ExMass_ADD_INFO.txt Output file
    fida = fopen('ExHCMass_AVG_PH_ADD_INFO.txt','wt') ;
    fprintf(fida, 'FileName'); fprintf(fida, '\t');
    fprintf(fida, 'm_exh_tot_calc (kg/cyc)'); fprintf(fida, '\t');
    fprintf(fida, 'm_tot_meas (kg/cyc)'); fprintf(fida, '\t');
    fprintf(fida, 'm_air_meas (kg/cyc)'); fprintf(fida, '\t');
    fprintf(fida, 'm_fuel_meas (kg/cyc)'); fprintf(fida, '\t');
    fprintf(fida, 'm_HC_exh_calc(kg/cyc)'); fprintf(fida, '\t');
    fprintf(fida, 'EIHC_meas (g/kg)'); fprintf(fida, '\t');
    fprintf(fida, 'EIHC_calc (g/kg)'); fprintf(fida, '\t');
    fprintf(fida, 'k'); fprintf(fida, '\t');
    fprintf(fida, 'P_exh_off'); fprintf(fida, '\t');
    fprintf(fida, 'Tevo'); fprintf(fida, '\t');
    fprintf(fida, '\n');
    for nf = 1 : nlines
        DT = TData{ nf } ;
        for dd = 1 : 13
          comp1( dd ) = strcmp( DT ( dd ) , str ) ;
        end
        if  comp1(1) == 0 & comp1(2) == 0 & comp1(3) == 0 & comp1(4) ==
0 & comp1(5) == 0 & comp1(6) == 0 & comp1(7) == 0 & comp1(8) == 0 &
comp1(9) == 0 & comp1(10) == 0 & comp1(11) == 0 & comp1(12) == 0&
comp1(13) == 0
            tx = DT( 1 ) ;
            tstart = handles.metricdata.sangle ; % Start Angle
            tend = handles.metricdata.eangle ;   % End Angle
            tivc = handles.metricdata.ivcv ;     % IVC timing - aTDC
            tevo = handles.metricdata.evov ;     % EVO timing - aTDC
            tevc = handles.metricdata.evcv ;     % EVC timing
            LHV = handles.metricdata.lhvv ;      % LHV(kJ/kg)
            D = handles.metricdata.borev ;       % Bore(m)
            stroke = handles.metricdata.strokev ;% Stroke(m)
            T_wall = handles.metricdata.twallv ; % T_wall(° K)
            tn_2=-30;                            % CA of 2nd point to
calcualte the polytropic index n
```

```
            tevc_tau = tevc ;                    % Tau
% File name concatenation
            [ nrtx , nctx ] = size ( tx ) ;      % Filename string size
            TX1 = tx ;
            rtx = tx ( 5 : nctx );               % Root Filename
            if tx(3)=='2'
                tx = strcat('O2_',rtx);          % Output Filename with
all data
            else
                tx = strcat('O1_',rtx);
            end
% Reading the main file with the Pressures and FFID info
           [hdrOfile, d] = hdrload(tx);          % Reading file
% Reading the Parameters of the table for each file from the table
            eta = str2num( DT( 2 ) ) ;           % eff._comb
            m_air = str2num( DT( 3 ) ) ;         % mass_air(kg/cycle)
            m_fuel = str2num( DT( 4 ) ) ;        % mass_fuel(kg/cycle)
            RPM = str2num( DT( 5 ) ) ;           % RPM
            T_exh = str2num( DT( 6 ) ) ;         % T_exhaust (°K)
            T_int = str2num( DT( 7 ) ) ;         % T_intake(  °K)
            X_O2_calc = str2num( DT( 8 ) ) ;     % Molar fraction O2
calc
            EIHC_exh = str2num(DT(9));           % Emissions index HC
(g/kg)
            MW_exh = str2num( DT( 10 ) ) ;       % Molecular weight
            AF = str2num(DT(11));                % Air fuel ratio (kg
air / kg fuel)
            X_O2 = str2num( DT( 12 ) ) ;         % Oxygen mole fraction
            EGR = str2num( DT( 13 ) ) ;          % EGR concentration
% Checking the GUI table inputs
            ee = isempty( eta );  mm = isempty( m_air );  mf = isempty(
m_fuel );  tin = isempty( T_int );
            rpp = isempty( RPM );  tex = isempty( T_exh );  mfocalc =
isempty( X_O2_calc );  eihcex = isempty( EIHC_exh );
            mwex = isempty( MW_exh );  afm = isempty( AF );  mfo =
isempty( X_O2 ); egr1 = isempty( EGR);
            if ee == 0 & mm == 0 & mf == 0 &rpp == 0 & tex == 0 &
mfocalc == 0 & eihcex == 0 & tin == 0 & mwex == 0 & afm == 0 & mfo == 0
& egr1 == 0
% Constants
                Ru = 8314 ;                      % Universal Gas
Constant J/kmol-K
                MW_air = 28.90 ;                 % Air molar mass
kg/kmol
                R= Ru / MW_air ;                 % Air constant, J/kg-K
                gamma = 1.4;    % Specific Heat Ratio for exhaust gases
% Vectors with data from the Output file
                 CA = d ( : , 1 ) ;              % Crank angle vector
                 V = d ( : , 2 ) ;               % Cyl.1 volume m^3
                 P = 1000 * d ( : , 3 ) ;        % Pressure Cylinder 1
in Pa
                 EP = 1000 * d ( : , 4 ) ;       % Exhaust Pressure Cyl
1, and with correction for cyl 2
```

```
                HCFFID=d(:,5);                  % Fast FID data ppm/3
of CH, or ppm C3
                [ Nd , f ] = size( d ) ;        % Data matrix size
                enc_res=d(2,1)-d(1,1);          % Encoder res from the
input data file
% Reading of the Valve Profile file EVL.txt
                [hdrEVL, LEV] = hdrload('EVL.txt'); % File with lift
in mm
                [ revl , cevl ] = size( LEV) ; % Data matrix size
                CAl  = LEV ( : , 1 );           % Crank angle exhaust
valve lift, deg
                evlift = LEV ( : , 2 ) ;        % Exhaust valve lift,mm
% Reading of the discharge coefficient file CD_ev.txt
                [hdrCD, Cdm]=hdrload('CD_ev.txt'); % File with the
Cd=Cd(Lv/Dv)
                [ rCd , cCd ] = size( Cdm ) ;  % Data matrix size
                LvDv = Cdm ( : , 1 );  % Lv/Dv for the valve
                Cd = Cdm ( : , 2 );    % Discharge coef. exhaust valve
% Calc.of the curtain area Ac, Lv/Dv and interpol. of Cd
                Dv = 29.5 ;             % Valve diameter in mm
                for i = 1 : (revl - 1 )* 2  / enc_res + 1
                    CAi ( i ) = ( i -1 ) * enc_res ;
                    LEVi ( i ) = interp1 ( CAl, evlift , CAi ( i ) ,
'linear' ) ;                                % Lift in mm
                    Lv_Dv ( i ) = LEVi(i)/Dv ; % mm
                    Ac ( i ) = pi * Dv * LEVi ( i ) * 1e-6 ; % Area in
m^2
                    Cdi ( i ) = interp1 ( LvDv , Cd , Lv_Dv ( i ),
'spline') ;
                end
% Pegging CA to the evo event
  CAshift=27; % Based in the 0.008 in criteria for open and close valve
% Cylinder and Exhaust Pressures in the integration window
                for i = 1 : (revl - 1 )* 2  / enc_res + 1
                    CAint ( i ) =  CA ( ( 180 + tevo - CAshift ) /
enc_res +  i ) ;
                    Pi ( i ) =  P ( ( 180 + tevo - CAshift ) / enc_res
+ i )  ;
                    EPi ( i ) = EP ( ( 180 + tevo - CAshift ) /
enc_res + i ) ;
                    HCFFIDi ( i ) = HCFFID ( ( 180 + tevo - CAshift )
/ enc_res + i ) ;
                 end
% Calculation of Additional Parameters
dCAint=CAint(1,2)-CAint(1,1);       % CA step integration, in Crank
Angle
dt=dCAint/(6*RPM);                  % Integration time step in sec for
each file changes with the velocity
vpsize=(revl-1)* 2  / enc_res + 1 ; % Size of the integration vector
% Volume and Pressure at evo and evc conditions Cyl1 and Cyl2
V_ivc=interp1(CA,V,tivc,'spline');                % m^3
V_evo=interp1(CA,V,tevo,'spline');                % m^3
V_evc=interp1(CA,V,tevc,'spline');                % m^3
P_evo=interp1(CA,P,tevo,'spline');                % Pa
```

```
P_ivc=interp1(CA,P,tivc,'spline');                % Pa
P_evc=interp1(CA,P,tevc,'spline');                % Pa
% Parameters at evo for the integration
P_evoi=interp1 (CA , P , CAint(1) , 'spline');    % in kPa
V_evoi=interp1 (CA , V , CAint( 1 ) , 'spline');  % m^3
% Pres. and Vol. to calc. compression politropic coefficient
P_1 = interp1( CA , P , tivc + 5 , 'spline') ;
P_2 = interp1( CA , P , tn_2 , 'spline') ;
V_1 = interp1( CA , V , tivc + 5 , 'spline') ;
V_2 = interp1( CA , V , tn_2 , 'spline') ;
n_comp = log( P_2 / P_1 ) / log( V_1 / V_2 ) ;
% Residual Mass Calculation
y_res_int1 = ( V_evc / V_evo ) * ( P_evc / P_evo ) ^ ( 1 / n_comp ) ;
% Calcualtion of the mass trapped
m_trapped1 = ( m_air + m_fuel ) * ( 1 + ( EGR / 100 ) / ( 1 - EGR / 100
) ) / ( 1 - y_res_int1 );
m_res_int1 = y_res_int1 * m_trapped1 ;
m_res_ext1 = m_trapped1-m_res_int1 - (m_air + m_fuel )
m_res1 = m_res_int1 + m_res_ext1 ;
y_res1 = m_res1 / m_trapped1 ;
% Blowdown Temperature Approximation
R_b = Ru / MW_exh ;                    % Burned gases constant in J/kg-K
Tevo1 = P_evoi * V_evoi / ( R_b * ( m_air + m_fuel + m_res1 ) ) ;   %
Tevo in K, Cyl. 1
                for i = 1 : (revl - 1 )* 2  / enc_res + 1
                    Tbd ( i ) = Tevo1 * ( Pi ( i ) / P_evoi ) ^ ( (
gamma - 1 ) / gamma );                 % Blow.Temp. Cyl. 1
                end
% Mass Flow through the exhaust valve
PRc=(2/(gamma+1))^(gamma/(gamma-1));  % Choke flow criteria
diff = 1 ;                             % Mass difference = abs (
calculated - measured), used for stop criteria
dPexh = 0.01 * 1e3 ;                   % Increse in exhaust pressure to
match the mass per cycle
k = 0 ;                                % Number of iteration required to
match the mass of the cylinder
dPup = 0 ;                             % Total increse in pressure to
match the meas. mass, in kPa
dPdown = 0 ;                           % Total decrease in pressure to
match the meas. mass, in kPa
                 while abs(diff) > 1e-6 && k < 5000  % Criteria to stop
the loop Cyl. 1
% Mass calculation - Cyl. 1
                  for i = 1 : (revl - 1 )* 2  / enc_res + 1
                    if Pi( i ) >= EPi( i )
                     if EPi( i ) / Pi( i ) < 0.52
                        eta1 = ( 2 / ( gamma + 1 ) ) ^ ( ( gamma + 1 )
/ ( 2 * ( gamma - 1 ) ) );
                     else
                        eta1 = ( 2 / ( gamma - 1 ) * ( ( EPi( i ) /
Pi( i ) ) ^ ( 2 / gamma ) - ( EPi( i ) / Pi( i ) ) ^( ( gamma + 1 ) /
gamma ) ) ) ^ 0.5 ;
                     end
```

```
                                    me ( i ) = Cdi ( i ) * Ac ( i ) * (
sqrt ( gamma / ( R_b * Tbd ( i )  ) ) * Pi ( i ) ) * eta1 ;
                    else
                     if Pi( i ) / EPi( i ) < 0.52
                        eta2i = ( 2 /( gamma + 1 ) ) ^ ( ( gamma + 1 )
/ ( 2 * ( gamma - 1 ) ) ) ;
                     else
                        eta2i = ( 2 / ( gamma - 1 ) * ( ( Pi( i ) /
EPi( i ) ) ^ ( 2 / gamma ) - ( Pi( i ) / EPi( i ) ) ^ ( ( gamma + 1 ) /
gamma ) ) ) ^ 0.5 ;
                     end
                                    me ( i ) = -Cdi ( i ) * Ac ( i ) *
(sqrt ( gamma /( R_b * Tbd ( i ) ) )* EPi( i ) )* eta2i ;
                     end
                    end
% Exh. mass per cycle Calc. Cyl. 1
                    for i = 1 : (revl - 1 )* 2  / enc_res
                        dme1( i ) = ( me ( i ) + me ( i + 1 ) ) / 2 *
dt ;  % Differetial of mass
                    end
                    m_exh_cycle1_calc = sum ( dme1 ) ; % Total mass
per cycle in kg, Cyl. 1
% if condition to match the measured mass flow
                    diff =  ( m_air + m_fuel ) - m_exh_cycle1_calc ;
                    if diff < 0
                       EPi = EPi + dPexh ;
                       dPup = dPup + dPexh ;
                    elseif diff > 0
                       EPi = EPi - dPexh ;
                       dPdown = dPdown + dPexh ;
                    end
                       k = k + 1 ;
                       Diff ( k ) = abs ( diff ) ;
                       K ( k ) = k ;
                   end
% Calculation of Mass Fuel
y = 1.804 ;
MW_C = 12.011 ;                     % Carbon Molecular Weigth
MW_H = 1.0079 ;                     % Hydrogen Molecular Weigth
MW_fuel = 12.011 + 1.0079 * y ;     % Fuel Molecular weight C1 based
for i = 1 : (revl - 1 )* 2  / enc_res + 1  % Calculation of the fuel
mass flow Cyl. 1
    HCFFID_mf ( i ) = 3 / 1000000 * HCFFIDi ( i )  ; % HC molar
fraction at the exhaust
    mfuel ( i ) = HCFFID_mf ( i ) * ( MW_fuel ) / ( MW_exh ) *  me ( i
) ;                                         % Fuel mass flow
end
for i = 1 : (revl - 1 )* 2  / enc_res
    dm_fuel1( i ) = ( mfuel ( i ) + mfuel ( i + 1 ) ) / 2 * dt ;
% Fuel mass differential
end
m_fuel1_total_calc = sum ( dm_fuel1 ) ;     % Total fuel per cycle in
Kg, Cyl. 1
```

```
EIHC_calc = m_fuel1_total_calc / m_fuel * 1000 ;  % Emission index in
g/kg_fuel
EIHC_meas = EIHC_exh ;                          % EIHC measured
%-------------------End of fue mass calculation ---------------------
me = 1000* me ;                         % Exhaust mass flow in g/s Cyl. 1
m_total_measured=(m_air + m_fuel);    % Total exh. mass measured
EP1i_offset = dPup -dPdown ;
%-------------------Output files ----------------------
if tx(2)=='2'
   OHR{nf}=strcat('EHCM2_',rtx);
   fidO=fopen(OHR{nf},'wt');
   TX = rtx;
   fprintf(fidO, 'CA2_'); fprintf(fidO, TX); fprintf(fidO, '\t');
   fprintf(fidO, 'Tbd2_'); fprintf(fidO, TX); fprintf(fidO, '\t');
   fprintf(fidO, 'P2_'); fprintf(fidO, TX); fprintf(fidO, '\t');
   fprintf(fidO, 'Pe2_'); fprintf(fidO, TX); fprintf(fidO, '\t');
   fprintf(fidO, 'm2_'); fprintf(fidO, TX); fprintf(fidO, '\t');
   fprintf(fidO, 'm_HCexh2_'); fprintf(fidO, TX);
   fprintf(fidO, '\n');
   for v = 1 : (revl - 1 )* 2  / enc_res + 1
       fprintf(fidO, '%3.3f\t', CAint(v));
       fprintf(fidO, '%g\t', Tbd(v));
       fprintf(fidO, '%g\t', Pi(v));
       fprintf(fidO, '%g\t', EPi(v));
       fprintf(fidO, '%g\t', me(v));
       fprintf(fidO, '%g\t', mfuel(v));
       fprintf(fidO, '\n');
   end
   fclose(fidO);
else
   OHR{nf}=strcat('EHCM1_',rtx);
   fidO=fopen(OHR{nf},'wt');
   TX = rtx;
   fprintf(fidO, 'CA1_'); fprintf(fidO, TX); fprintf(fidO, '\t');
   fprintf(fidO, 'Tbd1_'); fprintf(fidO, TX); fprintf(fidO, '\t');
   fprintf(fidO, 'P1_'); fprintf(fidO, TX); fprintf(fidO, '\t');
   fprintf(fidO, 'Pe1_'); fprintf(fidO, TX); fprintf(fidO, '\t');
   fprintf(fidO, 'm1_'); fprintf(fidO, TX); fprintf(fidO, '\t');
   fprintf(fidO, 'm_HCexh1_'); fprintf(fidO, TX);
   fprintf(fidO, '\n');
   for v = 1 : (revl - 1 )* 2  / enc_res + 1
       fprintf(fidO, '%3.3f\t', CAint(v));
       fprintf(fidO, '%g\t', Tbd(v));
       fprintf(fidO, '%g\t', Pi(v));
       fprintf(fidO, '%g\t', EPi(v));
       fprintf(fidO, '%g\t', me(v));
       fprintf(fidO, '%g\t', mfuel(v));
       fprintf(fidO, '\n');
    end
    fclose(fidO);
end
% ExHCMass_AVG_PH_ADD_INFO.txt
fprintf(fida, TX1 );
fprintf(fida, '\t');
```

```
fprintf(fida, '%g\t', m_exh_cycle1_calc);
fprintf(fida, '%g\t', m_total_measured);
fprintf(fida, '%g\t', m_air);
fprintf(fida, '%g\t', m_fuel);
fprintf(fida, '%g\t', m_fuel1_total_calc);
fprintf(fida, '%g\t', EIHC_meas);
fprintf(fida, '%g\t', EIHC_calc);
fprintf(fida, '%g\t', k);
fprintf(fida, '%g\t', EP1i_offset);
fprintf(fida, '%g\t', Tevo1);
fprintf(fida, '\n');
oplots = 1 ;
if oplots == 1 ;
   if tx(2)=='2'
      figure
      plot ( Diff)
      legend ( 'Error Cyl 2')
      xlabel ('k'); ylabel('Error-Cyl. 2');
      figure
      plot(CAint,Pi,CAint,EPi)
      legend('P2','P_exh2')
      xlabel('CA');ylabel('Pressure(kPa)');
      figure
      plot(CAint,mfuel)
      legend('Fuel mass flow Cyl. 2')
      xlabel('CA');ylabel('fuel mass flow');
      figure
      plot(CAint,me,CAint,HCFFIDi )
      legend('mexh-2', 'FFID2')
      xlabel('CA');ylabel('Exhaust Mass Flow Cyl. 2 (g/s)');
      figure
      plot(CAint,Tbd)
      legend('Texh-2')
      xlabel('CA');ylabel('Exhaust Temperature Cyl.2 (K)');
    else
      figure
      plot ( Diff)
      legend ( 'Error cyl 1')
      xlabel ('k'); ylabel('Error-Cyl. 1');
      figure
      plot(CAint,Pi,CAint,EPi)
      legend('P1','P_exh1')
      xlabel('CA');ylabel('Pressure(kPa)');
      figure
      plot(CAint,mfuel)
      legend('Fuel mass flow Cyl. 1')
      xlabel('CA');ylabel('fuel mass flow');
      figure
      plot(CAint,me,CAint,HCFFIDi )
      legend('mexh-1','FFID1')
      xlabel('CA');ylabel('Exhaust Mass Flow Cyl. 1 (g/s)');
      figure
      plot(CAint,Tbd)
      legend('Texh-1')
```

```
      xlabel('CA');ylabel('Exhaust Temperature Cyl.1 (K)');
     end
   end
   else
      errordlg('Parameters must be numeric','Error');
   end
   else
      errordlg('Table should be filled correcty','Error');
   end
   end
      fclose(fida);
else
   errordlg('Table should be filled','Error');
end
toc
set(handles.text36, 'String', toc);
set(handles.calculate, 'Enable', 'on');
set(handles.reset, 'Enable', 'on');
%========END OF DATA PROCESSING========
```

APPENDIX XVIII – OIL-FUEL DIFFUSION

```
%-----Oil Film -Cycle Simulation-Multicomponent Main Calculation------
%   Written by: Victor M. Salazar
%   ERC-UW Madison
%   June 12, 2008
clc
tic

%Known Parameters
Tw = 380 ;      % Cylinder Wall Temperature in K
th = 2e-6 ;      Oil layer thickness in m
RPM = 3060 ;    % Engien Speed in RPM

%------Diffusivity Calculation---------
%---- Estimation of the liquid molar volume at the normal boiling
point----
%This was performed usign the Tyn and Calus Method (1975), pg. 4.33,
%Eq. (4-10.2) from " The Properties of Gases and Liquids " by
%Poling, B., Prausnitz, J. M., and O'connell, J.P., 5th Edition.
% Critical Volumes (cm^3/g-mol) extracted from the SUPERTRAPP PORTLIB
% file, 1st row, second column

    Vc_C3H8 = 200 ;     % critical volume (cm^3/mol) of Propane"
    Vc_C5H12 = 306 ;    % critical volume (cm^3/mol) of "I-Pentane"
    Vc_C6H14 =  367 ;   % critical volume (cm^3/mol) of "3-
Methylpentane"
    Vc_C6H6 = 259 ;     % critical volume (cm^3/mol) of "Benzene"
    Vc_C7H16 = 431.97 ; % critical volume (cm^3/mol) of "N-Heptane"
    Vc_C7H8 = 316 ;     % critical volume (cm^3/mol) of "Toluene"
    Vc_C8H18 = 468 ;    % critical volume (cm^3/mol) of "I-Octane"
    Vc_C8H10m = 376 ;   % critical volume (cm^3/mol) of "m-Xylene"
    Vc_C8H10p = 379 ;   % critical volume (cm^3/mol) of p-Xylene
[kg/kmol]
    Vc_C9H12 = 427.35 ;  % critical volume (cm^3/mol) of 1,2,4
Trimethylbenzene [kg/kmol]
    Vc_C10H22 = 600 ;   % critical volume (cm^3/mol) of N-Decane
[kg/kmol]
    Vc_C12H26 = 719.7 ; % critical volume (cm^3/mol) of N-Dodecane
[kg/kmol]

    %--Liquid molar volume at the normal boiling point (cm^/mol)

    VA_C3H8 = 0.258 * Vc_C3H8 ^ 1.048 ;     % Liq. molar vol. @ NBP
(cm^3/mol) of Propane"
    VA ( 1,1 ) = 0.258 * Vc_C5H12 ^ 1.048 ;   % Liq. molar vol. @ NBP
(cm^3/mol) of "I-Pentane"
    VA ( 2,1 ) = 0.258 * Vc_C6H14 ^ 1.048 ;   % Liq. molar vol. @ NBP
(cm^3/mol) of "3-Methylpentane"
    VA ( 3,1 ) = 0.258 * Vc_C6H6 ^ 1.048 ;    % Liq. molar vol. @ NBP
(cm^3/mol) of "Benzene"
```

```
    VA ( 4,1 ) = 0.258 * Vc_C7H16 ^ 1.048 ;   % Liq. molar vol. @ NBP
(cm^3/mol) of "N-Heptane"
    VA ( 5,1 ) = 0.258 * Vc_C7H8 ^ 1.048 ;     % Liq. molar vol. @ NBP
(cm^3/mol) of "Toluene"
    VA ( 6,1 ) = 0.258 * Vc_C8H18 ^ 1.048 ;    % Liq. molar vol. @ NBP
(cm^3/mol) of "I-Octane"
    VA ( 7,1 ) = 0.258 * Vc_C8H10m ^ 1.048 ;  % Liq. molar vol. @ NBP
(cm^3/mol) of "m-Xylene"
    VA ( 8,1 ) = 0.258 * Vc_C8H10p ^ 1.048 ;  % Liq. molar vol. @ NBP
(cm^3/mol) of p-Xylene [kg/kmol]
    VA ( 9,1 ) = 0.258 * Vc_C9H12 ^ 1.048 ;   % Liq. molar vol. @ NBP
(cm^3/mol) of 1,2,4 Trimethylbenzene [kg/kmol]
    VA ( 10,1 ) = 0.258 * Vc_C10H22 ^ 1.048 ;   % Liq. molar vol. @ NBP
(cm^3/mol) of N-Decane [kg/kmol]
    VA ( 11,1 ) = 0.258 * Vc_C12H26 ^ 1.048 ; % Liq. molar vol. @ NBP
(cm^3/mol) of N-Dodecane [kg/kmol]

    [ncr, ncc ] = size (VA) ;

%------Input parameters to calculate the Concentration at the interface
(B.C.)---------

    phi = 1.2;                                %"Equivalence Ratio"
    T = Tw ; %380 ;                           %[K]
    m_fuelcyc = 15.902e-6 ;                   %"Mass of fuel per
cycle"[kg]

    %------Reading the Pressure File (Experimental data)------------

    tx = 'lu1_RP-3060-50-AF12-L.txt' ;              % File name
        fid = fopen( tx ) ;                         % To open the data
file
        line = '';
        while isempty( findstr( line , 'F3 fCr_pressure [kPa]' ) )  %
looking for the line with the data
            line = fgetl( fid ) ;
        end
        d = fscanf( fid , '%f' , [ 5 , inf ] )' ;       %Extracting the
data of the look Up file
        [ nr , nc ] = size( d ) ;           %Size of the file
        fclose( fid ) ;              % End of file reading
        CA = d( :, 1 ) ;             % CA vector
        P = d( :, 4 ) ;              % Pressure vector
        dCA = d(2,1) - d(1,1);       % Encoder resolution

        %--------- Shifiting of the pressure trace ------------
        CAi =( -360:0.5:359.5) ;
        CAs = 180 ;
        nps = CAs / 0.5 ;
        for i = 1: nps
            Ps ( i ) = P ( nr - nps + i ) ;
        end
```

```
        for i = ( nps + 1 ):nr
            Ps ( i ) = P ( - nps + i ) ;
        end
        P = Ps ;
        CA = CAi ;
        %-----------------End of shifting pressure trace-------------

        %-------- Piston vertical Position -------------

        a = 33.5*1e-3 ;         % Crankshaft radius in m
        l = 114 * 1e-3 ;        % Connecting rod length in m
        for i = 1 : nr
            s( i ) = a * cos ( CA ( i ) / 180 * pi ) + ( l^2 - a^2* (
sin (CA( i ) / 180 * pi ) )^2 )^(1/2) - ( l - a ) ;
        end
    %----------------------- Time simulation -------------------------

     ncyc = 20;           % Number of cycles for simulation
     nt = ncyc * nr ;     % Number of time steps for the simulation
     nx = 200 ;            % Number of space steps along the oil film
     dt = dCA * 60 / (RPM * 360) ;  % time step in the simulation
     j = 1 ;                        % Index counting the number of
cycles of simulation
     t1 = 1 ;                       % On or off of the concentration in
the combustion chamber
     dx = th / (nx-1) ;         % space step
     x = ( 0:dx:th);            % space dimension
     CAeoc = 39.50 ;            % CA of end of combustion

    %------ Number of Segments to be divided -----------

     ns = 40 ;                      % Number of segments that the
cyinder is being divided vertically
     L = max ( s ) - min ( s ) ;    % Total height of the cylinder
covered by the oil-film
     dL = L / ns ;                  % height of the vertical segment
     for i = 1 : ns
         Lc ( i ) = dL + ( i ) * dL ;   % heigth of each of the
vertical segements
     end

     %------- Initialization of the matrix wiht the concentration
accross
     %the oil layer
    phio = zeros ( nx , ns*ncr );   % Matrix with the concentration
profile for all vertical segment
    phis = zeros ( nx , 1 );        % Matrix with the concentration
profile for only one segment
    coun = 0 ;                      % Counter of number of plots
    mic = zeros (nr,ns*ncr);
    moc = zeros (nr,ns*ncr);
    mi = zeros (ncr,ns);
```

```
    mo = zeros (ncr,ns);

    %---------Initial Concentration of the mixture in the cylinder ----
----
         [A1, Y1 ] = Xim( phi, m_fuelcyc, T, 100, th) ;             %
Matrix with all the equil info from SUPERTRAPP
         r1blowby = Y1( 4:14, 1 ) ;

    %-------------------------------------------------------------
     for i = 1 : nt + 1440; %1000 %nt       % main loop for
         i = i - 1440 * ( j - 1 ) ;         % time index modification
as the number of cycles is increased
         [A, Y ] = Xim( phi, m_fuelcyc, T, P ( i ), th ) ;   % Matrix
with all the equil info from SUPERTRAPP
         X (:, i) = Y( 4:14, 1 );                            %
Concentration of propane at the interface
         if  CA ( i ) >= CAeoc && CA ( i ) <= 360            % Time
when combustion reaches the cylinder wall, the fuel conc. goes to zero
             t1 = 0 ;
         else
             t1 = 1 ;
         end
        X (:, i) = t1 * X (:, i);                        % Reasigment
of the concentration inside the cyl. considering the flame arrival
        r1 = X (:, i) ;                                  % Boundary
Condition with the concentration
        mu = A( 11, 3 ) / 10000 ;                        % oil
viscosity in centipoise cP (1/100 poise).

        %--------Solution of the Diffusion Equation--------------

        for ic = 1 : ncr                       % for loop for each
fuel component

        %-----Diffusivity Estimation----------
        %   This was done using the Hayduk and Minnas correlation, pg.
11.25
        %   Eq. (11-9.8) from " The Properties of Gases and Liquids "
by
        %   Poling, B., Prausnitz, J. M., and O'connell, J.P., 5th
Edition.

        E = ( 10.2 / VA ( ic ) ) - 0.791 ;
% Factor used in the Diff. eval.
        D= 13.3 * 1e-8 * ( T ^ 1.47 ) * ( mu  ^ E ) / ( VA ( ic ) ^0.71
) * 1e-4; % Diffusivity of fuel in oil in m2/s
            for k = 1 : ns                       % for loop for the
cylinder segments
                r1 = X (:, i) ;                  % Boundary Condition
with the concentration
                if s( i ) > Lc ( k )
```

```
                    r1 ( ic ) = r1blowby (ic)/4 ;% 0.25*1e-3 ;        %
Blowby concentration
                end
                phis = phio ( :, k +  ns * ( ic -1 ) ) ;              %
Initialization of the concetratin matrix at each time step
                C = OilDiff1DEq( phis, th, D, nx, dt, r1 (ic) ) ;     %
Solution of the Diff. Eq.
                phio ( : , k +  ns * ( ic -1 )) = C ;
% reasigmetn of the new value
            end                                          % end of for loop
for the cylinder segements
        end                                              % end of for loop
for each fuel component

        %-------Pictures at different times
                  if j > ncyc                                 % Loop for
the last cycle
                      for npi = 750 :50:1000
                       for ic = 1 : ncr
                             if i == npi
                               figure
                               for nsi = 1:ns
                                 hold on
                                 plot(phio( : , nsi  +  ns * ( ic -1 )
) ) ;
                               end
                             end
                          coun = coun + 1 ;
                       end
                      end
                                          %-----------Cummulative mass
in each element for all
                    %the fuel components
                    for ic = 1 : ncr                     % for for each
fuel component
                        for nim = 1 : ns                 % for
cummulative mass at each segment
                            if s( i ) < Lc (nim)
                                mo (ic,nim ) = trapz( x, phio( : , nim
+  ns * ( ic -1 ) ) ) ;        % mass out of the cylinder, in the film
                            end
                            if CA(i)>CAeoc && CA(i)<360
                                    if s(i) < Lc( nim )
                                        mi (ic,nim ) = trapz( x, phio(
: , nim +  ns * ( ic -1 ) ) ) ;    %mass in the cylinder, out of the
film
                                    end
                                     mo (ic,nim) = 0;
                            end
                            %------------------
                            moc( i, nim +  ns * ( ic -1 ) )  = mo
(ic,nim);
```

```
                            mic( i, nim +  ns * ( ic -1 ) )  = mi
(ic,nim) ;
                            if CA ( i ) >=360
                                mic( i, nim +  ns * ( ic -1 ) )  = 0*
mi (ic,nim);
                            end
                            %-----------------
                        end                          % end for
cummulative mass at each segment
                    end                              % end for of each
fuel component
                    %-------------------------------------------------
----
            end                                      % End of loop for
last cycle
        %--------------------------------------
         if i == 1440 ;
            j = j + 1 ;
         end
     end                  % main loop end for
%-----------------------------------------------------------------------
----
     micr = zeros(nr,ns*ncr);
     mocr = zeros(nr,ns*ncr);
     for ic = 1 : ncr                               % for throught each
fuel component
             for j = 1 : ns                        % for through each
cylinder segment
                 for i = 1 : nr                    % for through each
of the 1440 points of the cycle
                        if mic ( i, j +  ns * ( ic -1 ) ) >0
                            micr ( i, j +  ns * ( ic -1 )) = max( mic(
:, j +  ns * ( ic -1 ) ) ) - mic( i, j +  ns * ( ic -1 ) ) ;    % mass
in cylinder cummulative
                        end
                        if moc ( i, j +  ns * ( ic -1 ) ) >0
                            dmocr ( i, j +  ns * ( ic -1 ) ) = max(
moc( :, j +  ns * ( ic -1 ) ) ) - moc( i, j +  ns * ( ic -1 ) );   %
difference between the maximum and minimum
                        end
                 end                                % for through each
of the 1440 points of the cycle
                min_mocr = max( moc(:, j +  ns * ( ic -1 ) ) ) -
max(dmocr(:, j +  ns * ( ic -1 ) ) );   % Minimum value of the mass in
each element
                for i = 1 : nr
                        if moc ( i, j +  ns * ( ic -1 ) ) >0
                            mocr (i,  j +  ns * ( ic -1 ) ) = moc(i, j
+  ns * ( ic -1 ) ) - min_mocr;      % mass out of the cylinder
cummulative
                        end
                end
                 mcumi ( ic, j ) = max( micr( :,  j +  ns * ( ic -1 )
) ) ;
```

```
                mcumo ( ic, j ) = max( mocr( :,  j +  ns * ( ic -1 )
) ) ;
            end                                     % Enf of for through
each segment
     end                                            % End of for through
each component
     mci_totc = sum(mcumi,2);
     mco_totc = sum(mcumo,2);
     mci_tot = sum(mci_totc);
     mco_tot = sum(mco_totc);
     rho = (A ( 2, 3 ) * A( 4, 3 )) ;               % Mixture density
     Dc = 0.08;          % cylinder diameter m
     LC = pi * Dc ;      % cylinder circunference length
     mass_total = rho * dL * LC * mci_tot;
     masso_total = rho * dL * LC * mco_tot;
     pcti_fuel = mass_total/ m_fuelcyc * 100
     pcto_fuel = masso_total/ m_fuelcyc * 100
     hist_micr = rho * dL * ( LC / m_fuelcyc * 100 )* sum ( micr, 2 ) ;
     hist_mocr = rho * dL * ( LC / m_fuelcyc * 100 )* sum ( mocr, 2 ) ;
  %-------------------------------------------------------
  %-----------------------Output File----------------------

    OLPH{1}=strcat('CumMass_','N-Hexatriacontane-Multi');
    fid=fopen(OLPH{1},'wt');
    fprintf(fid, 'CA'); fprintf(fid, '\t');
    fprintf(fid, 'Cumm_mass_in'); fprintf(fid, '\t');
    fprintf(fid, 'Cumm_mass_out'); fprintf(fid, '\t');
    fprintf(fid, '\n');
    for v=1:nr
        fprintf(fid, '%3.3f\t',CA(v));
        fprintf(fid, '%g\t', hist_micr(v));
        fprintf(fid, '%g\t', hist_mocr(v));
        fprintf(fid, '\n');
    end
    fclose(fid);
%---------------- Plots ----------------------------
    figure
    for i = 1:ns
     hold on
     plot(CA,mic(:,i))
    end
    figure
    for i = 1:ns
     hold on
     plot(CA,micr(:,i))
    end
   figure
    for i = 1:ns
     hold on
     plot(CA,moc(:,i))
    end
    figure
    for i = 1:ns
```

```
     hold on
     plot(CA,mocr(:,i))
    end
    toc         % Time of end of calculation

function [phi] = OilDiff1DEq (phio, th, D, nx, dt, r1) ;
%Crank Nicholson, 1-D Diffusion Equation
%Know Parameters
phi = phio ;
Lx = th ;
dx = Lx / ( nx - 1 ) ;
Dbar = D * dt / ( dx ^ 2 ) ;
%--------- Coefficients of a, b, c, crwk of the thomas algoritm

    %------ Initialization of the coefficients ------
    a = zeros ( nx , 1 ) ;
    b = zeros ( nx , 1 ) ;
    c = zeros ( nx , 1 ) ;
    cwrk = zeros ( nx , 1 ) ;
    %----- Definition of the coefficients ---------
    b ( 1 ) = 1 ;
    r ( 1 ) = r1 ;
    for i = 2 : nx - 1
        a ( i ) = - 1/2 * Dbar ;
        b ( i ) = 1 + Dbar ;
        c ( i ) = - 1/2 * Dbar ;
    end
    a ( nx ) = - Dbar ;
    b ( nx ) = 1 + Dbar ;
    r ( nx ) = phi ( nx ) +  1/2 * Dbar * ( - 2 * phi ( nx ) + 2 * phi
( nx - 1 ) )  ;

        for i = 2 : nx - 1
            r ( i ) = phi ( i ) + 1/2 * Dbar * ( phi ( i + 1 ) - 2 *
phi ( i ) + phi ( i - 1)) ;
        end

        r ( nx ) = phi ( nx ) + 1/2 * Dbar * ( -2 * phi ( nx ) + 2 *
phi ( nx - 1 ) ) ;
        phi = thomas ( a, b, c, cwrk, r, nx ) ;


function [A, Y] = Xim(phi, m_fuelcyc, T, P, th ) ;
%Multicomponent equilibrium simulation

%Written by Victor M. Salazar
%Engine Research Center
%University of Wisconsin-Madison
%April 06,2008
P = P / 100 ;                                    %[bar]
method = 1 ;                                % method= 1, for PR and method
= 2 for CS
```

```
%-------------------------------------------------------------------
----
 Ai = NISTSUPPMATLB (P, T, method, 1,'C36');     %Properties of the N-
hexatriacontane
 rho_oil = (Ai ( 2, 3 ) * Ai( 4, 3 ));          %Density of the N-
hexatriacontane in Kg/m^3
%---------Oil mass, mass fraction, molar fraction Calc.-----------
L_Oil = 0.067 ;                          %"Stroke" [m]
D_cyl = 0.08 ;                           %"Cylinder diameter" [m]
Area_Oil = pi*L_Oil*D_cyl ;              %"Area of oil exposed to the
fuel" [m^2]
m_fuel = m_fuelcyc ;                     %"Mass of fuel per cycle"[kg]
m_oil = rho_oil*Area_Oil*th ;            %"Mass of oil" [kg]

%------------------Mixture molar fraction estimation-----------------
----

%"=================================================================
====="

    % For lean or stoic. mix. phi <=1, and for rich mix. phi>=1, Turns,
Pg. 19"

    %"The general equation has the following form, for the
stoichiometric case"
    %"CxHy + a ( O2 + 3.76N2) =====>   b CO2 + d H2O + f O2 + 3.76a N2"

    %"The general equation has the following form, for the rich case"
    %"CxHy + a ( O2 + 3.76N2) =====>   b CO2 + d H2O + e H2 +  3.76a N2
+ ..."

    %------------Molecular weight of C, O2, H, N2--------------
    MW_C = 12.00 ;                       %Carbon melecular weight
[kg/kmol]
    MW_H = 1.007825 ;                    %Hydrogen Molecular weight
[kg/kmol]
    MW_O2 = 31.9988 ;                    %O2 melecular weight
[kg/kmol]
    MW_N2 = 28.0134 ;                    %O2 melecular weight
[kg/kmol]
    %-------------------------------------------------------------------
--------
    MW_oil =MW_C *36 + MW_H*74 ;         %"Oil molecular weigth, N-
HEXATRIACONTANE, C36H74, equ. name: C36"
    N_oil = m_oil/MW_oil ;               %"Number of moles of oil"
    %------- Sintetic fuel composition from Linna et at SAE Paper
972892-------
    Y_f_C5H12 = 0.2 ;                    % mass fraction of "I-
Pentante"
    MW_C5H12 = 5 * MW_C + 12 * MW_H ;    % Molecular weight of I-
Pentane [kg/kmol]
    Y_f_C6H14 = 0.1 ;                    % mass fraction of "3-
Methylpentane"
```

```
    MW_C6H14 = 6 * MW_C + 14 * MW_H ;       % Molecular weight of 3-
Methylpentane [kg/kmol]
    Y_f_C6H6 = 0.03 ;                       % mass fraction of
"Benzene"
    MW_C6H6 =  6 * MW_C + 6 * MW_H ;        % Molecular weight of
Benzene [kg/kmol]
    Y_f_C7H16 = 0.05 ;                      % mass fraction of "N-
Heptane"
    MW_C7H16 =  7 * MW_C + 16 * MW_H ;      % Molecular weight of N-
Heptane [kg/kmol]
    Y_f_C7H8 = 0.2 ;                        % mass fraction of
"Toluene"
    MW_C7H8 =  7 * MW_C + 8 * MW_H ;        % Molecular weight of
Toluene [kg/kmol]
    Y_f_C8H18 = 0.15 ;                      % mass fraction of "I-
Octane"
    MW_C8H18 =  8 * MW_C + 18 * MW_H ;      % Molecular weight of I-
Octane [kg/kmol]
    Y_f_C8H10m = 0.085 ;                    % mass fraction of "m-
Xylene"
    MW_C8H10m =  8 * MW_C + 10 * MW_H ;     % Molecular weight of m-
Xylene [kg/kmol]
    Y_f_C8H10p = 0.085 ;                    % mass fraction of "p-
Xylene"
    MW_C8H10p =  8 * MW_C + 10 * MW_H ;     % Molecular weight of p-
Xylene [kg/kmol]
    Y_f_C9H12 = 0.05 ;                      % mass fraction of "1,2,4
Trimethylbenzene"
    MW_C9H12 =  9 * MW_C + 12 * MW_H ;      % Molecular weight of 1,2,4
Trimethylbenzene [kg/kmol]
    Y_f_C10H22 = 0.035 ;                    % mass fraction of "N-
Decane"
    MW_C10H22 =  10 * MW_C + 22 * MW_H ;    % Molecular weight of N-
Decane [kg/kmol]
    Y_f_C12H26 = 0.015 ;                    % mass fraction of "N-
Dodecane"
    MW_C12H26 =  12 * MW_C + 26 * MW_H ;    % Molecular weight of N-
Dodecane [kg/kmol]
    %----Molecular weight of the syntetic Fuel (mixture of
theircomponents)----
    MW_fuel_syn = 1 / ( Y_f_C5H12/MW_C5H12 + Y_f_C6H14/MW_C6H14 +
Y_f_C6H6/MW_C6H6...
        + Y_f_C7H16/MW_C7H16 + Y_f_C7H8/MW_C7H8 + Y_f_C8H18/MW_C8H18
...
        + Y_f_C8H10m/MW_C8H10m + Y_f_C8H10p/MW_C8H10p +
Y_f_C9H12/MW_C9H12...
        + Y_f_C10H22/MW_C10H22 + Y_f_C12H26/MW_C12H26 );
    %----------Molar fractions of each fuel-componet in the fuel-------
--
    X_f_C5H12 =   Y_f_C5H12/MW_C5H12 *  MW_fuel_syn ;
    X_f_C6H14 = Y_f_C6H14/MW_C6H14 *  MW_fuel_syn ;
    X_f_C6H6 = Y_f_C6H6/MW_C6H6 *  MW_fuel_syn ;
    X_f_C7H16 = Y_f_C7H16/MW_C7H16 *  MW_fuel_syn ;
    X_f_C7H8 = Y_f_C7H8/MW_C7H8 *  MW_fuel_syn ;
```

```
    X_f_C8H18 = Y_f_C8H18/MW_C8H18 *  MW_fuel_syn ;
    X_f_C8H10m = Y_f_C8H10m/MW_C8H10m *  MW_fuel_syn ;
    X_f_C8H10p = Y_f_C8H10p/MW_C8H10p *  MW_fuel_syn ;
    X_f_C9H12 = Y_f_C9H12/MW_C9H12 *  MW_fuel_syn ;
    X_f_C10H22 = Y_f_C10H22/MW_C10H22 *  MW_fuel_syn ;
    X_f_C12H26 = Y_f_C12H26/MW_C12H26 *  MW_fuel_syn ;
    X_Total_fuel  = X_f_C5H12 + X_f_C6H14 + X_f_C6H6 + X_f_C7H16
+X_f_C7H8 ...
            + X_f_C8H18 + X_f_C8H10m + X_f_C8H10p + X_f_C9H12 +
X_f_C10H22 + X_f_C12H26 ;

    %" x1 and y1 values of the syntetic fuel: Cx1Hy1, x1 = number of
carbon atoms, y1= number of hydrogen atoms "
    %----"Carbon"----
    x1 = 5 *  X_f_C5H12 + 6 *  X_f_C6H14 + 6 *  X_f_C6H6 +  7 *
X_f_C7H16 ...
        + 7 * X_f_C7H8 + 8* X_f_C8H18 + 8 * X_f_C8H10m + 8 *
X_f_C8H10p...
        + 9 * X_f_C9H12 + 10 * X_f_C10H22 + 12 * X_f_C12H26 ;
    %----"Hydrogen"----
    y1 = 12 *  X_f_C5H12 + 14 * X_f_C6H14 + 6 * X_f_C6H6 + 16 *
X_f_C7H16...
        + 8 * X_f_C7H8 + 18 * X_f_C8H18 + 10 * X_f_C8H10m ...
        + 10 * X_f_C8H10p + 12 * X_f_C9H12 + 22 * X_f_C10H22 + 26 *
X_f_C12H26;
    N_ffuel = m_fuel/MW_fuel_syn ;          %"Number of moles of fuel"
    a= ((x1 + y1/4)/phi ) ;                  %"Number of moles of air"
    N_T_R =( 1 + a*4.76)*N_ffuel ;          %"Total number of moles of
the reactants air+fuel"
    N_T = N_T_R + N_oil ;                   %"Total number of moles
including oil"
    X_fuel=N_ffuel/N_T ;                    %"Fuel molar fraction"
    X_O2 = a*N_ffuel/N_T ;                  %"Oxygen molar fraction"
    feed(1,1) = X_O2 ;
    X_N2 = 3.76*a*N_ffuel/N_T ;             %"Nitrogen molar fraction"
    feed(2,1) = X_N2 ;
    X_oil = N_oil/N_T ;                     %"Oil molar fraction"
    feed(3,1) = X_oil ;
    X_T_v = X_oil + X_N2 + X_O2 + X_fuel ;  %"Total number of moles
verification"
    %----" Mass of the air components O2 and N2 in the mixture "----
    m_O2 = ( a*N_ffuel ) * MW_O2 ;           %"Mass of O2 per
cycle"[kg]
    m_N2 = ( 3.76*a*N_ffuel  ) * MW_N2 ;     %"Mass of N2 per
cycle"[kg]
    %------------Total mass of the system---------------
    m_total = m_fuel + m_oil + m_O2 + m_N2 ;
    %---------" Moles of fuel in the Oil-Air-Fuel system"---------
    X_C5H12 = X_f_C5H12*N_ffuel/N_T ;        % mass fraction of "I-
Pentante"
    feed(4,1) = X_C5H12 ;
    X_C6H14 = X_f_C6H14*N_ffuel/N_T ;        %mass fraction of "3-
Methylpentane"
```

```
    feed(5,1) = X_C6H14 ;
    X_C6H6 = X_f_C6H6*N_ffuel/N_T ;          %mass fraction of
"Benzene"
    feed(6,1) = X_C6H6 ;
    X_C7H16 = X_f_C7H16*N_ffuel/N_T ;        %mass fraction of "N-
Heptane"
    feed(7,1) = X_C7H16 ;
    X_C7H8 = X_f_C7H8 *N_ffuel/N_T ;         %% mass fraction of
"Toluene"
    feed(8,1) = X_C7H8 ;
    X_C8H18 = X_f_C8H18*N_ffuel/N_T ;        % mass fraction of "I-
Octane"
    feed(9,1) = X_C8H18 ;
    X_C8H10m = X_f_C8H10m*N_ffuel/N_T ;      % mass fraction of "m-
Xylene"
    feed(10,1) = X_C8H10m ;
    X_C8H10p = X_f_C8H10p*N_ffuel/N_T ;      % mass fraction of "p-
Xylene"
    feed(11,1) = X_C8H10p ;
    X_C9H12 = X_f_C9H12*N_ffuel/N_T ;        % mass fraction of "1,2,4
Trimethylbenzene"
    feed(12,1) = X_C9H12 ;
    X_C10H22 = X_f_C10H22*N_ffuel /N_T ;     % mass fraction of "N-
Decane"
    feed(13,1) = X_C10H22 ;
    X_C12H26 = X_f_C12H26*N_ffuel/N_T ;      % mass fraction of "N-
Dodecane"
    feed(14,1) = X_C12H26 ;
    X_Total_mix  = X_C5H12 + X_C6H14 + X_C6H6 + X_C7H16 +X_C7H8 +
X_C8H18 + X_C8H10m...
        + X_C8H10p + X_C9H12 + X_C10H22 + X_C12H26 + X_oil + X_N2 +
X_O2 ;
    %--------------- Array with the components of the mixture----------
--------
    commix =
'O2+N2+C36+IC5+3MP+BNZ+C7+TOL+224TMP+MXYL+PXYl+124TMBNZ+C10+C12';
    feed ;
    A = NISTSUPPMATLB (P, T, method, feed,commix);
%------- "Percentage of fuel in oil " -------
%---"Mass fractions of the fuel components in the LIQUID phase"---
    Y_l_O2 =   A(1,1) *MW_O2 /  A(2,3) ;
    Y_l_N2 =   A(2,1) *MW_N2 /  A(2,3) ;
    Y_l_oil =    A(3,1) *MW_oil/ A(2,3) ;
    Y_l_C5H12 =   A(4,1) *MW_C5H12 /  A(2,3) ;
    Y_l_C6H14 = A(5,1) *MW_C6H14  /  A(2,3) ;
    Y_l_C6H6 = A(6,1) *MW_C6H6  /  A(2,3) ;
    Y_l_C7H16 = A(7,1) *MW_C7H16  /  A(2,3) ;
    Y_l_C7H8 = A(8,1) *MW_C7H8  /  A(2,3) ;
    Y_l_C8H18 = A(9,1) *MW_C8H18  /  A(2,3) ;
    Y_l_C8H10m = A(10,1) *MW_C8H10m  /  A(2,3) ;
    Y_l_C8H10p = A(11,1) *MW_C8H10p  /  A(2,3) ;
    Y_l_C9H12 = A(12,1) *MW_C9H12  /  A(2,3) ;
    Y_l_C10H22 = A(13,1) *MW_C10H22  / A(2,3) ;
    Y_l_C12H26 = A(14,1) *MW_C12H26  /  A(2,3) ;
```

```
    %---- Mass Fraction of especies--------------
    Y(1,1) = Y_l_O2 ;
    Y(2,1) = Y_l_N2 ;
    Y(3,1) = Y_l_oil ;
    Y(4,1) = Y_l_C5H12 ;
    Y(5,1) = Y_l_C6H14 ;
    Y(6,1) = Y_l_C6H6 ;
    Y(7,1) = Y_l_C7H16 ;
    Y(8,1) = Y_l_C7H8 ;
    Y(9,1) = Y_l_C8H18 ;
    Y(10,1) = Y_l_C8H10m ;
    Y(11,1) = Y_l_C8H10p ;
    Y(12,1) = Y_l_C9H12 ;
    Y(13,1) = Y_l_C10H22 ;
    Y(14,1) = Y_l_C12H26 ;
    %-------------Mass fraction of the fuel in oil ----------------
    Y_fuel_l = Y_l_C5H12 + Y_l_C6H14 + Y_l_C6H6 + Y_l_C7H16 ...
        + Y_l_C7H8 + Y_l_C8H18 + Y_l_C8H10m + Y_l_C8H10p + Y_l_C9H12 +
Y_l_C10H22 + Y_l_C12H26;
    Y_fuel_total_liquid_phase = Y_fuel_l + Y_l_O2 + Y_l_N2 + Y_l_oil ;
% Check
    m_liq_ph = m_total / (  A(1,4)* A(2,4) / ( A(1,3) * A(2,3) ) + 1 )
;    % Mass of the liquid phase
    m_fuel_l = m_liq_ph * Y_fuel_l ;
% mass of fuel in the liquid pashe (Oil)
    Per_fuel_oil   = m_liq_ph * Y_fuel_l / m_fuel * 100 ;
% Percent of mass of fuel stored in oil
    PF = Per_fuel_oil;

function [x] = thomas(a,b,c,cwrk,r,n)
% written by Prof. Chris Rutland
% solve tridiagonal system with thomas algorithm.  tri(a,b,c)*x = r.
% solution returned in r array.
% input
%   a,b,c   arrays containing the tridiag matrix (these are not
changed)
%   r       array containing the right hand side (destroyed in call)
%   n       size of the system
% output
%   x       solution returned in x array
%   cwrk    work array so that original matrix is not destroyed
% forward elimination
fac     = 1.0/b(1);
cwrk(1) = c(1) * fac;
r(1)    = r(1) * fac;
for i = 2:n
    fac     = 1.d0/( b(i) - a(i)*cwrk(i-1) );
    cwrk(i) =                   c(i)   * fac;
    r(i)    = ( r(i) - r(i-1) * a(i) ) * fac;
end
% back substitution
% put solution into x array, r(n) already has solution
x(n) = r(n);
for i = n-1:-1:1
```

```
    x(i) = r(i) - cwrk(i)*x(i+1);
end


c**********************************************************************
c
c     MEX Function to call the NIST SUPPERTRAPP Source Fortran code
c     from  Matlab
c     from Matlab it can be call typing:
c           mex HNISTSUPPMATL.for
c     this creates the gateway file between Matlab and Fortran
c     then type:
c           A = NISTSUPPMATL ( PX , TX , N, FEED, INSTR1);
c     where : PX and TX are the pressure and temperature of the system,
c     N is the method used for solve either: 1 Peng Robinson or 2
c     corresponding states,
c     FEED is the array containing the molar fractions of the
c     components
c     INSTR1 is the string containing all the names of the system. It
c     must have the following form: 'CM1,CM2,CM3,......', where: CM1,
c     CM2,...
c                 are the names of the components of the system
c     following the convention of the NIST manual.
c     Writen by: Victor M. Salazar
c     Madison, April 06, 2008
c
c**********************************************************************
c
c
      SUBROUTINE mexFunction
     $(NARGOUT,PARGOUT,NARGIN,PARGIN)
      INTEGER NARGOUT, NARGIN
      INTEGER PARGOUT (*), PARGIN (*)
      INTEGER mxGetN, mxGetPr, mxGetScalar
      INTEGER mxCreateDoubleMatrix
      INTEGER mxCreateString, mxGetString
      CHARACTER INSTR1*200

      STATUS = mxGetString(pargin(5), INSTR1, 200)
      PARGOUT(1) = mxCreateDoubleMatrix (20, 4, 0)

      CALL NISTSUPPMATL (%VAL (mxGetPr (PARGIN (1))),
     $ %VAL (mxGetPr (PARGIN (2))),
     $ %VAL (mxGetPr (PARGIN (3))),
     $ %VAL (mxGetPr (PARGIN (4))),
     $ INSTR1,
     $ %VAL (mxGetPr (PARGOUT (1))))
      RETURN
      END
C     -----------NISTSUPPMATL subroutine-----------------------
c**********************************************************************
      SUBROUTINE NISTSUPPMATL ( PX , TX , N, FEED, INSTR1 ,XP)
      IMPLICIT DOUBLE PRECISION (A-H,O-Z)
      CHARACTER NAME(20)*50, INSTR1*200
```

```
      DIMENSION  X(20,2), FEED(20), AK(20), PROPS(20,2),XP(20,4)
      DIMENSION  XL(20),XV(20)
      DOUBLE PRECISION XP
      C     --------READING OF THE ARRAY CONTAINING THE NAMES---------
      I = LEN(INSTR1)
      DO WHILE (INSTR1(I:I) .EQ. ' ')
        I = I - 1
      ENDDO
      LN = I
      KT = 1
      J =1
      DO 115 I = 1,LN
       IF(INSTR1(I:I).EQ.'+')THEN
            NAME ( J ) = INSTR1(KT:I-1)
            KT = I+1
            J = J+1
        ENDIF
        IF(I.EQ.LN)THEN
            NAME ( J ) = INSTR1(KT:LN)
        ENDIF
115   CONTINUE
C     -----END OF THE READING AND ASIGMENT OF THE COMPONENT NAMES
CC                       INITIALIZE PARAMETERS
      CALL INITP
C=====================================================================
C
C    ENTER NAMES, NUMBER OF COMPONENTS, FEEDS, MODEL
C    NOTE: MOLE FRACTIONS (FEED) MUST SUM TO UNITY!
C     -------SELECTION OF THE METHOD , PR OR CS-----------
      IF(N.EQ.1) THEN
            METHOD = 1
      ELSE
            METHOD = 2
      ENDIF
      NC = J ! Number components, must match the mole fractions
C           ADDITIONAL SET UP, REQUIRED EVRY TIME COMPONENTS
C                       OR FEED CHANGED
      CALL SETCOM(NAME,FEED,NC,IER)
c      IF(IER.NE.0)THEN
C        WRITE(*,*)' COMPONENT NAME SPELLED INCORRECTLY, OR '
C        WRITE(*,*)' IT IS NOT PRESENT IN THE DATABASE '
C        STOP
C      ENDIF
C
C      ----------CALLING THE: T,P FLASH ROUTINE-------------
      CALL FLASH(PX,TX,FEED,AK,X,PSI,NPH,IER)
      DO 117 I = 1,NC
        XL(I)=X(I,1)
        XV(I)=X(I,2)
117   CONTINUE

C     ------EVALUATE PROPERTIES IF NO ERRORS FROM FLASH------
      IF(IER.EQ.0)THEN
        CALL PHASEP(PX,TX,XL,XV,PSI,NPH,METHOD,PROPS,IERPP)
```

```
      ENDIF
C     --------------SSIGMENT OF PROPERTIES--------------------
      DO 119 I = 1,NC
        XP(I,1)=X(I,1)
        XP(I,2)=X(I,2)
119   CONTINUE
      DO 121 I = 1,20
        XP(I,3)=PROPS(I,1)
        XP(I,4)=PROPS(I,2)
121   CONTINUE
          XP(17,3)= PSI
          XP(18,3)= NPH
C     ---------------End of evaluation of properties-----------
      RETURN
      END               ! End of subroutine

C*********************************************************************
C*********************************************************************
C     Below this line are the fortran subroutines of: STPV2A.for and
STPV2B.for
C     Do not modify these subroutines at all!
```